

**Cellular viability and the occurrence and significance of chlorophyll  
allomers during phytoplankton turnover**

by

Deborah Jane Steele



*A thesis submitted for the degree of*  
**DOCTOR OF PHILOSOPHY**

Faculty of Science and Technology  
Bournemouth University

*In collaboration with*  
Plymouth Marine Laboratory

September 2014

## **Copy Statement**

This copy of the thesis has been supplied on condition that anyone who consults it is understood to recognise that its copyright rests with its author and due acknowledgement must always be made of the use of any material contained in, or derived from, this thesis.

## Abstract

### *Cellular viability and the occurrence and significance of chlorophyll allomers during phytoplankton population turnover*

Deborah Jane Steele

Phytoplankton can exist in the water column, whole but non-functional, and the percentage of these dead cells is highly variable. These dead cells can contain chlorophyll and contribute to ocean colour, and hence estimates of oceanic primary productivity. The aim of this project was to assess indicators of phytoplankton physiological state, focusing on the formation of chlorophyll *a* oxidation products (allomers) and a chlorophyll precursor.

Initially, to establish an appropriate method for the identification and quantification of chlorophyll allomers, a method selection and optimisation study was carried out. This assessment revealed that chlorophyll was prone to oxidation during sample analysis. Instrumentation, sample manipulation, method duration and HPLC solvent composition were all contributors to sample oxidation. The application of a method by Zapata et al. (2000) was found to produce minimal and consistent chlorophyll oxidation and was applied in subsequent studies.

During a culture study of the picoeukaryote *Ostreococcus tauri* (Prasinophyceae), two chlorophyll allomers were formed solely during viral-infection, and not during environmental limitation of growth. Allomers began to increase 24 hours post viral-infection (hpi), simultaneously with decreases in population density and  $F_v/F_m$ , and an increase in membrane permeability. During viral-infection allomers reached a maximum level 48 hpi, which was 10-fold higher than the maximum level of allomers formed during environmental limitation.

Chlorophyll *a* allomers were measured over an annual cycle for the first time, at the Western Channel Observatory (UK). Allomer occurrence (relative to chl-*a*) was maximal during April with a total allomer to chl-*a* ratio of 0.093 in surface water. Peaks in allomers were associated with blooms of *Phaeocystis* spp., *Guinardia delicatula*, *Chaetoceros socialis* and *Emiliania huxleyi* and associations were dependent on the cause of the taxas' declines.

In situ allomer measurements were also taken during a research cruise in the central and southern North Sea, where the maximum ratio of allomers to chl-*a* (0.15) was measured at the Flamborough Front.

## Contents

<b>1. Chapter I : Variability and detection of micro-eukaryote phytoplankton viability....</b>	<b>17</b>
1.1. Role of phytoplankton primary production in the Earth System.....	17
1.2. Ecology of Phytoplankton Death .....	17
1.2.1. The proportion of functional cells is highly variable .....	18
1.3. Defining Phytoplankton Death.....	19
1.3.1. Modes of death.....	19
1.3.2. Defining “Viability” .....	20
1.3.3. Defining “Senescence” .....	20
1.3.4. Batch culture growth cycle.....	21
1.4. Process of Cell Death .....	22
1.4.1. Death by environmental factors .....	22
1.4.2. Death by viral lysis.....	22
1.4.3. Oxidative stress .....	23
1.5. Indicators of viability and reactive oxygen species.....	24
1.5.1. Cell digestion assay .....	24
1.5.2. Molecular probes.....	24
1.5.2.1. For membrane permeability: SYTOX-Green.....	25
1.5.2.2. For ROS: CM-H <sub>2</sub> DCFDA and DHR .....	25
1.5.2.3. CMFDA for hydrolytic enzyme activity .....	25
1.5.3. Limitations of viability staining .....	25
1.6. Theory and uses of chlorophyll fluorescence.....	26
1.6.1. Description of light absorption and fluorescence.....	26
1.6.2. Interpretation of $F_v/F_m$ in a mixed community .....	27
1.6.3. Using fluorescence to estimate photosynthesis in situ .....	28
1.7. Chlorophyll and phytoplankton cell death .....	29
1.7.1. Chlorophyll and estimating primary productivity .....	29
1.7.2. Chlorophyll alteration products linked to phytoplankton death.....	31
1.8. Chlorophyll <i>a</i> allomers.....	32
1.8.1. Detecting allomers.....	32
1.8.2. Chlorophyll <i>a</i> allomers in the natural environment.....	33
1.8.3. Allomer formation under laboratory conditions.....	33
1.8.3.1. Formation of hydroxychlorophyll <i>a</i> .....	33
1.9. Research aims & objectives .....	34
<b>2. CHAPTER II : HPLC method selection and optimisation for allomer separation.....</b>	<b>35</b>
2.1. Introduction .....	35
2.2. Description of Samples used for Chromatography Optimisation.....	37
2.3. Selection and Optimisation of Airs et al. (2001).....	37
2.3.1. Method selection and optimisation of eluent composition.....	37
2.3.2. Application of Method 1 to pelagic particulate samples .....	39
2.4. Oxidation of chlorophyll <i>a</i> during sample preparation and analysis .....	41
2.4.1. Oxidation during extract preparation for injection.....	41
2.4.2. Comparison of oxidation in HPLC systems .....	44
2.4.3. Ultra-High Performance Liquid Chromatography .....	47
2.5. Optimisation of Zapata et al (2000) method .....	49
2.6. Assignment of peaks using LC/MS <sup>n</sup> .....	52
2.6.1. Particulate sample from station L4, analysed using the Zapata et al. (2000) method.....	52
2.6.2. Particulate sample from station L4, analysed using Method 1.....	54
2.7. Conclusions .....	56

<b>3. CHAPTER III : Chlorophyll oxidation and indicators of viability during viral infection and senescence in the prasinophyte <i>Ostreococcus tauri</i> .....</b>	<b>57</b>
3.1. Introduction .....	57
3.1.1. Marine viruses of phytoplankton.....	57
3.1.1.1. Viruses affect carbon cycling .....	57
3.1.1.2. Viruses affect phytoplankton diversity.....	58
3.1.2. Phytoplankton senescence due to nutrient limitation .....	59
3.1.3. Description and importance of <i>Ostreococcus</i> .....	60
3.1.4. Comparing viral lysis to senescence .....	61
3.2. Experimental Outline .....	62
3.3. Results and Discussion of <i>O. tauri</i> microcosm study .....	64
3.3.1. OtV5-infected cultures; physiological indicators.....	64
3.3.1.1. <i>O. tauri</i> /OtV5 infection cycle.....	64
3.3.1.2. $F_v/F_m$ during <i>O. tauri</i> /OtV5 infection.....	66
3.3.1.3. Staining for membrane permeability during <i>O. tauri</i> /OtV5 infection.....	66
3.3.1.4. Staining for reactive oxygen species during <i>O. tauri</i> /OtV5 infection.....	67
3.3.2. Physiological indicators during <i>O. tauri</i> growth and senescence.....	69
3.3.2.1. <i>O. tauri</i> batch culture growth and death.....	69
3.3.2.2. Chlorophyll <i>a</i> content and $F_v/F_m$ during <i>O. tauri</i> senescence .....	71
3.3.2.3. Membrane permeability during <i>O. tauri</i> senescence.....	71
3.3.2.4. Staining for reactive oxygen species during <i>O. tauri</i> senescence .....	72
3.3.3. Assignment of chlorophyll alteration products .....	73
3.3.3.1. Assignment of peak I.....	74
3.3.3.2. Assignment of peak II .....	76
3.3.3.3. Assignment of peaks III and IV .....	77
3.3.3.4. Assignment of peak VI.....	77
3.3.3.5. Assignment of peaks VII and VIII .....	77
3.3.4. Chlorophyll alterations during viral infection versus nutrient limitation .....	79
3.3.4.1. Chlorophyll <i>b</i> allomers during viral infection of <i>Ostreococcus tauri</i> .....	79
3.3.4.2. Chlorophyll <i>a</i> allomers during viral infection of <i>Ostreococcus tauri</i> .....	79
3.3.4.3. Chlorophyll <i>b</i> allomers during <i>Ostreococcus tauri</i> growth and senescence .....	82
3.3.4.4. Chlorophyll <i>a</i> allomers during <i>Ostreococcus tauri</i> growth and senescence .....	82
3.4. Chapter III Conclusions .....	85
<b>4. CHAPTER IV : Seasonal changes of chlorophyll <i>a</i> allomers in the Western English Channel during 2012.....</b>	<b>87</b>
4.1. Introduction .....	87
4.2. Material and Methods.....	88
4.2.1. Study site and Sampling Protocol .....	88
4.3. Results and Discussion.....	90
4.3.1. Physical conditions.....	90
4.3.2. Nutrient concentrations at L4 during 2012.....	91
4.3.3. Phytoplankton community structure and progression .....	93
4.3.4. Seasonality of chlorophyll <i>a</i> , hydroxychlorophyll <i>a</i> and precursor .....	95
4.3.5. Allomer hydroxychlorophyll <i>a</i> .....	97
4.3.5.1. Occurrence relative to phytoplankton blooms.....	97
4.3.5.2. Contributors to pelagic hydroxychlorophyll <i>a</i> maxima .....	99
4.3.5.3. Contributors to minor peaks in pelagic hydroxychlorophyll <i>a</i> .....	102
4.3.6. Precursor Chlorophyll $a_{P276}$ .....	104
4.4. Conclusions .....	105

<b>5. CHAPTER V : Survey of chlorophyll allomers, precursor and eukaryote population viability in the North Sea .....</b>	<b>107</b>
5.1. Introduction .....	107
5.1.1. Chapter V hypotheses.....	108
5.2. Location and sampling synopsis.....	109
5.3. Statistical methods.....	110
5.3.1. Phytoplankton community multivariate analysis .....	110
5.4. North Sea cruise Results and Discussion .....	111
5.4.1. Overview of nutrient conditions during the cruise.....	111
5.4.2. Overview of phytoplankton communities during the cruise .....	112
5.4.3. Overview of community variable fluorescence during the cruise.....	113
5.4.4. Overview of community viability during the cruise.....	114
5.4.4.1. SYTOX staining at stations 17 and 18 .....	114
5.4.4.2. CMFDA staining at stations 17 and 18 .....	115
5.4.5. Overview of chlorophyll, allomers and chl- <i>a</i> precursor measurements (by HPLC) .....	116
5.4.5.1. Chlorophyll <i>a</i> concentration.....	116
5.4.5.2. Example pigment chromatogram from the North Sea.....	117
5.4.5.3. Hydroxychlorophyll <i>a</i> detected in the North Sea .....	118
5.4.5.4. Methoxychlorophyll <i>a</i> -like allomer detected in the North Sea .....	120
5.4.5.5. Chlorophyll <i>a</i> <sub>P276</sub> detected in the North Sea .....	120
5.4.6. Multivariate analysis .....	121
5.4.6.1. Phytoplankton community compositions and nutrient concentration .....	121
5.4.7. Hydroxychlorophyll <i>a</i> through the water column .....	123
5.4.8. Allomer to chlorophyll <i>a</i> ratios at thermally stratified stations .....	124
5.4.9. Allomer to chlorophyll ratios in context of recent history of chlorophyll <i>a</i> (satellite derived).....	127
5.4.10. Allomer to chlorophyll ratios in the context of $F_v/F_m$ .....	130
5.5. Chapter V conclusions .....	131
<b>6. CHAPTER VI : Overview and Future Work.....</b>	<b>133</b>
6.1. Overview of Research .....	133
6.2. HPLC method selection and optimisation.....	133
6.3. <i>O. tauri</i> senescence/viral-infection .....	134
6.3.1. Novelty of Study .....	134
6.3.2. Novel Results .....	134
6.3.3. Further culture work.....	135
6.4. Annual cycle of allomer and precursor occurrence in the Western English Channel .....	135
6.4.1. Novelty of study .....	136
6.4.2. Novel Results .....	136
6.4.3. Further in situ work.....	136
6.5. Allomer detection in the North Sea.....	137
6.5.1. Novelty of study .....	137
6.5.2. Novel Results .....	138
6.5.3. Further in situ work.....	138
6.6. Conclusions .....	139

<b>7. CHAPTER VII : Materials and Methods .....</b>	<b>141</b>
7.1. Materials for Biological use .....	141
7.1.1. Preparation of glassware .....	141
7.1.2. Algal and Viral stocks .....	141
7.1.2.1. Preparation of OtV5 stock.....	141
7.1.2.2. Algal maintenance.....	142
7.1.2.3. Culture conditions .....	142
7.1.3. Preparation of Growth Media.....	142
7.1.3.1. ASW and media recipes .....	143
7.2. Biological measurements for culture study (Chapter III).....	145
7.2.1. Maximum quantum efficiency of Photosystem II photochemistry ( $F_v/F_m$ ).....	145
7.2.2. Population density of cultures by flow cytometry.....	145
7.2.3. Membrane permeability probe (SYTOX-Green) .....	147
7.2.4. Reactive Oxygen Species probe (CM-H <sub>2</sub> DCFDA) .....	147
7.2.5. Viral enumeration.....	148
7.3. Sampling procedure for Station L4 (Chapter IV).....	148
7.3.1. Sample collection, PAR and temperature.....	148
7.3.2. Nutrients.....	148
7.3.3. Phytoplankton enumeration and identification.....	149
7.3.3.1. Enumeration by flow cytometry.....	149
7.3.3.2. Identification by microscopy.....	149
7.4. Sampling procedure for North Sea Cruise (Chapter V) .....	150
7.4.1. Sample collection .....	150
7.4.2. $F_v/F_m$ .....	150
7.4.3. Nutrients.....	150
7.4.4. Phytoplankton abundance and community composition.....	150
7.4.5. Cellular staining .....	151
7.4.6. Satellite data .....	151
7.5. Materials for Analytical use .....	151
7.5.1. Solvents for HPLC/MS .....	151
7.5.2. Preparation of HPLC/MS eluents.....	151
7.5.3. Preparation of chlorophyll a standard .....	152
7.6. Analytical Procedures .....	152
7.6.1. Sampling procedure for pigments .....	152
7.6.1.1. From phytoplankton culture .....	152
7.6.1.2. From marine water samples .....	152
7.6.1.3. From marine surface sediment samples .....	153
7.6.2. Concentration by SPE primed in methanol .....	153
7.6.3. Pigment analysis.....	154
7.6.4. Pigment HPLC calibration .....	154
7.6.5. HPLC/MS of selected samples.....	155
<b>8. References .....</b>	<b>156</b>

## List of Figures

- Figure 1.1.** Growth phases of microalgal batch cultures. Modified from an *Ostreococcus tauri* culture cycle to include a lag phase..... 21
- Figure 1.2.** Structures of chlorophyll *a* (I), two of its common alteration products (II & III) and four allomers (IV to VII). ..... 30
- Figure 2.1.** Partial HPLC chromatograms (660 nm) of chlorophyll *a* standard using (A) Airs et al. (2001) method and (B) Method 1 (Table 2.1). ..... 39
- Figure 2.2.** A partial chromatogram (660 nm) obtained during HPLC analysis of a pelagic marine particulate extract (0 m from L4 on 27-03-2012), using Method 1 (Table 2.1). ..... 40
- Figure 2.3.** Partial HPLC-Diode Array Detector (660 nm) chromatograms of chlorophyll *a* and chlorophyll *a* allomer elution after preparation of extract by; (A) automated mixing in injector seat, (B) automated mixing in vial, and (C) manual mixing. .... 43
- Figure 2.4.** Allomer to chl-*a* ratios resulting from injections of chlorophyll *a* standard into System 1 (Agilent instrument running Method 1) ● and System 2 (Accela Instrument running Zapata et al. 2000 method) ○. Ratios calculated from peak areas in 660 nm DAD chromatograms. Arrows indicate times of new standard preparation. .... 44
- Figure 2.5.** Allomer production during chromatography of chlorophyll *a* standard using Agilent and Accela instruments with 3 HPLC methods and 2 column types. Mean ratios of allomer to chl-*a* are shown with SE bars (n=5). ..... 46
- Figure 2.6.** Partial UPLC chromatogram (660 nm) of chlorophyll *a* standard at time of chl-*a* and allomer elution, using Saesaengseerung (2013) method. .... 48
- Figure 2.7.** Partial HPLC chromatograms (660 nm) of chlorophyll *a* standard using (A) Zapata et al. (2000) method, (B) Method 2 and (C) Method 3. For assignment of peaks see text, section 2.6. .... 51
- Figure 2.8.** Partial HPLC chromatogram (660 nm) of a pigment extract from a marine pelagic surface sample collected from Station L4 on 10-04-12, analysed using the Zapata et al. (2000) method. .... 53
- Figure 3.1.** Viruses enhance the flow of carbon and nutrients from phytoplankton to heterotrophic bacteria by causing lysis of cells and shunting the pool of dissolved and particulate organic matter (P-D-OM). Original diagram taken from Suttle (2005); additions are marked in orange and represent the production of recalcitrant DOM (R-DOM) via processing by heterotrophic bacteria and Archaea, which can persist in the water column for millennia (Jiao et al. 2010). .... 58
- Figure 3.2.** Eukaryotic phytoplankton community at time-series station L4 (50.150°N; 4.130°W) in 2012, averaged across depths 0.2, 10, 25 and 50 m (n=12), determined by flow cytometry (See methods chapter 7.3.3.1 for details). Raw data provided by Glen Tarran (PML). The average population densities of picoeukaryotes (□) and other eukaryotes (■), including coccolithophores, dinoflagellates, cryptophytes, *Phaeocytis* and other nanoeukaryotes are shown. The average percentages of picoplankton in the eukaryotic community are also shown (o) as mean ± SE (n=12). .... 60
- Figure 3.3.** Schematic diagram of *Ostreococcus tauri* and OtV5 culture experiment including set-up, sampling frequency and sampling volumes. .... 63

**Figure 3.4.** *Ostreococcus tauri* RCC745 cultures infected with virus OtV5 and non-infected controls: (A) Population densities of *O. tauri* and virus OtV5, (B) maximum quantum efficiency of PSII photochemistry ( $F_v/F_m$ ), (C) SYTOX-Green (for membrane permeability) and CM-H<sub>2</sub>DCFDA (for intracellular reactive oxygen species) staining, insert displays % of cells stained with CM-H<sub>2</sub>DCFDA, on a smaller scale (0 to 1%); and (D) Chlorophyll *a* content per cell. Mean and SE bars shown (n=3), - - - indicates time of virus addition. .... 65

**Figure 3.5.** (A) Population density, specific growth rate ( $\mu$ , d<sup>-1</sup>), (B) maximum quantum efficiency of PSII photochemistry ( $F_v/F_m$ ) and chlorophyll *a* content per cell, (C) SYTOX-Green (for membrane permeability) and CM-H<sub>2</sub>DCFDA (for reactive oxygen species) staining of triplicate *Ostreococcus tauri* batch cultures during growth, stationary and senescent phases. Mean and SE bars shown (n=3). .... 70

**Figure 3.6.** Partial HPLC-PDA chromatogram (660 nm) showing elution position relative to chl-*a* (IX) and chl-*b* (V) of chlorophyll alteration products detected in (A) OtV5-infected *O. tauri* cultures 48 hours post-infection (day 5), (B) growing non-infected cultures on day 5 and (C) senescent non-infected cultures on day 29. For peak assignment see Table 3.1. .... 73

**Figure 3.7.** MS<sup>2</sup> spectra of ions; A. *m/z* 905 and B. *m/z* 873 resulting from peak I in OtV5-infected *Ostreococcus tauri* pigment extract. .... 75

**Figure 3.8.** MS<sup>2</sup> spectra of the major ion at *m/z* 887 resulting from peak II in OtV5-infected *Ostreococcus tauri* pigment extract. .... 76

**Figure 3.9.** Ratios of chlorophyll *b* allomers to chl-*b* in OtV5-infected ●, and non-infected ○, *O. tauri* cultures including (A) hydroxychlorophyll *b* and (B) hydroxychlorophyll *b'*. - - - indicates time of virus addition. Mean and SE bars shown (n=3). .... 79

**Figure 3.10.** Ratios of chlorophyll *a* allomers to chl-*a* in OtV5-infected ● and non-infected ○ *O. tauri* cultures including (A) methoxychlorophyll *a*-like allomer, (B) HO-chl-*a*-like allomer, (C) hydroxychlorophyll *a* and (D) hydroxychlorophyll *a'*. - - - indicates time of virus addition. Mean and SE bars shown (n=3). .... 80

**Figure 3.11.** Ratios of chlorophyll *a* alteration products to chl-*a* in viral-infected ● and non-infected ○ *O. tauri* cultures including (A) chlorophyllide *a*, (B) chl-*a*<sub>P276</sub> and (C) pheophytin. - - - indicates time of virus addition. Mean and SE bars shown (n=3). .... 80

**Figure 3.12.** Ratios of chl-*b* allomers to chl-*b* in growing (days 0 to 15), and senescent (days 15 to 29) *Ostreococcus tauri* cultures including (A) hydroxychlorophyll *b* and (B) hydroxychlorophyll *b'*. Mean and SE bars shown (n=3). .... 82

**Figure 3.13.** Ratios of allomers to chlorophyll *a* in growing (days 0 to 15) and senescent (days 15 to 29) *Ostreococcus tauri* cultures including (A) hydroxychlorophyll *a* and (B) hydroxychlorophyll *a'*. Mean and SE bars shown (n=3). .... 84

**Figure 3.14.** Ratios of chlorophyll *a* alteration products to chl-*a* in growing (days 0 to 15) and senescent (days 15 to 29) *Ostreococcus tauri* cultures including (A) chlorophyllide *a*, (B) chl-*a*<sub>P276</sub> and (C) pheophytin. Mean and SE bars shown (n=3). .... 84

**Figure 4.1.** Location of station L4 within the western English Channel, UK. Bathymetry map derived from www.gebco.net. .... 90

**Figure 4.2.** (A) Depth profile of water temperature at station L4, Western English Channel, UK during 2012. (B) Total monthly rainfall at Camborne MET station (50° 21.30' N, 5° 3.00' W) during 2012 as a percentage of the average monthly total between 1978 and 2013. Data from MET office (www.metoffice.gov.uk) contains public sector information licensed

under the Open Government License v1.0. (C) Monthly averages of resultant wind speed ( $\text{m s}^{-1}$ ) at L4. (D) Surface Photosynthetically Active Radiation (PAR) at L4. Box represents the interquartile range. Bars represent the 10<sup>th</sup> and 90<sup>th</sup> quartiles. Points represent all outliers... 91

**Figure 4.3.** Contour plots of nutrient concentrations ( $\mu\text{M}$ ) through the depth profile at sample station L4, Western English Channel, UK, during 2012; (A) Nitrate, (B) Phosphate and (C) Silicate. .... 92

**Figure 4.4.** Plankton abundances measured at station L4, Western English Channel, during 2012. (A) Open circles represent the total phytoplankton abundance averaged through the water column measured by flow cytometry (combined data from the 7 phytoplankton groups:  $\text{cells mL}^{-1}$ ), the bar chart representing the proportional contribution of each group (as a percentage of total phytoplankton assemblage). (B) Microscopy enumeration of eukaryote phytoplankton ( $\text{cells mL}^{-1}$ ) and biomass ( $\text{pg C mL}^{-1}$ ) from 10 m depth, and (C) microzooplankton abundance and biomass from 10 m depth. .... 94

**Figure 4.5.** Concentrations of (A) chlorophyll *a* in pelagic particulate samples ( $\mu\text{g L}^{-1}$ ), (B) hydroxychlorophyll *a* in pelagic particulate samples ( $\text{ng L}^{-1}$ ), (C) hydroxychlorophyll *a* in surface sediment samples ( $\text{ng g}^{-1}$  dry sediment) and (D) chlorophyll  $a_{\text{P276}}$  ( $\text{ng L}^{-1}$ ) in pelagic particulate samples, from station L4, Western English Channel, UK during 2012. .... 96

**Figure 4.6.** (A) The ratio of hydroxychlorophyll *a* (HO-chl-*a*) to chl-*a* averaged through the water column depth profile (mean $\pm$ SE). (B) The ratio of hydroxychlorophyll *a* to chl-*a* in the depth profile (contour plot) and surface sediment ( $\square$ ) from station L4, Western English Channel, UK during 2012. .... 98

**Figure 4.7.** Phytoplankton abundances at station L4, Western English Channel, UK during 2012 of: (A) *Phaeocystis* spp including single flagellated cells and colonies measured by microscopy at 10 m (o) and flow cytometry through the water column (contour plot). (B) *Guinardia delicatula*, abundance measured by microscopy at 10 m, and (C) *Chaetoceros socialis* measured at 10 m by microscopy. .... 100

**Figure 4.8.** Ratio of nitrate to phosphate at station L4, Western English Channel, UK during 2012. .... 102

**Figure 4.9.** Phytoplankton abundances at station L4, Western English Channel, UK during 2012 of: (A) Coccolithophores and (B) Dinoflagellates, measured by microscopy at 10 m (o), and flow cytometry through the depth profile (contour plot). .... 103

**Figure 4.10.** (A) The ratio of chlorophyll  $a_{\text{P276}}$  (chl- $a_{\text{P276}}$ ) to chl-*a* averaged through the water column depth profile (mean $\pm$ SE). (B) The ratio of chlorophyll  $a_{\text{P276}}$  to chl-*a* in the depth profile (contour plot) from station L4, Western English Channel, UK during 2012. 104

**Figure 5.1.** Location of sampling stations during a research cruise from 8<sup>th</sup> to 11<sup>th</sup> May. ... 109

**Figure 5.2.** (A) Concentrations of dissolved inorganic nitrate, phosphate and silicate, and the corresponding N to P ratios. (B) Average phytoplankton abundance through the water column measured by flow cytometry and (C) The proportional contribution of *Synechococcus*, picoeukaryotes, cryptophytes, coccolithophores, *Phaeocystis*, and other nanoeukaryotes averaged through the water column, measured by flow cytometry, at 12 stations in the central and southern North Sea sampled in May 2011. See Figure 5.1 for station locations. .... 113

**Figure 5.3.** Cytogram plots from station 17, off Schevingen in the southern North Sea. The phytoplankton population was dominated by *Phaeocystis* spp. (A). Box encloses the *Phaeocystis* spp. population. The assemblage was stained for (B) membrane permeability

(SYTOX-Green), and (C) hydrolytic enzyme activity (CMFDA), showing the *Phaeocystis* population only. .... 115

**Figure 5.4** Concentration of chlorophyll *a* in pelagic particulate samples throughout the water column, including replicates and multiple depths, from 18 stations in the central and southern North Sea during May 2011, determined by HPLC. .... 116

**Figure 5.5.** Partial HPLC-PDA chromatogram (660 nm) showing elution position relative to chl-*a* (VII) and chl-*b* (III) of chlorophyll allomers and precursor detected in the southern North Sea, at station 1 (at 6 m depth, located at lat: 53.518 and lon: 1.0722). For peak assignments, see Table 5.2. .... 117

**Figure 5.6.** Ratios of allomers (A) hydroxychlorophyll *a* and (B) methoxychlorophyll *a*-like allomer, and precursor (C) chlorophyll *a*<sub>P276</sub>, to chlorophyll *a* in pelagic particulate samples throughout the water column from 14 stations in the central and southern North Sea during May 2011, determined by HPLC. .... 119

**Figure 5.7.** Multi-Dimensional Scaling (MDS) analysis of (A) phytoplankton community, composition showing Bray-Curtis similarity, and (B) concentrations of nitrate, phosphate, nitrite, silicate, ammonium and silicate and N to P ratios, (C) chl-*a* concentration and (D) ratios of HO-chl-*a* and chl-*a*<sub>P276</sub> to chl-*a*, showing Euclidian distance. .... 122

**Figure 5.8.** All measurements of hydroxychlorophyll *a* to chl-*a* taken during a North Sea cruise in May 2011, through the depth profile. .... 123

**Figure 5.9.** Continuous chlorophyll fluorescence (RFU) profiles through the water column at 14 sampling stations in the central and southern North Sea. .... 125

**Figure 5.10.** Satellite derived surface chlorophyll *a* concentration at 15 stations in the central and southern North Sea from 20<sup>th</sup> April to 20<sup>th</sup> May 2011. - - - indicates date of water column sampling. .... 128

**Figure 5.11.** (A) HO-chl-*a* to chl-*a* ratio and (B) chl-*a*<sub>P276</sub> to chl-*a* ratio, during periods of decreasing and increasing chl-*a* concentration. .... 129

**Figure 5.12.** Surface  $F_v/F_m$  and maximum HO-chl-*a* to chl-*a* ratio at 12 sampling stations in the North Sea. .... 131

**Figure 7.1.** Example cytograms of *Ostreococcus tauri* culture after 5 days of growth (A) and (B). Cellular stains SYTOX-Green for membrane permeability (C and D) and H<sub>2</sub>DCFDA (E and F) were applied to untreated cultures (left side) and positive controls (right side). Region R2 contains non-stained cells, region R3 contains stained cells. .... 146

## List of Tables

<b>Table 2.1.</b> Solvent gradient program of Airs et al. (2001) method and Method 1. ....	38
<b>Table 2.2.</b> Injection program for the automated mixing of sample with water (Vial 10) in A. the injector seat and B. a clean vial. An acetone wash step (Vial 9) is included. ....	43
<b>Table 2.3.</b> Solvent gradient programs from Airs et al. (2001) method and Saesaengseerung (2013) method. ....	48
<b>Table 2.4.</b> Solvent gradient programs and average allomer to chl- <i>a</i> ratio (mean $\pm$ SE), n=5. ....	49
<b>Table 2.5.</b> Assignment of chlorophylls <i>a</i> , <i>b</i> and allomers in marine surface water sample (from station L4) after HPLC using Zapata et al. (2000) method, using UV/vis maxima and the most abundant ions resulting from LC/MS/MS ( <i>m/z</i> , <b>major ions</b> ).....	54
<b>Table 3.1.</b> Peak assignment from 660 nm chromatogram resulting from HPLC separation of <i>Ostreococcus tauri</i> pigment samples. ....	74
<b>Table 3.2.</b> Most abundant ions in MS/MS of allomers eluting before chlorophyll <i>a</i> in <i>O. tauri</i> samples. ....	78
<b>Table 5.1.</b> Description of sampling stations from a research cruise in the central and southern North Sea, May 2011. ....	110
<b>Table 5.2.</b> Peak assignment from 660 nm chromatogram resulting from HPLC separation of particulate photopigment samples from the central and southern North Sea.....	117
<b>Table 5.3.</b> Hydroxychlorophyll <i>a</i> ratios at stations sampled for photopigments at multiple depths. ....	126
<b>Table 7.1.</b> Components of ESAW Salt solution I: Anhydrous salts. Quantity to produce 5 L of stock.....	143
<b>Table 7.2.</b> Components of ESAW Salt solution II: Hydrated salts. Quantity to produce 5 L of stock.....	143
Table 7.3. Components to produce Vitamins for ESAW media .....	143
<b>Table 7.4.</b> Components to produce Iron-EDTA stock solution for ESAW media. ....	143
<b>Table 7.5.</b> Components to produce Trace Metals Solution II for ESAW media.....	144
Table 7.6. Additions for F/2 enriched media .....	144
Table 7.7. Growth Media components.....	144

## Publications and presentations

Arising from this research:

### Publications

- **Steele DJ**, Tarran GA, Widdicombe CE, Woodward EMS, Kimmance SA., Franklin DJ, and Airs RL. Seasonal changes of chlorophyll *a* allomers in the Western English Channel during 2012. *Progress in Oceanography* (in press).
- **Steele DJ**, Kimmance SA, Franklin DJ and Airs RL. Chlorophyll *a* allomers as indicators of death during *Ostreococcus tauri* viral infection and senescence. *In preparation*.
- **Steele DJ** and Airs RL. HPLC method selection and optimisation for chlorophyll allomer separation. *In preparation*.

### Oral Presentations

- **September 2014**: “Chlorophyll *a* transformation pigments potentially indicate eukaryote phytoplankton viability”. Challenger Society Conference, Plymouth, UK.
- **December 2012 and 2011**: “Chlorophyll alteration products as indicators of nanoeukaryote phytoplankton viability.” Plymouth Marine Science Education Fund Conference, Plymouth, UK.
- **September 2011**: “Chlorophyll alteration products as indicators of nanoeukaryote phytoplankton viability.” Challenger Society Marine Biogeochemistry and Optics Forum, Southampton, UK.
- **May 2011**: “Phytoplankton fate processes and chlorophyll degradation”. Bournemouth University graduate forum, Bournemouth, UK.

### Posters presented

- **June 2014**: “Cell viability and chlorophyll oxidation in phytoplankton”. Integrated Marine Biogeochemistry and Ecosystem Research (IMBER) Open Science Conference, Bergen, Norway (Poster Prize-1st).
- **February 2014**: “Cell viability and chlorophyll alteration in phytoplankton”. Society of General Microbiology (SGM) Ocean Sciences Meeting, Honolulu, USA.
- **December 2013**: “Chlorophyll *a* allomers as indicators of death in *Ostreococcus tauri*: viral infection and senescence.” Plymouth Marine Science Education Fund Conference, Plymouth, UK (Poster Prize-1st).

## **Acknowledgements**

My foremost thanks go to my supervisors: Ruth Airs, Susan Kimmance and Dan Franklin. Dan has been a constant source of sound advice and support throughout the project; Susan patiently taught me microbiology lab skills to a standard that I can only hope to maintain; and Ruth taught me pigment analysis from the very beginning and has shared my trials, tribulations and eventual successes in the lab with an infectious enthusiasm. I am truly grateful for each of their contributions to my PhD and I have no doubt that their influence will stay with me through my research career.

I am obliged to the Natural Environmental Research Council for funding by studentship; and to all those organisations who have provided funding to attend courses and conferences which have made my PhD all the richer. These thanks go to Bournemouth University, the Plymouth Marine Science Education Fund, the Challenger Society and the British Phycological Society. Thanks especially to the University Centre of Svalbard for providing me a place on the Arctic Microbiology summer school, which was an unforgettable experience. The research cruise was funded by the DyMaphy INTERREG 2 Seas European project, and I thank the crew of the RV Endeavour and Rodney Forster for providing me with a space during the ProTool cruise.

Plymouth Marine Laboratory has provided a friendly and dynamic working environment for the duration of my PhD. Thank you to all my colleagues at PML who have helped me throughout the project. I am indebted to Paul Rooks and Claire Evans who helped me out in the virus lab, especially at the beginning! Particular thanks to Ben Taylor and Tony Staff for dealing with odd data/equipment requests; and to all who contribute to the Western Channel Observatory, in particular Tim Smyth, James Fishwick, Glen Tarran, Claire Widdicombe, Denise Cummings, Carolyn Harris, Gunjan Motwani and the boat guys of the PML RV Quest.

I have met many wonderful people in Plymouth, and I appreciate all those who have made me smile over the years – during shared trips to the climbing wall or pool, pints at the Yard Arm or wine at the Terrace. Thank you to those who have been with me for soggy walks on the moor and fresh swims in the Sound; and to those who looked after me during those hideous months of broken limbs. Thanks in particular to my housemate Kate for quiet evenings, and the voice of experience; to Sam and Tom, for providing welcome escapes, generous cooking, music and dancing; and to Woody for surfing trips, boundless energy and his extreme generosity.

My warmest thanks go to my office mates. I would not have survived the project, nor been so happy, if it weren't for them: to Charlotte and Matt who were there from the start; to Steve's bottle opener; to Ruth's calm; to Steph who taught me to rock out while writing up and lent me her Jackadoodle and Whippet; to Ellie for looking after me when I needed it most; to Jackie, for late night nerding, whale spotting and snorkel sporting; to communal coffee; to Poetry Fridays; to All Of The Cake; to Kristian's endless questions, annex archery, Jelly Circus and office Aikido; to 100 lengths and chilled IMDB nights with Rich; to Kieran's bad puns; to family time; and massively to Kylie, for celebrating the little wins, water baby swims, peanut M&Ms, yoga-times, emerald Mai Tais, Hulking, sulking and gigantic sneezing.

I owe many thanks and years of friendship to all those who have helped me take breaks from city life and lab-obsession. To Andrew for climbs, plans and silliness; to Molly for quiet company, sympathy and occasional propaganda; to Dave for always having time to chat; to Kev (MD) for doing it the other way; and to my brother Charlie, with whom I have travelled vicariously across the globe!

Finally to my parents, I owe simply everything. Mum and Dad – your support has been all I needed to pursue this path and I have navigated through the past few years inspired by you both.

*“If we knew what we were doing, it would not be called research, would it?”*

*Albert Einstein, 1879-1955*

## **Declaration**

I declare that the work in this dissertation was carried out in accordance with the requirements of the University's Code of Practice for Research Degrees and that it has not been submitted for any other academic award. Except where indicated by specific references in the text, the work is the candidate's own. Work done in collaboration with, or with the assistance of others, is indicated as such.

## **Chapter I**

### ***Introduction***

#### **Variability and detection of eukaryote phytoplankton viability**

##### ***1.1. Role of phytoplankton primary production in the Earth System***

Primary production is the fixation of aquatic or atmospheric carbon dioxide into organic compounds. The main process by which this happens is photosynthesis. Photosynthetic primary production is essential to life on earth as almost every organism is formed and fuelled by organic compounds. Primary production is therefore fundamental to the global carbon cycle; hence its quantification is paramount to understanding how the earth supports life.

Phytoplankton are responsible for about half of global primary production (Geider et al. 2001). Production is modelled using estimates of chlorophyll *a* (chl-*a*), derived from ocean colour satellite measurements (Longhurst et al. 1995, Field et al. 1998), along with *in situ* truthing (a C-fixation measurement). Aquatic primary production was estimated at  $51.2 \pm 0.29$  Gigatons of carbon in 2005 ( $\text{Gt C y}^{-1}$ , Brewin et al. 2010). However the derivation of marine primary production does not currently account for the chl-*a* resulting from non-photosynthetically functional phytoplankton cells. Hence, to more accurately quantify primary production, it is necessary to include a measurement of phytoplankton physiological state.

##### ***1.2. Ecology of Phytoplankton Death***

At any time a large proportion (up to 95%) of the marine phytoplankton community can be dead and not photosynthetically functional (Veldhuis et al. 2001, Agustí and Sánchez 2002). It is generally assumed that intact cells are either working (growing, repairing, dividing) or capable of it. However, whole non-functional cells can be abundant and contribute to ocean colour, and hence to estimates of chlorophyll *a* biomass, and primary production. During phytoplankton death (when caused by environmental factors) intact but dead cells remain in the water column. The remaining chlorophyll contained in dead cells is not photosynthetically active, which causes an uncoupling of chlorophyll *a* biomass and primary production (Werdell and Bailey 2005). Dead cells potentially confound interpretations of *in situ* productivity measurements. Therefore it is necessary to distinguish functional from non-functional phytoplankton cells. The methods

for detection are complex, as are the definitions of cell death, cell viability and functionality; topics that are discussed below.

### *1.2.1. The proportion of functional cells is highly variable*

Studying the rate and processes of phytoplankton death is important in understanding marine biogeochemical cycling, the ecology of marine food webs and the fate of phytoplankton blooms (Brussaard et al. 1995, Agustí et al. 1998, Agustí and Duarte 2000, Agustí and Duarte 2013). However, despite the importance of the topic, there are only a limited number of studies investigating variability in phytoplankton cell state or viability.

An early study by Veldhuis et al. (2001) into phytoplankton viability used the nucleic acid stain SYTOX-Green as an indicator of membrane permeability. Cells which were exposed to SYTOX-Green but not stained had structurally sound membranes and so were classed as viable. In water samples from the North Atlantic Ocean the proportion of viable phytoplankton varied with depth and between taxa from 50% to 95% viable cells (Veldhuis et al. 2001).

All viability studies of natural populations since Veldhuis et al. (2001) have used the cell digestion method (Agustí and Sánchez 2002) (see section 1.5.1 for details). This method involves counting the phytoplankton population, introducing enzymes which enter cells with compromised membranes to digest them, and finally counting the remaining “viable”/undigested phytoplankton cells. This assay has generally been applied to cyanobacteria-dominated communities (Agustí 2004, Alonso-Laita and Agustí 2006). The population viability of cyanobacteria was reported to vary between taxa and across nutrient concentrations, from 4% to 100% (Agustí 2004, Alonso-Laita and Agustí 2006); with sea surface temperature (Alonso-Laita and Agustí 2006) and seasonality (Duarte et al. 1999, Agustí and Duarte 2000, Agustí and Sánchez 2002, Hayakawa et al. 2008).

There are fewer reports of the application of the cell digestion assay to eukaryote dominated assemblages. At the North West African upwelling, dominated by microphytoplankton (mainly diatoms) and nanophytoplankton (unspecified taxa), populations had viabilities of 80% and 98.9% respectively, during May/June 2003 (Alonso-Laita and Agustí 2006). This result contrasts the finding of low viabilities in the oligotrophic waters of the North East Atlantic (11.8% and 18.6% respectively) (Alonso-Laita and Agustí 2006). Viability of eukaryotic phytoplankton populations have been reported to vary seasonally: in the North West Pacific

during the spring bloom, viability was 70-90%; this contrasted their viability during the summer when cyanobacteria dominated and the eukaryotic population had a viability of 26-41%. Seasonal patterns of phytoplankton viability have also been reported, from the NW Mediterranean, using the cell digestion method (Agustí and Sánchez 2002). At the beginning of summer, diatoms dominated with a population viability of 34%, increasing to 50% at the end of summer and further to 81% in autumn (Agustí and Sánchez 2002).

This variability in the proportion of viable cells in the water column may result in a changeable level of decoupling between ocean colour (chl-*a* “signal”) and primary productivity. Viability of cells also varies with light level and over the diel cycle, indicating that cell cycle stage could be important in the detection and classification of cell viability (Veldhuis et al. 2001).

### **1.3. Defining Phytoplankton Death**

#### *1.3.1. Modes of death*

There are numerous possible causes of phytoplankton death and population decline in the natural environment. Several of these are well established, for example herbivory and sedimentation (Walsh 1983). Phytoplankton termination by micro-zooplankton grazing (Baudoux et al. 2008) or viral lysis (Suttle et al. 1990, Brussaard 2004) rapidly removes or disintegrates cells; hence they are removed from the particulate pool and their chlorophyll is then transferred into the coloured dissolved organic matter (CDOM) pool (Lønborg et al. 2013), or rapidly destroyed. Entire phytoplankton blooms such as *Phaeocystis* (Jacobsen et al. 1996) and *Emiliania huxleyi* (Bratbak et al. 1993, Brussaard et al. 1995), can be terminated by viruses. A less established mode of death is a process of genetically controlled ‘auto-mortality’, however limited evidence exists for its occurrence in microalgae (Berges and Falkowski 1998, Franklin et al. 2006, Vardi et al. 2006, Bidle and Bender 2008, Lane 2008, Segovia and Berges 2009). Cell mortality can also be caused by environmental stressors such as temperature stress (Alonso-Laita and Agustí 2006), light level (Berman-Frank et al. 2004), UVB radiation (Llabrés and Agustí 2006, Llabrés et al. 2010), hydroxyl radicals (Llabrés et al. 2012), darkness, and nutrient (Berges and Falkowski 1998, Alonso-Laita and Agustí 2006) or micronutrient (e.g. iron and zinc) (Timmermans et al. 2005, Timmermans et al. 2007) limitation.

Mortality caused by environmental stress can leave the phytoplankton cells intact but not capable of functioning (i.e. photosynthesis, repair or divide). Cells may sink or eventually

disintegrate into dissolved organic carbon, mediated by bacterial dissolution. Virally-induced lysis of cells or bacterially-mediated disintegration are important sources of organic carbon for the microbial food web (Brussaard et al. 1995, Agusti et al. 2001). As succinctly put by Kirchman (1999) “How phytoplankton die largely determines how other marine organisms live”. Meaning that, the fixed carbon from phytoplankton cells terminated by herbivory will be utilised by the consumer and further by higher trophic levels. Whereas the fixed carbon from cells terminated by virally-induced lysis or environmental stressors, will be utilised by the microbial assemblage.

### 1.3.2. Defining “Viability”

The term “viability” is used by microbiologists to describe the physiological state of populations as well as individual cells. Cells can exist in many different states, from the live, metabolising cell to dead cell fragments. This is a continuous range of states, including intact cells with reduced or no metabolic activity, and cells with damaged membranes or DNA. Over this range the exact point of death is unknown, as is the stage at which a cell cannot restore its damaged self (Davey 2011). Hence the unknown tipping point in this continuum does not allow for a clear and distinct definition of viability in terms of life and death. Therefore, for the purpose of this study “viable” will be used to describe a phytoplankton cell that has the capacity to function, i.e. to photosynthesise, repair and divide. “Non-viable” will describe a cell that has lost its capacity to function or when this loss is imminent (i.e. moribund cells). The term “population viability” will be used to describe the proportion of viable cells in a population.

### 1.3.3. Defining “Senescence”

The term “senescence” has been used for a range of processes from the cellular to the ecological level (Thomas et al. 2009). In organic geochemistry literature “senescence” is used rather generally, mostly in reference to periods of declining and degrading chlorophyll, both in the context of seasonal declines in the natural marine environment and in cultures (Louda et al. 1998, Louda et al. 2011). Studies on the fate of phytoplankton have often used “senescence” to describe cells which have undergone cell death resulting from environmental stresses such as nutrient limitation (Franklin et al. 2006). This study will use “senescence” in the same sense, including the description of phytoplankton batch cultures in the late stationary phase and declining phases of their growth curve (See next section 1.3.4, Figure 1.1).

### 1.3.4. Batch culture growth cycle

The cycle of phytoplankton population growth and decline in the marine environment is often demonstrated using the model system of a batch culture. The growth of an axenic (without bacteria) mono-culture usually has five phases (Fogg and Thake 1987). During the first phase, the “lag phase” (Figure 1.1), the population density only marginally increases. The duration of the lag phase depends on the condition of the inoculum and any change of conditions. During the lag phase, the cells’ metabolisms physiologically acclimate to growth, i.e. the cells increase levels of enzymes and metabolites involved in cell division and C-fixation. During the second phase, the “exponential growth phase”, the population density increases as a function of time (t) according to the logarithmic function  $C_t = C_0 \cdot e^{rt}$  where  $C_t$  and  $C_0$  are population densities at times t and 0 respectively and r (intrinsic rate of increase) =  $[\ln(C_t) - \ln(C_0)]/\Delta t$ . During exponential growth  $r \geq 0.69 \text{ d}^{-1}$ . Note:  $r = \mu - m$ , where  $\mu$  = specific growth rate and m = mortality (Wood et al. 2005). The population then undergoes a period of declining growth rate when cell division slows. This occurs when nutrients, light, or other physical or chemical factors begin to limit growth. When the limiting factor and growth rate are balanced the population density can become relatively constant, this is known as “stationary phase”. During the final stage, population density decreases rapidly due to environmental limitation and the culture collapses. This can be due to numerous causes, for example, nutrient depletion, oxygen deficiency or self-shading.

Chlorophyll content and photosynthetic efficiency (gauged by  $F_v/F_m$ ) can also change during the batch culture cycle (Ebata and Fujita 1971, Kruskopf and Flynn 2006).  $F_v/F_m$  is a measurement of the maximum photochemical efficiency of photosystem II (PSII) photochemistry. It quantifies the proportion of incident light that is used for photosynthesis. Although  $F_v/F_m$  is known to decrease when cells experience “stressful” conditions (Kolber et al. 1988, Geider et al. 1993b, Kolber et al. 1994), the proportion of dead cells in a population has a limited effect on  $F_v/F_m$  (Franklin et al. 2009a). Hence  $F_v/F_m$  is a poor indicator of population viability. This is due to the non-linear nature of the  $F_v/F_m$  ratio (see section 1.6.2 for details).

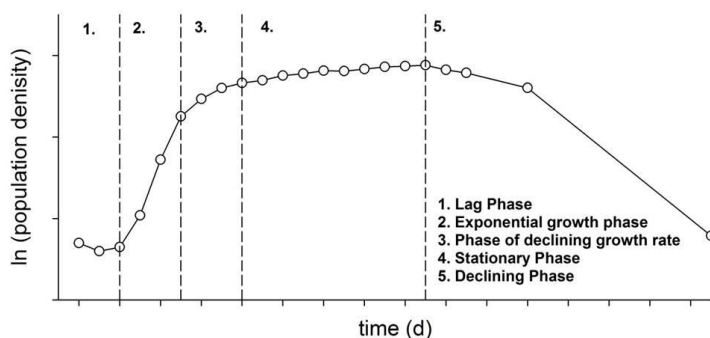


**Figure 1.1.** Growth phases of microalgal batch cultures. Modified from an *Ostreococcus tauri* culture cycle to include a lag phase.

## 1.4. Process of Cell Death

### 1.4.1. Death by environmental factors

Cell mortality can be caused by environmental stressors such as nutrient (Berges and Falkowski 1998, Alonso-Laita and Agustí 2006) or micronutrient (e.g. iron and zinc) (Timmermans et al. 2005, Timmermans et al. 2007) limitation, darkness, or UVB radiation (Llabrés and Agustí 2006, Llabrés et al. 2010). It can be predicted that the processes of cell death will vary depending on the stressors affecting the cell. There are very few studies that combine indicators of functionality e.g.  $^{14}\text{C}$ -method for primary productivity, or fluorescein diacetate (FDA) for enzyme activity; and indicators of viability e.g. SYTOX-staining for membrane permeability, or Fluorodeoxyuridine triphosphate (f-dUTP) for fragmentation of the genome, which illuminate the process of cell death. One multi-factor study by Franklin et al. (2012) assessed viability and enzyme activity during nutrient limitation of *Thalassiosira pseudonana*. During N-limitation the *T. pseudonana* cells progressively lost membrane integrity and then hydrolytic enzyme activity.

Another such study of cell state during death was carried out by Veldhuis et al. (2001) on the diatom *Chaetoceros calcitrans*, under environmental limitation. Cultures in stationary growth phase had an increased proportion of cells with compromised membrane integrity (as tested by SYTOX-Green stain), which preceded a reduction in population size. Loss of membrane integrity caused increased permeability and loss of homeostasis in the cell. This indicated that the loss of membrane integrity was a late stage in cell death and preceded total disintegration of the cell (Kroemer et al. 1995, Naganuma 1996). Cells with reduced membrane integrity were able to photosynthesise but because of membrane permeability, it is likely that more small metabolites were released (Veldhuis et al. 2001). The final stages of cell death were the degradation of chlorophyll (Berges and Falkowski 1998); when cells lost their ability to photosynthesise (as indicated by  $^{14}\text{C}$ -method), and fragmentation of the genome occurred. After this process came complete degradation of the cell (Veldhuis et al. 2001).

### 1.4.2. Death by viral lysis

Viruses are the most abundant biological entities in the ocean and are a major cause of phytoplankton death. They are ubiquitous in all aquatic environments; and are most abundant in productive coastal seas, where numbers are estimated at  $\sim 10^8$  virus particles  $\text{mL}^{-1}$  (Suttle 2005). Marine viruses are typically 20-300 nm long and consist of genetic material (nucleic acid, either

DNA or RNA, single- or double-stranded) contained in a protein case (capsid). Viruses are incapable of independent growth and metabolism and therefore require the cellular machinery of a host to replicate. As non-motile entities, viruses contact their hosts by passive motion in the water column. Adsorption to the host occurs via attachment to external structures on the cell membrane, and entry is gained. During lytic infection the attached virus injects its nucleic acids, which redirect the host's replication machinery to produce virus progeny. The new virus particles can be released through the cell wall or via cell lysis to begin the cycle again (Fuhrman 1999). To date, all described viruses which infect microalgae are lytic, however an alternate infection mechanism is known from higher organisms, i.e. lysogenic infection, during which viral DNA combines with the host's DNA and is replicated, but the host remains alive.

#### 1.4.3. Oxidative stress

Oxidative stress occurs in a cell when the production of reactive oxygen species (ROS) exceeds the antioxidant defence mechanisms of the cell. Environmental conditions such as high light, temperature, salt stress and nutrient limitation have been found to cause oxidative stress in cyanobacteria (Latifi et al. 2009), dinoflagellates (Lesser 1996) and diatoms (Rijstenbil et al. 1994, Rijstenbil 2002). Oxidative stress can also occur during photosynthesis and respiration (Apel and Hirt 2004). ROS are produced by the cell and include hydrogen peroxide ( $H_2O_2$ ), singlet oxygen and hydroxyl radicals (Gadjev et al. 2008). ROS can damage the cell in many different ways, but they are also thought to be a ubiquitous signalling molecule and part of the cells recognition and response to stress (Apel and Hirt 2004). ROS also have an unresolved role in viral lysis and senescence death pathways. Further, ROS production has been linked to viral infection of coccolithophore populations (Evans et al. 2006, Bidle et al. 2007, Vardi et al. 2009). It is thought that ROS mediates virally-induced cell death (Bidle and Vardi 2011, Vardi et al. 2012) and is required to trigger functions in the cell required for viral replication (Vardi et al. 2012).

The links between oxidative stress and cell death have recently been explored in the toxic cyanobacteria *Microcystis aeruginosa* (CCAP 1450/16) (Bouchard and Purdie 2011). Cultures were exposed to hydrogen peroxide which resulted in a 2-fold increase in intracellular ROS (measured by the probe dihydrorhodamine 123, DHR). The  $H_2O_2$  exposed cultures showed no growth, reduced chl-*a* content and  $F_v/F_m$  reduced to zero within 24 hours. The percentage of cells with permeable membranes (SYTOX-positive) also increased. It was deduced that ROS played a destructive role in the cell (Bouchard and Purdie 2011).

### 1.5. *Indicators of viability and reactive oxygen species*

As demonstrated in the studies detailed above, there are many tests and indicators used for phytoplankton viability. Most of these were not designed to determine algal viability, and therefore must be tested and optimised thoroughly for the algal strain in question (Garvey et al. 2007, Peperzak and Brussaard 2011, Zetsche and Meysman 2012). It is common for viability indicators to be reliant on the state of the cell membrane; this is because a compromised membrane is the first detectable instance that the cell may not recover by self-repair (Davey 2011). However, unless the test agent is designed very rigorously, there may be a gap or overlap between the level of permeability required for incorporation of the indicator and the minimum level of membrane permeability where a cell cannot repair, i.e. molecules of the test agent could in theory pass through membranes that could still be repaired, giving false-positive results. In addition, if the staining concentration is too high, it may force its way into live cells, also giving false-positive results.

#### 1.5.1. *Cell digestion assay*

The viability indicator most widely used for assessing natural phytoplankton populations is the cell digestion assay (Agustí and Sánchez 2002). When a population is exposed to the assay, cells with compromised membrane structure allow the assay to enter into their cytoplasm. DNase I causes fragmentation and hydrolysis of DNA and Trypsin causes phospholipid hydrolysis, digesting the cell. Cells with intact membranes are unaffected by the assay but cells with compromised membranes are digested and disintegrate, and are therefore unobservable and show no auto-fluorescence or staining fluorescence. Counting the number of visible cells in the population before and after use of the assay allows calculation of the proportion of cells which had compromised membranes.

#### 1.5.2. *Molecular probes*

Molecular probes that use the properties of damaged cell membranes, originally developed for biomedical use, have been adopted by phycologists (Wyllie et al. 1980, Ellis et al. 1991, Darzynkiewicz et al. 1994). As loss of cell homeostasis is brought about by the loss of membrane integrity, the approach has remained popular in the determination of viability. These probes are discussed below.

#### 1.5.2.1. For membrane permeability: SYTOX-Green

SYTOX-Green (Molecular Probes Inc.) is a nucleic acid stain which penetrates into cells with compromised plasma membranes and binds to DNA, hence staining non-viable cells. The resulting molecule fluoresces green under 488 nm excitation (Molecular Probes, 2010) .

#### 1.5.2.2. For ROS: CM-H<sub>2</sub>DCFDA and DHR

Indicators for cellular Reactive Oxygen Species (ROS) include 5-(and-6)-chloromethyl-2',7'-dichlorodihydrofluorescein diacetate (CM-H<sub>2</sub>DCFDA, Invitrogen) and dihydrorhodamine 123 (DHR). CM-H<sub>2</sub>DCFDA is non-fluorescent and membrane permeable, allowing it to diffuse into cells. It is hydrolysed (by esterases) to 2',7'-dichlorohydrofluorescein (DCFH), which is polar and becomes trapped in the cells. There it is oxidised by ROS to the fluorescent dichlorofluorescein (DCF) (emission at 522 nm) (Haugland 2002), which can be measured by flow cytometry (Evans et al. 2006). DHR also passively diffuses across the cell membrane and is oxidized by ROS or reactive nitrogen species (RNS) to rhodamine 123 which concentrates in the mitochondria and fluoresces green (Crow 1997). DHR has been used to detect intracellular ROS levels in cyanobacteria (Bouchard and Purdie 2011).

#### 1.5.2.3. CMFDA for hydrolytic enzyme activity

Assessment of enzyme activity has also been employed in determining cell viability using the probe 5-chloromethylfluorescein diacetate (CMFDA, Invitrogen). The non-fluorescent CMFDA enters into cells where intracellular esterases cleave the acetate group, releasing the fluorescent product (emission at 517 nm). This conversion only occurs by enzyme activity, and hence only cells with hydrolytic enzymatic activity become fluorescent (Kaneshiro et al. 1993, Porter et al. 1995).

#### 1.5.3. *Limitations of viability staining*

The performance of molecular probes (also known as cellular stains) in phytoplankton cultures have been recently evaluated by Peperzak and Brussaard (2011). Probe performance varied with species, strain and culture age; hence method optimisation is crucial to the use of these molecular probes for determining viability of algal populations.

Even after optimisation, staining methods have limitations. Stain concentration and incubation time are difficult to standardise for natural water samples. Cell identification can also be problematic in natural samples and auto-fluorescence from phytoplankton cells can interfere with the probe signal during analysis (Veldhuis and Kraay 2000). For these reasons, the use of molecular probes alone to determine viability in mixed natural populations is challenging.

## **1.6. Theory and uses of chlorophyll fluorescence**

Maximum quantum photochemical efficiency ( $F_v/F_m$ ) is widely used both as a general measure of phytoplankton health and for estimating primary production. To better understand this measurement the process of light absorption is briefly described.

### *1.6.1. Description of light absorption and fluorescence*

The photosynthetic process can be separated into the light reactions and the dark reactions. The light reactions are carried out by photosystems I and II (PSI & PSII), and are made possible by light energy absorbed by the chloroplast pigments. Each photosystem has a reaction centre comprised of a specific chlorophyll *a*, complexed with a specific protein (Kirk 1994). The reaction centre chlorophyll receives excitation energy either by direct absorption of a photon of light, or much more often, via the transfer of energy by inductive resonance transfer, from light-harvesting (or antenna) pigment molecules (Förster 1967). When the reaction centre chlorophyll receives excitation energy, it is raised to an excited electronic state. The excited reaction centre chlorophyll then transfers an electron to an acceptor molecule. The electron transfer from PSI and PSII eventually results in the reduction of NADP and the splitting of water to pass hydrogen to the NADP, respectively, forming NADPH<sub>2</sub> (Kirk 1994). However, if the acceptor molecule is already reduced, the energy can be dissipated by fluorescence or non-photochemical quenching.

Under low light conditions the transfer of electrons from the PSII reaction centres to the acceptor molecules is efficient and hence fluorescence is minimal ( $F_o$ ). At higher irradiance the acceptor molecules are progressively reduced and so at any instant more of the reaction centres will be “closed” and fluorescence increases. Therefore under high irradiance the proportion of energy received from incident light that is used for photosynthesis is reduced, i.e. the quantum efficiency of photosynthesis is reduced (Kolber and Falkowski 1993). When all the reaction

centres are closed, fluorescence reaches a maximum ( $F_m$ ). Variable fluorescence ( $F_v$ ) is defined as  $F_v = F_m - F_o$ . However the relationship between fluorescence and photochemistry is not simply inverse, as some excitation energy can also be dissipated by non-photochemical quenching (Schreiber et al. 1986) which may include, for example, the conversion of fluorescence to heat by carotenoids in the xanthophyll cycle (Demmig-Adams 1990), or photodegradation of the PSII reaction centres (Horton and Hague 1988). Biophysical models of photosynthesis account for non-photochemical quenching when using fluorescence to determine photosynthesis (Kolber and Falkowski 1993).

### 1.6.2. Interpretation of $F_v/F_m$ in a mixed community

The ratio  $F_v/F_m$  is directly related to the maximum photochemical quantum efficiency of PSII (Cullen 1982, Falkowski and Kolber 1995, Cullen and Davis 2003).  $F_v/F_m$  quantifies the proportion of incident actinic photons which are used in photochemical quenching, i.e. for photosynthesis. The maximum PSII photochemical efficiency is known to decrease when autotrophs experience “stressful” conditions for example nutrient starvation or very high irradiance (Kolber et al. 1988, Geider et al. 1993b, Kolber et al. 1994). Hence the  $F_v/F_m$  measurement was established as an indicator of photosynthetic “health” of mixed phytoplankton communities on large scales (Moore et al. 2005, Behrenfeld et al. 2006, Suggett et al. 2006). However recent work has identified that having a proportion of cells within the population that are not photosynthetically functional, has a limited effect on  $F_v/F_m$  (Franklin et al. 2009a). Further, high  $F_v/F_m$  cannot be used as evidence of low mortality, revealing  $F_v/F_m$  to be a poor indicator of phytoplankton assemblage health (Franklin et al. 2009a). Oceanic measurements of  $F_v/F_m$  range from 0.65 in nutrient-replete, highly-productive regions to <0.3 in the surface water of oligotrophic gyres (Falkowski and Kolber 1995, Smyth et al. 2004).

The ratio  $F_v/F_m$  and the measure of the maximum PSII effective absorption cross-section ( $\sigma_{\text{PSII}}$ ) are known to vary with phytoplankton taxa (Suggett et al. 2009). The variability of these measurements between taxa can exceed changes due to nutrient limitation, with the exception of high-nutrient, low-chlorophyll *a* (often iron-limited) regions (Suggett et al. 2009). In natural, mixed phytoplankton assemblages,  $F_v/F_m$  tends to reduce with cell diameter (Cermenon et al. 2005, Suggett et al. 2009). As the maximum ratio of  $F_v/F_m$  varies between taxa, direct comparison across different phytoplankton assemblages is not simple.

### 1.6.3. Using fluorescence to estimate photosynthesis in situ

Chlorophyll fluorescence can be used to estimate photosynthetic rate (Kolber and Falkowski 1993, Suggett et al. 2004). Two forms of fluorometry which measure active fluorescence have been used for this purpose. 1. Probe and Pump Fluorometry (PPF), and 2. Fast Repetition Rate Fluorometry (FRRF). The method of PPF uses weak “probe” flashes of artificial light to measure the controlled change in active fluorescence yield induced by a strong “pump” flash of actinic light. These measurements are used to derive  $\sigma_{\text{PSII}}$ , the quantum yield for photochemistry and the maximum rate of photosynthetic electron transport at light saturation (Kolber and Falkowski 1993).

Fast Repetition Rate Fluorometry (FRRF) is an evolution of PPF and is also based on the measurement of active fluorescence (Suggett et al. 2001). Acutely controlled sub-saturating flashes are applied allowing manipulation of PSII acceptor molecule reduction (Kolber et al. 1998). This allows calculation of a wider suite of photosynthetic parameters including  $F_v/F_m$  (Weis and Berry 1987),  $\sigma_{\text{PSII}}$  (Samson and Bruce 1995), quantification of primary and secondary electron acceptors (Malkin and Kok 1966, Murata et al. 1966) and the kinetics of electron transport on the acceptor side of PSII (Kramer et al. 1990). FRRF has been used to calculate primary production, with comparison to radiocarbon or oxygen measurements (Suggett et al. 2001, Moore et al. 2003, Suggett et al. 2003).

## 1.7. Chlorophyll and phytoplankton cell death

A possible new approach to the assessment of phytoplankton viability may exist in the study of chlorophyll (Bale 2010, Bale et al. 2011). Chlorophyll *a* (I, Figure 1.2) is the primary pigment required for all eukaryotic photosynthesis. It is ubiquitous amongst organisms that perform oxygenic photosynthesis. Chlorophyll is a labile molecule when removed from its pigment-protein complex, and is very sensitive to environmental conditions, e.g. light intensity. Chlorophyll molecules fuel the photosynthetic pathway by resonance energy transfer, after absorbing light. The process brings chlorophyll into its excited state, which as a by-product, converts ground state triplet oxygen into the destructive excited state singlet oxygen (ROS), hence it must be under tight control by the cell.

Loss of chlorophyll is thought to occur at a late stage of phytoplankton death (Veldhuis et al. 2001). This is based on measurements of bulk chlorophyll, estimated using chlorophyll fluorescence.

### 1.7.1. Chlorophyll and estimating primary productivity

Satellite measurements of ocean colour are used to make estimates of oceanic chlorophyll from which primary production is determined (Antoine and Morel 1996, Sathyendranath and Platt 2007). These primary productivity models are dependent on *in situ* truthing by measurement of photosynthesis through the radiocarbon  $^{14}\text{C}$ -method. Chlorophyll *a* is used as an index of phytoplankton biomass and the algorithms which retrieve phytoplankton “biomass” from colour data rely on changes in the reflectance at the sea surface corresponding to changes in biomass. Gross primary production can then be modelled using the derived biomass, incident irradiance and sometimes also photo-adaptation parameters and inherent optical properties of the phytoplankton (Sathyendranath and Platt 2007). It is assumed, when modelling production in this way, that all of the detected chlorophyll *a* signal has originated from chlorophyll which is actively contributing to photosynthesis. However, some of the detected chlorophyll *a* signal actually originates from chlorophyll contained in dead cells, or other pigments with similar spectral properties (e.g. chlorophyll *a* allomers, see section 1.7) which do not contribute to photosynthesis. The presence of allomers or chlorophyll contained in dead cells will confound estimates of global primary productivity.

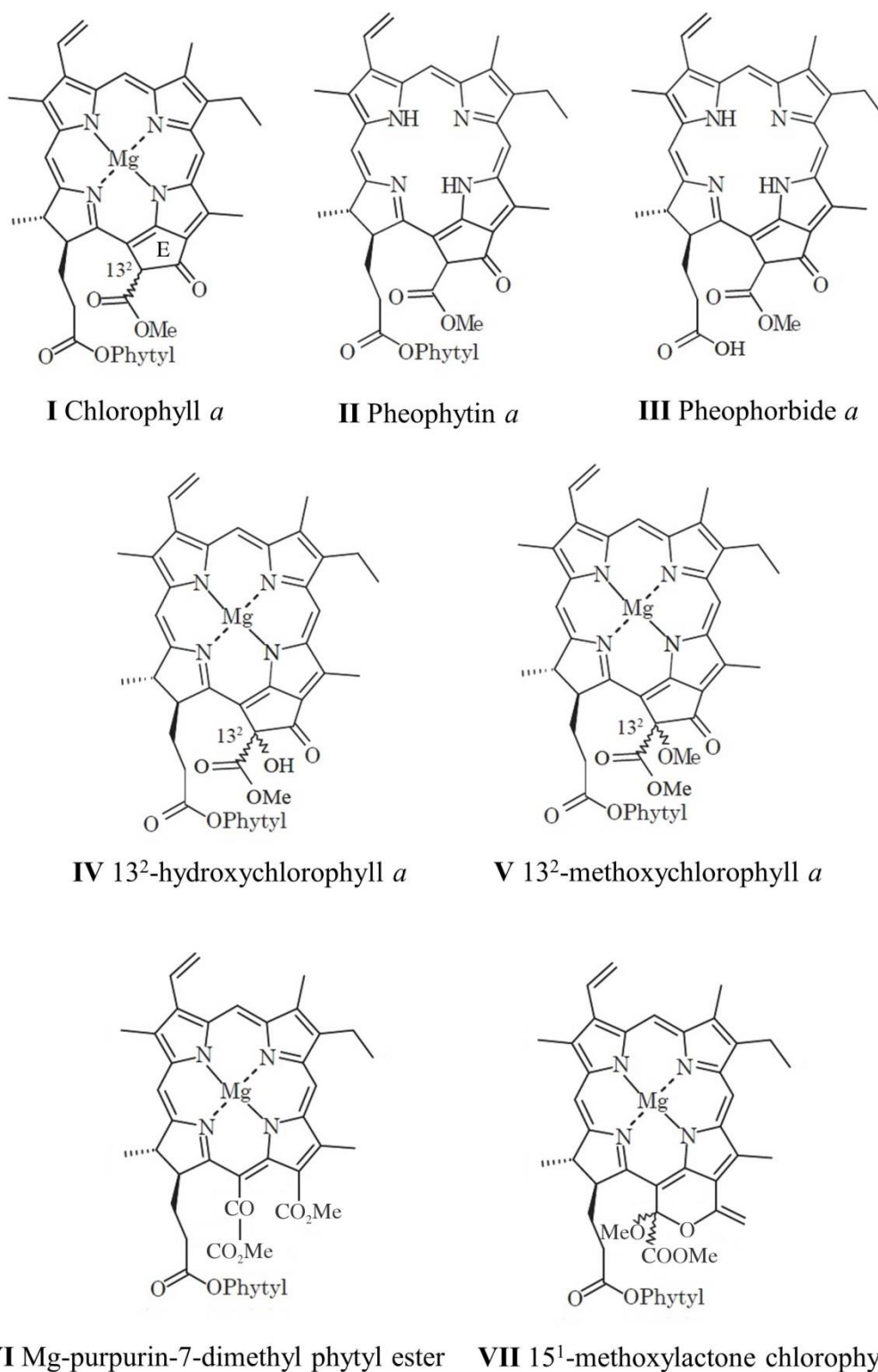


**Figure 1.2.** Structures of chlorophyll *a* (I), two of its common alteration products (II & III) and four allomers (IV to VII).

### 1.7.2. Chlorophyll alteration products linked to phytoplankton death

Chlorophyll transformation, i.e. alteration to the chlorophyll molecule, can arise from any disruption to the phytoplankton cell (Jeffrey et al. 1997) and there are many different processes by which transformation products are formed. Transformation products have been linked to different modes of phytoplankton mortality (Head and Horne 1993, Head et al. 1994, Walker and Keely 2004, Bale 2010, Bale et al. 2011). The defunctionalization products pheophytin *a* (**II**, Figure 1.2), pheophorbide *a* (**III**, Figure 1.2) and their pyro-derivatives have been associated with the senescence of diatoms (Spooner et al. 1994a, Spooner et al. 1994b, Louda et al. 1998, Louda et al. 2002). It has been found that in the presence of a trace amount of acid, chlorophyll *a* is demetallated (-Mg) forming pheophytin *a*, and can occur in the acidic guts of grazers. Pheophytin *a* also occurs by enzyme action and has been linked to senescence in *Phaeodactylum tricorutum* cultures (Spooner et al. 1994b). Pheophorbide *a* formed by demetallation and loss of the phytyl chain from chlorophyll has been associated with senescence of *T. weissflogii* cultures (Spooner et al. 1994c). The above products (along with others) have also been linked with herbivory (Hallegraeff 1981) and bacterial activity (Spooner et al. 1994a, Spooner et al. 1995). However, many of the past “senescence” experiments used non-axenic cultures, hence the conditions under which the chlorophyll transformation products were formed were not closely controlled and chlorophyll transformation could have been mediated by bacterial action (Bale 2010).

Chlorophyll and its degradation products are also found in the geochemical record and undergo diagenetic changes on a geological time scale (Louda et al. 2000). The long term decay of phytoplankton chlorophyll over 31 months in light/dark and oxic/anoxic conditions has been used to link pigments found in live phytoplankton to those found in the geochemical record (Louda et al. 1998).

## 1.8. Chlorophyll *a* allomers

Allomers are oxidation products of chlorophyll which can form in the chloroplast or in the water column, where the oxidation is centred on ring E (**I**, Figure 1.2). They are predecessors of sedimentary porphyrins, which can be derived from chlorophyll (or alternatively, heme) and are the basis of organic geochemistry (Treibs 1936). Laboratory reactions of chlorophyll *a* with triplet oxygen in alcoholic solutions produce a complex array of allomers (Jie et al. 2002). Chlorophyll *a* allomers such as 13<sup>2</sup>-hydroxychlorophyll *a* (HO-chl-*a*, **IV**, Figure 1.2) are thought to be formed by autooxidation through a reaction with ground state oxygen (Hynninen 1991). Several allomers similar to those found by laboratory reaction have been identified in the natural marine environment and in phytoplankton cultures, as discussed below. One hypothesised reason for their presence inside the chloroplast is a build-up of reactive oxygen species, when oxidative stress overwhelms defence mechanisms of the cell, i.e. during stress to the phytoplankton cell or when membrane integrity is lost (Franklin et al. 2012).

### 1.8.1. Detecting allomers

Chlorophyll *a* allomers comprise a complex array of components, many with very similar structures. Due to the similarity of the UV/vis spectra of many chlorophyll allomers, assignment of components requires a combination of UV/vis spectra obtained on-line during HPLC analysis, and mass spectral protonated molecule and fragmentation information obtained during LC/MS<sup>n</sup> analysis. As the array of possible allomers is complex, complete separation by chromatography is very challenging. Reversed phase HPLC in combination with LC/MS<sup>n</sup> has been used to assign allomer structures in natural systems; in lake sediments (Squier et al. 2004); seawater (Walker and Keely 2004, Bale 2010) and also in culture studies (Bale et al. 2011, Franklin et al. 2012, Bale et al. 2013). This approach permitted 13<sup>2</sup>-methoxychlorophyll *a* (MeO-chl-*a*, **V**, Figure 1.2) detection in a phytoplankton culture (Franklin et al. 2012). Although commonly detected using routine HPLC methods for phytoplankton pigments (Hooker et al. 2005) they are rarely assigned, and are often quantified together with chl-*a*. Assignment of chlorophyll allomers in natural waters is a new challenge as phytoplankton numbers are lower. Pre-concentration of extracts prior to analysis may be necessary (Walker and Keely 2004).

### 1.8.2. Chlorophyll *a* allomers in the natural environment

Chlorophyll *a* allomers have been previously assigned in the water column (Walker and Keely 2004, Bale 2010), within sediments (Airs et al. 2000, Walker et al. 2002, Chen et al. 2003, Szymczak-Żyła et al. 2011) and in phytoplankton cultures (Louda et al. 1998, Szymczak-Żyła et al. 2008, Bale et al. 2011, Bale et al. 2013). Hydroxychlorophyll *a* and Mg-purpurin-7 dimethyl phtyl ester (**VI**, Figure 1.2) were detected during the spring bloom of the Celtic Sea (49°37'N 10°20'W) in 2002 (Walker and Keely 2004). Allomer abundances were greatest in the later stages of the bloom, in the oxygenated zone of the water column (the upper water column) (Walker and Keely 2004). This is in contrast to results by Bale (2010), who reported that during a North Atlantic spring bloom the ratio of HO-chl-*a* to chl-*a* suspended in the water column stayed relatively constant (between 0.01 and 0.03). Bale (2010) also reported that the HO-chl-*a* to chl-*a* ratio in sinking particles was higher (0.05-0.08) than that of suspended particles. These contrasting results may be due to differences between the compositions of the phytoplankton assemblages or dominant species; however, these two studies did not include taxonomic data.

### 1.8.3. Allomer formation under laboratory conditions

Chlorophyll allomers were originally observed when alcoholic chlorophyll solutions were opened to the air. This approach formed Mg-purpurin-7 dimethyl phtyl ester, 15<sup>1</sup>-methoxylactone-chlorophyll *a* (MeO-lact-chl-*a*, **VII**, Figure 1.2), MeO-chl-*a* and HO-chl-*a*, by autoxidation (Willstätter and Stoll 1913, Jie et al. 2002). Allomer formation has also been reported in phytoplankton cultures aged for months to years (Louda et al. 1998, Szymczak-Żyła et al. 2008).

#### 1.8.3.1. Formation of hydroxychlorophyll *a*

In laboratory reactions HO-chl-*a* has been shown to be the sole allomerisation product of chlorophyll *a* in the presence of hydrogen peroxide (Walker et al. 2002). Hence HO-chl-*a* is likely to be formed in phytoplankton cells during loss of viability, in conjunction with an increase in reactive oxygen species (ROS). Hydroxychlorophyll *a* has been found in senescent and virally infected cultures (Bale et al. 2013). Preliminary work has shown that MeO-chl-*a* and HO-chl-*a* both increase in *Thalassiosira pseudonana* cultures at the onset of senescence, along with a decline in  $F_v/F_m$  and loss of membrane integrity (Franklin et al. 2012). However, the role of ROS during this process has not been investigated previously. Very little is known about the

formation of allomers during phytoplankton mortality. A limited number of chlorophyll *a* allomers have been assigned during culture studies of a total of 4 phytoplankton species (Bale et al. 2011, Franklin et al. 2012, Bale et al. 2013). The formation of chlorophyll allomers in cells in combination with measurements of  $F_v/F_m$  and cell viability has been determined in only one study (Franklin et al. 2012). Hence additional culture studies are required to test the ubiquity or specificity of allomer formation, in comparison with viability indicators, in different taxa.

### **1.9. Research aims & objectives**

The focus of this project was the detection, identification and quantification of allomers in cultures and the marine environment with the aim to determine if allomers could be used as indicators of phytoplankton viability. The first objective was to select an HPLC method for assignment and quantification of allomers. A method selection and optimisation study was required to minimise artefact formation and to enable optimum resolution and quantification of chl-*a* allomers.

The selected HPLC method was applied to phytoplankton populations in a culture study. The objective of this study was to measure the timing and extent of chlorophyll allomerization in relation to loss of membrane permeability, cellular ROS and photosynthetic efficiency ( $F_v/F_m$ ) during population decline. Given the differences in the cell-death pathways mediated by viruses versus environmental factors and previous results (Bale et al. 2013), these 2 modes of death were chosen. Indicators of viability were measured during both viral infection, and decline due to environmental limitation of a phytoplankton culture.

The third objective of this project was to assign and quantify allomers in the water column during the natural growth and decline phases of phytoplankton populations over an annual cycle. This work expands on two studies of chlorophyll *a* allomers in the marine water column, which are temporally limited to several days (Walker and Keely 2004) and several weeks (Bale 2010).

Further objectives sought to assign and quantify chl-*a* allomers with depth through the water column in areas of different phytoplankton assemblages; and to investigate the occurrence of allomers in relation to the stage of population growth/decline.

## **Chapter II**

### **HPLC method selection and optimisation for allomer separation**

#### **2.1. Introduction**

In recent years several HPLC methods have been developed which separate chlorophyll *a* from its allomers (Zapata et al. 2000, Airs et al. 2001a, Saesaengseerung 2013). Airs et al. (2001a) developed a method to separate complex distributions of pigments and their alteration products from sediment samples (Walker et al. 2002, Hodgson et al. 2003, Squier et al. 2004, Hodgson et al. 2006). This method has also been applied to distributions of bacteriochlorophylls (Airs et al. 2001b, Airs and Keely 2002, 2003, Gich et al. 2003, Wilson et al. 2004, Gich and Overmann 2006), pigments in particulates from marine water columns (Walker and Keely 2004, Bale 2010), coral extracts (Venn et al. 2006) and microalgal cultures (Airs and Llewellyn 2006, Bale et al. 2010, Bale et al. 2013). The Airs et al. (2001a) method separates several allomers including 13<sup>2</sup>-hydroxychlorophyll *a* (HO-chl-*a*), purpurin-7 dimethyl phtyl ester and purpurin-18 methyl ester (Walker and Keely 2004) and has been used to quantify these allomers in culture extracts (Bale 2010), seawater (Walker and Keely 2004) and sediments (Squier et al. 2004). Recently, the Airs et al. (2001a) method has been used to separate and assign 13<sup>2</sup>-methoxychlorophyll *a* (MeO-chl-*a*) and HO-chl-*a* in extracts from microalgal cultures during nutrient limitation (Franklin et al. 2012). Despite the length and complexity of the Airs et al. (2001) method and its use in conjunction with LC/MS<sup>n</sup>, some components in natural pigment distributions remain unidentified (Squier et al. 2004, Airs and Llewellyn 2006). Some of the unidentified components show allomer-type elution positions and UV/vis spectra (Airs et al. 2001a, Hodgson et al. 2003, Bale et al. 2011) and some co-elutions are evident e.g. HO-chl-*a* and a chl-*a* precursor-like compound (Bale et al. 2011).

The Zapata et al. (2000) method was designed to separate phytoplankton pigments and has been applied extensively for this purpose (Zapata et al. 2001, Rodríguez et al. 2003, Latasa et al. 2004, Not et al. 2005, Wright et al. 2010, Yao et al. 2010). The Zapata et al. (2000) method is one of two methods recommended for the analysis of phytoplankton pigments, and achieves excellent separation of polar components, e.g. Chlorophyll *c*<sub>2</sub>, Mg-2,4-divinyl pheoporphyrin and chlorophyllide (Zapata et al. 2000). The Zapata et al. (2000) method is also reported to separate an unidentified chl-*a* allomer from algal cultures (Zapata et al. 2011) as well as divinyl chlorophyll *a* from cyanobacteria cultures (Hutchins et al. 2003).

Saesaengseerung (2013) developed an Ultrahigh Performance Liquid Chromatography (UPLC) method based on the method of Airs et al. (2001), designed to separate complex pigment distributions from sediments in short run times (e.g. 18 min). The Saesaengseerung (2013) method was reported to separate HO-chl-*a* from chl-*a* and a number of unidentified chlorins in an extract from a lake sediment core (Saesaengseerung, 2013).

Normal phase HPLC has been applied to the separation of chlorophyll allomers in higher plant extracts (Kuronen et al. 1993, Jie et al. 2002) and bacteriochlorophylls (Walker et al., 2003). Normal phase HPLC methods were used by Kuronen et al. (1993) and Jie et al. (2002) to separate HO-chl-*a*, MeO-chl-*a*, 15<sup>1</sup>-methoxylactone chlorophyll *a* (MeO-lact-chl-*a*) and their epimers in the methanolic reaction of chl-*a* extracted from clover and spinach leaves, respectively. The Jie et al. (2002) method has also been applied to allomers produced during the methanolic reaction of bacteriochlorophyll *a* and bacterioviridin *a* prepared from *Chromatium D* cell paste (Walker et al. 2003). However these high resolution normal phase methods have not been applied to microalgal extracts.

When applying HPLC to the separation of chlorophyll allomers it is essential to avoid oxidation during analysis as chlorophyll allomers are products of oxidation reactions (Walker et al. 2003). Chlorophyll is susceptible to oxidation reactions in alcoholic solutions (Willstätter and Stoll 1913), therefore alcohols are avoided in the extraction process in favour of acetone (Keely 2006). Photo-oxidation is a mode of chlorophyll degradation in phytoplankton (Llewellyn et al. 1990), hence extracts are protected from strong light. Chlorophyll autoxidation occurs slowly in acetone (Keely 2006), hence rapid extraction methods are used, e.g. sonication (Airs et al. 2001a).

For an informative and realistic study of the proportions of chlorophyll *a* and naturally occurring oxidation products, artefact formation during sample extraction, manipulation and analysis must be prevented. To examine subtle changes in the proportions of chlorophyll *a* and individual chl-*a* allomers, optimum resolution of peaks in the region of allomer elution, during HPLC, was required. A method selection and optimisation study was therefore undertaken to fulfil this objective.

## **2.2. Description of Samples used for Chromatography Optimisation**

For method evaluation and optimisation two different sample types were used; standards (see Methods chapter 7.5.3 for details) and pelagic, marine particulate samples from station L4 of the Western Channel Observatory (<http://www.westernchannelobservatory.org.uk>) (see Methods chapter 7.6.1.2). Standard solutions of chlorophyll *a* were prepared monthly and stored at -20 °C. These solutions contained a low proportion of allomers with an allomer to chlorophyll *a* ratio of 0.02 (approximately 2% allomers). Chlorophyll *a* standard solutions were used to provide sample reproducibility during chromatography optimisation. Pelagic marine particulate samples taken from station L4 of the Western Channel Observatory were used to test chromatographic methods with a more complex pigment distribution, and were subjected to LC/MS<sup>n</sup> for peak assignment.

## **2.3. Selection and Optimisation of *Airs et al. (2001)***

### *2.3.1. Method selection and optimisation of eluent composition*

The *Airs et al. (2001)* HPLC method was selected for optimisation for this study as it achieves good resolution of several allomers and provides separation of a wide polarity range of chlorophylls and carotenoids (*Bale et al. 2010*). The method is also directly amenable to LC/MS<sup>n</sup> which is essential for assignment of components. Within *Airs et al. (2001)*, three gradient programs are presented. The main method, (gradient program A) is the full length version designed to be delivered by a ternary HPLC pumping system (requiring 3 separate solvent lines). Method B is a shortened version of the full gradient program designed for extracts that lack the most apolar components which are observed in sediment extracts, e.g. culture extracts. The paper also presents a second version of the full method, gradient program C, which can be delivered by a binary pumping system (Table 2.1). Gradient program C was selected for use as it was directly transferable to the PML LC/MS system which was equipped with a binary pump.

The *Airs et al. (2001)* method employs two Waters Spherisorb cartridge columns joined to create an overall column length of 30 cm. The mobile phase comprises ammonium acetate solution, methanol, acetonitrile and ethyl acetate in a gradient elution with total run time of 110 minutes (Table 2.1). Previously, increasing the proportion of ammonium acetate in the initial solvent composition from that of *Airs et al. (2001)* method, was used to improve the

chromatography of early eluting components (Bale 2010). For the purpose of this study, the polarity of the starting composition was increased by raising the proportion of ammonium acetate solution from 5 % (Airs et al., 2001) to 10 % (Method 1, Table 2.1). The higher aqueous content increased the partition coefficient of chlorophyll *a* and its allomers, holding them on the column for longer (Figure 2.1), enabling improved separation.

The target region for chromatography optimisation was the elution region of hydroxychlorophyll *a* and methoxychlorophyll *a* i.e. just prior to the elution position of chlorophyll *a* ( $t_R$  54 min). The method was therefore shortened to reduce solvent waste by ending the run at 65 min. Steps thereafter were designed to clean and re-equilibrate the column back to the starting composition, as in the original method (Table 2.1), giving a total run time of 79 min. A chromatogram obtained from analysis of chl-*a* standard using Method 1 (Figure 2.1), showed improved separation of the allomer group from chl-*a* as well as partial separation of additional components within the allomer group, evident from shoulders on components II and IV (Figure 2.1.B).

**Table 2.1.** Solvent gradient program of Airs et al. (2001) method and Method 1.

Time (min)	% Ammonium acetate (0.01M)	% Methanol	% Acetonitrile	% Ethyl acetate
Airs et al. (2001) method				
0	5	80	15	0
5	5	80	15	0
100	0	19	1	80
105	5	80	15	0
110	5	80	15	0
Method 1				
0	10	75	15	0
5	10	75	15	0
65	5	41	3	51
66	0	19	1	80
78	0	19	1	80
79	10	75	15	0

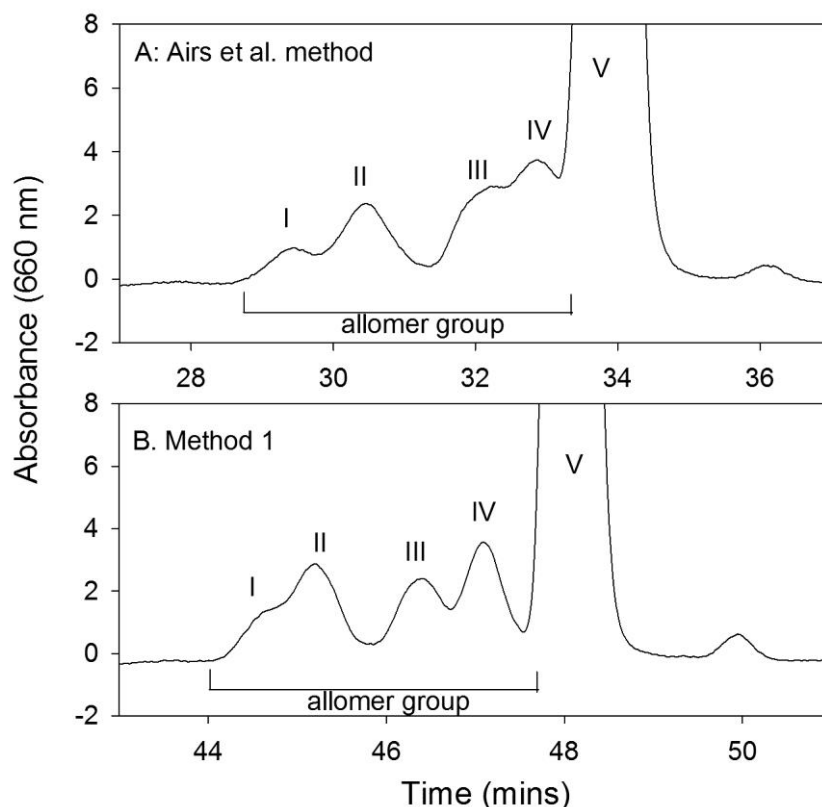


**Figure 2.1.** Partial HPLC chromatograms (660 nm) of chlorophyll *a* standard using (A) Airs et al. (2001) method and (B) Method 1 (Table 2.1).

### 2.3.2. Application of Method 1 to pelagic particulate samples

The HPLC composition for improved allomer separation (Method 1) was applied to pelagic, marine particulate samples from station L4 taken during the spring of 2012. The resulting chromatogram contained 4 peaks which eluted in the region expected for chlorophyll *a* allomers, preceding chl-*a* (peak V, Figure 2.2). Their on-line UV/vis absorption spectra were consistent with those expected for chl-*a* allomers. The chromatogram, however, showed a very high allomer peak area compared to chl-*a*. The peak area ratio of total allomer to chl-*a* was  $2.61 \pm 0.51$  (mean  $\pm$  Standard Error,  $n=18$ ). The individual ratio of HO-chl-*a* to chl-*a* was  $0.26 \pm 0.03$  ( $n=18$ ) with values ranging from 0.07 to 0.47. This range can be compared directly to the HO-chl-*a* to chl-*a* ratio detected in pelagic particulate samples from the North Atlantic published by Bale (2010) of 0.015 to 0.04. Therefore, the maximum ratio of HO-chl-*a* to chl-*a* observed in the Western Channel Observatory samples was more than ten times that observed in the North Atlantic samples (Bale 2010). Such a high ratio of HO-chl-*a* to chl-*a* was unexpected,

and indicated chlorophyll oxidation may have occurred post sampling. Interrogation of chromatograms of chl-*a* standards analysed during the same period revealed an allomer to chl-*a* ratio of  $0.091 \pm 0.001$  ( $n=6$ ), which corresponded to an increase from the expected allomer to chl-*a* ratio in the standard (0.02).

A high degree of chlorophyll *a* allomerisation has been observed previously by Van Heukelem and Thomas (2001) during chromatography of concentrated samples, when ammonium acetate was present in the primary eluent. Therefore, components of the mobile phase in this study may have contributed to allomerisation. The antioxidant butylated hydroxy toluene (BHT) has been used as an eluent additive to prevent allomerisation of bacteriochlorophyll *a* (Koblížek et al. 2003). In subsequent use of Method 1 (Table 2.1), BHT was added to eluent A (solvent composition at  $t=0$ ) at the final concentration of 0.01 % (w/v) (Koblížek et al. 2003).

To further investigate possible contributions to chlorophyll oxidation, elements of the analysis process, including extract preparation, instrument type and HPLC method were assessed. Chlorophyll *a* standard solutions were used for this purpose to provide analytes with consistent allomer content.

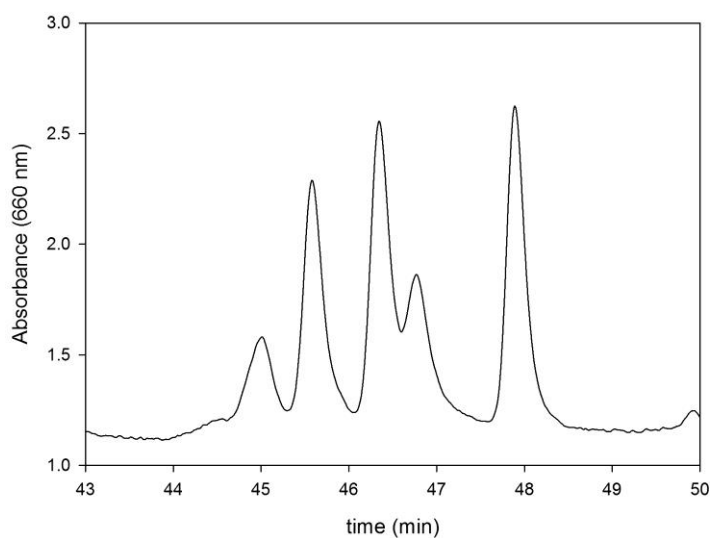


**Figure 2.2.** A partial chromatogram (660 nm) obtained during HPLC analysis of a pelagic marine particulate extract (0 m from L4 on 27-03-2012), using Method 1 (Table 2.1).

## 2.4. Oxidation of chlorophyll *a* during sample preparation and analysis

### 2.4.1. Oxidation during extract preparation for injection

The processes of pigment sampling by filtration, storage at -80 °C (Sosik 1999) and extraction in acetone using sonication, under dim light, are well established and commonly used for routine pigment analysis (Pickney et al. 2011). Known artefacts of extraction include chlorophyllide, which forms through contact between the enzyme chlorophyllase and chlorophyll *a* during cellular disruption (Jeffrey and Hallegraeff 1987), particularly in diatom samples. The transesterification reaction that produces chlorophyllide from chlorophyll *a* can also proceed via acid or base catalysis in the absence of enzyme. Notably chlorophyllide can also be present naturally in cells as a biosynthetic precursor to chlorophyll *a*. With the exception of loss of the extremely labile cyclophaeophorbide enols during extraction in acetone (Kashiyama et al. 2012) no other artefacts of extraction in acetone have been reported. As oxidation of chlorophyll occurs readily in alcoholic solutions (Jie et al. 2002), acetone is recommended for extraction (Keely 2006). The extraction process was therefore not investigated as a possible source of chlorophyll allomers. For the purpose of assessing post-sampling oxidation, chlorophyll *a* standard was used, avoiding the need for an extraction step.

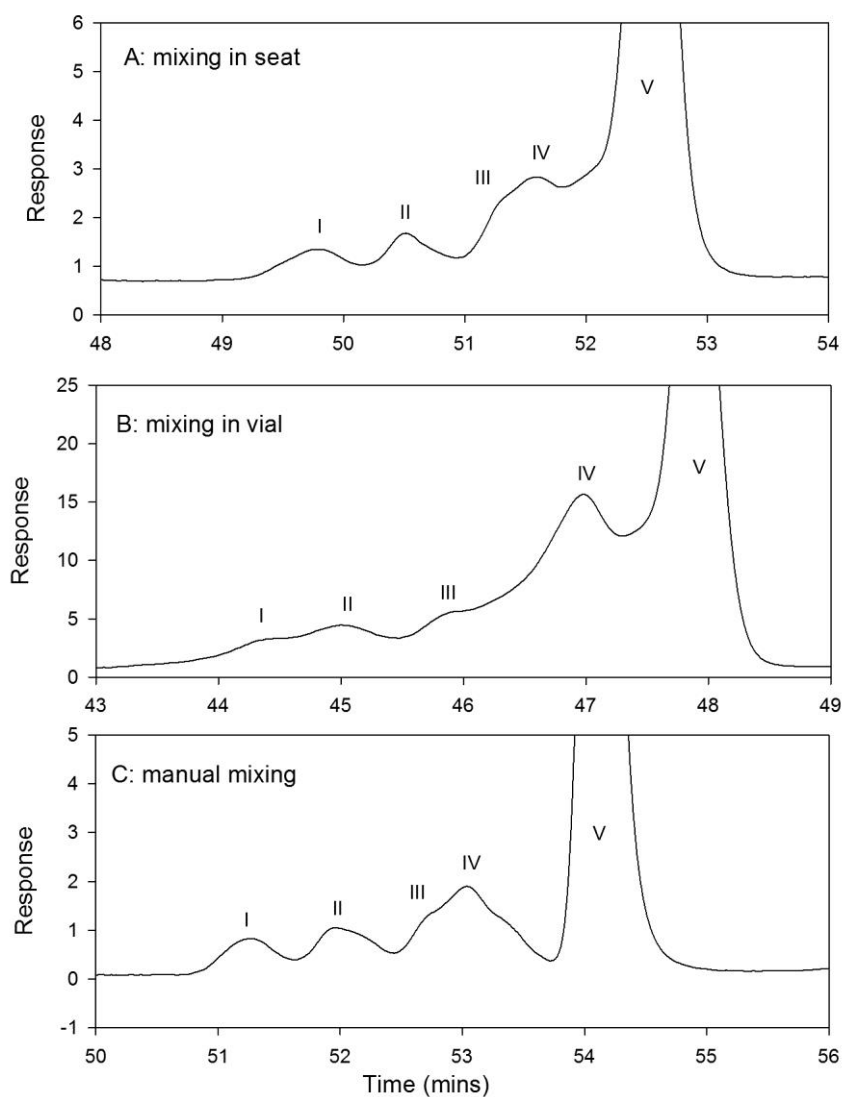
During HPLC analysis of pigments, the extract is commonly mixed with water or a salt solution (Vidussi et al. 1996, Barlow et al. 1997, Latasa and Bidigare 1998), in order to match the polarity of the extract with the initial mobile phase composition. In this study, the injected samples contained acetone and water mixed in a ratio of 10:1. The process of mixing the extract with water, normally performed by the HPLC autosampler, was a possible source of oxidation. For the purpose of testing for oxidation, chlorophyll *a* standard was prepared with 100% acetone. Comparisons were made between mixing the standard with water manually and using an Agilent 1200 autosampler to mix both in the injector seat and in a separate vial (Table 2.2). In both cases the autosampler was programmed to draw the sample volume from the vial in two parts with water sandwiched between. Contamination of the vial containing the water was avoided by programming the autosampler to dip the needle into a vial containing acetone immediately after drawing sample. A wait time of 30 s after the mixing step was included to allow thorough mixing of the sample and water components before injection.

Automated mixing of sample and water in the injector seat, resulted in a ratio of allomer to chl-*a* of  $0.38 \pm 0.03$  ( $n=3$ ). The resulting chromatogram contained peaks III and IV which had merged, and were poorly separated from chl-*a* (peak V; Figure 2.3.A) compared to the direct injection of chl-*a* standard in 90% acetone (Figure 2.1.B). Automated mixing in a separate vial caused peak fronting and overlapping (Figure 2.3.B) and increased the allomer to chl-*a* ratio to  $1.4 \pm 0.23$  ( $n=3$ ), the highest of the mixing methods. Manual mixing gave rise to a chromatogram with improved resolution between peaks III and IV compared to the automated mixing methods (Figure 2.3). Manual mixing resulted in an allomer to chl-*a* ratio of  $0.21 \pm 0.02$  ( $n=3$ ). When a mixing step was not required i.e. for a chl-*a* standard prepared in 90% acetone (Figure 2.1.B), the allomer to chl-*a* ratio was decreased ( $0.09 \pm 0.001$ ,  $n=6$ ), but the chromatography of the allomers was very similar (Figures 2.1.B and 2.3.C), indicating additional components were not produced during manual mixing.

Automated mixing increased the quantity of chlorophyll oxidation products and possibly the number of oxidation product types, causing the allomer peaks to merge and hence decrease peak resolution (Figure 2.3). During automated mixing in the Agilent autosampler, a piston in the sampling unit moves back and forth drawing fluid through a needle. If the needle is positioned in the injector seat (as in Table 2.2.A) it will pull fluid through a waste line which is open to the atmosphere. When the needle is positioned in a vial, fluid is drawn out of and into the vial (as in Table 2.2.B) and providing the vial contains adequate sample, no air is included. As the mixing vial contained only 100  $\mu\text{L}$  and this total volume was drawn into and out of the needle during the mixing step (Table 2.2.B), it is highly likely that air was included in the process. This inclusion of air is likely to be the main cause of oxidation observed in chl-*a* standard mixed in a vial prior to chromatography (Figure 2.3.B). The mix step involves interaction between the analyte and mobile phase present in the sample loop capillary; this may be an additional cause of sample oxidation. The needle and capillaries used in the Agilent autosampler are stainless steel; hence they are not a cause of sample oxidation. The manual mixing method provided chromatograms with the greatest peak resolution and least allomer production during analysis of chl-*a* standard. Manual mixing was therefore used when a sample required mixing with water before injection.

**Table 2.2.** Injection program for the automated mixing of sample with water (Vial 10) in A. the injector seat and B. a clean vial. An acetone wash step (Vial 9) is included.

#	A. Mixing in Injector Seat	B. Mixing in Vial
1	DRAW 45 $\mu$ L from sample, max. speed, def. offset	DRAW 45 $\mu$ L from sample, max. speed, def. offset
2	DRAW 0 $\mu$ L from Vial 9, max. speed, def. offset	DRAW 0 $\mu$ L from Vial 9, max. speed, def. offset
3	DRAW 10 $\mu$ L from Vial 10, max. speed, def. offset	DRAW 10 $\mu$ L from Vial 10, max. speed, def. offset
4	DRAW 0 $\mu$ L from Vial 9, max. speed, def. offset	DRAW 0 $\mu$ L from Vial 9, max. speed, def. offset
5	DRAW 45 $\mu$ L from sample, max. speed, def. offset	DRAW 45 $\mu$ L from sample, max. speed, def. offset
6	MIX 100 $\mu$ L in seat, max. speed, 6 times	MIX 100 $\mu$ L in vial+1, max. speed, 6 times
7	WAIT 0.50 min	WAIT 0.50 min
8	INJECT	INJECT

**Figure 2.3.** Partial HPLC-Diode Array Detector (660 nm) chromatograms of chlorophyll *a* and chlorophyll *a* allomer elution after preparation of extract by; (A) automated mixing in injector seat, (B) automated mixing in vial, and (C) manual mixing.



To determine the overall contribution to chlorophyll oxidation from instrumentation, Method 1 was set up on both instruments. Injections of chlorophyll *a* standard revealed a lower ratio of allomer to chl-*a* for standards analysed using the Accela instrument ( $0.0757 \pm 0.0004$ ;  $n=5$ ; Figure 2.5), compared to those analysed using the Agilent instrument ( $0.091 \pm 0.013$ ;  $n=18$ ). The variability of the allomer to chl-*a* ratio was also reduced when Method 1 was applied to the Accela instrument as judged by the lower standard error (Figure 2.5). Notably this allomer to chl-*a* ratio and variability (from Method 1 on the Accela instrument) was much higher than that observed for chl-*a* standard injected onto the Accela system using the Zapata et al (2000) method (Figure 2.5), indicating a larger contribution to the high allomer to chl-*a* ratio from the HPLC method than the instrumentation.

The ratio of allomer to chl-*a* observed during analysis of chl-*a* standard using Method 1 was compared with the Airs et al (2001) method, both ran on the Accela instrument. The ratio of allomer to chl-*a* observed was higher when the Airs et al. 2001 method was used ( $0.12 \pm 0.009$ ,  $n=5$ ) compared to Method 1 ( $0.078 \pm 0.004$ ,  $n=5$  Figure 2.5).

The difference in the ratio of allomer to chl-*a* observed from chl-*a* standard analysed using the Zapata et al. (2000) method and Method 1, is striking (Figure 2.5), and results from allomerisation due to the mobile (solvent composition) and stationary (column) phases. The Airs et al (2001) method and Method 1 are both performed using a Waters Spherisorb polymeric ODS2 (OctaDecyl, C<sub>18</sub>) column (300 x 4.6 mm, 3 µm particle size, 80 Å pore size) on silica with a carbon load of 11.5% and surface area 220 m<sup>2</sup> g<sup>-1</sup>, whereas the Zapata et al (2000) method uses a Waters Symmetry monomeric C<sub>8</sub> column (150 x 4.6 mm, 3.5 µm particle size, 100 Å pore size) on high purity silica with a carbon load of 19% and surface area 335 m<sup>2</sup> g<sup>-1</sup>. To investigate the contribution to chlorophyll oxidation from the stationary phase, chlorophyll *a* standard was analysed using the mobile phase composition of Method 1, with the Spherisorb ODS2 and Symmetry C<sub>8</sub> columns on the Accela instrument. Changing the stationary phase from Spherisorb ODS2 C<sub>18</sub> to Symmetry C<sub>8</sub> reduced the allomer to chl-*a* ratio from  $0.078 \pm 0.004$  to  $0.024 \pm 0.005$  ( $n=5$ , Figure 2.5). Chromatography on the Symmetry C<sub>8</sub> produced 3 allomer peaks, and the chl-*a* elution time was reduced to 29 min, from 51 min, however the separation between the chl-*a* peak and the adjacent allomer was reduced. The lowest ratio of allomer to chl-*a* and lowest variability, however, was achieved using the Zapata et al. (2000) mobile and stationary (Symmetry C<sub>8</sub>) phases together (Figure 2.5).

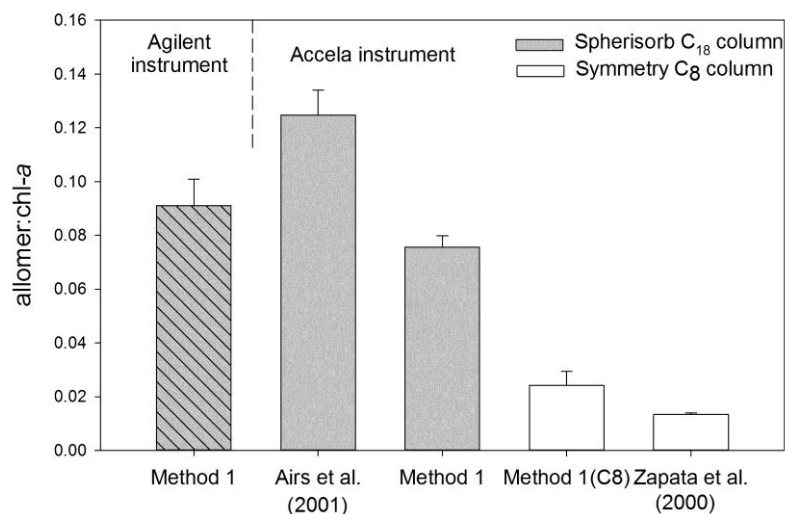


**Figure 2.5.** Allomer production during chromatography of chlorophyll *a* standard using Agilent and Accela instruments with 3 HPLC methods and 2 column types. Mean ratios of allomer to chl-*a* are shown with SE bars (n=5).

A lower ratio of allomer to chl-*a* was observed in chlorophyll *a* standards than in marine particulate samples, both analysed by System 1 during the same period (section 2.3.2). This high variability of allomer production observed when using System 1 (Figure 2.4) could contribute to this difference between chl-*a* standard and marine samples. The level of oxidation observed in marine samples using Method 1 ( $2.61 \pm 0.51$ , n=18, Figure 2.2) has been previously reported during routine pigment analysis at Plymouth Marine Laboratory using an earlier model of the Agilent instrument (PML, unpublished results). The Agilent 1100 HPLC system contained a similar pump and injection system to the 1200 model described above. This earlier analysis used a mobile phase gradient, containing ammonium acetate, based on Barlow et al. (1997). This previous report also identified variation in the allomer to chl-*a* ratio between 2 individual columns (both Thermo C<sub>8</sub> hypersil mos-2, 100 mm x 4.6 mm, 3  $\mu$ m) (PML, unpublished results).

The type of stationary phase used was a major contributor to the high allomer to chl-*a* ratio observed during analysis of chl-*a* standard and marine particulate samples by Method 1 (Figure 2.4 & 2.5). This was partly due to the length of time the analyte spent on the column, i.e. Method 1 on the C<sub>8</sub> column eluted chl-*a* faster than the C<sub>18</sub> column. The mobile phase composition and gradient had a smaller contribution to this high allomer to chl-*a* ratio (Figure 2.5).

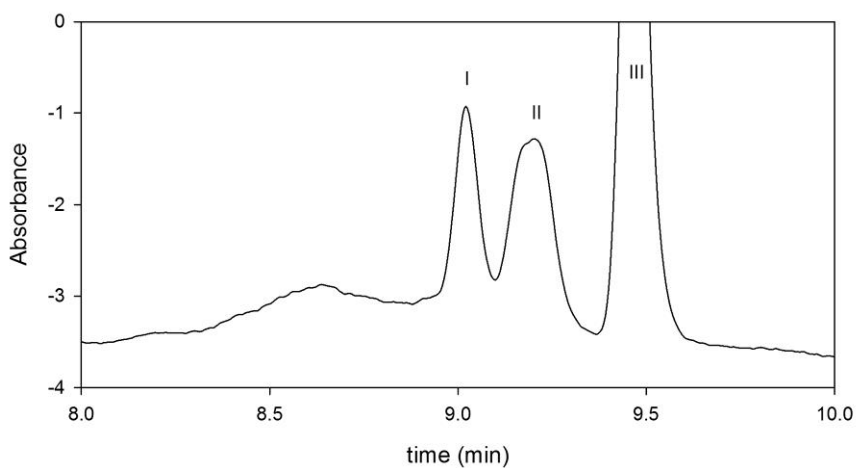
### 2.4.3. Ultra-High Performance Liquid Chromatography

A recent development in HPLC technology, Ultra-High Performance Liquid Chromatography (UPLC) utilised high pressure conditions to reduce method duration and solvent consumption. The short run times of UPLC methods minimises the time the analyte spends on the column. As column type is a major contributor to high allomer to chl-*a* ratios (Figure 2.5), decreasing method duration may reduce allomerisation. Several UPLC methods have been developed for microalgal pigment analysis from sediments (Saesaengseerung 2013) and phytoplankton cultures (Mulders et al. 2013). The Mulders et al. (2013) method achieves separation of chlorophyll *a* from one allomer peak reported as being either MeO-chl-*a* or MeO-lact-chl-*a* and has a run time of 20 min. Saesaengseerung (2013) developed 2 UPLC methods based on the Airs et al. (2001a) method. Method 6 was designed for use on two Acclaim 120 C<sub>18</sub> columns (100 mm × 2.1 mm i.d., with 2.2 µm particle size), with a run time of 23 minutes. Method 10 was developed for use on an Acquity UPLC BEH C<sub>18</sub> column (150 mm x 3mm i.d with 1.7 µm particle size), and had a run time of 20 minutes. Both methods were designed for complex pigment distributions from sediment samples. Method 10 achieved separation of HO-chl-*a* and several unidentified chlorins from sediment samples (Saesaengseerung 2013) and was therefore selected for use in this study.

The Saesaengseerung (2013) method (Table 2.3) was applied to the Accela instrument. Analysis of chlorophyll *a* standard by the Saesaengseerung (2013) method produced a chromatogram which exhibited 2 allomer peaks preceding chl-*a* (Figure 2.6) with UV/vis absorption spectra as expected for chl-*a* allomers. The ratio of allomer to chl-*a*,  $0.61 \pm 0.014$  (n=6), was higher compared to any of the other methods or column types used to analyse chl-*a* standard in this study. The C<sub>18</sub> column type may have been a contributor to this high allomer to chl-*a* ratio. Another possible cause of the high allomer to chl-*a* ratio resulting from the UPLC method may have been irregularity in the Accela quaternary pump, indicated by an unstable baseline during system preparation and analysis of chl-*a* standard.

**Table 2.3.** Solvent gradient programs from Airs et al. (2001) method and Saesaengseerung (2013) method.

Time (mins)	% Ammonium acetate (0.01M)	% Methanol	% Acetonitrile	% Ethyl acetate
Airs et al. (2001) method				
0	5	80	15	0
5	5	80	15	0
100	0	20	15	65
105	0	1	1	98
110	0	1	1	98
115	5	80	15	0
Saesaengseerung (2013) method				
0	10	80	10	0
0.5	10	80	10	0
7	5	64	10	21
16	0	50	10	40
18	0	31	6	63
18.5	0	19	1	80
19.5	0	19	1	80
20	10	80	10	0

**Figure 2.6.** Partial UPLC chromatogram (660 nm) of chlorophyll a standard at time of chl-a and allomer elution, using Saesaengseerung (2013) method.

### 2.5. Optimisation of Zapata et al (2000) method

As the Zapata et al. (2000) method resulted in the smallest ratio of allomer to chl-*a* (Figure 2.5), it was selected for optimisation of chl-*a* and allomer chromatography, by modification of the mobile phase composition and gradient (Table 2.4). The aqueous content of the mobile phase was increased from 25 to 35 % (Table 2.4) in order to retain chlorophyll *a* on the column for longer, to enable increased interaction with the stationary phase and hence improve separation (Table 2.4, Method 2). The composition at 22 min was also altered from Zapata et al. (2000) method, to modify the rate of change of aqueous content in the gradient. The rate of change of aqueous content was decreased between 0 and 22 min and increased between 22 and 28 min (Table 2.4, Method 2).

**Table 2.4.** Solvent gradient programs and average allomer to chl-*a* ratio (mean  $\pm$  SE), n=5.

Time (mins)	% Methanol	% Acetonitrile	% Aqueous Pyridine (0.248M)	% Acetone
Zapata et al. (2000), Method a				
0	50	25	25	0
22	38	39	15	8
28	21.5	58.25	1.25	19
38	21.5	58.25	1.25	19
40	50	25	25	0
Average allomer to chl- <i>a</i> ratio = 0.012 $\pm$ 0.006				
Method 2				
0	40	25	35	0
22	32	39	21	8
28	21	58.25	1.75	19
38	21	58.25	1.75	19
40	40	25	35	0
Average allomer to chl- <i>a</i> ratio = 1.4 $\pm$ 0.3				
Method 3				
0	50	25	25	0
5	50	25	25	0
27	38	39	15	8
33	21.5	58.25	1.25	19
43	21.5	58.25	1.25	19
45	50	25	25	0
Average allomer to chl- <i>a</i> ratio = 0.036 $\pm$ 0.001				

Increasing the percentage of the aqueous component of the mobile phase resulted in a slight increase in chlorophyll *a* retention time from 33.5 min to 35.2 min (Figure 2.7, A & B). The altered mobile phase composition, however, had a dramatic effect on the ratio of allomer to chl-*a*, which increased to 1.4 $\pm$ 0.35 (n=3) compared to 0.012 $\pm$ 0.0006 (n=5) from the unaltered

Zapata et al. (2000) method. This is a far larger increase than that observed between column types, indicating that the increased aqueous component of the mobile phase greatly affected the allomer to chl-*a* ratio. Furthermore, the chromatogram obtained using Method 2 contained an additional peak in the allomer region (with UV/vis maxima at 430 and 660 nm) compared to the chromatogram obtained using the Zapata et al. (2000) method (Peak vi', Figure 2.7, A & B). The resolution of peaks from Method 2 were reduced between peaks v and vi and between peak vi and chl-*a* (vii) compared to the Zapata et al (2000) method (from R=0.7 to R=0.55 and from R=1.28 to R=0.96 respectively).

An alternative method to increase chl-*a* retention, without increasing the aqueous content of the mobile phase was required. To this aim, an isocratic hold of the initial mobile phase composition was included in the method (Table 2.4, Method 3). The elution time of chl-*a* was increased to 39 min (Figure 2.7.C), but the ratio of allomer to chl-*a* also increased to  $0.036 \pm 0.001$  (n=3), compared to  $0.012 \pm 0.0006$  (n=5) obtained using the Zapata et al (2000) method. The increase in allomer to chl-*a* ratio from 0.012 to 0.036 indicates that increased time on the column may contribute to allomerisation. Method 3 also caused a slight reduction in peak resolution compared to that obtained using the Zapata et al. (2000) method, between peaks v and vi (R=0.61) and between peak vi and chl-*a* (R=1.16). The allomer components observed from a chl-*a* standard analysed using Method 3 were the same as those observed using Method 2, which differed from the components observed after analysis using the Zapata et al. (2000) method. Method 3 resulted in a much lower ratio of allomer to chl-*a* than Method 2, which indicates that the proportion of aqueous content has a larger effect on the ratio of allomer to chl-*a* than the length of time spent on the column.

Chromatograms obtained from chlorophyll *a* standard using the Zapata et al. (2000) method contained 3 allomer peaks (peaks vi, v and vi, Figure 2.7, A), whereas 4 allomer peaks resulted from Method 1 (Figure 2.1, B). However, direct comparison of Method 1 and the Zapata et al. (2000) method, on the Accela instrument using a Symmetry C<sub>8</sub> column, revealed a larger allomer to chl-*a* ratio observed from chl-*a* standards analysed using Method 1 ( $0.024 \pm 0.005$ , n=5) than from using the Zapata et al. (2000) method ( $0.013 \pm 0.0007$ , n=5). Method 1 also resulted in higher variability of the allomer to chl-*a* ratio than the Zapata et al. (2000) method. The low and repeatable allomer to chl-*a* ratio observed in chromatograms of chl-*a* standard analysed using the Zapata et al. (2000) method indicated the lowest level of chlorophyll oxidation was occurring, compared to any of the other methods tested in this study.

Minimising oxidation in the HPLC system was highly important for this study as it aims to measure the occurrence of allomers in marine particulate and phytoplankton culture samples, therefore the Zapata et al. (2000) method was chosen for analysis. The lower number of allomer peaks observable by the Zapata et al. (2000) method, compared to Method 1 was a compromise necessary for reliable data collection.

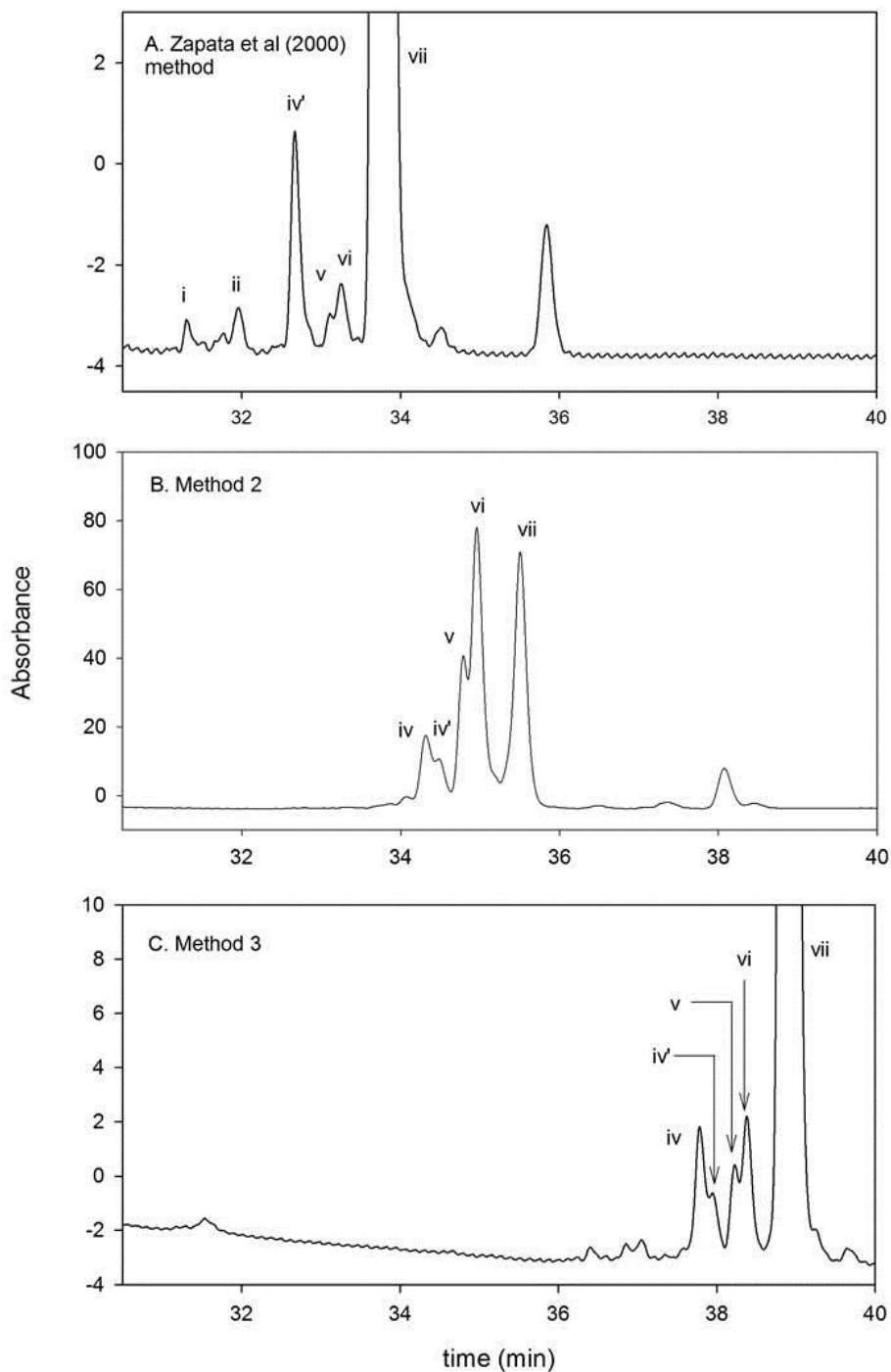


**Figure 2.7.** Partial HPLC chromatograms (660 nm) of chlorophyll a standard using (A) Zapata et al. (2000) method, (B) Method 2 and (C) Method 3. For assignment of peaks see text, section 2.6.

## 2.6. Assignment of peaks using LC/MS<sup>n</sup>

### 2.6.1. Particulate sample from station L4, analysed using the Zapata et al. (2000) method

The Zapata et al. (2000) method was applied to a pelagic particulate sample from station L4 and allomers were assigned according to their UV/vis spectra and Full MS and MS<sup>2</sup> spectra obtained during LC/MS/MS analysis. Three peaks eluted in the region expected for chlorophyll *a* allomers (peaks iv, v & vi, Figure 2.8). Peaks v and vi had UV/vis absorption spectra indistinguishable from that of chl-*a* with UV/vis absorption maxima at 428 nm and 663 nm (Table 2.5). Peak v gave rise to a UV/vis spectrum exhibiting a Soret band blue shifted compared to chl-*a* (Table 2.5), previously associated with MeO-chl-*a* (Franklin et al. 2012).

Peaks i and ii, eluted in the region expected for chlorophyll *b* allomers, just before chlorophyll *b* (peak iii, Figure 2.8). However, peaks i and ii gave rise to UV/vis absorption spectra consistent with chl-*a* allomers (Table 2.5). From LC/MS/MS analysis with post-column addition of acid (Methods chapter 7.6.5), peak i gave rise to a major ion at *m/z* 901 corresponding to the expected mass of [M+H-Mg]<sup>+</sup> for hydroxychlorophyll *b* (Table 2.5). A minor ion at *m/z* 923 represented a small proportion of [M+H]<sup>+</sup>, which had not undergone demetallation. On resonance induced fragmentation of the ion at *m/z* 901, major ions were observed in the MS<sup>2</sup> spectrum at *m/z* 623, *m/z* 883 and *m/z* 605 corresponding to [M+H-Mg-C<sub>20</sub>H<sub>38</sub>]<sup>+</sup>, [M+H-Mg-H<sub>2</sub>O]<sup>+</sup> and [M+H-Mg-H<sub>2</sub>O-C<sub>20</sub>H<sub>38</sub>]<sup>+</sup> respectively (Table 2.5). The loss of H<sub>2</sub>O from the protonated molecule, and position relative to chl-*b* are consistent with hydroxychlorophyll *b*. The MS signal from peak ii was not adequate for identification. Hydroxychlorophyll *b* has been reported to have a UV/vis spectrum indistinguishable from chlorophyll *b* (Hyvärinen and Hynninen 1999), however the LC/MS/MS analysis allows assignment of peak i as hydroxychlorophyll *b*.

Peak iv gave rise to a major ion at *m/z* 869 corresponding to [M+H-Mg]<sup>+</sup> (Table 2.5). On resonance induced fragmentation, the ion at *m/z* 869, gave rise to *m/z* 593 in the MS<sup>2</sup> spectrum (Table 2.5), equating to a loss of 276 Da. Chlorins esterified to a phytol chain at C17<sup>3</sup> commonly fragment during LC/MS<sup>2</sup> to lose 278 Da (Airs et al. 2001b). The loss of 276 Da thus indicates an additional double bond in the phytol chain. Peak iv is therefore assigned as the biosynthetic precursor to chlorophyll *a* (Rüdiger 2006); chlorophyll *a*<sub>P276</sub> as detected previously in *Thalassiosira pseudonana*, *Emiliana huxleyi* (Franklin et al. 2012) and *Pavlova gyrans* (Bale 2010).

From LC/MS/MS with post-column addition of formic acid, peaks v and vi gave rise to major ions at  $m/z$  887 and  $m/z$  869 corresponding to  $[M+H-Mg]^+$  and  $[M+H-Mg-H_2O]^+$  for 13<sup>2</sup>-hydroxychlorophyll *a* (Table 2.5). A minor ion at  $m/z$  909 was observed, corresponding to  $[M+H]^+$  representing a small proportion of HO-chl-*a* that had not undergone demetallation. On resonance induced fragmentation of the ions at  $m/z$  887 and  $m/z$  869, major ions were detected at  $m/z$  869,  $m/z$  591 and  $m/z$  531 in MS<sup>2</sup> corresponding to  $[M+H-Mg-H_2O]^+$ ,  $[M+H-Mg-H_2O-C_{20}H_{38}]^+$  and  $[M+H-Mg-OH-C_{20}H_{38}-CO_2Me]^+$  respectively (Table 2.5). This loss of H<sub>2</sub>O from the protonated molecule is diagnostic of the HO-chl-*a* structure (Jie et al. 2002, Franklin et al. 2012). Although peak v had UV/vis absorption spectra (Table 2.5) previously associated with methoxychlorophyll *a* (Franklin et al. 2012), the diagnostic MS<sup>2</sup> spectrum permits assignment as 13<sup>2</sup>-hydroxychlorophyll *a*. No evidence of methoxychlorophyll *a* or methoxylactonechlorophyll *a* was found in the marine particulate samples analysed by LC/MS using the Zapata et al. (2000) method.

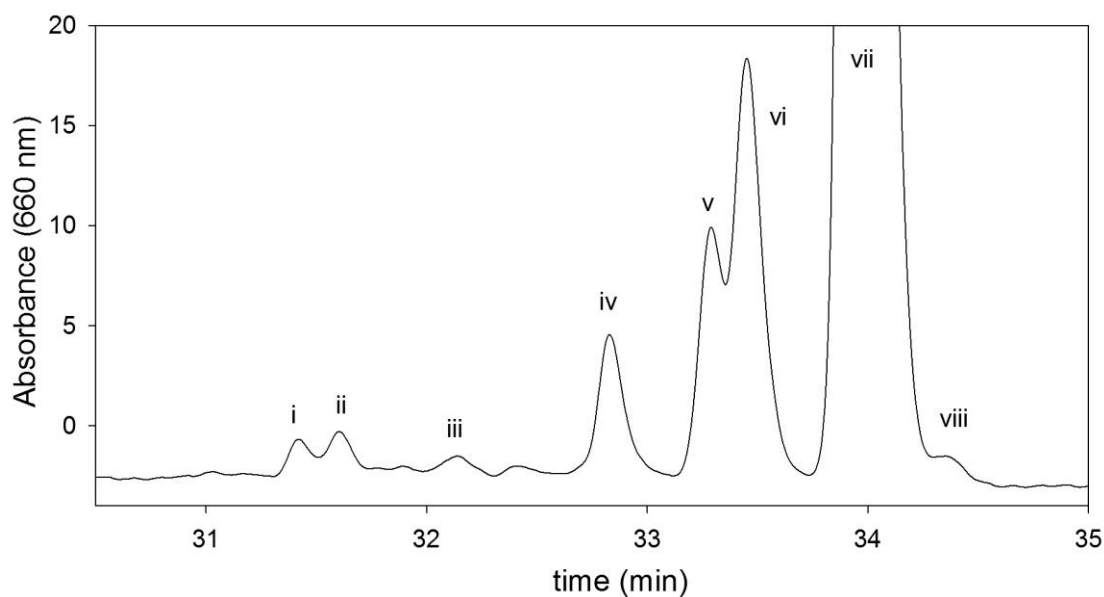


**Figure 2.8.** Partial HPLC chromatogram (660 nm) of a pigment extract from a marine pelagic surface sample collected from Station L4 on 10-04-12, analysed using the Zapata et al. (2000) method.

**Table 2.5.** Assignment of chlorophylls *a*, *b* and allomers in marine surface water sample (from station L4) after HPLC using Zapata et al. (2000) method, using UV/vis maxima and the most abundant ions resulting from LC/MS/MS (*m/z*, **major ions**).

Peak no.	Main UV/vis absorption bands (nm)	Assignment	Full MS ions ( <i>m/z</i> )	MS <sup>2</sup> major ions ( <i>m/z</i> )
i	428, 662	Hydroxychlorophyll <i>b</i>	923, <b>901</b>	<b>623, 883, 605</b>
ii	428, 662	Unidentified allomer 3		
iii	460, 648	Chlorophyll <i>b</i>		
iv	429, 663	Chlorophyll <i>a</i> <sub>P276</sub>	<b>869</b>	<b>593, 533</b>
v	420, 659	Hydroxychlorophyll <i>a</i>	<b>887, 869</b>	887, 609, <b>869, 591, 531</b>
vi	427, 662	Hydroxychlorophyll <i>a</i>	909, <b>887, 869</b>	887, 609, <b>869, 591, 531</b>
vii	429, 663	Chlorophyll <i>a</i>		
viii	429, 663	Chlorophyll <i>a</i> '		

### 2.6.2. Particulate sample from station L4, analysed using Method 1

Method 1 was applied to a particulate sample from station L4 and the chlorophyll *a* allomers were assigned using UV/vis spectra and LC/MS<sup>n</sup>. Four components in the marine sample chromatogram gave UV/vis spectra as expected for chl-*a* allomers (Table 2.6) (Kuronen et al. 1993). Peaks I, II and III gave rise to UV/vis spectra indistinguishable to chl-*a* (Table 2.6) and peak IV gave rise to a UV/vis spectrum with a blue-shifted Soret band (Table 2.6).

Peaks I gave rise to major ions at *m/z* 887 and 869 corresponding to [M+H-Mg]<sup>+</sup> and [M+H-Mg-H<sub>2</sub>O]<sup>+</sup> for 13<sup>2</sup>-hydroxychlorophyll *a*, respectively (Table 2.6). Their MS<sup>2</sup> spectra were consistent with the HO-chl-*a* structure, as described above (Table 2.6) (Jie et al. 2002). Peak I was therefore assigned as 13<sup>2</sup>-hydroxychlorophyll *a*.

Peaks II and III (Figure 2.2) gave rise to major ions at *m/z* 901 and *m/z* 869, corresponding to [M+H-Mg]<sup>+</sup> and [M+H-Mg-MeOH]<sup>+</sup> for 13<sup>2</sup>-methoxychlorophyll *a* (MeO-chl-*a*) (Franklin et al. 2012) with minor ion at *m/z* 923 corresponding to the protonated molecule (Table 2.6). On fragmentation, the ion at *m/z* 901 gave rise to MS<sup>2</sup> spectra exhibiting major ions at *m/z* 869, *m/z* 613, *m/z* 591 and *m/z* 531 corresponding to [M+H-Mg-MeOH]<sup>+</sup>, M+H-MeOH-C<sub>20</sub>H<sub>38</sub><sup>+</sup>, [M+H-Mg-MeOH-C<sub>20</sub>H<sub>38</sub>]<sup>+</sup> and M+H-Mg-MeOH-C<sub>20</sub>H<sub>38</sub>-COCO<sub>2</sub>Me<sup>+</sup> respectively (Table 2.6). The dominance of the loss of MeOH is diagnostic of the MeO-chl-*a* structure (Jie et al. 2002, Franklin et al. 2012). These two peaks can therefore be assigned as 13<sup>2</sup>-methoxychlorophyll *a* and its epimer.

Peak IV gave rise to an abundance of ions at  $m/z$  939 (Table 2.6) representing the protonated molecule. Unlike the other allomers described, this component was not readily demetallated. The MS<sup>2</sup> spectra generated from the ion at  $m/z$  939 contained a major ion at  $m/z$  852 corresponding to  $[M+H-COCO_2Me]^+$ . It also contained ions at  $m/z$  574 and 821 corresponding to  $[M+H-C_{20}H_{38}-COCO_2Me]^+$  and  $[M+H-MeOCOCO_2Me]^+$  (Table 2.6). The loss of MeOCOCO<sub>2</sub>Me is diagnostic of 15<sup>1</sup>-methoxylactonechlorophyll *a* (Jie et al., 2002).

As no evidence of MeO-chl-*a* or MeO-lact-chl-*a* was found in the marine particulate samples or chl-*a* standard analysed using the Zapata et al. (2000) method, it is possible that these compounds were produced artificially by Method 1 or were not resolved by the Zapata et al. (2000) method.

**Table 2.6.** Assignment of chlorophylls *a*, *b* and allomers in marine surface water sample (from station L4) after HPLC using Method 1, using UV/vis maxima and the most abundant ions resulting from LC/MS/MS ( $m/z$ , major ions).

Peak no.	Main UV/vis absorption bands (nm)	Assignment	Full MS ions ( $m/z$ )	MS <sup>2</sup> major ions ( $m/z$ )
I	430, 664	Hydroxychlorophyll <i>a</i>	909, <b>887</b> , <b>869</b>	906, 869, 591, 531
II	430, 664	Methoxychlorophyll <i>a</i>	923, <b>901</b> , <b>869</b>	<b>869</b> , 645, 623, <b>613</b> , <b>591</b> , <b>531</b>
III	432, 664	Methoxychlorophyll <i>a</i>	923, <b>901</b> , <b>869</b>	<b>869</b> , 645, 623, <b>613</b> , <b>591</b> , <b>531</b>
IV	420, 664	Methoxylactone chlorophyll <i>a</i>	<b>939</b> , 917	907, <b>852</b> , 821, 661, 629, 574, 537
V	430, 664	Chlorophyll <i>a</i>		

## 2.7. Conclusions

This study highlights how readily chlorophyll *a* allomers can be formed as artefacts during HPLC and LC/MS analysis and how variable this allomerisation can be. For the purpose of detecting allomers in culture and marine particulate samples, this level of artefact formation is prohibitive. Extract manipulation, HPLC instrumentation and method duration were all contributors to sample oxidation, with the aqueous component of the mobile phase and the interaction between the stationary and mobile phases being the largest contributors to allomerisation found in this study. Although most of this study was carried out using standards, some of the natural samples analysed using Method 1 showed high levels of allomerisation, indicating both sample types can be prone to this effect. Notably, the effect of HPLC method on allomerisation of extracts from sediments was not investigated during this study.

The selection of a robust analytical method and careful testing for artefacts is crucial when undertaking pigment analysis. The HPLC system must be assessed for artefact formation and measures taken to reduce the level and variability of oxidation before the method is applied to samples. The allomer to chl-*a* ratio should be assessed daily using standards before samples are processed, to ensure confidence in the HPLC method.

The sensitivity of extracted chlorophyll to allomerisation during pigment analysis has implications for previous studies that did not employ rigorous testing of artefact formation. A large proportion of the allomers observed may have been artificially created in the HPLC system (eg. Figure 2.4). Further, allomers reported to occur in natural particulates may have been formed as artefacts. From the HPLC methods assessed here, the Zapata et al (2000) method conceded a minimal and repeatable level of allomers during analysis of standards (Figure 2.5) however the range of allomers detected was reduced compared to Method 1. It was therefore necessary to compromise peak resolution for robust and trustworthy results.

## **Chapter III**

# ***Chlorophyll oxidation and indicators of viability during viral infection and senescence in the prasinophyte *Ostreococcus tauri****

### ***3.1. Introduction***

Viral infection, leading to host cell lysis, is an important regulator of phytoplankton communities (Bratbak et al. 1993, Kirchman 1999, Brussaard 2004) and can influence bloom dynamics (Baudoux et al. 2008). Viral infection is also an important process in the biological pump (Suttle 2007) and the microbial carbon pump (Jiao et al. 2010).

#### *3.1.1. Marine viruses of phytoplankton*

##### 3.1.1.1. Viruses affect carbon cycling

Viruses are thought to be responsible for the release of one quarter of photosynthetically fixed carbon into the water column (Fuhrman 1999, Suttle 2007). Induced by viruses, cell lysis alters the pathways of carbon through the biological pump (Suttle 2007) and microbial carbon pump (Jiao et al. 2010), i.e. processes leading to the sequestration of carbon, in the form of sinking or transported particulate organic matter (POM), and recalcitrant dissolved organic material (R-DOM) respectively. These processes both affect the atmospheric concentration of carbon dioxide.

Viruses redirect the flow of carbon and nutrients away from the higher trophic levels, back into the pool of dissolved and particulate organic matter, a process known as the viral shunt (Wilhelm and Suttle 1999, Suttle 2005) (Figure 3.1). Organic material that is released by virally mediated cell lysis (a portion of which will be refractory) tends to remain in the surface waters for longer and sinks more slowly. In the surface waters most of this P-D-OM will be converted to dissolved inorganic constituents (Gobler et al. 1997, Middelboe and Lyck 2002) by bacterial respiration and solar radiation (Fuhrman 1992, Fuhrman 1999, Wilhelm and Suttle 1999). Viral lysis can liberate phytoplankton growth limiting elements that are in complex with organic molecules, for example iron (Poorvin et al. 2004). Ultimately, viral action can increase the

efficiency of the biological pump by altering the proportion of C that is exported, relative to the nutrients that limit primary production (Suttle 2007). Therefore viral infection is important for the global C and N cycles. Viral infection can also increase the sinking rate of infected cells, as measured in *Heterosigma akashiwo* (Lawrence and Suttle 2004), which is large (18-34  $\mu\text{m}$ ) compared to *O. tauri* ( $\sim 1 \mu\text{m}$ ).

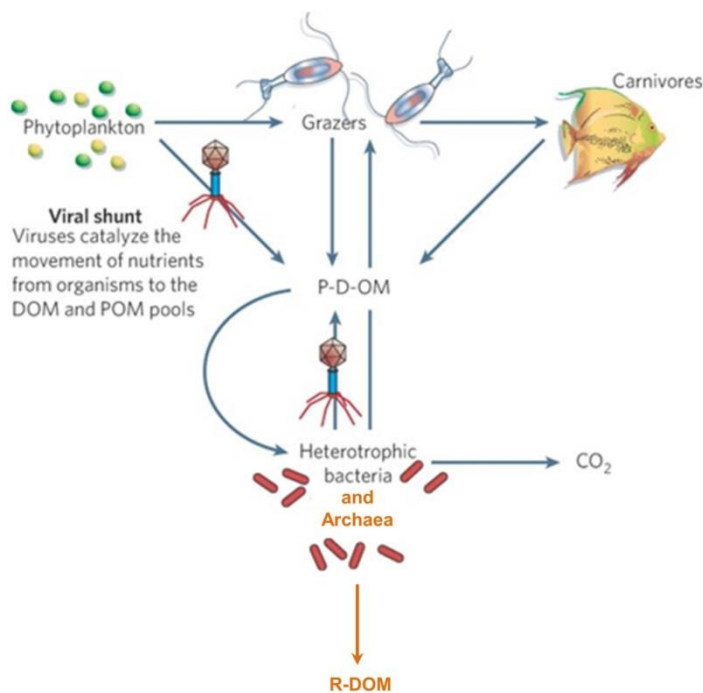


**Figure 3.1.** Viruses enhance the flow of carbon and nutrients from phytoplankton to heterotrophic bacteria by causing lysis of cells and shunting the pool of dissolved and particulate organic matter (P-D-OM). Original diagram taken from Suttle (2005); additions are marked in orange and represent the production of recalcitrant DOM (R-DOM) via processing by heterotrophic bacteria and Archaea, which can persist in the water column for millennia (Jiao et al. 2010).

### 3.1.1.2. Viruses affect phytoplankton diversity

Viruses affect phytoplankton community composition by several mechanisms: 1. The release of nutrients due to virus-induced cell lysis facilitates growth of particular phytoplankton taxa. 2. Horizontal gene transfer can result in new genetic traits in species, which are affected by natural selection (Suttle 2007). 3. Viruses affect phytoplankton diversity more directly as vectors of death, as host-virus interactions are species-, and sometimes strain-specific (Weinbauer and Rassoulzadegan 2004). A model describing viral control of diversity, the “Kill the Winner” model (Suttle 2007) depends on viral infection of the most abundant groups (Murray and Jackson 1992), however its translation to natural systems is as-yet unresolved (Suttle 2007). Viruses can terminate phytoplankton blooms (Vardi et al. 2012), however viral infection of a

bloom does not always result in complete termination (Waterbury and Valois 1993), due to diversity within the host species. Individuals within a population can have differing levels of resistance, by either carrying genes that affect susceptibility/resistance, or by the action of infection causing a shift in phenotype which enhances resistance (Thomas et al. 2011). Partial resistance to viral infection has been measured in *O. tauri* PCC745 populations infected with virus OtV5 (Thomas et al. 2011).

### 3.1.2. *Phytoplankton senescence due to nutrient limitation*

Phytoplankton blooms can also be terminated by environmental limitation (Lancelot 1983), i.e. senescence (see section 1.3.3 for definition). Death due to environmental limitation eventually results in cell lysis and the release of dissolved organic carbon, the same fate as cells lysed by viral action (Veldhuis et al. 2001). Commonly, phytoplankton growth in the surface ocean is limited by inorganic nutrient availability, e.g. nitrogen in the low latitudes, and iron in the upwelling regions (Moore et al. 2013). Population viability (described in section 1.3.2) in mixed phytoplankton assemblages is reduced when nutrient availability is low (Agustí 2004, Alonso-Laita and Agustí 2006, Hayakawa et al. 2008, Lasternas et al. 2010, Llabrés et al. 2010). Moreover, due to an increased proportion of dying cells in areas of low nutrient availability, the proportion of photosynthetic carbon that is released as DOC is increased and thus POC is decreased (Agustí and Duarte 2013). Hence, in the oligotrophic ocean phytoplankton mortality is basal to understanding carbon flow (Agustí and Duarte 2013).

Nutrient limitation has been used previously to induce senescence in algal cultures. In such studies the nutrient responsible for senescence is either measured (Berges and Falkowski 1998) or deduced through “add-back” experiments, where nutrients are added to cultures in stationary phase and monitored for growth (Franklin et al. 2012). The nutrient which is causing phytoplankton growth limitation can also be deduced by comparing the proportions of the major nutrients with their predicted use with reference to the Redfield Ratio (Guillard and Ryther 1962).

### 3.1.3. Description and importance of *Ostreococcus*

Picoeukaryotes are particularly important primary producers in the open ocean (Grob et al. 2011) and have a relatively high rate of carbon fixation (Li 1994, Worden et al. 2004). They are also generally abundant in the world's oceans; in the Western English Channel (UK) at time series station L4 (50.150°N; 4.130°W) during 2012, picoeukaryotes represented the majority of the eukaryote phytoplankton assemblage throughout the year (Figure 3.2). Picoeukaryotes are particularly susceptible to death caused by UV radiation (Llabrés and Agustí 2006) and hydroxyl radicals (Llabrés et al. 2012).

*O. tauri* is the smallest (0.8-1.3  $\mu\text{m}$ , Marin 2014) known free living eukaryote (Chrétiennot-Dinet et al. 1995), and by size class is a picoeukaryote (< 3  $\mu\text{m}$ ). It is a naked coccoid cell without cell wall or flagella, contains 1 chloroplast, and belongs to the class Prasinophyceae. *Ostreococcus* has an extensive distribution and has been found in coastal seas, the oligotrophic North Atlantic, the Mediterranean, and the Indian and Pacific Oceans (Worden et al. 2004, Zhu et al. 2005, Countway and Caron 2006), from the surface to 120 m depth (Worden et al. 2004). Hence *Ostreococcus* is an important and relevant genera to study.

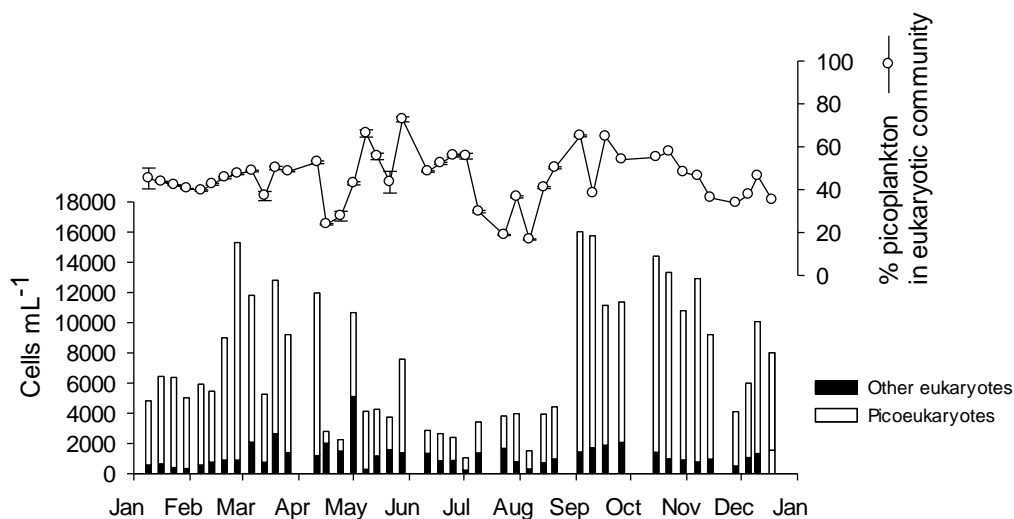


**Figure 3.2.** Eukaryotic phytoplankton community at time-series station L4 (50.150°N; 4.130°W) in 2012, averaged across depths 0.2, 10, 25 and 50 m (n=12), determined by flow cytometry (See methods chapter 7.3.3.1 for details). Raw data provided by Glen Tarran (PML). The average population densities of picoeukaryotes (□) and other eukaryotes (■), including coccolithophores, dinoflagellates, cryptophytes, *Phaeocystis* and other nanoeukaryotes are shown. The average percentages of picoplankton in the eukaryotic community are also shown (o) as mean  $\pm$  SE (n=12).

#### 3.1.4. Comparing viral lysis to senescence

Although the fate of carbon released from phytoplankton which have undergone virally and environmentally induced cell death is the same, the pathways which lead from healthy functional cells to cell particles are different (Veldhuis et al. 2001, Derelle et al. 2008, Vardi et al. 2012). Hence timings of disruption to photosynthesis, loss of homeostasis and loss of cell membrane integrity will be different during these pathways. The alteration products of chlorophyll *a* may present novel insight into these death processes, in particular the early oxidation products (allomers) of chlorophyll *a* (Bale et al. 2013).

Current knowledge of the effects of viral infection versus senescence on photopigments is limited to two studies of *Emiliana huxleyi* (Llewellyn et al. 2007, Bale et al. 2013). In the later, more detailed study, more chl-*a* allomer was found in virally infected cells, than in senescent cells (Bale et al. 2013). Information about chlorophyll alteration during viral infection in species other than *E. huxleyi* is lacking. Therefore, in this study death-induced changes in allomer production were assessed in the ecologically important picoeukaryote *Ostreococcus tauri*.

Thus, indicators of viability, including allomer production, ROS production and membrane permeability, were assessed during death by two modes. Assessment was made in cultures of the picoeukaryote *Ostreococcus tauri*, monitored during a carefully controlled viral lysis event and through a complete population growth cycle: from exponential growth phase (population is increasing exponentially), through stationary phase (where population growth is approximately equal to loss), to population decline due to environmental limitation (senescence, see Introduction chapter I, section 1.3.4). The main objective of this study was to compare chlorophyll *a* allomer production in environmentally limited and virally infected phytoplankton cells. The timing of the production of allomers was compared to the timing of loss of membrane permeability and increases in reactive oxygen species beyond the buffering capacity of the cells. Hence, this enabled comparison of the physiological and chemical changes during viral infection and senescence.

### 3.2. Experimental Outline

To study the alteration products of chlorophyll *a* during death by viral lysis, an established host/virus culture system was used; *Ostreococcus tauri* (RCC745) and *Ostreococcus tauri* virus 5 (OtV5), a lytic virus. Both host and virus were originally isolated from Bages Lagoon, France in 2006 (Derelle et al. 2008). Six replicate *O. tauri* cultures were grown in 5 L glass, conical flasks containing 1 L of artificial seawater (ESAW recipe) (Harrison and Berges 2005) enriched with F/2 nutrients (for further details see Methods chapter 7.1.3), under controlled temperature and light conditions (see chapter 7.1.2.3). Three of the exponentially growing cultures (with growth rate  $\mu \geq 0.69 \text{ d}^{-1}$ , measured by flow cytometry) were infected with freshly prepared (chapter 7.1.2.1) OtV5 lysate (Figure 3.3) at a host to virus ratio of 1. The triplicate non-infected flasks were primed with an equivalent volume of ESAW creating the controls. These non-infected flasks proceeded through a population growth cycle of growth, stationary phase and decline, creating the senescence study.

Samples were taken daily at 09:00 h, immediately followed by measurement of maximum quantum efficiency of PSII photochemistry (chapter 7.2.1) ( $F_v/F_m$ ; 15 min dark acclimation, Kromkamp and Forster, 2003). Population density (chapter 7.2.2), uptake of SYTOX-Green (membrane permeability, chapter 7.2.3) and uptake of CM-H<sub>2</sub>DCFDA (5-and-6-chloromethyl-2',7'-dichlorodihydrofluorescein diacetate, reactive oxygen species, chapter 7.2.4) were determined by flow cytometry (using an Accuri C6). Daily samples were also collected for pigment analysis (7 – 50 mL, see chapter 7.6.1.1) and samples were fixed for quantification of virus particles (chapter 7.2.5). The populations were monitored daily (Figure 3.3) until virus addition and twice daily thereafter. Sampling of the OtV5-infected flasks ceased after the population had crashed (day 6). The non-infected flasks were sampled daily until their population density began to decline (day 17).

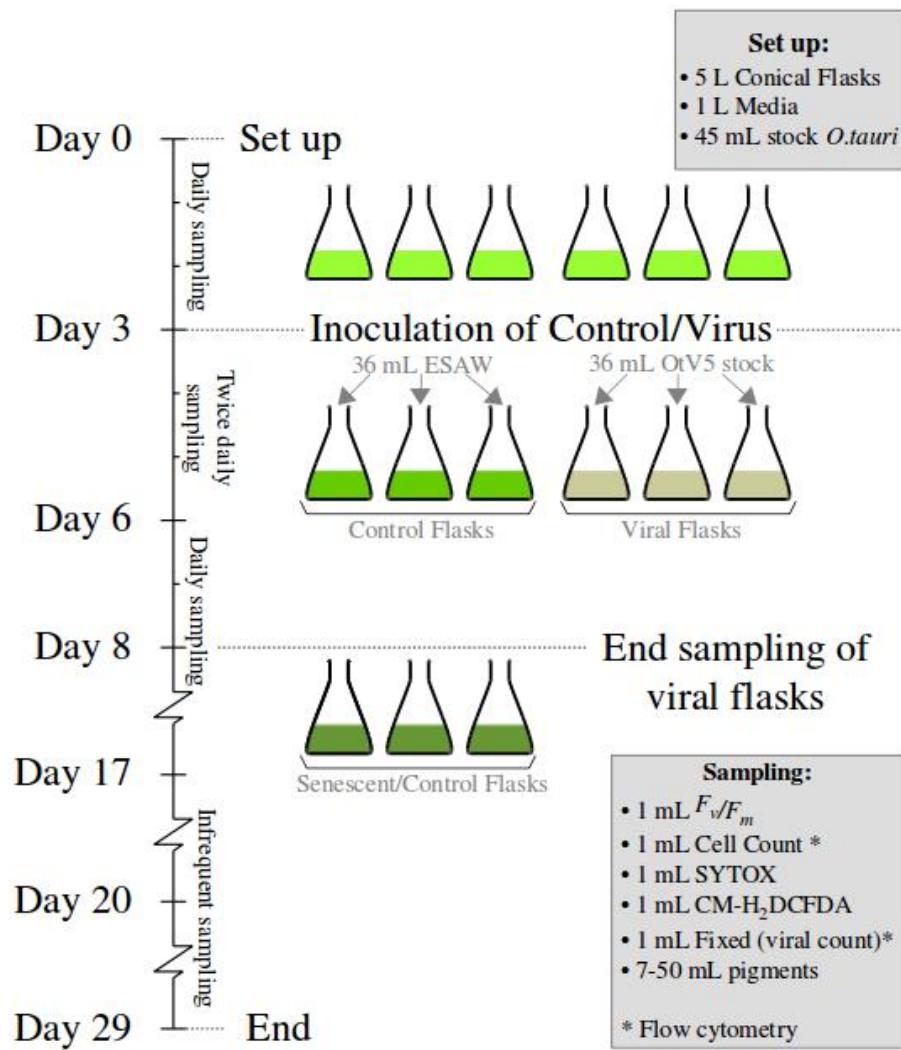


**Figure 3.3.** Schematic diagram of *Ostreococcus tauri* and OtV5 culture experiment including set-up, sampling frequency and sampling volumes.

### 3.3. Results and Discussion of *O. tauri* microcosm study

#### 3.3.1. *OtV5*-infected cultures; physiological indicators

##### 3.3.1.1. *O. tauri*/*OtV5* infection cycle

The growth curves of all six *Ostreococcus tauri* cultures demonstrated exponential growth from day 1 onwards, defined as growth rate ( $\mu$ ) greater than or equal to 0.69 per day (Figure 3.4.A). The virus *OtV5* was applied to triplicate flasks after 3 days of exponential growth ( $\mu = 1.05 \pm 0.03 \text{ d}^{-1}$ , mean  $\pm$  SE,  $n=3$ ). The population density of the infected cultures began to decrease between 12 and 24 hours post-infection (hpi) and the non-infected cultures continued in exponential growth (Figure 3.4.A). Virus numbers had increased by 80 000 fold, by 12 hpi as evident by the increase in virus particles (Figure 3.3.A). However, the major cell lysis event co-occurred with the major *OtV5* increase, between 24 and 36 hpi, when the *O. tauri* population declined by  $93.4 \pm 2.0\%$  (mean  $\pm$  SE). During this time viral numbers peaked at  $9.13 \pm 0.18 \times 10^8 \text{ mL}^{-1}$  (Figure 3.4.A).

The timing of the infection cycle of *O. tauri* and *OtV5* is consistent with previous work by Derelle et al. (2008). More frequent sampling by Derelle et al. (2008) revealed an increase in *OtV5* numbers at 8 hpi during which time the *O. tauri* population continued to grow. *OtV5* numbers were seen to increase most rapidly between 16 and 20 hpi, before the major *O. tauri* decrease ( $\sim 20$  hpi) (Derelle et al. 2008). The slight lag in major *OtV5* increase in the present study compared to that reported by Derelle et al. (2008), may be due to differences in experimental conditions, such as frequency of agitation or light environment, i.e. continuous light (Derelle et al., 2008) versus the 16 h/8 h, light/dark cycle applied in this study. However host-virus systems are evolutionarily very dynamic (Suttle 2007) and hence changes in the timings of infection events is not unexpected.

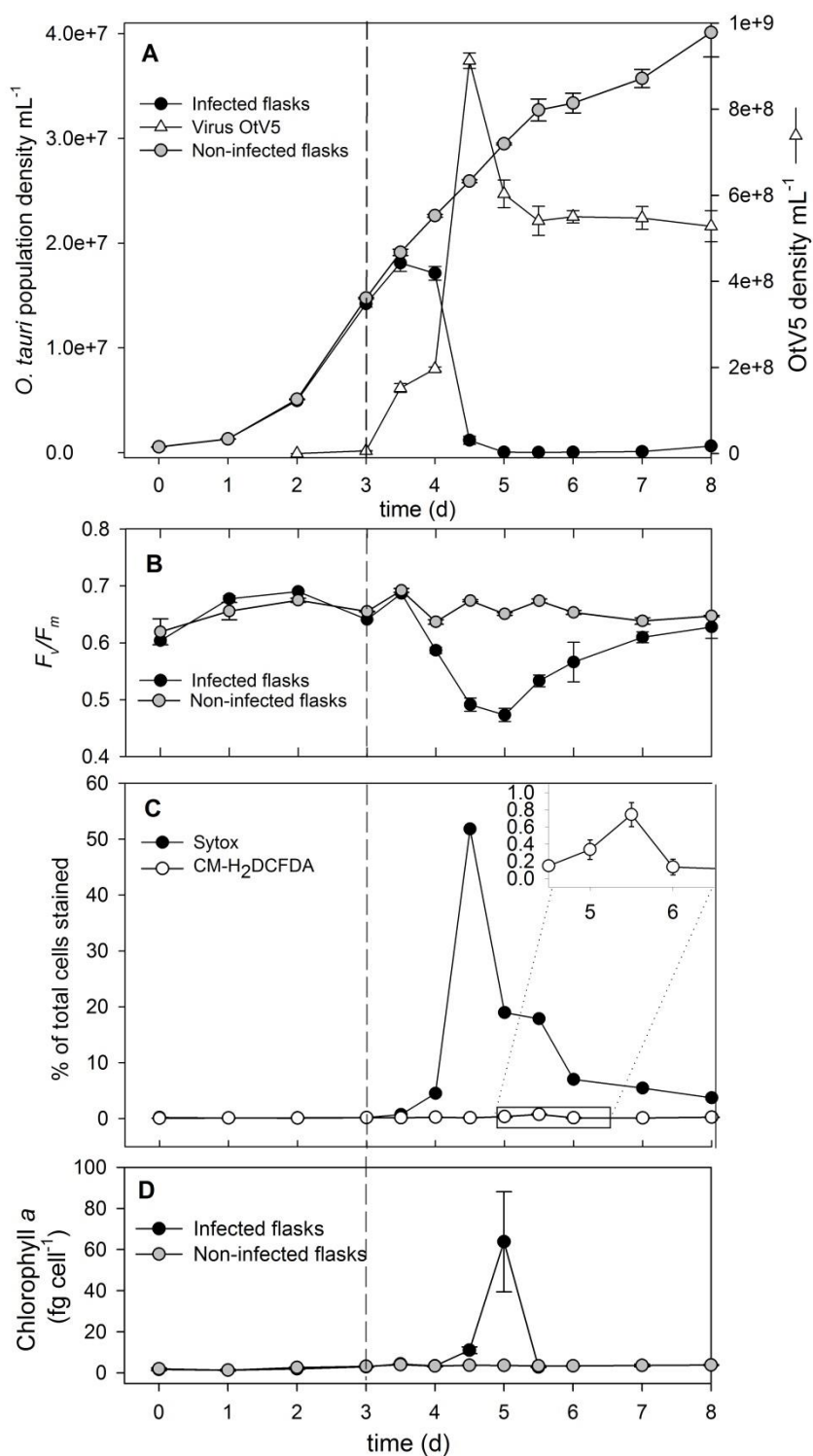


**Figure 3.4.** *Ostreococcus tauri* RCC745 cultures infected with virus OtV5 and non-infected controls: (A) Population densities of *O. tauri* and virus OtV5, (B) maximum quantum efficiency of PSII photochemistry ( $F_v/F_m$ ), (C) SYTOX-Green (for membrane permeability) and CM-H<sub>2</sub>DCFDA (for intracellular reactive oxygen species) staining, insert displays % of cells stained with CM-H<sub>2</sub>DCFDA, on a smaller scale (0 to 1%); and (D) Chlorophyll a content per cell. Mean and SE bars shown (n=3), - - - indicates time of virus addition.

### 3.3.1.2. $F_v/F_m$ during *O. tauri*/OtV5 infection

The *O. tauri* population density began to decline by 24 hpi, which coincided with a decrease in  $F_v/F_m$ , the maximum quantum efficiency of PSII photochemistry (Figure 3.4.B). At this time  $F_v/F_m$  of infected cultures reduced by 8 %, from  $0.643 \pm 0.004$  to  $0.590 \pm 0.005$  (mean  $\pm$  SE). This decrease indicated that the photosynthetic apparatus was disrupted during viral infection, prior to cell lysis.  $F_v/F_m$  also decreased 24 hpi during viral infection of *E. huxleyi* (Evans et al. 2006). Typically, during viral infection of phytoplankton, photosynthesis is inhibited through the loss of PSII electron transport efficiency (Teklemariam et al. 1990, Seaton et al. 1995). The degree of depression depends on the timing in the viral cycle, and is species specific (Waters and Chan 1982, Suttle et al. 1990, Suttle and Chan 1993, Juneau et al. 2003).

By 36 hpi, the remaining *O. tauri* population had a decreased  $F_v/F_m$  of  $0.49 \pm 0.012$ , which is  $26.8 \pm 1.8\%$  lower than the  $F_v/F_m$  of the control cultures. Chlorophyll *a* content per cell significantly increased in infected flasks 36 and 48 hpi, compared to non-infected flasks (Figure 3.4.D), by  $195 \pm 44\%$  and  $1634 \pm 660\%$  respectively. A small surviving population of *O. tauri* began to regrow on day 7 as found previously (Thomas et al. 2011), accounting for the residual photosynthetic capacity evident from the increase in  $F_v/F_m$  from day 5 (Thomas et al. 2011).

### 3.3.1.3. Staining for membrane permeability during *O. tauri*/OtV5 infection

Simultaneously, with the major *O. tauri* cell decline and reduction in  $F_v/F_m$  (24 hpi), the proportion of cells positively stained with SYTOX-Green (SYTOX-positive, indicating permeable plasma membranes) in infected cultures was significantly increased above the non-infected control cultures ( $4.49 \pm 0.41\%$  from  $0.18 \pm 0.01\%$ ). By 36 hpi (day 4.5) more than 90% of the *O. tauri* population had lysed; of the population that remained  $52.5 \pm 4.5\%$  were SYTOX-positive, indicating an increase in the proportion of cells with permeable membranes.

As OtV5 does not degrade the host's chromosomes before lysis (Derelle et al. 2008), there is opportunity for the nucleic acid stain SYTOX-Green to bind to the DNA during viral infection. However, lysis may occur quickly, with only a brief window when plasma membranes are compromised but cells are still relatively intact i.e. SYTOX-positive.

SYTOX-Green has not been previously applied to virally-infected *O. tauri* cultures, however a similar level of SYTOX-positive cells (60%) were detected during viral infection of *Phaeocystis pouchetii* (Brussaard et al. 2001), compared to the maximum percentage of virally-infected

*O. tauri* in the present study ( $52.5 \pm 4.5\%$ ). SYTOX-staining results were also similar in virus (MpV-UF10-38-)infected *Micromonas pusilla*, where a maximum of ~60% of cells were SYTOX-positive during viral infection (Brussaard et al. 2001). These studies indicate that whilst SYTOX-Green is clearly capable of detecting the loss of viability associated with viral infection, the rapidity of the process may mean that not all the cells destined to die are detected. This is reinforced by the consistency of the maximum percentage of SYTOX-positive cells detected between studies of different sampling intensities. Even in the *M. pusilla* study, where sampling intensity was once every 2 to 6 h, the maximum percentage of SYTOX-positive cells (Brussaard et al. 2001) was not higher than detected with a sampling intensity of once every 12 hours (as for *O. tauri*).

SYTOX-Green has also been applied to natural mixed picoplankton communities in the North Sea (Baudoux 2007). Mortality due to viral infection was detected at several of the sampling stations. At these specific stations, the percentage of SYTOX-positive cells within the picoeukaryote populations varied from ~5% to a maximum of ~85% (Baudoux 2007). The ability to detect this high maximum percentage of stained cells may be due to several different environmental effects such as light level and composition. The maximum rate of mortality due to viral lysis was 0.23 (Baudoux 2007). This low rate of lysis may also have enhanced the detection of SYTOX-positive cells.

#### 3.3.1.4. Staining for reactive oxygen species during *O. tauri*/OtV5 infection

Only modest percentages of cells with elevated (un-scavenged) cellular reactive oxygen species (CM-H<sub>2</sub>DCFDA-positive) were detected during this study. However, after viral addition, the percentage of CM-H<sub>2</sub>DCFDA-positive cells was significantly increased relative to the non-infected flasks (Mann-Whitney U=4.5, P<0.05). The percentage of CM-H<sub>2</sub>DCFDA-positive cells increased over time in infected cultures to a maximum on day 5 of  $0.72 \pm 0.14\%$  (Spearman rank; R=0.714, P<0.05, Figure 3.4.C), which was a  $722 \pm 154\%$  increase.

CM-H<sub>2</sub>DCFDA has been used previously to detect elevated intracellular reactive oxygen species levels during *E. huxleyi* viral infection (Evans et al. 2006, Vardi et al. 2012), where the fluorescent intensity of the probe inside cells was approximately doubled compared to non-infected cells. In *E. huxleyi* the increase in un-scavenged intracellular ROS was delayed until the latter part of culture decline, and was therefore associated with disruption to the cell caused by the virus. As ROS did not increase directly after infection of the *E. huxleyi* culture, but only from 48 hpi, during the late lytic phase of infection, it was deduced that ROS production was

not a defensive mechanism and was thought to indicate that ROS was necessary for viral replication (Evans et al. 2006). ROS production has been linked to viral infection of *E. huxleyi* populations elsewhere (Bidle et al. 2007, Vardi et al. 2009) and recent evidence suggests virally-induced *E. huxleyi* death is mediated by viral sphingolipid-induced ROS production (Bidle and Vardi 2011, Vardi et al. 2012).

Increased ROS has also been associated with viral infection of natural coccolithophore populations; with a maximum of 40% of cells CM-H<sub>2</sub>DCFDA-positive during the late lytic phase of viral infection (Vardi et al. 2012). Thus, it is surprising that only <1% of the virally infected *O. tauri* population was CM-H<sub>2</sub>DCFDA-positive during this study. The staining concentration and incubation conditions used by Vardi et al. (2012) was the same as in the present study (*O. tauri*). However, this low level of staining may be due to differences in the host species, or in the infection process in the different host/viral systems, or may be a short coming in the sensitivity of the fluorescent probe used.

This is the first application of CM-H<sub>2</sub>DCFDA to a picoeukaryote culture. The CM-H<sub>2</sub>DCFDA staining concentration and incubation conditions were optimised for response in *O. tauri* cultures before use (see methods chapter 7.2.4 for details). The CM-H<sub>2</sub>DCFDA-positive control used for optimisation was *O. tauri* culture exposed to H<sub>2</sub>O<sub>2</sub>. This resulted in a ROS concentration much higher than occurs naturally in the cell. Hence, although the staining conditions were optimised before use, the probe sensitivity may not have been adequate to detect changes of un-scavenged ROS inside the *O. tauri* cells. Hydroxyl radicals react very rapidly and it is not known when during the *O. tauri*/OtV5 infection cycle that un-scavenged ROS is maximum.

Intracellular ROS is expected to increase after viral infection via several mechanisms. As a defensive response to infection, some cells rapidly accumulate ROS (Doke 1985), which damages the pathogen (De Gara et al. 2003). ROS production above scavenging capabilities may also be linked to disruption to photosynthesis (Montalbini and Lupattelli 1989). The production of ROS has been linked with viral replication in some plant systems (Schwarz 1996), as in *E. huxleyi* (Evans et al. 2006).

Reaction centres PSI and PSII are a major generation site of photo-produced ROS, the production of which are affected by physiological and environmental factors (Asada 2006). ROS production increases during disruption to the electron transport chain. Viral infection has been shown to affect electron flow between PSII and PSI (Seaton et al. 1995). Therefore, it can

be speculated that the decreased  $F_v/F_m$  during viral infection of *O. tauri* was caused by increased ROS production during viral-infection via either destabilisation of PSII turnover (Balachandran et al. 1997) or stimulation of ROS production required for viral replication (Vardi et al. 2012), as has been suggested previously for virally-infected *E. huxleyi* populations (Kimmance et al. 2014).

### 3.3.2. *Physiological indicators during O. tauri* growth and senescence

#### 3.3.2.1. *O. tauri* batch culture growth and death

Prior to the study the *O. tauri* was closely monitored and kept growing in semi-continuous batch culture with a specific growth rate ( $\mu$ ) between 0.3 and 0.7 d<sup>-1</sup>. These (non-infected) *O. tauri* populations increased with exponential growth rates between days 1 and 3. Between days 3.5 and 5.5 growth rates were reduced but remained above  $\mu=0.1$  d<sup>-1</sup> (Figure 3.5.A). Thereafter growth rates reduced further but stayed positive until day 16. The growth rates of the triplicate flasks all became negative on day 16 ( $-0.12\pm 0.005$  d<sup>-1</sup>), when population density started to decline (Figure 3.5.A) and hence the population entered senescence phase. Negative growth rates indicated that cell lysis was occurring at a rate faster than cell division.

Assuming cells used nutrients according to the Redfield ratio; by calculation phosphate was potentially the initial nutrient to become limiting, as F/2 media has an N:P ratio of 24:1 (Guillard and Ryther 1962).

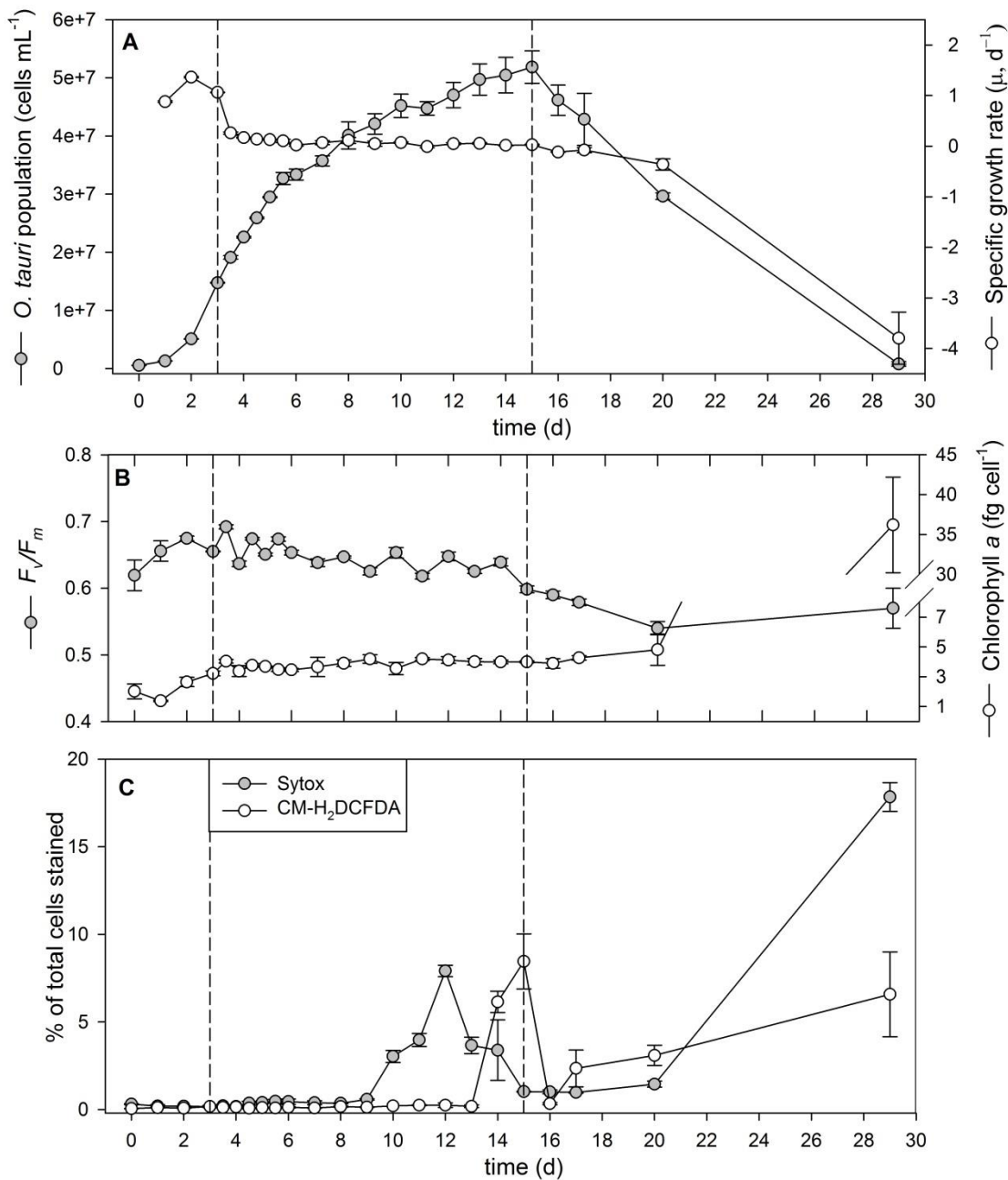


**Figure 3.5.** (A) Population density, specific growth rate ( $\mu$ , d<sup>-1</sup>), (B) maximum quantum efficiency of PSII photochemistry ( $F_v/F_m$ ) and chlorophyll a content per cell, (C) SYTOX-Green (for membrane permeability) and CM-H<sub>2</sub>DCFDA (for reactive oxygen species) staining of triplicate *Ostreococcus tauri* batch cultures during growth, stationary and senescent phases. Mean and SE bars shown (n=3).

### 3.3.2.2. Chlorophyll *a* content and $F_v/F_m$ during *O. tauri* senescence

The *O. tauri* population showed an increase in its chlorophyll *a* quota from  $2.04 \pm 0.51$  to  $4.81 \pm 1.05$  fg cell<sup>-1</sup> between days 0 and 20 and with a further increase to  $36.2 \pm 6.3$  fg cell<sup>-1</sup> by day 29 (Figure 3.5.B). At the end of the study on day 29, the small remaining population had 18 times more chlorophyll *a* per cell than cells in the exponential growth phase (on day 1). As *Ostreococcus* sp. RCC410 is known to respond to nutrient limitation (N) and starvation (P) by increasing its chlorophyll content (Kulk et al. 2013), there is evidence to suggest that the cells in the present study were nutrient limited. A difference in cellular chl-*a* content is also expected under altered light conditions, however by day 29, population density was low and the remaining cells were not self-shaded. The huge difference in chlorophyll concentration per cell, between cells in exponential growth and stationary phase to senescent cells (day 29), is confirmation of the physiological range that can occur within *O. tauri* cells.

Photosynthetic efficiency ( $F_v/F_m$ ), declined gradually after the population growth rate slowed on day 6 (Figure 3.5.B).  $F_v/F_m$  then declined from  $0.650 \pm 0.002$  in stationary phase to  $0.57 \pm 0.003$  in senescent phase. This is comparable to the decline of  $F_v/F_m$  in P limited *Ostreococcus* cultures from  $\sim 0.60$  to  $\sim 0.55$  (Kulk et al. 2013). In the same study N limitation had a greater effect on  $F_v/F_m$ , which declined from  $\sim 0.6$  to  $\sim 0.4$ . We therefore assume the decline in *O. tauri* cultures (non-infected), after day 16, was due to phosphate limitation (Figure 3.5.A).

### 3.3.2.3. Membrane permeability during *O. tauri* senescence

SYTOX-Green staining, indicating the proportion of cells with permeable membranes (i.e. non-viable cells) increased from day 10 and peaked on day 12, before declining (Figure 3.5.C). After the onset of population decline, the number of SYTOX-positive cells increased again (on day 20) as the cultures entered the senescent phase. The percentage of SYTOX-positive cells reached a maximum on day 29, of  $17.8 \pm 0.8\%$ .

Previously, SYTOX-Green was applied to *Ostreococcus* sp. RCC410 cultures under nutrient (N or P) starvation (Kulk et al. 2013). The viability of nutrient starved cultures was not reduced and was reported as  $99.0 \pm 0.4\%$  (Kulk et al. 2013). SYTOX-Green has also been applied previously to unidentified picoeukaryotes as part of mixed natural assemblages (Veldhuis et al. 2001, Baudoux et al. 2008). A previous study reported SYTOX-Green staining of up to 50% of the picoeukaryote community from a North Atlantic station ( $37 \pm 45^\circ$ N and  $23^\circ$ W; Veldhuis et al. 2001) in a population that was likely composed of *Ostreococcus*, *Micromonas*, or a mixture of

the two (Veldhuis et al. 2001). Similarly, between 1 and 85 % of the picoeukaryote cells in a mixed assemblage from the North Sea were stained with SYTOX-Green (Baudoux et al. 2008). These applications of SYTOX-Green to natural communities highlight the variability in the viability of natural phytoplankton communities.

The maximum percentage of SYTOX-positive cells detected during *O. tauri* senescence ( $17.8 \pm 0.8\%$ ) is low compared to that measured in mixed communities of picoeukaryotes (Veldhuis et al. 2001, Baudoux et al. 2008). The same concentration of SYTOX-Green was used in all of these studies but incubation times varied, from 10 min in the present *O. tauri* study, through 15 min (Baudoux et al. 2008), to 1 h (Veldhuis et al. 2001). The different stressors of the natural environment for example, light intensity and composition may affect the deterioration of cells and hence the percentage that would be SYTOX-positive.

#### 3.3.2.4. Staining for reactive oxygen species during *O. tauri* senescence

Only modest percentages of cells with elevated (un-scavenged) cellular reactive oxygen species (CM-H<sub>2</sub>DCFDA-positive) were detected during *O. tauri* growth and senescence. However, CM-H<sub>2</sub>DCFDA-positive cells, peaked at the onset of population density decline (day 15) at  $8.5 \pm 1.6\%$ . After the onset of population decline, the number of CM-H<sub>2</sub>DCFDA-positive cells increased again (on day 17) as the cultures entered the senescent phase. This peak in reactive oxygen species before population decline has also been detected in the diatom *Thalassiosira oceanica* (Steele, unpublished).

CM-H<sub>2</sub>DCFDA-positive cells only represented a small percentage of the total *O. tauri* population. The stains were optimised before use, with particular attention to improving the discrimination between positive and negative controls (Davey 2011) (see methods section 7.2.4 for details), however, the probe response remained very limited. This may be due to variability between individuals within the population, in their production of ROS or ability to scavenge ROS.

### 3.3.3. Assignment of chlorophyll alteration products

Pigment extracts from OtV-infected *Ostreococcus tauri* cultures and non-infected cultures were analysed for chlorophyll alteration products. Assignments of chlorophyll *a* and chlorophyll *b* were made by comparison of their retention times to standards and comparison of UV/vis absorption spectra and major ions observed during MS analysis to published data (Table 3.1, Zapata et al., 2000). The extracts gave rise to several peaks which eluted in the region expected for chlorophyll allomers, prior to chlorophyll *a* (peak IX, Figure 3.6, Walker et al., 2002), with UV/vis absorption spectra consistent with chl-*a* allomers (Table 3.1, Franklin et al., 2010). An array of peaks exhibiting chlorin-like UV/vis spectra were also detected eluting prior to chl-*b* (Peak V, Figure 3.6).

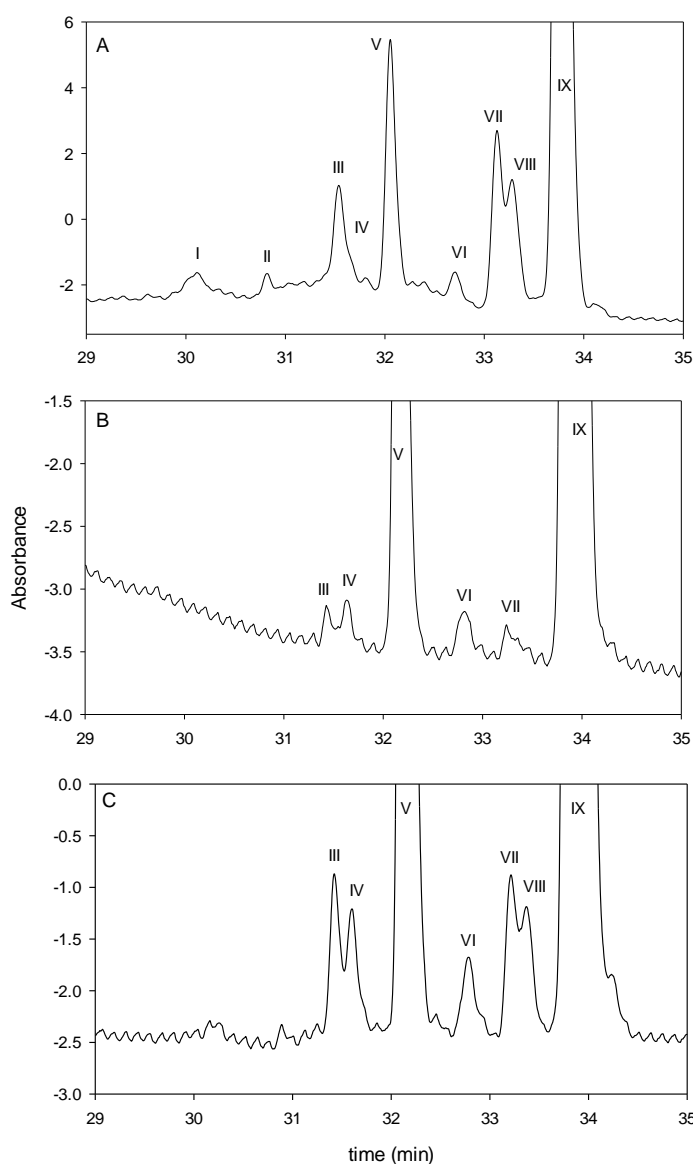


**Figure 3.6.** Partial HPLC-PDA chromatogram (660 nm) showing elution position relative to chl-*a* (IX) and chl-*b* (V) of chlorophyll alteration products detected in (A) OtV5-infected *O. tauri* cultures 48 hours post-infection (day 5), (B) growing non-infected cultures on day 5 and (C) senescent non-infected cultures on day 29. For peak assignment see Table 3.1.

**Table 3.1.** Peak assignment from 660 nm chromatogram resulting from HPLC separation of *Ostreococcus tarui* pigment samples.

Peak no.	Main UV/vis absorption bands (nm)	Assignment
I	427, (462), 653	Methoxychlorophyll a-like allomer*
II	430, 481, 658	Hydroxychlorophyll a-like allomer*
III	430, 660	Hydroxychlorophyll <i>b</i>
IV	430, 660	Hydroxychlorophyll <i>b'</i>
V	460, 648	Chlorophyll <i>b</i>
VI	430, 663	Chlorophyll <i>a</i> <sub>P276</sub>
VII	420, 663	Hydroxychlorophyll <i>a</i>
VIII	430, 663	Hydroxychlorophyll <i>a</i>
IX	430, 663	Chlorophyll <i>a</i>

\* tentative assignments

### 3.3.3.1. Assignment of peak I

Peak I eluted at 30.1 min (Figure 3.6.A) and was present only in pigment extracts from the OtV5-infected cultures; it was not detected at any time in the non-infected cultures. Peak I had UV/vis absorption spectra with maxima at 427 nm and 653 nm and a secondary absorption band at 462 nm (Table 3.1). During LC/MS, ions associated with peak I were determined as those that had maximum intensities coincident with the UV/vis absorption maximum at 660 nm for the peak. This approach was particularly relevant for peaks I and II, as their low relative intensity led to co-eluting ions of significant abundance in the mass spectrum.

Using post column addition of acid to demetallate the chlorins before they entered the mass spectrometer, and hence improve their ionisation (Airs and Keely 2000), peak I gave rise to major ions at  $m/z$  905 and 873. In the absence of acid, a major ion at  $m/z$  927 was observed, consistent with the mass of component  $m/z$  905 with a central chelating magnesium (+22 Da).

Using post-column acidification, the demetallated ion at  $m/z$  905, on resonance induced fragmentation, gave rise to major ions in the MS<sup>2</sup> spectra at: a)  $m/z$  627 via the loss of  $m/z$  278 indicating esterification by phytol; b)  $m/z$  567 from  $m/z$  627, via the loss of  $m/z$  60 indicating the presence of a CO<sub>2</sub>Me group [M+H-Mg-phytyl-HCO<sub>2</sub>Me]<sup>+</sup>; c)  $m/z$  435 and d) minor ions including  $m/z$  595 [M+H-Mg-phytyl-MeOH]<sup>+</sup> (Figure 3.7.A).

The MS<sup>2</sup> spectra of the ion at  $m/z$  873 in full MS gave rise to a major ion at  $m/z$  535 and minor ions including  $m/z$  595, 507, 478, 435 and 407 (Figure 3.7. B). The MS<sup>2</sup> spectra of both of these ions ( $m/z$  905 and 873) gave the same pattern of losses (Figure 3.7) but with a mass difference

of 32 Da, indicating that the ion at  $m/z$  873 resulted from the ion at  $m/z$  905 through loss of a MeOH group, which is constant with the fragmentation of a methoxy group at position C13<sup>2</sup> (Franklin et al. 2012). Both major ions arising from peak I (at  $m/z$  905 and  $m/z$  873), after the losses of phytol and CO<sub>2</sub>Me, fragmented in the pattern of loss: 28 Da, 28 Da and 72 Da, which are common losses of chlorophyll derivatives during MS<sup>n</sup>, indicating that peak I resulted from a chlorophyll derived product (Airs and Keely 2002).

The ions at  $m/z$  435 and  $m/z$  407, common to the MS<sup>2</sup> spectra of both parent ions (Figure 3.7), are 2 Da higher than expected for the corresponding macrocycle masses of pyropheophorbide *a* (433) or pyro methoxychlorophyll *a* (405). However the demetallated mass of MeO-chl-*a* ( $m/z$  901) is 4 Da heavier than the major ion at  $m/z$  905. The component is therefore assigned as a methoxychlorophyll *a*-like allomer (MeO-chl-*a*-like).

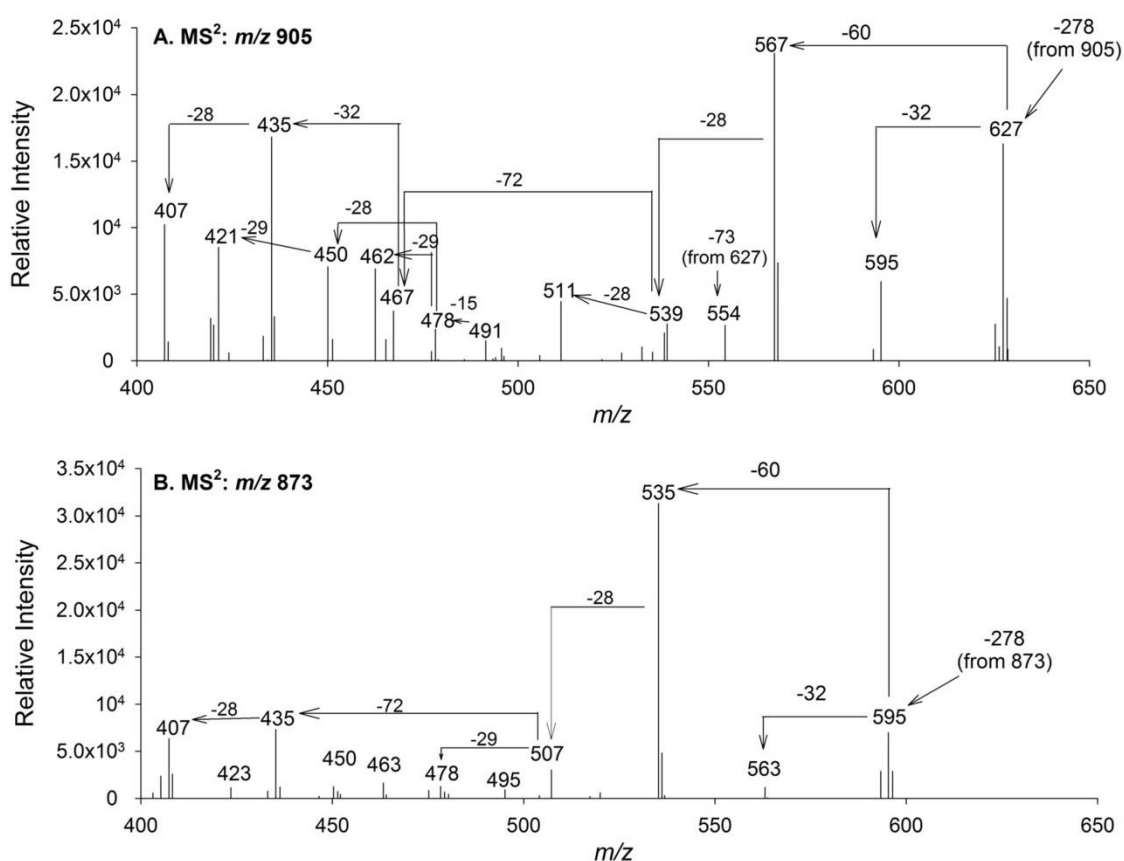


**Figure 3.7.** MS<sup>2</sup> spectra of ions; A.  $m/z$  905 and B.  $m/z$  873 resulting from peak I in OtV5-infected *Ostreococcus tauri* pigment extract.

### 3.3.3.2. Assignment of peak II

Peak II gave rise to a UV/vis absorption spectrum with maxima at 430 nm and 658 nm, as expected for a chl-*a* allomer but with an additional absorption band at 481 nm (Table 3.1). From LC/MS analysis with post-column acidification, peak II gave rise to one major ion at  $m/z$  887  $[M+H-Mg]^+$ . The MS<sup>2</sup> spectra of the ion at  $m/z$  887 contained a major ion at  $m/z$  593 (Figure 3.8), corresponding to a loss of 294 Da. Notably, the phytol chain of chlorophylls *a* and *b* usually cleaves at the C-O bond during MS/MS resulting in the loss of a fragment of 278 Da. The mass of the entire phytol constituent is, however 295 Da. It is possible therefore, that peak II was a chlorin esterified by phytol, but in such a stereochemical configuration to promote fragmentation via the loss of 294 Da instead of 278 Da. Notably, the MS<sup>2</sup> spectrum shows a less abundant ion at  $m/z$  609, arising from the loss of 278 Da from the parent ion, providing support for the assignment of phytol as the esterifying alcohol, and indicating that both fragmentation mechanisms were taking place. It is important to note that the relative intensity of the MS<sup>2</sup> spectrum was low, and therefore the spectrum must be interpreted cautiously. Other fragmentations indicate the presence of a CO<sub>2</sub>Me group (60 Da loss to produce an ion at  $m/z$  533), and HO-substituent (18 Da loss to produce an ion at  $m/z$  575), consistent with a hydroxychlorophyll *a* structure. The component is therefore tentatively assigned as a hydroxychlorophyll *a*-type structure with unusual stereochemistry. Hence peak II remains an unidentified hydroxychlorophyll *a*-like allomer (HO-chl-*a*-like).

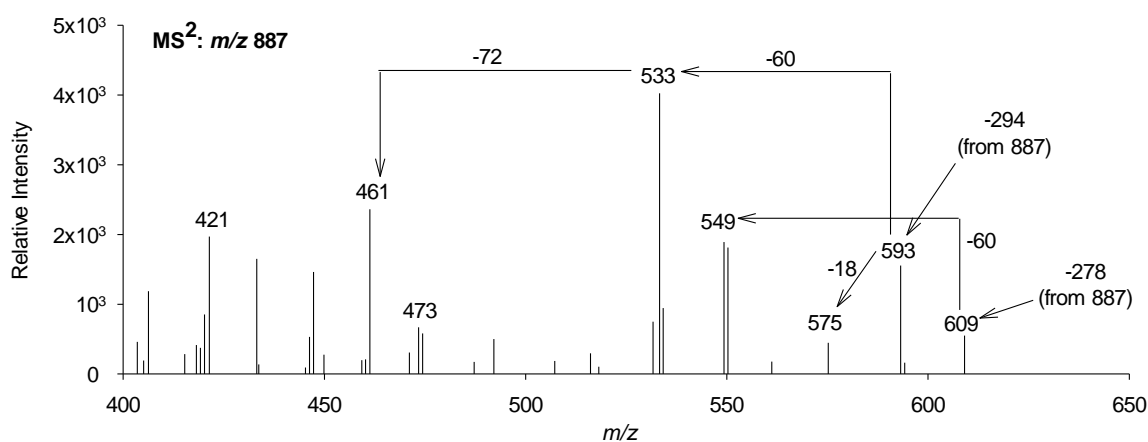


**Figure 3.8.** MS<sup>2</sup> spectra of the major ion at  $m/z$  887 resulting from peak II in OtV5-infected *Ostreococcus tauri* pigment extract.

### 3.3.3.3. Assignment of peaks III and IV

Peaks III and IV eluted in the region expected for chlorophyll *b* allomers, directly prior to chl-*b*, however their UV/vis maxima were as expected for chlorophyll *a* allomers, with maxima at 430 nm and 660 nm, and not consistent with chl-*b* allomers (Hyvärinen and Hynninen 1999). This may be due to differences in the solvents used in the present study (methanol dominated) and those used for analysis of chl-*b* allomers by Hyvärinen and Hynninen (1999) (hexane dominated), which is known to affect the UV/vis spectra of pigment extracts (Roy et al. 2011).

Both peaks III and IV gave rise to major ion at  $m/z$  901 (with post-column addition of acid) which corresponded to  $[M+H-Mg]^+$  for 13<sup>2</sup>-hydroxychlorophyll *b* (Table 3.2). The MS<sup>2</sup> spectra of the ion at  $m/z$  901 gave rise to major ions at  $m/z$  883 and 605 which corresponded to  $[M+H-Mg-C_{20}H_{38}]^+$ ,  $[M+H-Mg-H_2O]^+$  and  $[M+H-Mg-H_2O-C_{20}H_{38}]^+$  respectively. These losses of 18 Da correspond to H<sub>2</sub>O, which is typical of hydroxy components (Hyvärinen and Hynninen 1999, Walker et al. 2003). Peaks III and IV were assigned as 13<sup>2</sup>-hydroxychlorophyll-*b* and its epimer. The assignment of these peaks as hydroxychlorophyll *b* allomers highlights the importance of confirming assignments with LC/MS/MS as the UV/vis spectrum alone can be misleading. Although the UV/vis spectra of peaks III and IV were strong, the possibility that the UV/vis spectra detected arose due to chl-*a*-like co-elutions cannot be ruled out.

### 3.3.3.4. Assignment of peak VI

Peak VI had UV/vis absorption spectra as expected for a component structurally similar to chl-*a* (Airs et al. 2001a) (Table 3.1). From LC/MS/MS with post-column addition of acid, peak VI gave rise to a major ion at  $m/z$  869 corresponding to  $[M+H-Mg]^+$  (Table 3.2). On resonance induced fragmentation, the ion at  $m/z$  869, gave rise to  $m/z$  593 in the MS<sup>2</sup> spectrum (Table 3.2), equating to a loss of 276 Da indicating an extra double bond in the phytol chain. The component at peak VI is therefore identified as a biosynthetic precursor to chlorophyll *a* (Rüdiger 2006), chlorophyll *a*<sub>P276</sub>. This component has been detected previously in *Thalassiosira pseudonana*, *Emiliania huxleyi* (Franklin et al. 2012) and *Pavlova gyrams* (Bale 2010).

### 3.3.3.5. Assignment of peaks VII and VIII

Peak VIII had UV/vis absorption spectrum identical to chl-*a* (maxima at 430 and 660 nm) however, the UV/vis absorption spectrum of peak VII had maxima at 420 and 663 nm. This 10 nm shift to the blue of the Soret band maxima has previously been associated with HO-chl-*a* (chapter 2.6.1) and MeO-chl-*a* (Franklin et al. 2012). Peaks VII and VIII both gave rise to major ions at  $m/z$  887 and 869, corresponding to  $[M+H-Mg]^+$  and  $[M+H-Mg-H_2O]^+$  respectively for

$13^2$ -hydroxychlorophyll *a* (Table 3.2). On fragmentation, a number of ions were observed in the MS<sup>2</sup> spectra consistent with the hydroxychlorophyll *a* structure (Table 3.2) (Jie et al. 2002). Peaks VII and VIII are therefore assigned as  $13^2$ -hydroxychlorophyll *a* and its epimer.

**Table 3.2.** Most abundant ions in MS/MS of allomers eluting before chlorophyll *a* in *O. tauri* samples.

Relationship to molecular ion	Structural assignment	Peak no.							
		I	II	III	IV	V	VI	VII	VIII
MH	[M+H] <sup>+</sup>	927		923	923	907			909
MH -22	[M+H-Mg] <sup>+</sup>	905	887	901	901	885	869	887	887
MH -32	[M+H-MeOH] <sup>+</sup>	873							
MH-32-278-60	[M+H-MeOH-C <sub>20</sub> H <sub>38</sub> -CO <sub>2</sub> Me] <sup>+</sup>	535							
MH -22-278	[M+H-Mg-C <sub>20</sub> H <sub>38</sub> ] <sup>+</sup>	627		623	623			609	609
MH-22-294	[M+H-Mg-C <sub>20</sub> H <sub>38</sub> O] <sup>+</sup>		593						
MH -22-276	[M+H-Mg-C <sub>20</sub> H <sub>36</sub> ] <sup>+</sup>						593		
MH -22-278-60	[M+H-Mg-C <sub>20</sub> H <sub>38</sub> -HCO <sub>2</sub> Me] <sup>+</sup>	567							
MH -22-276-60	[M+H-Mg-C <sub>20</sub> H <sub>36</sub> -HCO <sub>2</sub> Me] <sup>+</sup>						533		
MH -22-18	[M+H-Mg-H <sub>2</sub> O] <sup>+</sup>			883	883				869
MH -22-18-278	[M+H-Mg-H <sub>2</sub> O-C <sub>20</sub> H <sub>38</sub> ] <sup>+</sup>			605	605			591	591
MH -22-278-18-60	[M+H-Mg-C <sub>20</sub> H <sub>38</sub> -H <sub>2</sub> O-HCO <sub>2</sub> Me] <sup>+</sup>							531	531
MH -22-294-18	[M+H-Mg- C <sub>20</sub> H <sub>38</sub> O-H <sub>2</sub> O] <sup>+</sup>		575						
MH-278-60	[M+H-C <sub>20</sub> H <sub>38</sub> -CO <sub>2</sub> Me] <sup>+</sup>	567							
MH-278-32	[M+H-C <sub>20</sub> H <sub>38</sub> -MeOH] <sup>+</sup>	595							

### 3.3.4. Chlorophyll alterations during viral infection versus nutrient limitation

#### 3.3.4.1. Chlorophyll *b* allomers during viral infection of *Ostreococcus tauri*

Hydroxychlorophyll *b* (HO-chl-*b*) and its epimer (HO-chl-*b'*) occurred in non-infected cultures with a HO-chl-*b* to chl-*b* ratio of  $0.027 \pm 0.003$ . The ratio of HO-chl-*b* increased relative to chl-*b* during OtV5-infection to a maximum of  $0.73 \pm 0.06$  at 48 hpi (Figure 3.9). The ratio of HO-chl-*b'* to chl-*b* did not increase above the non-infected culture which may be due to its low abundance compared to HO-chl-*b*. This is the first report of chlorophyll *b* allomers increasing with viral infection.

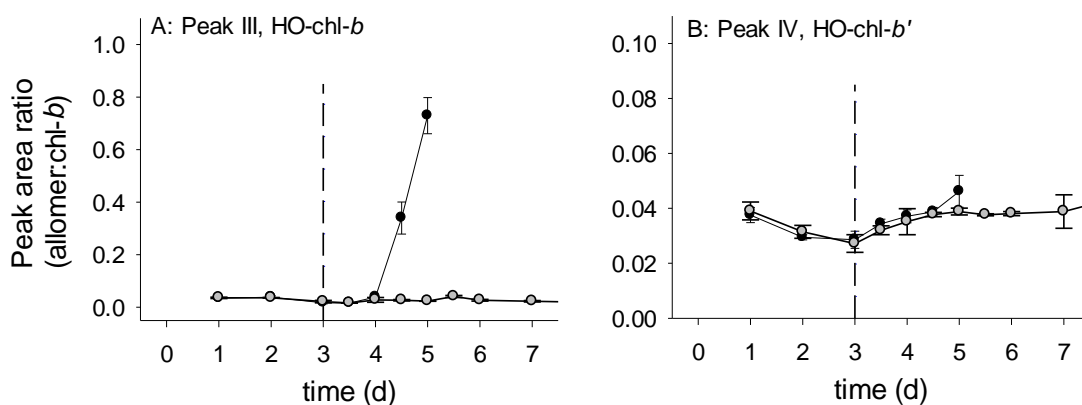


**Figure 3.9.** Ratios of chlorophyll *b* allomers to chl-*b* in OtV5-infected ●, and non-infected ○, *O. tauri* cultures including (A) hydroxychlorophyll *b* and (B) hydroxychlorophyll *b'*. - - - indicates time of virus addition. Mean and SE bars shown ( $n=3$ ).

#### 3.3.4.2. Chlorophyll *a* allomers during viral infection of *Ostreococcus tauri*

Pigment samples from OtV5-infected cultures contained methoxychlorophyll *a*-like (MeO-chl-*a*-like) and hydroxychlorophyll *a*-like allomers (HO-chl-*a*-like), evident at 36 and 48 hours post-infection (hpi) with average allomer to chl-*a* ratios of  $0.015 \pm 0.003$  and  $0.011 \pm 0.002$  respectively ( $n=6$ ) (Figure 3.10.A&B). The dominant chl-*a* allomer produced during viral infection was hydroxychlorophyll *a*. HO-chl-*a* and its epimer reached their maxima of  $0.110 \pm 0.008$  and  $0.08 \pm 0.009$  respectively (equal to 26-fold and 78-fold increases) at 48 hpi (Figure 3.10, C&D), when 99% of the *O. tauri* population had been lysed by OtV5. At this time, non-infected cultures maintained low levels of HO-chl-*a* of  $0.004 \pm 0.000$ .

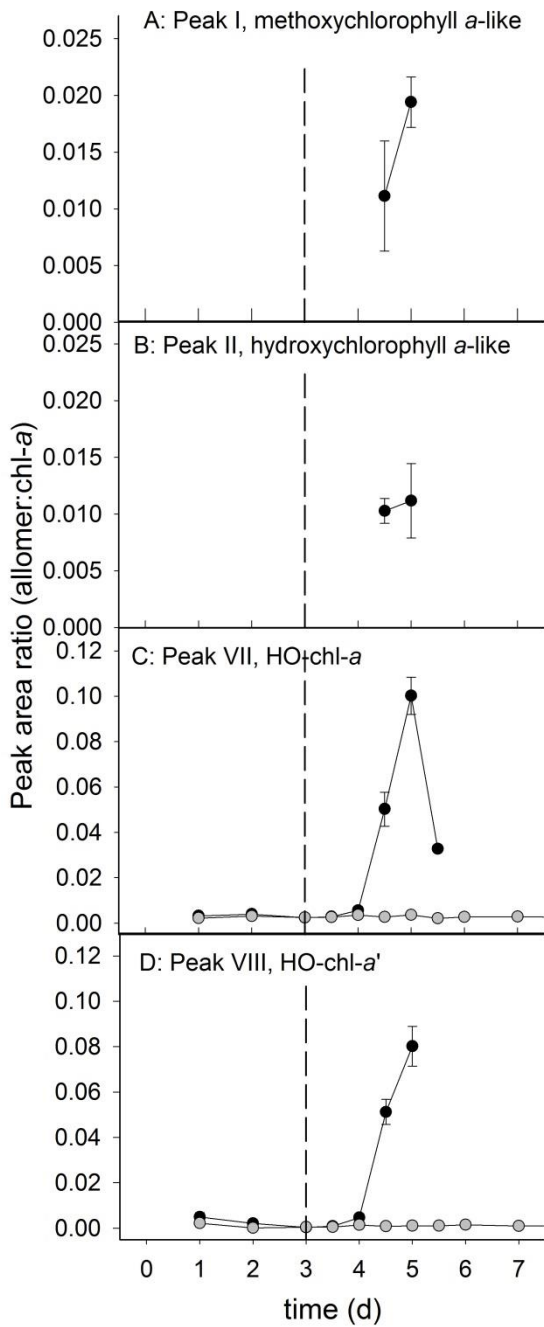


**Figure 3.10.** Ratios of chlorophyll a allomers to chl-a in OtV5-infected ● and non-infected ○ *O. tauri* cultures including (A) methoxychlorophyll a-like allomer, (B) HO-chl-a-like allomer, (C) hydroxychlorophyll a and (D) hydroxychlorophyll a'. - - - indicates time of virus addition. Mean and SE bars shown (n=3).

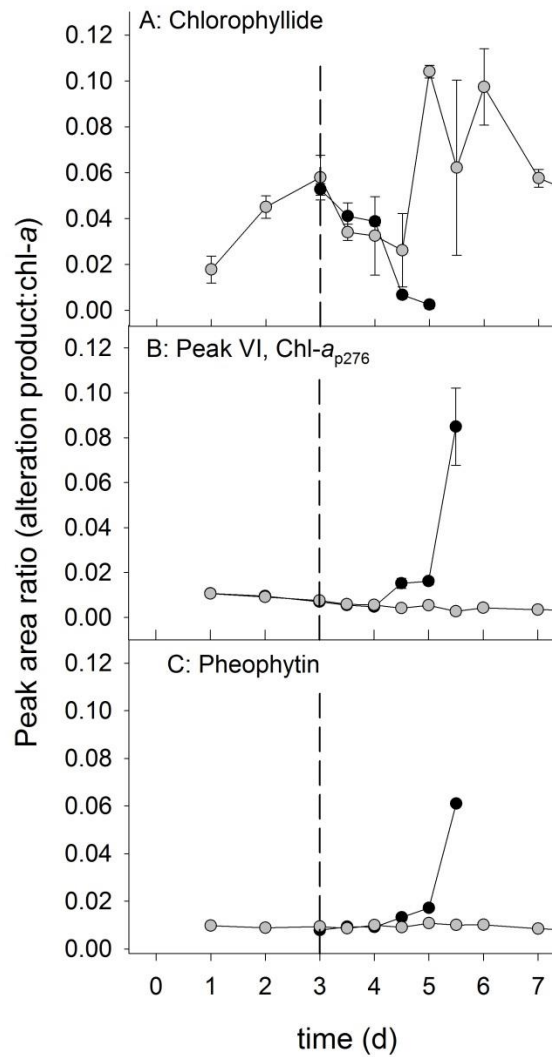


**Figure 3.11.** Ratios of chlorophyll a alteration products to chl-a in viral-infected ● and non-infected ○ *O. tauri* cultures including (A) chlorophyllide a, (B) chl-a<sub>p276</sub> and (C) pheophytin. - - - indicates time of virus addition. Mean and SE bars shown (n=3).

Hydroxychlorophyll *a* has been reported previously to increase during viral infection of *E. huxleyi* CCMP 1516 (Bale et al. 2013); presented as an increase of approximately 200%, from 0.11 to 0.33 fg cell<sup>-1</sup>. The change in the ratio of HO-chl-*a* to chl-*a* during *E. huxleyi* viral infection can be calculated as ~0.06 at the beginning of population decline (4 days post infection), reducing to ~0.04 after the loss of 94% of the population (16 days post-infection). Notably this decline period was 3 times longer than mesocosm studies of *E. huxleyi* bloom infection, which recorded the loss of 95% of the population 5 days after the maximum population density (Bratbak et al. 1993, Vardi et al. 2012). Although the *E. huxleyi* viral infection was extended, similar levels of hydroxychlorophyll *a* (relative to chl-*a*) were detected during viral infection of *E. huxleyi* as in *O. tauri*.

Less of the chl-*a* alteration product chlorophyllide was detected in OtV5-infected cultures, compared to non-infected cultures (Figure 3.11.A), at 36 and 48 hpi. The chlorophyll *a* precursor chl-*a*<sub>p276</sub> increased relative to chl-*a* from 36 hpi from 0.007±0.000 to a maximum of 0.102±0.008 (Figure 3.11, B), this peak may be due to the re-growth of a small residual, virus-resistant *O. tauri* population (Figure 3.4.A), as previously described by Thomas et al. (2011).

Pheophytin increased relative to the non-infected cultures by 36 hpi, up to a maximum of 0.069±0.001 (n=3), 60 hpi, compared to 0.011±0.001 of non-infected cultures (Figure 3.11, C). Pheophytin *a* also increased in EhV86 infected *E. huxleyi* cultures, relative to senescent cultures during the late stage of population decline, 12 days after addition of the virus (Bale et al. 2013).

Chlorophyll *a* allomers (relative to chl-*a*) began to increase above the level of the control cultures 24 hpi. This was co-incident with the start of the decline in  $F_v/F_m$  and increase in SYTOX-positive cells. Hydroxychlorophyll *b* and pheophytin *a* began to increase (relative to chl-*a*) later, at 36 hpi. This was still prior to the detected increase in CM-H<sub>2</sub>DCFDA-positive cells which occurred from 48 hpi. Therefore, this data does not suggest a link between an increase in un-scavenged cellular reactive oxygen species detected (CM-H<sub>2</sub>DCFDA-positive cells) and production of chlorophyll oxidation products. Interestingly a meso-chlorophyll *a* allomer was found to form in aged cyanobacterial cultures under anoxic conditions (Louda et al. 2011). However as the ROS detection method used in the present study appeared to have limited sensitivity, no definite conclusions can be drawn on the link between ROS and chlorophyll allomerization.

### 3.3.4.3. Chlorophyll *b* allomers during *Ostreococcus tauri* growth and senescence

As well as being detected during viral infection, hydroxychlorophyll *b* and its epimer were also detected throughout the growth (days 0 to 15) and senescence (days 15 to 29) of *O. tauri*. The HO-chl-*b* to chl-*b* ratio increased during the senescent phase to a maximum of  $0.075 \pm 0.013$  on day 29 (Figure 3.12). This increase is small compared to the maximum HO-chl-*b* to chl-*b* ratio reached during viral infection ( $0.73 \pm 0.06$ ).

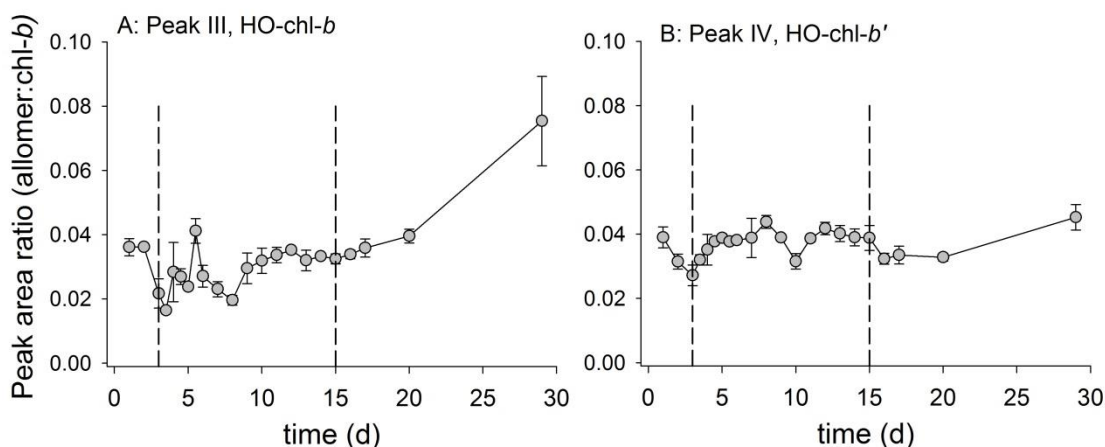


**Figure 3.12.** Ratios of chl-*b* allomers to chl-*b* in growing (days 0 to 15), and senescent (days 15 to 29) *Ostreococcus tauri* cultures including (A) hydroxychlorophyll *b* and (B) hydroxychlorophyll *b*'. Mean and SE bars shown ( $n=3$ ).

### 3.3.4.4. Chlorophyll *a* allomers during *Ostreococcus tauri* growth and senescence

All chlorophyll *a* allomers detected increased relative to chl-*a* during the senescent phase, between days 20 and 29 (Figure 3.13). HO-chl-*a* and HO-chl-*a*' reached maxima of  $0.0074 \pm 0.0005$  and  $0.0072 \pm 0.0007$  (increases of 2-fold and 7-fold respectively from day 5). These levels of the HO-chl-*a* to chl-*a* ratio were small compared to maximum levels during viral infection ( $0.110 \pm 0.008$ ). An increase in the ratio of hydroxychlorophyll *a* to chl-*a* has been reported previously during senescence of the diatom *Thalassiosira pseudonana* (at ratio  $\sim 0.05$ , Franklin et al., 2012). Whereas, hydroxychlorophyll *a* was reported to not increase during senescence of *E. huxleyi* cultures (Franklin et al. 2012, Bale et al. 2013). These study species belong to different classes and as such have widely diverse physiology which may affect the intracellular processes leading to allomer formation, which may explain the different responses observed. The variability in the occurrence and abundance relative to chl-*a* between taxa (so far measured) highlights the challenges in trying to make general predictions for phytoplankton.

Levels of chlorophyllide (relative to chl-*a*) generally increased over the study period (Figure 3.14.A) from  $0.045 \pm 0.005$  to  $0.28 \pm 0.06$ , a 6-fold increase. This was in direct contrast to the OtV5-infected cultures, where the chlorophyllide to chl-*a* ratio was reduced. Chlorophyllide is a traditional marker for senescence (Jeffrey and Hallegraeff 1987, Spooner et al. 1994a, Louda et al. 1998, Bale et al. 2011). The de-esterification of chl-*a* to chlorophyllide *a* by activity of the enzyme chlorophyllase is species specific (Jeffrey and Hallegraeff 1987, Louda et al. 1998) and known to be formed in low quantities (relative to chl-*a*) in a few prasinophyte species (Jeffrey and Hallegraeff 1987). *Tetraselmis chui* was found to form chlorophyllide with a chlorophyllide to chl-*a* ratio of up to 0.01 during extraction in acetone. (Jeffrey and Hallegraeff 1987). The proportion of chlorophyllide (relative to chl-*a*) found in *O. tauri* cells was much greater, up to  $0.28 \pm 0.06$  during senescence.

Pheophytin *a* increased only at the late stages of senescence between day 20 and day 29 (Figure 3.14.C) and maximum levels were low when compared to OtV5-infected cultures. Pheophytin *a*, i.e. demetallated chl-*a*, is formed under acidic conditions and has been found previously in association with senescence of *Phaeodactylum tricornutum* (Spooner et al. 1994b) and *Thalassiosira weissflogii* (Spooner et al. 1994c) but this is the first such association in a prasinophyte species and picoeukaryote.

The component chl-*a*<sub>P276</sub> was found in the highest concentrations relative to chl-*a* in exponentially growing *O. tauri*, (days 0 to 3, when  $\mu \geq 0.69$ , Figure 3.14.B), consistent with its assignment as a biosynthetic precursor to chl-*a*. There was also an increase in the chl-*a*<sub>P276</sub> to chl-*a* ratio between days 20 and 29 which indicates that the remaining *O. tauri* population was increasing its synthesis of chl-*a*. This is reflected in the increase in chl-*a* content per cell on day 29 (Figure 3.4.B) and is expected for nutrient limited (N) or starved (P) *Ostreococcus* (Kulk et al. 2013).

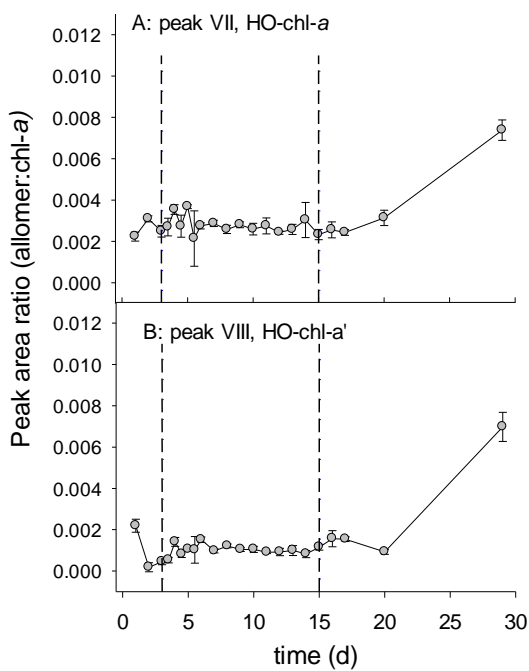


**Figure 3.13.** Ratios of allomers to chlorophyll *a* in growing (days 0 to 15) and senescent (days 15 to 29) *Ostreococcus tauri* cultures including (A) hydroxychlorophyll *a* and (B) hydroxychlorophyll *a*'. Mean and SE bars shown ( $n=3$ ).

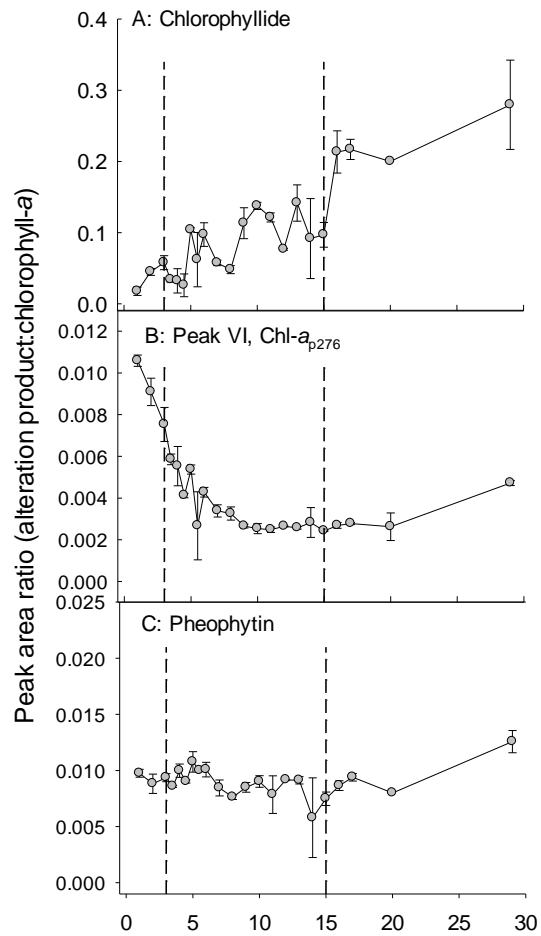


**Figure 3.14.** Ratios of chlorophyll *a* alteration products to chl-*a* in growing (days 0 to 15) and senescent (days 15 to 29) *Ostreococcus tauri* cultures including (A) chlorophyllide *a*, (B) chl-*a*<sub>P276</sub> and (C) pheophytin. Mean and SE bars shown ( $n=3$ ).

### 3.4. Chapter III Conclusions

During this work, indicators of viability were assessed during viral lysis and senescence of *Ostreococcus tauri*. Chlorophyll allomer production was compared during these two modes of death, and related to loss of membrane permeability and changes in un-scavenged cellular ROS. This work is the most detailed study of chlorophyll alteration to date during viral infection and senescence of a cultured phytoplankton.

The unidentified methoxychlorophyll *a*-like (MeO-chl-*a*-like) and hydroxychlorophyll *a*-like (HO-chl-*a*-like) allomers were found solely in association with viral infection of *O. tauri* and not during senescence. These allomers are potentially biomarkers for viral infection in natural phytoplankton populations. More work needs to be undertaken with additional cultures to chemically assign these components and to assess whether these markers are common across strains, species and taxa. This would establish the usefulness of the MeO-chl-*a*-like and HO-chl-*a*-like allomers as biomarkers for viral infection.

Hydroxychlorophyll *b* (HO-chl-*b*) was found in *O. tauri* cells undergoing viral infection and senescence. Hydroxychlorophyll *a* (HO-chl-*a*) was produced during viral infection of *O. tauri*, starting 24 hours post inoculation (hpi), with a maximum 16-fold increase in the ratio of HO-chl-*a* to chl-*a*, at 48 hpi (day 5). The allomers HO-chl-*a* and HO-chl-*b* were the earliest to be produced during viral infection, before the major lysis event, closely followed by the MeO-chl-*a*-like and HO-chl-*a*-like allomers.

In the senescent populations, HO-chl-*b* was the first to increase, just before the decline of the *O. tauri* population, followed by HO-chl-*a*. Hydroxychlorophyll *a* was also elevated relative to chl-*a*, but to a lesser extent during senescence of *O. tauri*, compared to viral infection. The production of chlorophyll allomers in *O. tauri* cells during viral infection and senescence are clearly different. Therefore, it may be possible for chlorophyll allomers to be used as indicators of mode of phytoplankton mortality. However further work using more strains and species is required to assess if these differences in allomer production due to mode of mortality are preserved across taxa.

During viral infection the percentage of SYTOX-positive cells increased from 24 hpi and ROS-positive cells increased from 48 hpi. The increase in percentage of cells with permeable membranes occurred prior to the increase in allomers (relative to chlorophyll), which was

delayed until 36 hpi. Therefore during *O. tauri* viral lysis, membrane permeability was an earlier marker of cell death than chlorophyll allomers.

In the senescence study a clear peak in SYTOX-positive cells occurred on day 12, followed by a peak in CM-H<sub>2</sub>DCFDA-positive cells (day 15), just prior to the start of population decline (day 16, Figure 3.4). The ratios of chlorophyll allomers to chlorophyll did not increase until the later part of population decline (days 20-29). Therefore during *O. tauri* senescence, membrane permeability and increased un-scavenged cellular ROS were earlier markers of cell death than chlorophyll allomers.

Although CM-H<sub>2</sub>DCFDA had a limited response in this *O. tauri* study, differences were seen between infected and non-infected cells. Therefore it would be worthwhile optimising the most recent ROS detection method to *O. tauri* cells. Recently the ROS sensitive probe ',7'-dichlorodihydrofluorescein diacetate (DCFH-DA, Molecular probes) has been applied, in combination with fluorescence microscopy and spectrofluorophotometry, to phytoplankton taxa including cyanobacteria (Rastogi et al. 2010, Wang et al. 2011, Rastogi et al. 2014), diatoms (Liu et al. 2012a, Xie et al. 2014) and chlorophytes (Liu et al. 2012b) but not to prasinophytes. This probe also requires cellular esterase activity to fluoresce which may limit its usefulness in studies of mortality as esterase activity may also be disrupted during cell death.

This study has exposed some features of the residual *O. tauri* population after the majority had been lysed by viral action. Sampling the surviving population would allow comparison with the original; interesting from an evolutionary perspective, but also to compare allomer production. If the *O. tauri* population which survived viral addition was grown and then left to senesce, would it produce the MeO-chl-*a*-like and HO-chl-*a* like allomers as seen under viral infection of the original population? Further, would the immune population produce these allomers in the presence of the OtV5 virus?

The allomer hydroxychlorophyll *a* has been associated with phytoplankton death in several previous incidences in culture studies, i.e. during *Thalassiosira pseudonana* senescence (Franklin et al. 2012) and *E. huxleyi* viral infection (Bale et al. 2013). Adding the elevated HO-chl-*a* during viral infection and senescence of *O. tauri* measured in this study, elevated HO-chl-*a* levels in phytoplankton populations should be considered an early indicator of ensuing death. Further, with additional work chlorophyll *a* allomers may also have the potential to indicate the mode of phytoplankton death.

## **Chapter IV**

### ***Field study time series***

# **Abundance of the oxidation product hydroxychlorophyll *a* and a chlorophyll *a* precursor during seasonal phytoplankton community progression in the Western English Channel**

*Aspects of this chapter have been published in:*

Steele DJ, Tarran GA, Widdicombe CE, Woodward EMS, Kimmance SA., Franklin DJ, and Airs RL. (2015). Seasonal changes of chlorophyll *a* allomers in the Western English Channel during 2012. *Progress in Oceanography*.

#### **4.1. Introduction**

If the detection of allomers is to be useful as an indicator of phytoplankton mortality, allomer occurrence and abundance must be assessed in the field, during natural phytoplankton turnover. To date, chlorophyll allomers have been measured in the marine environment during discrete research cruises (Chapter V, Walker and Keely 2004, Bale 2010) or in marine sediments (Tait et al. in review). The seasonality of allomer production with relation to phytoplankton population turnover has not been established.

In UK shelf seas, changing environmental conditions throughout the year drive the progression of the phytoplankton assemblage through both promotion and limitation of growth. Monitoring the phytoplankton assemblage over a yearly cycle allows the measurement of allomers during the growth and decline phases of many different phytoplankton groups and individual species. When ambient conditions are conducive for growth, phytoplankton species divide rapidly, creating blooms. These events are transient and phytoplankton populations decline with altered conditions, like environmental limitation (Alonso-Laita and Agustí 2006), viral infection (Jacobsen et al. 1996, Brussaard 2004) or zooplankton grazing (Baudoux et al. 2008). In the Western English Channel (UK), the productive spring period is typically characterised by a rapid depletion of nitrate. The duration of the spring bloom is therefore controlled by nitrate availability (Smyth et al. 2010) and its species composition is typically dominated by chain forming diatoms (Southward et al. 2004, Widdicombe et al. 2010). Thermal stratification of the

water column generally occurs in the summer period and a second bloom of smaller pennate or centric diatoms (e.g. *Pseudo-nitzschia* spp. or *Leptocylindrus* spp.) is usual (Widdicombe et al. 2010). A second productive period in autumn is typically induced in September by mixing of the water column, replenishing nitrate to the surface waters (Smyth et al. 2010).

The measurement of chlorophyll *a* allomers and other alteration products over an annual cycle may reveal patterns of occurrence linked to seasonal phytoplankton population turnover. Analysis of the population growth cycles is aided by the detection of chlorophyll *a*<sub>P276</sub> (chl-*a*<sub>P276</sub>), which is thought to be a precursor in the biosynthesis of chlorophyll *a* (Bale 2010). Although not an allomer, due to its structural similarity, chl-*a*<sub>P276</sub> has previously been detected during analysis of chlorophyll *a* allomers (Franklin et al. 2012). Measurement during a growth cycle of the picoeukaryote phytoplankton, *Ostreococcus tauri*, revealed an association of the chl-*a*<sub>P276</sub> to chl-*a* ratio with population growth rate (Chapter 3). It therefore may be a useful proxy for phytoplankton population growth.

This work aimed to resolve the sources of the chlorophyll allomer hydroxychlorophyll *a* (HO-chl-*a*) in water column particulates and surface sediment in the Western English Channel, during the seasonal turnover of the phytoplankton assemblage. Changes in particulate pelagic allomer abundance (relative to chlorophyll *a*) were related to temporal changes in phyto- and microzooplankton community structure, nutrient concentration, temperature, and light levels.

## 4.2. *Material and Methods*

### 4.2.1. *Study site and Sampling Protocol*

Samples for this study were collected between 9<sup>th</sup> January and 18<sup>th</sup> December 2012 and analysed as part of the long-term oceanographic and marine biodiversity time series study at the Western Channel Observatory (WCO, [www.westernchannelobservatory.org.uk](http://www.westernchannelobservatory.org.uk)), from station L4, in the Western English Channel, 10 km south of Plymouth Breakwater, England, UK (50° 15.00' N, 4° 13.02' W, Figure 4.1). Surface photosynthetically active radiation (PAR) was calculated from a hyperspectral irradiance sensor (Satlantic) and monitored continuously from an autonomous buoy moored at station L4 (for details see methods chapter 7.3.1). Rainfall measurements from Camborne MET station (50° 21.30' N, 5° 3.00' W), ~80 km from station L4 (Figure 4.1), were accessed from [www.metoffice.gov.uk](http://www.metoffice.gov.uk).

Water samples were collected weekly (weather permitting) using Niskin bottles (10 L) mounted on a rosette and temperature was measured by weekly CTD casts deployed from the Plymouth Marine Laboratory vessel, RV Quest. Water samples were collected from 2, 10, 25 and 50 m depth and sampled for analysis of nutrients (chapter 7.3.2), pigments from pelagic particulates (chapter 7.6.1.2) and surface sediment (chapter 7.6.1.3). Chromatograms obtained by HPLC for the routine analysis of pigment samples (Zapata et al. 2000) were re-processed specifically for the investigation of chlorophyll alteration products.

Two methods were used to enumerate phytoplankton in different pico-, nano- and microplankton size fractions. Firstly, fresh samples from 2, 10, 25 and 50 m depth were analysed on an Accuri C6 flow cytometer (for details see methods chapter 7.3.3.1). Cells were separated into 7 groups according to their distinct red and orange fluorescence and side scatter profiles; *Synechococcus*, picoeukaryotes, coccolithophores, cryptophytes, *Phaeocystis* spp. single cells, small dinoflagellates (< 20 µm) and other nanoeukaryotes. The flow cytometry data for the *Phaeocystis* spp. single cells and small dinoflagellates are speculative, and relied on verification of the significant presence of *Phaeocystis* spp. or small dinoflagellates by microscopy at the same time as the appearance of clusters of events in flow cytometric analysis plots.

The second method considered only plankton sampled from 10 m depth which were fixed upon collection (see methods chapter 7.3.3.2). Phytoplankton were identified by microscopy to species level where possible, following the protocol detailed in Widdicombe et al. (2010) and enumerated using the Utermöhl (1958) technique. Autotrophs were divided into 5 functional groups; diatoms, coccolithophores, dinoflagellates, *Phaeocystis* spp. and phytoflagellates, which includes 2-6 µm flagellated chlorophytes and prasinophytes (Holligan and Harbour 1977). The microzooplankton groups: heterotrophic dinoflagellates, ciliates and zooflagellates were also identified and enumerated. Biomass was calculated from measurements of the average dimensions of each species which were then converted to cellular volumes (Kovalá and Larrance 1966) and carbon content (Menden-Deuer and Lessard 2000). Microscopy and flow cytometry data were obtained from the WCO repository ([www.westernchannelobservatory.org.uk](http://www.westernchannelobservatory.org.uk)).

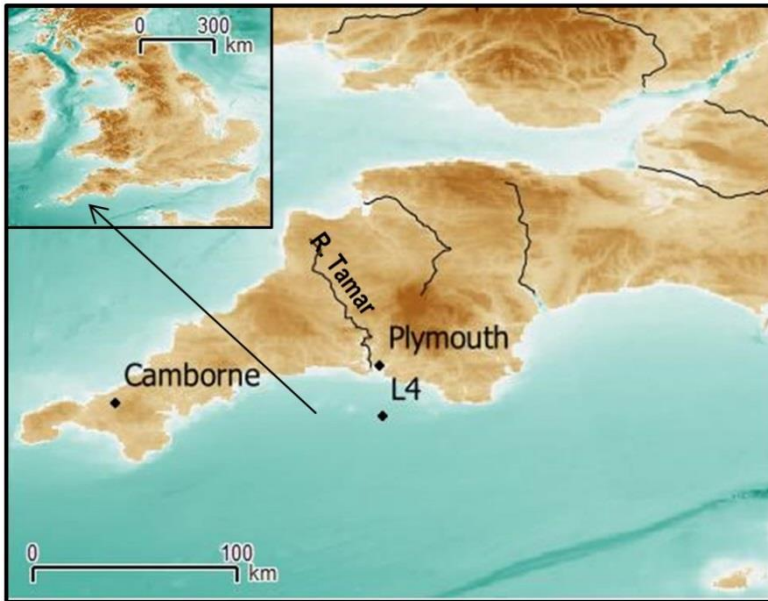


**Figure 4.1.** Location of station L4 within the western English Channel, UK. Bathymetry map derived from [www.gebco.net](http://www.gebco.net).

### 4.3. Results and Discussion

#### 4.3.1. Physical conditions

Conditions at L4 in early 2012 were typical for the winter season, with temperature consistent throughout the water column at  $\sim 10^{\circ}\text{C}$  from January to May (Figure 4.2.A., Smyth et al., 2010). By mid-May the surface and bottom temperatures differed by  $+0.46^{\circ}\text{C}$  (Figure 4.2.A), indicating the existence of an early summer thermocline (Smyth et al. 2010). Although this is consistent with the expected timing for the onset of stratification, the water column was re-mixed by storm events in the spring and summer months (Figure 4.2.B); in April, June and August rainfall was  $>200\%$  higher than historical averages (Figure 4.2.B). Wind speeds of over  $15\text{ m s}^{-1}$  were recorded in April, June, September and October (Figure 4.2.C). These periods of high wind speed indicated storm events that re-mixed the water column. During the months of increasing water temperature (from April) the monthly average photosynthetically active radiation (PAR) levels were not greater than the average winter levels (Figure 4.2.D). Around a 10-fold increase is expected in daily PAR levels from January to July (Smyth et al. 2010), hence the physical conditions during the spring months of March to May were not typical of the L4 spring bloom period compared to historical data.

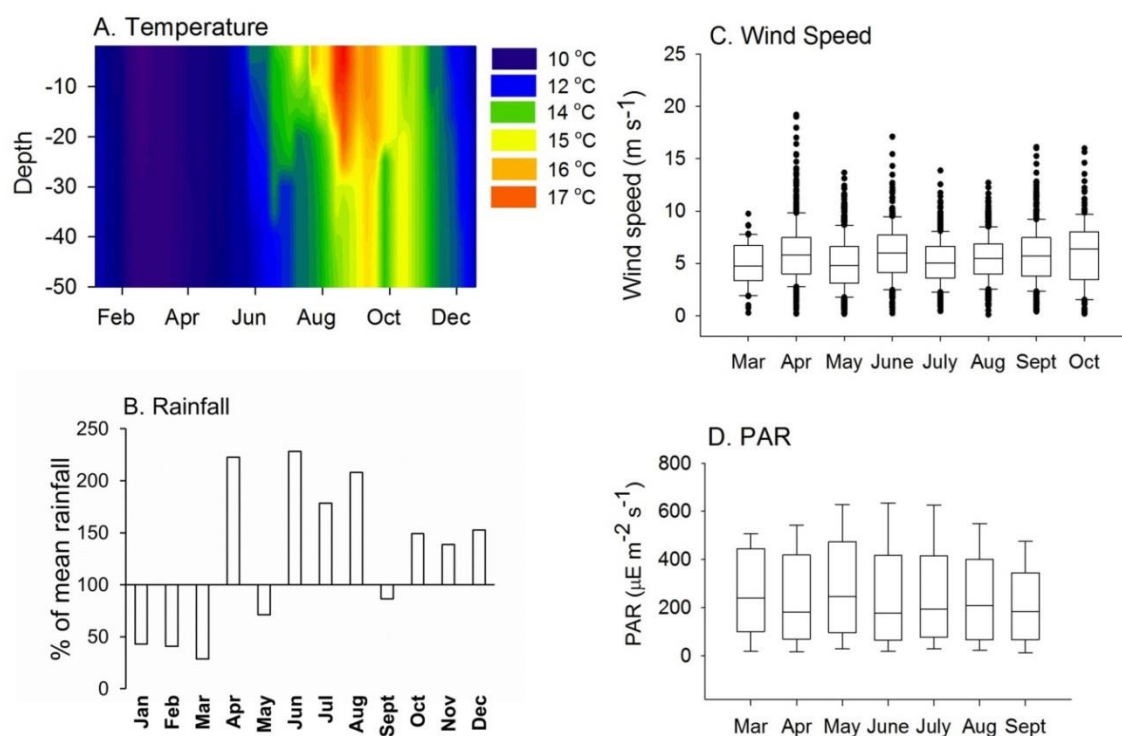


**Figure 4.2.** (A) Depth profile of water temperature at station L4, Western English Channel, UK during 2012. (B) Total monthly rainfall at Camborne MET station ( $50^{\circ} 21.30' \text{ N}$ ,  $5^{\circ} 3.00' \text{ W}$ ) during 2012 as a percentage of the average monthly total between 1978 and 2013. Data from MET office ([www.metoffice.gov.uk](http://www.metoffice.gov.uk)) contains public sector information licensed under the Open Government License v1.0. (C) Monthly averages of resultant wind speed ( $\text{m s}^{-1}$ ) at L4. (D) Surface Photosynthetically Active Radiation (PAR) at L4. Box represents the interquartile range. Bars represent the 10<sup>th</sup> and 90<sup>th</sup> quartiles. Points represent all outliers.

#### 4.3.2. Nutrient concentrations at L4 during 2012

Nitrate concentrations during 2012 showed a typical annual pattern for the L4 station, with a maximum of  $7.9 \mu\text{M}$  in January (Figure 4.3.A). Nitrate then declined rapidly to below the detection limit ( $0.02 \mu\text{M}$ ) during the spring bloom period in April (Southward et al. 2004, Smyth et al. 2010). During May and July surface nitrate concentration ranged between  $0.2 \mu\text{M}$  and  $2.6 \mu\text{M}$ . Summer peaks in surface nitrate concentration, up to  $2.26 \mu\text{M}$ , have previously been associated with elevated inputs from the nearby River Tamar (Figure 4.1) after high rainfall (164% of the summer time historical average) (Rees et al. 2009).

Phosphate and silicate lagged the nitrate trend by 1 to 2 months, with maximum concentrations in February of  $0.62 \mu\text{M}$  and  $4.06 \mu\text{M}$  respectively (Figures 4.3.B&C), which are as expected for L4 (Southward et al. 2004, Smyth et al. 2010). During the spring and summer months,

concentrations of silicate and phosphate were reduced in the surface waters, however, concentrations at 25 and 50 m depth increased either due to remineralisation from grazers (Fileman et al. 2010) or the establishment of the seasonal thermocline (Smyth et al. 2010). As expected, the winter silicate maximum at L4 of  $5.54 \mu\text{M}$  occurred in December (Figure 4.3.C) and has been attributed to an alternate source of silicate other than Atlantic water, which is most likely to be outflow from the River Tamar (Figure 4.1) (Smyth et al. 2010).

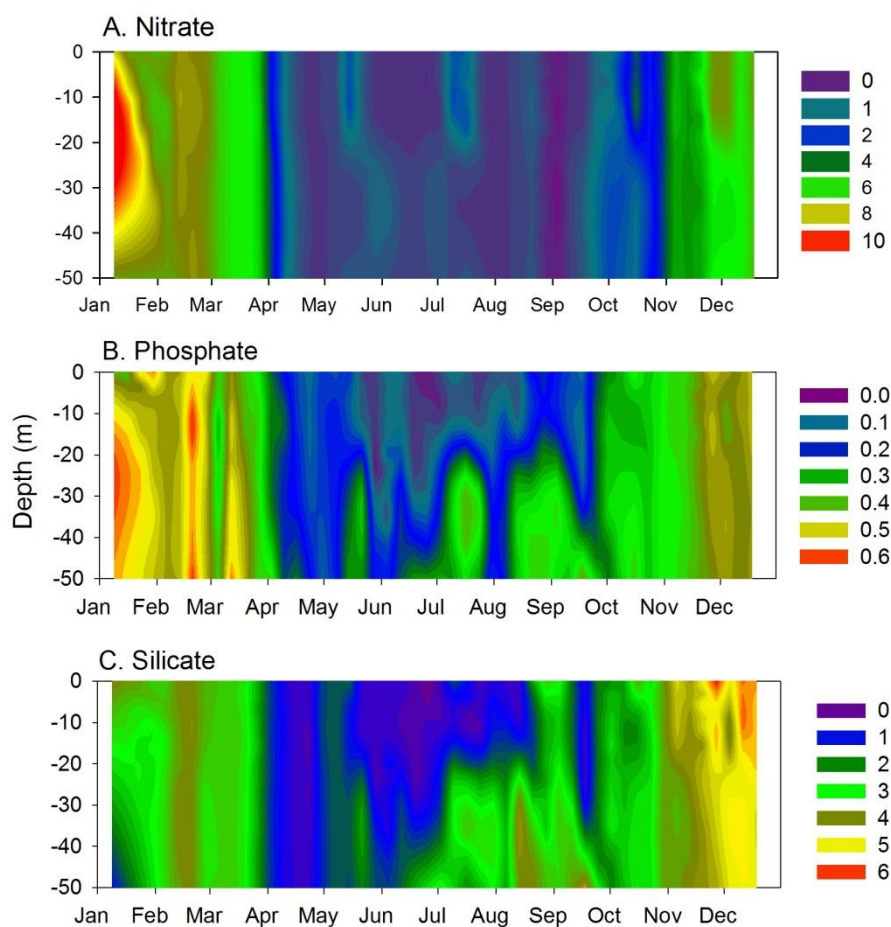


**Figure 4.3.** Contour plots of nutrient concentrations ( $\mu\text{M}$ ) through the depth profile at sample station L4, Western English Channel, UK, during 2012; (A) Nitrate, (B) Phosphate and (C) Silicate.

#### 4.3.3. Phytoplankton community structure and progression

The L4 phytoplankton community abundance peaked twice in 2012; during the early spring with maximum abundance on 27<sup>th</sup> February (measured by flow cytometry) and unusually for station L4, during the autumn months, with maximum abundance of 30 400 cells mL<sup>-1</sup> recorded on 10<sup>th</sup> September (measured by flow cytometry, Figure 4.4.A). *Synechococcus* and picoeukaryotes numerically dominated the phytoplankton community throughout the year, with picoeukaryotes dominating during periods of highest phytoplankton abundance and *Synechococcus* in early February and in August and November. (Figure 4.4.A). During the spring bloom period of April to July, increases in *Synechococcus*, *Phaeocystis* spp. and diatoms, in particular *Chaetoceros socialis* and *Guinardia delicatula*, were all significant contributors to the increase in total phytoplankton abundance. The spring bloom period at L4 is well known to be dominated by chain-forming diatoms, however, unusually for L4, another significant diatom bloom occurred in October.

Although picoeukaryotes and *Synechococcus* numerically dominated the water column for most of the year, the nano- and microeukaryote size fractions (i.e. those enumerated by microscopy) contributed most to phytoplankton biomass throughout the year (Kovala and Larrance 1966, Menden-Deuer and Lessard 2000). The eukaryote population density maxima measured by microscopy were 4700 cells mL<sup>-1</sup> and 5800 cells mL<sup>-1</sup> on the 14<sup>th</sup> of May and the 8<sup>th</sup> of October respectively (Figure 4.4.B). Phytoplankton biomass followed a similar trend to population density and ranged from 6 to 651 pg C mL<sup>-1</sup>. An exception occurred during the autumn bloom period in October, as phytoplankton biomass only reached 65 pg C mL<sup>-1</sup> (Figure 4.4.B). Microzooplankton had several peaks in abundance during the spring months with a maximum of 900 mL<sup>-1</sup> in mid-June. During the rest of the year microzooplankton abundance was low, ranging from 2 to 80 mL<sup>-1</sup> (Figure 4.4.C). Microzooplankton biomass followed a separate trend and generally increased from the winter to autumn months, from 1 pg C mL<sup>-1</sup> to a maximum of 36 pg C mL<sup>-1</sup> on the 17<sup>th</sup> September (Figure 4.4.C).

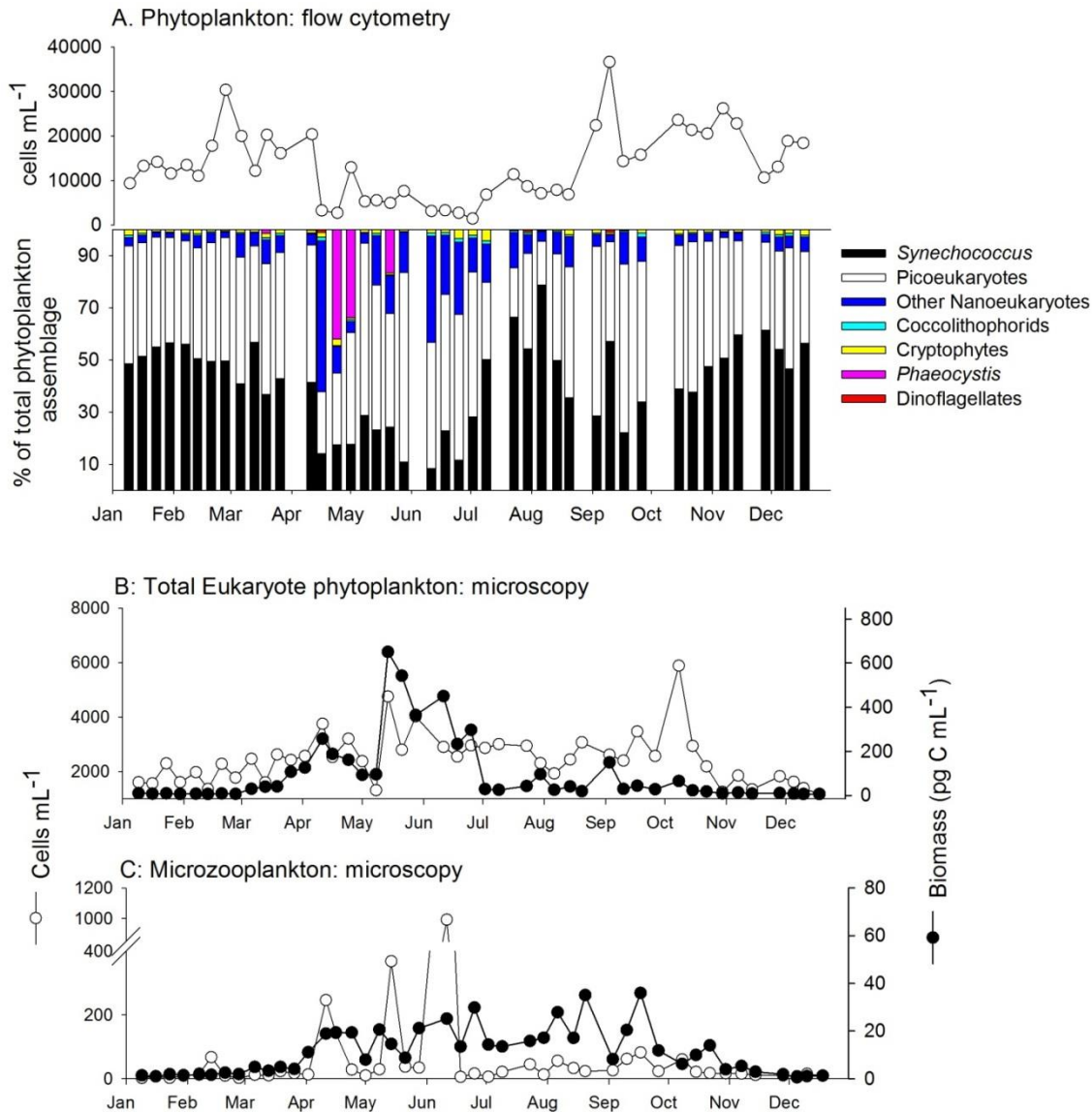


**Figure 4.4.** Plankton abundances measured at station L4, Western English Channel, during 2012. (A) Open circles represent the total phytoplankton abundance averaged through the water column measured by flow cytometry (combined data from the 7 phytoplankton groups: cells  $\text{mL}^{-1}$ ), the bar chart representing the proportional contribution of each group (as a percentage of total phytoplankton assemblage). (B) Microscopy enumeration of eukaryote phytoplankton (cells  $\text{mL}^{-1}$ ) and biomass ( $\mu\text{g C mL}^{-1}$ ) from 10 m depth, and (C) microzooplankton abundance and biomass from 10 m depth.

#### 4.3.4. Seasonality of chlorophyll *a*, hydroxychlorophyll *a* and precursor

At the beginning of 2012 the winter concentrations of chlorophyll *a* at station L4 were between 0.13 and 0.5  $\mu\text{g L}^{-1}$  (Figure 4.5.A) in surface waters, then increased to a maximum concentration of 4.48  $\mu\text{g L}^{-1}$  on 11<sup>th</sup> April. These surface concentrations were within the range expected for L4 (Southward et al. 2004, Smyth et al. 2010). The first chl-*a* maximum on 11<sup>th</sup> April (11  $\mu\text{g L}^{-1}$ ) corresponded to a minor peak in phytoplankton abundance (Figure 4.5.A & 4.4.A), possibly due to a *Phaeocystis* spp. bloom which had a concurrent maximum abundance (Figure 4.7.A). This chl-*a* maximum in April was coincident with a peak in chl-*a* concentration in the surface sediment (Tait et al. in review). A second chl-*a* maximum occurred at 50 m depth on the 28<sup>th</sup> of May (10.9  $\mu\text{g L}^{-1}$ ), just after the spring maximum eukaryote phytoplankton abundance as measured by microscopy (Figure 4.4.B), and may have resulted from sinking diatom cells, as their peak abundance preceded the deep chlorophyll maximum. During September and October, chl-*a* concentrations increased throughout the water column to an autumn maximum of 2.4  $\mu\text{g L}^{-1}$ .

The allomer hydroxychlorophyll *a* was detected throughout the year at station L4, and exhibited seasonal variations (Figure 4.5.B). Previous time-series of HO-chl-*a* in pelagic waters have been limited to the bloom period (Walker and Keely 2004, Bale et al. 2010), hence, these are the first reported measurements over an almost complete annual cycle. Hydroxychlorophyll *a* concentration had a similar annual distribution to chlorophyll *a*. A spring peak occurred on the 11<sup>th</sup> April throughout the water column with a maximum concentration of 548  $\text{ng L}^{-1}$  at 10 m depth (Figure 4.5.B). In comparison, concentrations of up to ~600  $\text{ng L}^{-1}$  of hydroxychlorophyll *a* were also measured during a spring bloom in the Celtic Sea (Walker and Keely 2004). Smaller peaks in pelagic particulate hydroxychlorophyll *a* occurred on the 28<sup>th</sup> May at 50 m and on the 11<sup>th</sup> June at 2 m.

HO-chl-*a* was detected in all analysed sediment samples with a range of concentration from 6.7 to 170  $\text{ng g}^{-1}$  dry sediment (Figure 4.5.C). To the best of our knowledge, this is the first quantification of hydroxychlorophyll *a* in marine sediments. This is comparable with the HO-chl-*a* concentration detected in sinking particles (Bale, 2010) and freshwater lake surface sediments (Walker et al. 2002).

The annual cycle of chlorophyll *a* concentration was mirrored by the chlorophyll *a* precursor, chlorophyll  $a_{P276}$  (chl- $a_{P276}$ , Figure 4.5.D). A spring peak of 143  $\text{ng L}^{-1}$  chl- $a_{P276}$  at 10 m depth on 11<sup>th</sup> April co-occurred with peaks in chl-*a* concentration (Figure 4.5.A) and phytoplankton

biomass (Figure 4.4.B). The maximum concentration of chl- $a_{P276}$  ( $210 \text{ ng L}^{-1}$ ) occurred on the 28<sup>th</sup> May at 50 m depth and was mirrored by the maximum chl- $a$  concentration at 50 m. This study is the first report of chl- $a_{P276}$  from natural phytoplankton assemblages.

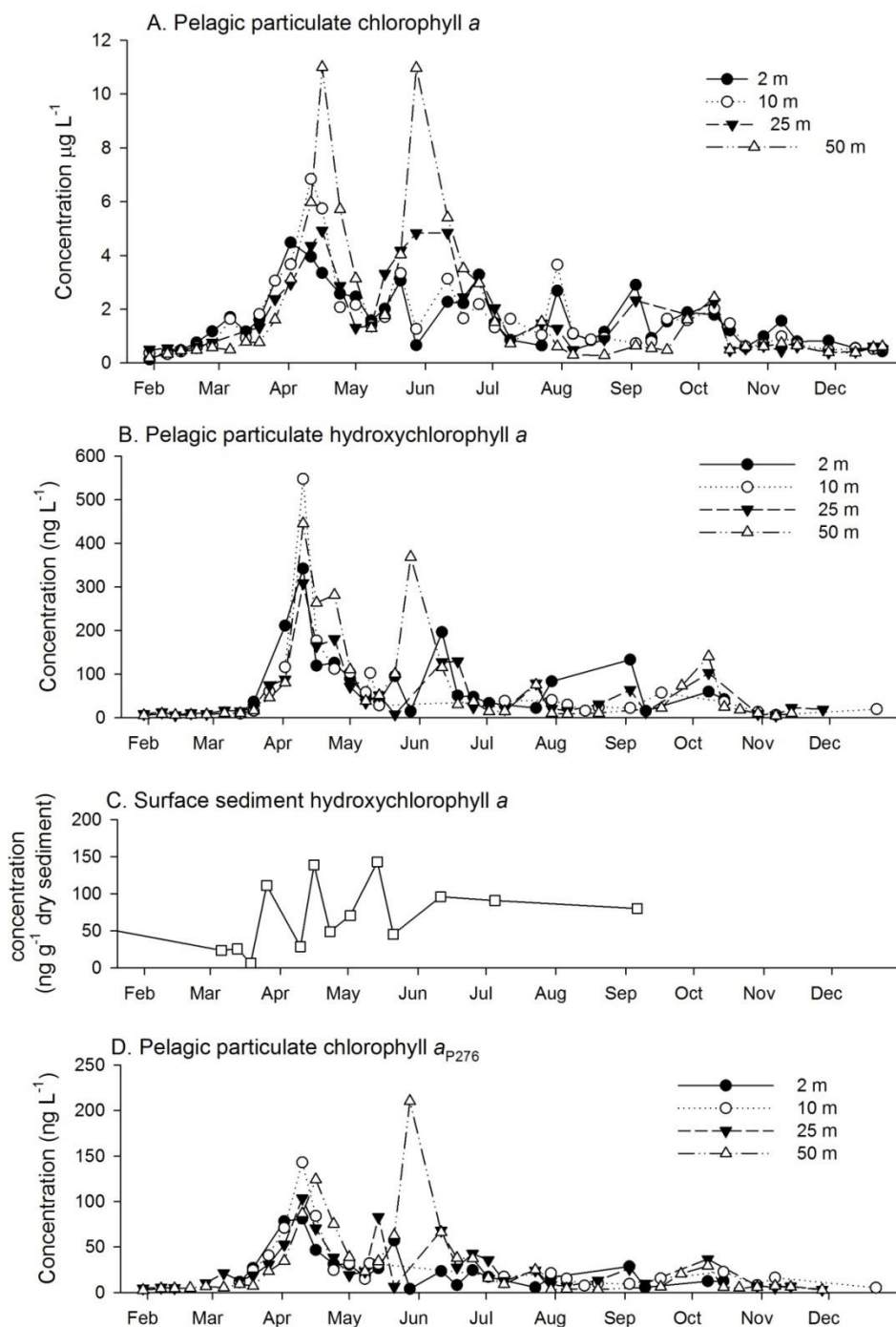


**Figure 4.5.** Concentrations of (A) chlorophyll  $a$  in pelagic particulate samples ( $\mu\text{g L}^{-1}$ ), (B) hydroxychlorophyll  $a$  in pelagic particulate samples ( $\text{ng L}^{-1}$ ), (C) hydroxychlorophyll  $a$  in surface sediment samples ( $\text{ng g}^{-1}$  dry sediment) and (D) chlorophyll  $a_{P276}$  ( $\text{ng L}^{-1}$ ) in pelagic particulate samples, from station L4, Western English Channel, UK during 2012.

#### 4.3.5. Allomer hydroxychlorophyll *a*

##### 4.3.5.1. Occurrence relative to phytoplankton blooms

The annual cycle of hydroxychlorophyll *a*, relative to chl-*a*, i.e. the HO-chl-*a* to chl-*a* ratio, was discrete from that of chl-*a* concentration (Figure 4.5.A and 4.6). At the beginning of the year during February and March, the ratio of HO-chl-*a* to chl-*a* was between 0.008 and 0.029 (Figure 4.6.A). A maximum ratio of 0.093 was detected in surface waters (2 m) in April. These measurements were within the ranges of the HO-chl-*a* to chl-*a* ratios previously reported: during a North Atlantic spring bloom, where the pelagic maximum ratio of HO-chl-*a* to chl-*a* was ~0.05 (Bale 2010) and during a spring bloom in the Celtic Sea where the HO-chl-*a* to chl-*a* ratios can be calculated to be between ~0.05 and ~0.5 from the work of Walker and Keely (2004). Unidentified chlorophyll *a* allomers have been reported from measurements in the Baltic Sea as 14% of the total chloropigments (i.e. a ratio of allomers to total chloropigments of 0.14) (Szymczak-Żyła and Kowalewska 2007).

In periods where the water column contained a thermocline, from mid-May onward (Figure 4.2.A), HO-chl-*a* was found in higher concentrations (relative to chl-*a*) below the thermocline, at 25 m and 50 m depth. Stratification of phosphate concentration occurred during this period (Figure 4.3.B) when higher concentrations occurred below 25 m. From mid-May to late September phosphate may have been a limiting factor for phytoplankton growth at station L4 in the upper 25 m of the water column. The elevated HO-chl-*a* to chl-*a* ratio below 25 m may be attributed to sinking phytoplankton cells (Walker and Keely 2004), presumably some of which were therefore phosphate-limited. The HO-chl-*a* to chl-*a* ratio then decreased during May and June to between 0.014 and 0.045, before increasing during the summer months, with a maximum ratio of 0.059; ratio values remained in this range until late October (Figure 4.6.A). The HO-chl-*a* to chl-*a* ratio then decreased to between 0.006 and 0.053 for the remainder of the year.

Hydroxychlorophyll *a* was detected in the surface sediment at station L4 with a HO-chl-*a* to chl-*a* ratio ranging from 0.07 to 0.49 (Fig 6B); up to 10 times higher than the overlying pelagic levels. A similar HO-chl-*a* to chl-*a* ratio was measured in freshwater lake surface sediments of ~0.25 (Walker et al. 2002). Unassigned chlorophyll allomers have previously been quantified in marine sediments from the Baltic Sea, where they accounted for 10% of the chloropigments (Szymczak-Żyła and Kowalewska 2007); they have also been detected in marine sediments

from the Louisiana shelf (Chen et al. 2003), the Levantine Basin and the Mediterranean Ridge (Cariou-Le Gall et al. 1998), but were not quantified.

A peak in the surface sediment HO-chl-*a* to chl-*a* ratio on the 21<sup>st</sup> May of 0.322 was coincident with the water column phytoplankton maximum biomass (Figure 4.4.B). The high concentrations of hydroxychlorophyll *a* (relative to chl-*a*) in the surface sediment compared to overlying waters indicate that the majority of chl-*a* oxidation occurred during the sedimentation process. This is consistent with a previous report of increased hydroxychlorophyll *a* to chl-*a* ratios measured in sinking particulates, collected by sediment traps (0.085), compared to suspended particulates sampled by Niskin bottles (0.03) (Bale 2010).

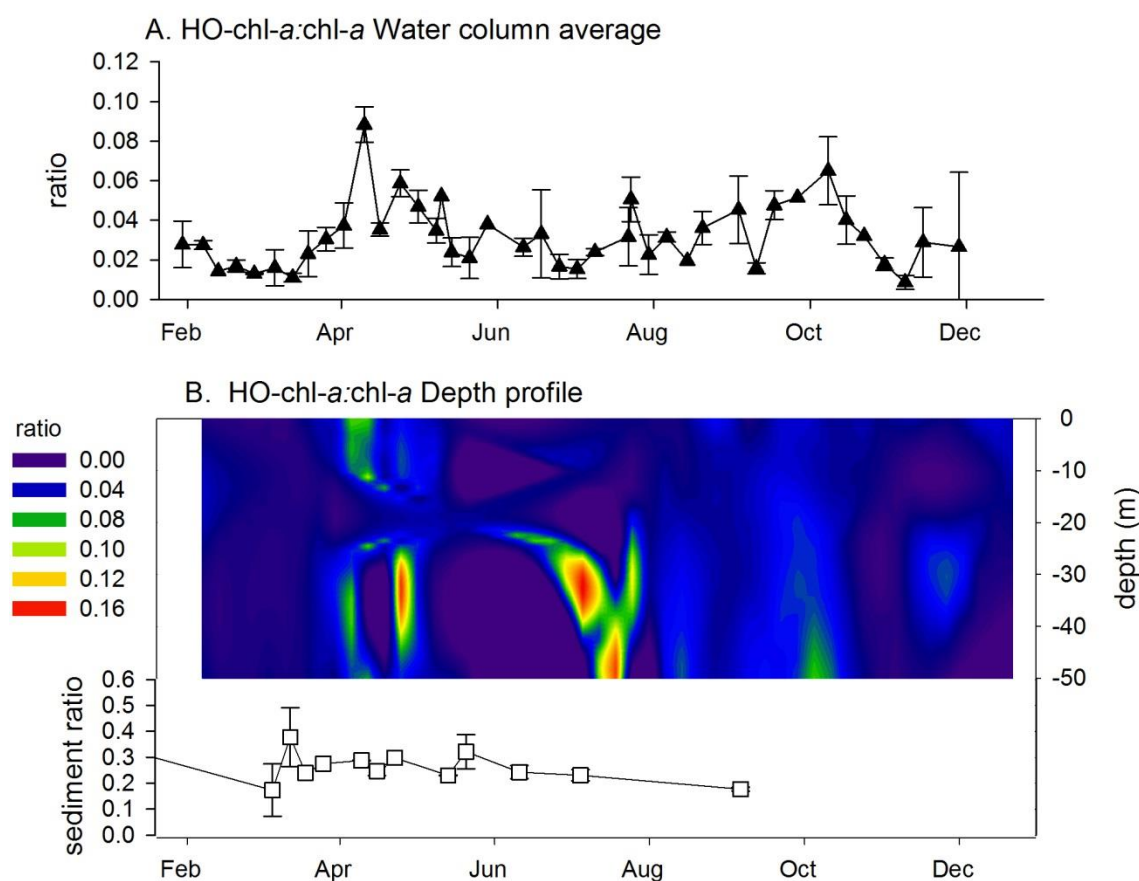


**Figure 4.6.** (A) The ratio of hydroxychlorophyll *a* (HO-chl-*a*) to chl-*a* averaged through the water column depth profile (mean $\pm$ SE). (B) The ratio of hydroxychlorophyll *a* to chl-*a* in the depth profile (contour plot) and surface sediment ( $\square$ ) from station L4, Western English Channel, UK during 2012.

#### 4.3.5.2. Contributors to pelagic hydroxychlorophyll *a* maxima

During April, hydroxychlorophyll *a* was elevated throughout the water column. A surface maximum in the ratio of HO-chl-*a* to chl-*a* of 0.093 was recorded on the 11<sup>th</sup> April (Figure 4.6.B), which coincided with maximum recorded *Phaeocystis* abundance measured by microscopy at 10 m (Figure 4.7.A). The maximum *Phaeocystis* and hydroxychlorophyll *a* abundances occurred between the 2<sup>nd</sup> and 16<sup>th</sup> April. The temporal sampling resolution (<1 week<sup>-1</sup>) does not allow a more precise prediction of the timing of the phytoplankton or allomer maximum abundances. A second maximum ratio of HO-chl-*a* to chl-*a* on 24<sup>th</sup> April at 25 and 50 m may be due to the senescing and sinking *Phaeocystis* cells which were detected at 50 m as single cells by flow cytometry (Figure 4.7.A). A link between hydroxychlorophyll *a* and phytoplankton mortality was previously postulated by Walker and Keely (2004), where HO-chl-*a* maxima were observed slightly below the chl-*a* maxima in the water column, which provided evidence that HO-chl-*a* was produced after chlorophyll was released from unidentified phytoplankton during senescence or herbivory. In comparison, HO-chl-*a* to chl-*a* has been found to be consistent in the water column during a diatom bloom and not linked to any particular ecological processes (Bale 2010).

Previous studies of allomer occurrence in water column particulates did not include phytoplankton taxonomy. Hence, this is the first report of a possible association between HO-chl-*a* occurrence and *Phaeocystis*. During the spring months of March to May the HO-chl-*a* to chl-*a* ratio was significantly correlated with the summated measurements of *Phaeocystis* abundance by microscopy and flow cytometry ( $P=0.032$ , Spearman Rank correlation coefficient=0.304).

At station L4 during the *Phaeocystis* spp. bloom the N/P ratio declined from 15 to <1, indicating that nitrate availability possibly limited *Phaeocystis* spp. population growth. This has been previously reported in a *Phaeocystis* spp. bloom in the North Sea near the Belgian coast (Lancelot 1983). A minor peak in microzooplankton abundance also occurred on 11<sup>th</sup> April (Figure 4.4.C), indicating grazing as an additional contributor of *Phaeocystis* spp. decline as observed previously in *Phaeocystis* sp. blooms in the Dutch Wadden Sea and the coastal North Sea (Admiraal and Venekamp 1986). In addition, viral infection is a possible cause of *Phaeocystis* spp. bloom decline (Baudoux et al. 2006), however it was not measured in this study.

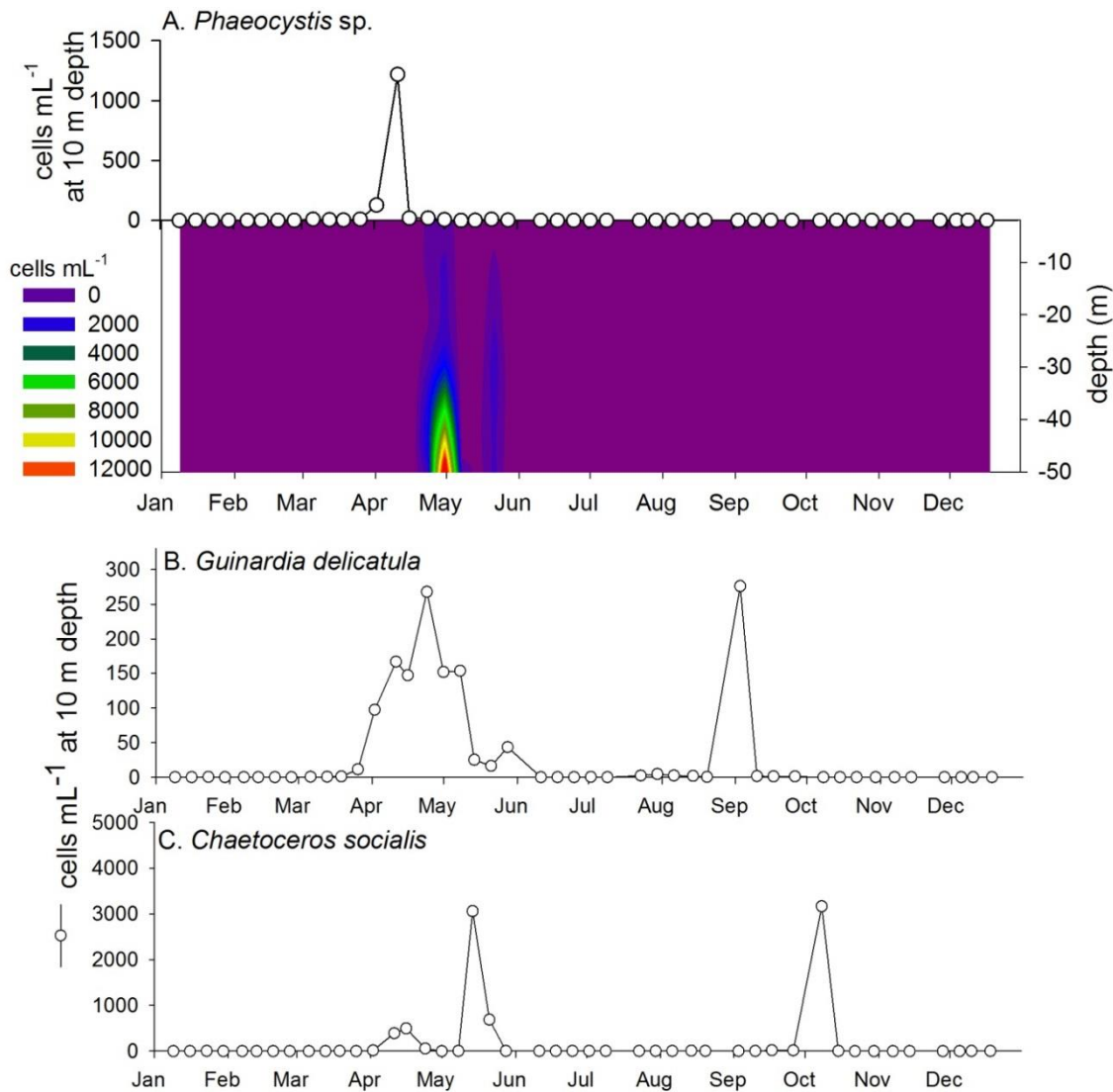


**Figure 4.7.** Phytoplankton abundances at station L4, Western English Channel, UK during 2012 of: (A) *Phaeocystis* spp including single flagellated cells and colonies measured by microscopy at 10 m (o) and flow cytometry through the water column (contour plot). (B) *Guinardia delicatula*, abundance measured by microscopy at 10 m, and (C) *Chaetoceros socialis* measured at 10 m by microscopy.

The elevated ratio of HO-chl-*a* to chl-*a* in the water column on the 24<sup>th</sup> April had a maximum of 0.068 at 25m depth. This was co-incident with the maximum abundance at 10 m of the diatom *Guinardia delicatula* (Figure 4.7.B). This bloom began on the 26<sup>th</sup> March which was co-incident with the start of a decline in the nitrate to phosphate ratio (Figure 4.8); during which the surface N/P ratio reduced from 14.4 to 0.5 on the 24<sup>th</sup> April. By the 8<sup>th</sup> May *G. delicatula* had become infected with a parasite, *Pirsonia* sp. and the bloom was waning (Widdicombe, pers

comm.). After this time *G. delicatula* abundance declined and the N/P ratio began to rise; it can therefore be deduced that population growth of *G. delicatula* was possibly limited by both nitrate availability and parasitic infection, as previously reported in a North Sea *Phaeocystis* population (Admiraal and Venekamp 1986, Veldhuis et al. 1986).

*G. delicatula* also had an autumn bloom which peaked on the 3<sup>rd</sup> September; however no hydroxychlorophyll *a* maximum was detected at this time (Figures 4.7.B and 4.6.B). During this bloom surface nitrate concentration dropped from 0.85  $\mu\text{M}$  to below the limit of detection (Figure 4.3.A) and surface phosphate concentration decreased from 0.17  $\mu\text{M}$  to 0.11  $\mu\text{M}$  (Figure 4.3.B). The N/P ratio decreased from 5 to 0 (Figure 4.8), hence implying that nitrate was limiting population growth of *G. delicatula* during its autumn bloom. This indicates that increased HO-chl-*a* to chl-*a* ratio was associated with the parasitic infection of *G. delicatula* by *Pirsonia* sp. (as in April) but not with the *G. delicatula* population declined due to nitrate limitation (as in September).

An autumn maximum of hydroxychlorophyll *a* occurred at 50 m on 8<sup>th</sup> October, with a HO-chl-*a* to chl-*a* ratio of 0.084. This was concurrent with a *Chaetoceros socialis* bloom (Figure 4.7.C), during which concentrations of both nitrate and phosphate increased, hence this bloom was assumed not to be nitrate or phosphate limited. *C. socialis* also bloomed in the spring with a maximum abundance on the 14<sup>th</sup> May, however during this bloom the HO-chl-*a* to chl-*a* ratio was not elevated. A sporadic period of nutrient input occurred during this time (Figure 4.3.A) and nitrate concentration reached 2.62  $\mu\text{M}$ . By the end of the bloom on the 21<sup>st</sup> May, nitrate concentration had declined to 0.08, hence this bloom may have declined due to nitrate limitation.

Hence, increased HO-chl-*a* to chl-*a* ratio was associated with *C. socialis* in October when population decline was not due to nutrient limitation, but some other factor, for example viral lysis (Tomaru et al. 2009). Increased HO-chl-*a* to chl-*a* ratio was not associated with nitrate limited *C. socialis*, as was deduced above for *G. delicatula*.

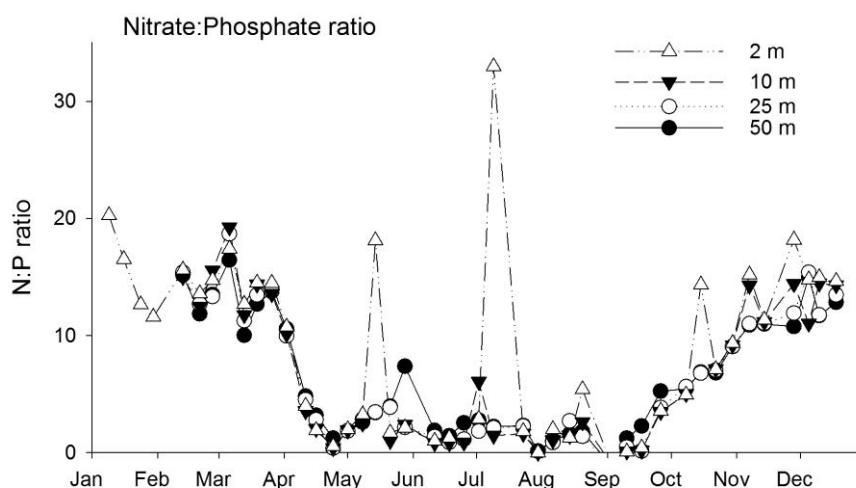


**Figure 4.8.** Ratio of nitrate to phosphate at station L4, Western English Channel, UK during 2012.

#### 4.3.5.3. Contributors to minor peaks in pelagic hydroxychlorophyll *a*

Several minor peaks in hydroxychlorophyll *a* occurred during the summer and autumn months. On the 23<sup>rd</sup> July the HO-chl-*a* to chl-*a* ratio increased at 25 and 50 m to a maximum of 0.057; at this time the water column was stratified with a mixed layer depth (MLD) of 15m. However, on the 26<sup>th</sup> September the ratio at 50 m was 0.052 (Figure 4.6.B) and the water column was completely mixed. These minor peaks were paralleled by increases in coccolithophore abundance (Figure 4.9.A). The coccolithophore *E. huxleyi* has been studied in culture and shown not to alter its HO-chl-*a* to chl-*a* ratio during adaptation to low nutrient conditions (Franklin et al. 2012, Bale et al. 2013). However, when *E. huxleyi* was infected with viruses, hydroxychlorophyll *a* increased from  $\sim 0.1$  fg cell<sup>-1</sup> to  $\sim 0.33$  fg cell<sup>-1</sup> (Bale et al. 2013). The ratio of HO-chl-*a* to chl-*a* can be calculated (from Bale et al., 2013) to increase from  $\sim 0.006$  to  $\sim 0.035$  during decline due to viral infection in culture.

Bloom termination of coccolithophores by viral lysis is known to occur in the summer period in the North Sea (Schroeder et al. 2002, Wilson et al. 2002). Hence the coccolithophore populations in September associated with increased HO-chl-*a* to chl-*a* ratio may have been subject to viral lysis. Thus the increase in HO-chl-*a*, relative to chl-*a* may prove to be a useful indicator of viral infection, in addition to senescence, but this needs to be assessed further in a wider range of phytoplankton taxa.

On the 30<sup>th</sup> July the HO-chl-*a* to chl-*a* ratio reached 0.058 at 25 m (Figure 4.6.A), which was coincident with the maximum abundance of the dominant dinoflagellate *Karenia mikimotoi* at 10 m depth (evident as the initial peak in total dinoflagellate abundance, Figure 4.9.B). At this time the water column had a MLD of 20 m. A deep water peak in the HO-chl-*a* to chl-*a* ratio of 0.052 occurred at 50 m on the 17<sup>th</sup> September (Figure 4.6.B), when the water column was thermally stratified with a MLD of 25 m (Figure 4.2.A). This increase in hydroxychlorophyll *a* followed the maximum dinoflagellate abundance measured by flow cytometry on the 10<sup>th</sup> of September (Figure 4.9.B), suggesting a potential contribution to hydroxychlorophyll *a* from dinoflagellate cells.

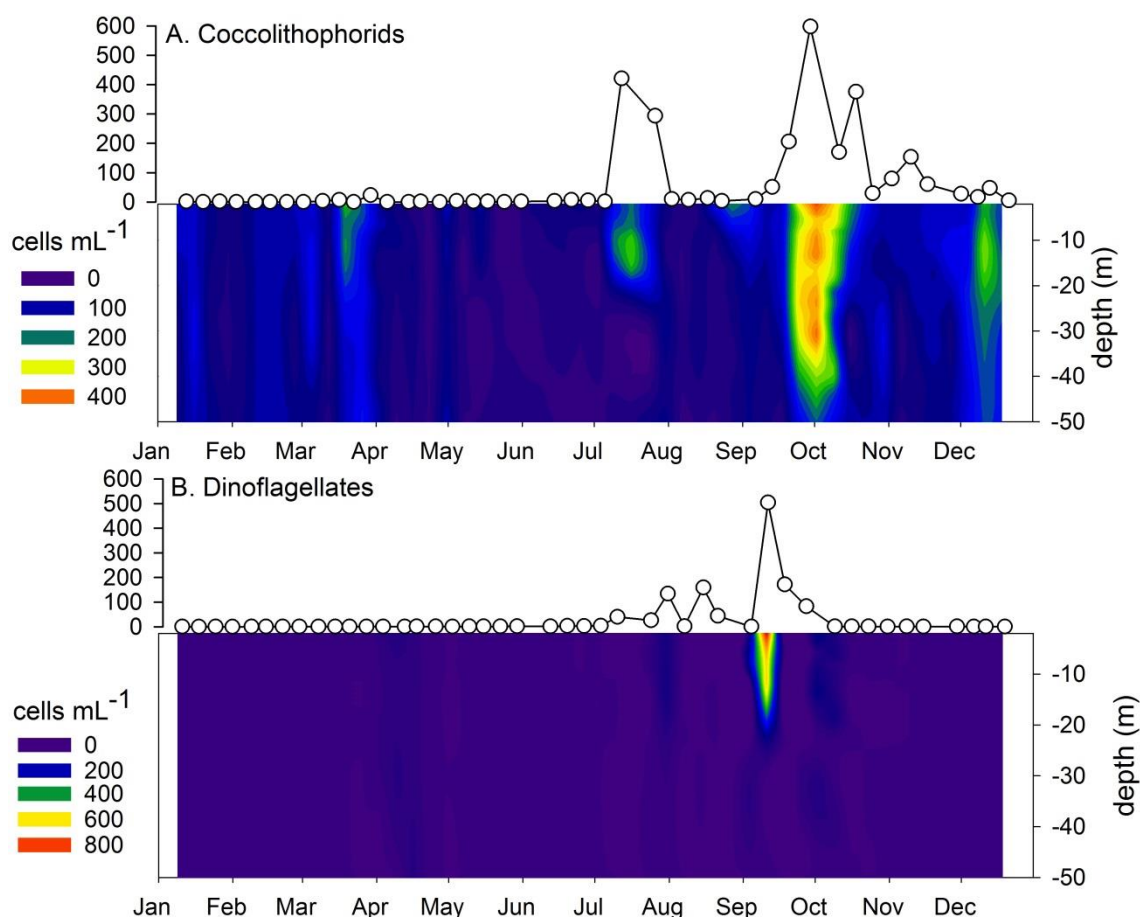


**Figure 4.9.** Phytoplankton abundances at station L4, Western English Channel, UK during 2012 of: (A) Coccolithophores and (B) Dinoflagellates, measured by microscopy at 10 m (o), and flow cytometry through the depth profile (contour plot).

#### 4.3.6. Precursor Chlorophyll $a_{P276}$

Chlorophyll  $a_{P276}$  occurred, relative to chl- $a$ , with a ratio between 0.003 and 0.027 (Figure 4.10). The ratio of chl- $a_{P276}$  to chl- $a$  increased between April and July with higher ratios measured at 25 and 50 m depth compared to surface waters. This period of increased chl- $a_{P276}$  (relative to chl- $a$ ) coincides with the period of high phytoplankton abundance (Figures 4.4.A & 4.4.B), i.e. the spring bloom period. The chl- $a_{P276}$  to chl- $a$  ratio maxima occurred before the chlorophyll  $a$  maxima (Figures 4.5.A & 4.10.). The ratio of chl- $a_{P276}$  to chl- $a$  correlates with chl- $a$  concentration ( $P < 0.001$ , rank correlation coefficient = 0.446). This is expected and adds support for the assignment of chl- $a_{P276}$  as a precursor during chl- $a$  biosynthesis (Rüdiger 2006, Franklin et al. 2012). There are no previous field measurements of chlorophyll  $a_{P276}$ , however it has been previously detected in *Pavlova gyrans* cultures at a ratio of  $\sim 0.003$  with chl- $a$  (Bale et al. 2010) which is consistent with the ratios found in this study. Chl- $a_{P276}$  has also been detected in cultures of *E. huxleyi* and *Thalassiosira pseudonana*, however it was quantified in combination with hydroxychlorophyll  $a$  (Franklin et al. 2012).

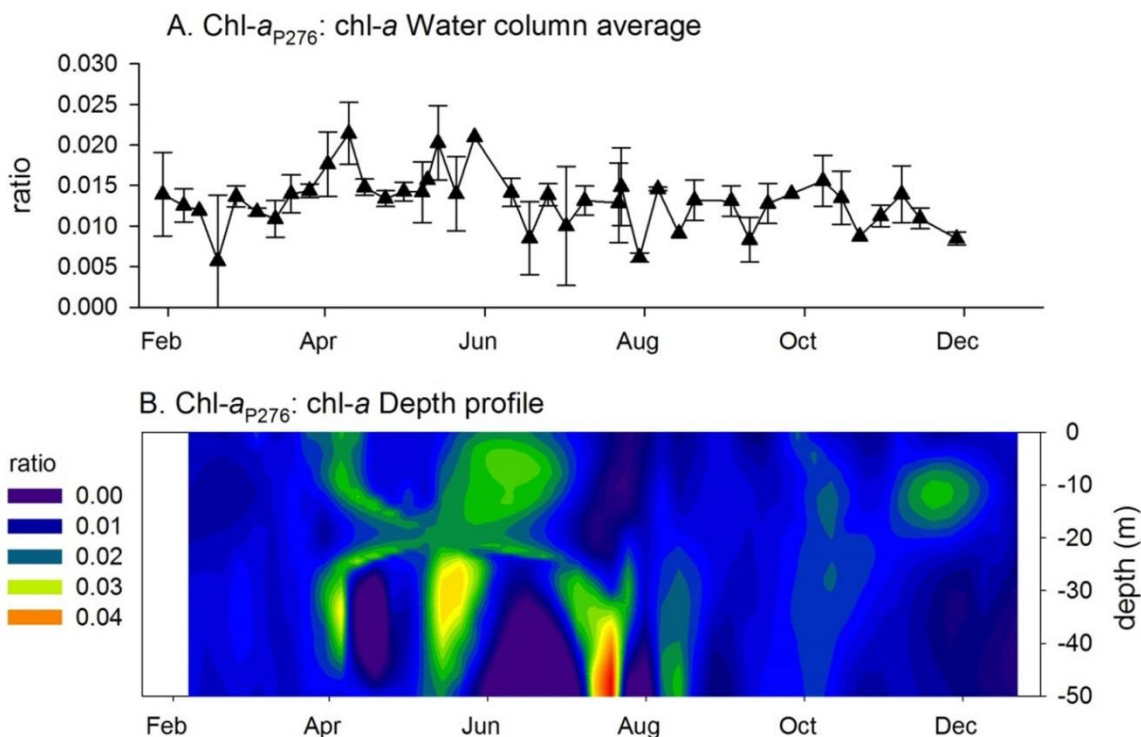


**Figure 4.10.** (A) The ratio of chlorophyll  $a_{P276}$  (chl- $a_{P276}$ ) to chl- $a$  averaged through the water column depth profile (mean $\pm$ SE). (B) The ratio of chlorophyll  $a_{P276}$  to chl- $a$  in the depth profile (contour plot) from station L4, Western English Channel, UK during 2012.

#### 4.4. Conclusions

Chlorophyll  $a_{P276}$  correlates with chl-*a* concentration, thus supporting its assignment as a chl-*a* precursor. The annual trend in the hydroxychlorophyll *a* to chl-*a* ratio shown here indicates that formation of HO-chl-*a* is a variable process in the water column, in this case associated with *Phaeocystis* spp, *G. delicatula*, *C. socialis* and *E. huxleyi* population dynamics and, reported for the first time, during dinoflagellate blooms. However, the inconsistency of the species' associations with hydroxychlorophyll *a* suggests a dependency on the mode of phytoplankton mortality or population decline, as has been observed in *E. huxleyi* cultures (Bale et al. 2013).

Due to the weekly sampling resolution of this study, it remains challenging to relate hydroxychlorophyll *a* production more precisely to the population dynamics of this phytoplankton assemblage. To determine which combination of taxa were responsible for allomer production in natural systems, more detailed surveys and further assessment in laboratory studies is necessary. Analysis across a diverse array of phytoplankton taxa subjected to viral lysis, environmental limitation and grazing will clarify their occurrence in natural systems.

During periods of thermal stratification the HO-chl-*a* to chl-*a* ratio was higher below the thermocline. Further, the HO-chl-*a* to chl-*a* ratio measured in the sediment was 10 times that detected in the water column, indicating that the process of sedimentation or the processing of phytoplankton cells by other organisms within the water column or at the sediment surface, is a larger contributor to hydroxychlorophyll *a* than production in phytoplankton cells suspended in the water column. Thus, more emphasis is needed on measuring allomer production and loss processes in the sediments, and importantly, the relationships between the pelagic and benthic interface.

[Blank Page]

## **Chapter V**

### ***Research Cruise, May 2011***

## **Survey of chlorophyll allomers, precursor and eukaryote population viability in the North Sea**

### ***5.1. Introduction***

To expand the geographical range of chlorophyll allomer measurements, to include a range of environmental conditions and phytoplankton community compositions, sampling was undertaken during a research cruise in the southern and central North Sea.

Regions within the southern and central North Sea are influenced by inflow from the Atlantic via the English Channel (Becker and Pauly 1996), industrial aquaculture on the continental coast, and riverine outflow. During this research cruise, the water column was sampled at regions influenced by these factors to varying degrees. This range of abiotic environments supported varied phytoplankton communities. Hence the cruise track enabled a survey of chlorophyll allomers in uniquely influenced and varied phytoplankton assemblages.

This study also provided the opportunity for comparison between allomer concentrations and measurements of population viability using SYTOX-Green (Chapter 1, section 1.5.2.1) and CMFDA staining (section 1.5.2.3), for membrane permeability and hydrolytic enzyme activity respectively, as well as bulk chlorophyll fluorescence measurements (i.e.  $F_v/F_m$ , section 1.6.2). These data were collected in parallel with the chlorophyll allomers and the chl-*a* precursor and hence provided an opportunity to examine associations between parameters.

### 5.1.1. Chapter V hypotheses

The aim of this study was to establish if chlorophyll *a* allomers and the precursor chlorophyll  $a_{P276}$  could be used as indicators of phytoplankton physiological status. As allomers are thought to be produced when phytoplankton cells are experiencing stressful conditions, it follows that they could be an indicator of cellular stress. The precursor chlorophyll  $a_{P276}$  has previously been measured in highest abundance (relative to chl-*a*) during exponential growth of phytoplankton populations in culture (Chapter 3, Franklin et al. 2012) and therefore could act as a marker for population growth.

There are currently 3 studies which include measurement of the allomer hydroxychlorophyll *a* (HO-chl-*a*) in the marine water column. They report contrasting evidence for a relationship between the HO-chl-*a* to chl-*a* ratio with depth (Walker and Keely 2004, Bale 2010). Therefore the first hypothesis is that the ratio of allomer to chl-*a* is maximal at depths below the chlorophyll maximum. However, this hypothesis depends on the degree of mixing or thermal stratification of the water column. Hence, at several sampling stations, allomers were measured at multiple depths in the water column. As the production of allomers is linked to senescing phytoplankton cells as has been measured in *Ostreococcus tauri* (chapter 3) and other taxa (Bale et al. 2011, Franklin et al. 2012, Bale et al. 2013), it follows that if the senescing phytoplankton sink through the water column, the ratio of allomer to chl-*a* will increase with depth.

Allomers may also be increased relative to chlorophyll *a* during the decline of a population, as was observed in *O. tauri* cultures (Chapter 3) and other phytoplankton cultures (Bale et al. 2011, Franklin et al. 2012, Bale et al. 2013). This leads to the second hypothesis - that the allomer to chl-*a* ratio increases when the overall chl-*a* concentration is decreasing. This study also leads to the third hypothesis - that the ratio of the precursor chl- $a_{P276}$  to chl-*a* is highest when the overall chl-*a* concentration is increasing.

The final hypotheses follow; that allomers would be found in highest abundance (relative to chl-*a*) when the maximum photosynthetic efficiency,  $F_v/F_m$ , is lower than expected for the phytoplankton community; and similarly, a low ratio of allomers to chl-*a* would occur when the  $F_v/F_m$  ratio was in the upper range expected for the phytoplankton community. However as maximum  $F_v/F_m$  varies with taxa (Suggett et al. 2009), comparison across phytoplankton assemblages comprised of varying taxa is complex (see Chapter 1, section 1.6.2 for details of the interpretation of  $F_v/F_m$ ).

## 5.2. Location and sampling synopsis

The cruise was part of a multidisciplinary research program (ProTool, <http://www.protool-project.eu/>; Dymaphy <http://www.dymaphy.eu/>) aboard the RV *CEFAS Endeavour* in May 2011 in the central and southern North Sea, between Lowestoft and the Netherlands (Figure 5.1). Sampling was conducted at a variety of sampling locations guided in some cases by satellite chlorophyll estimations from the previous day, during the period 8<sup>th</sup> to 12<sup>th</sup> May. The recent history of chlorophyll *a* concentration at each station was extracted from ocean colour data collected by satellite (see Methods chapter 7, section 7.4.6 for details). The sampling stations are shown in Figure 5.1 and Table 5.1. Seawater samples were collected throughout the water column using 10 L Niskin bottles mounted on a CTD rosette sampler. The sampling depths ranged from surface to bottom and water depth ranged from 21 to 82 m. Water samples were processed for pigments and allomers (chapter 7.6.1.2), nutrients (by R Forster, chapter 7.4.3), and analyzed for phytoplankton community composition and abundance using a Cytosense flow cytometer by M Thyssen (Thyssen et al. 2014, chapter 7.4.4.). The phytoplankton assemblage at stations 17 and 18 were also assessed for membrane permeability (using SYTOX-Green) and hydrolytic enzyme activity (using CMFDA) using an Accuri C6 flow cytometer (by D Franklin, chapter 7.4.5). Seawater was also collected continuously from 6 m depth, which entered a Pocket Ferry Box and was analysed for optical measurements including an estimation of  $F_v/F_m$  by Phytoflash (chapter 7.4.2).

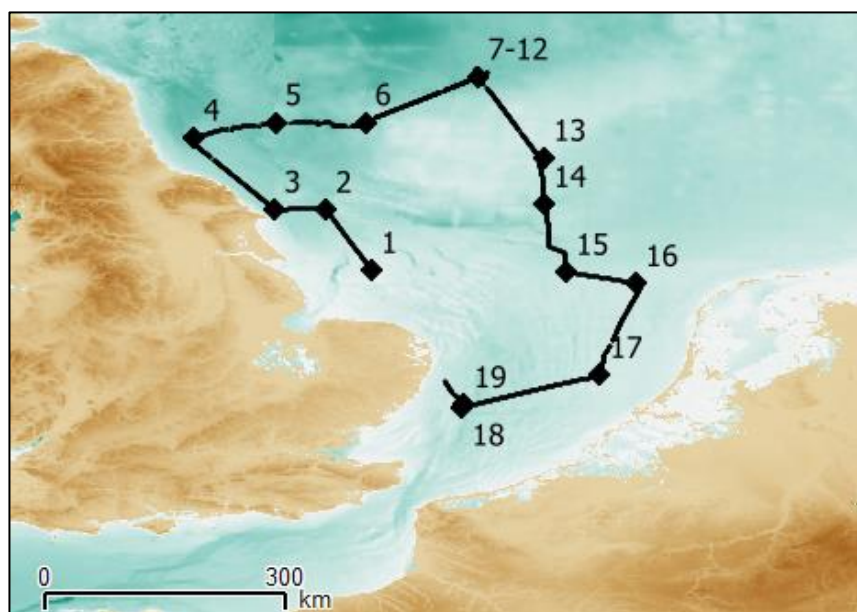


**Figure 5.1.** Location of sampling stations during a research cruise from 8<sup>th</sup> to 11<sup>th</sup> May.

**Table 5.1.** Description of sampling stations from a research cruise in the central and southern North Sea, May 2011.

Station site	Station no.	Date	GMT_time	Water column depth (m)
Dowsing	1	08/05/2011	08:35	21
Flamborough Outer	2	08/05/2011	14:12	58
Flamborough Inner	3	08/05/2011	17:06	52
Tyne	4	09/05/2011	07:43	80
Outer Tyne	5	09/05/2011	13:05	70
West Dogger	6	09/05/2011	17:50	65
North Dogger	7	10/05/2011	05:38	81
North Dogger	8	10/05/2011	07:38	81
North Dogger	9	10/05/2011	10:14	82
North Dogger	10	10/05/2011	13:11	82
North Dogger	11	10/05/2011	17:40	82
North Dogger	12	10/05/2011	18:00	82
South Dogger	13	11/05/2011	05:31	23
South Rough	14	11/05/2011	09:36	47
Nam field	15	11/05/2011	15:27	32
Pen field	16	11/05/2011	18:44	27
off Schevingen	17	12/05/2011	05:30	28
West Gabbard	18	12/05/2011	12:37	32

### 5.3. Statistical methods

#### 5.3.1. Phytoplankton community multivariate analysis

The cruise stations were analysed for similarity using the multivariate statistics programme PRIMER-E (version 6, PRIMER-Ltd, Ivybridge, UK). The proportional contribution of each phytoplankton taxa was square-root transformed (Poulton et al. 2007, Franklin et al. 2009b) and a Bray-Curtis similarity index was computed. The resulting matrix was interpreted using Hierarchical Cluster analysis to produce a dendrogram of similarity and using non-metric multidimensional scaling (MDS).

The pattern with which the stations clustered based on the proportional contribution of phytoplankton taxa was compared to clustering of stations based on nutrient concentration (nitrate, phosphate, nitrite, silicate and ammonium) and the N to P ratio. The nutrient data was

log transformed and normalised, before using BEST analysis for comparison of the biotic and abiotic data, performed using PRIMER-E. This analysis finds the “best” match between the multivariate among-sample patterns of an assemblage and that from the environmental variables associated with those samples. The extent to which these 2 patterns match, reflects the degree to which the chosen abiotic data “explains” the biotic pattern (Clarke and Gorley 2006).

Patterns in clustering based on individual pigments of interest (i.e. ratios of HO-chl-*a*, MeO-chl-*a*-like or chl-*a*<sub>P276</sub> to chl-*a*) were compared to the biotic proportional contribution of each phytoplankton taxa and abiotic nutrient concentrations and N to P ratios of each station using BEST analysis. The chlorophyll *a*, allomer and precursor data were first square-root transformed and their Euclidean Distance indexes were computed. The BEST analysis assessed which variables best explained the station clustering resulting from the individual allomer or precursor ratios and resulted in a correlation co-efficient ( $\rho$ ) and significance level ( $p$ ).

#### **5.4. North Sea cruise Results and Discussion**

##### *5.4.1. Overview of nutrient conditions during the cruise*

This cruise track in the central and southern North Sea encompassed a wide range of environmental conditions. The nutrient-rich region of the Outer Tyne (station 5, Figure 5.1) had a nitrate concentration of 2.57  $\mu\text{M}$  and phosphate concentration of 0.5  $\mu\text{M}$  (Figure 5.2.A). In contrast, the low nutrient West Gabbard (station 18) had a nitrate concentration of 0.05  $\mu\text{M}$  and a phosphate concentration of 0.07  $\mu\text{M}$ . This nitrate concentration is greatly reduced compared to that measured at the Gabbard in March 2000; reported as 9.2  $\mu\text{M}$  (Weston et al. 2004) likely indicating that station 18 was sampled after the bulk of the nitrate had been consumed by the Spring bloom. Station 7 (North Dogger) had nitrate, phosphate and silicate concentrations of 0.05  $\mu\text{M}$ , 0.24  $\mu\text{M}$  and 0.3  $\mu\text{M}$  respectively. This is consistent with measurements of surface nitrate, phosphate and silicate of 0.03-0.06  $\mu\text{M}$ , 0.02-0.03  $\mu\text{M}$ , 0.04-0.81  $\mu\text{M}$  respectively, measured at the Dogger Bank during July 2003 (Baudoux et al. 2008). The nitrate concentrations at stations 15 and 16, at the Nam Field and Pen Field, were 1.95  $\mu\text{M}$  and 0.05  $\mu\text{M}$  respectively. This range is outside previous measurements in this area, during May 2000, of 0.2 to 0.7  $\mu\text{M}$ , but is within the range for July 2000 (maximum 2.56  $\mu\text{M}$ ) (Weston et al. 2004). It is therefore likely that station 16 was sampled after a phytoplankton bloom. The ratio of nitrate to phosphate also varied widely, from 16.3 at station 15 at the Nam Field to less than 1 in the majority of stations (1, 4, 6, 7, 10, 14 and 18, Figure 5.2.A).

#### 5.4.2. Overview of phytoplankton communities during the cruise

The maximum phytoplankton abundance of 45 000 cells mL<sup>-1</sup>, detected by flow cytometry, was recorded at station 18, in the West Gabbard. In contrast, the minimum phytoplankton abundance of 850 cells mL<sup>-1</sup> was recorded at the Outer Tyne (station 5) (Figure 5.2.B). Throughout the cruise track, picoeukaryotes were the most abundant phytoplankton group, followed by *Phaeocystis* spp. and *Synechococcus* (Figure 5.2.C). Generally, during periods of high phytoplankton productivity, i.e. the spring period, picoeukaryotes are expected to be numerically dominant in the water column, whereas *Synechococcus* generally takes-over at other times (Baudoux et al. 2008), as previously described in the Western English Channel (chapter 4.3.3). In the Dogger area, during July 2003, the water column was numerically dominated by *Synechococcus* with an average maximum abundance of  $\sim 7 \times 10^4$  cells mL<sup>-1</sup>, whereas the total picoeukaryote abundance was  $\sim 1.4 \times 10^4$  cells mL<sup>-1</sup> (Baudoux et al. 2008). This example of the July assemblage represents a summer period dominated by *Synechococcus* (as expected) with abundance 1.5 times higher than in May 2011, which was the more productive spring period. The coccolithophore abundance was low across the cruise study sites, which corresponds to previous measurements in the southern North Sea (van Bleijswijk et al. 1994).

A *Phaeocystis* spp. bloom at stations 17 and 18 was recorded with a maximum abundance of 9300 cells mL<sup>-1</sup> (Figure 5.2). This abundance is 4 orders of magnitude lower than a previous *Phaeocystis* bloom in the Southern Bight of the North Sea, where abundance was detected to be  $140 \times 10^6$  cells mL<sup>-1</sup> (measured by flow cytometry) (van der Woerd et al. 2011). During the bloom in 2003, chlorophyll *a* concentration reached  $\sim 40$   $\mu\text{g L}^{-1}$ , whereas the maximum chl-*a* concentration measured *in situ* at stations 17 and 18 was 3.05  $\mu\text{g L}^{-1}$ . Hence it is likely that stations 17 and 18 were not sampled during the peak of the *Phaeocystis* spp bloom. In addition, from ocean colour observations, it is likely that station 17 and 18 were sampled after the peak of the bloom (see section 5.4.9).

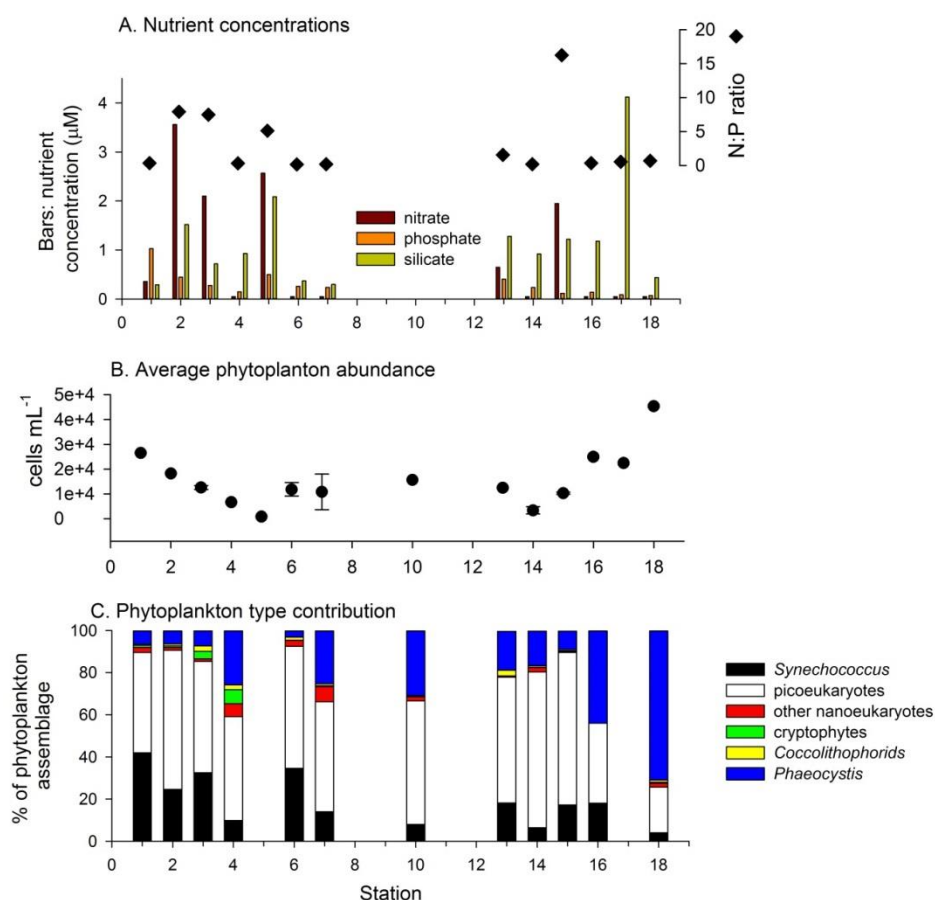


**Figure 5.2.** (A) Concentrations of dissolved inorganic nitrate, phosphate and silicate, and the corresponding N to P ratios. (B) Average phytoplankton abundance through the water column measured by flow cytometry and (C) The proportional contribution of *Synechococcus*, picoeukaryotes, cryptophytes, coccolithophores, *Phaeocystis*, and other nanoeukaryotes averaged through the water column, measured by flow cytometry, at 12 stations in the central and southern North Sea sampled in May 2011. See Figure 5.1 for station locations.

#### 5.4.3. Overview of community variable fluorescence during the cruise

The maximum quantum efficiency of PSII photochemistry ( $F_v/F_m$ ) of the communities ranged from 0.168 at station 15 to a maximum of 0.443 at station 4. Although no North Sea measurements of  $F_v/F_m$  have been located for comparison, the measurements of  $F_v/F_m$  recorded during this cruise can be compared to measurements from the Celtic Sea and North Atlantic Ocean. The maximum  $F_v/F_m$  recorded during the cruise was within the range measured in the Celtic Sea (measured by FRRF in May, 2000) from 0.44 to 0.50 (Smyth et al. 2004). This maximum  $F_v/F_m$  is also within ranges recorded in the North Atlantic Ocean; measured by FRRF, May/June 2001), from 0.2 to 0.65 during a diatom bloom (Moore et al. 2005); and measured using a pump-and-probe fluorometer in May/June 1993, from 0.22 and 0.55 (Olaizola et al.

1996). The minimum  $F_v/F_m$  recorded during this cruise was below the previously recorded ranges. This may be due to interference in the water column caused by non-physiological factors, for example dissolved fluorescence and particulate fluorescence from chlorophyll degradation products (Geider et al. 1993a, Olaizola et al. 1996, Fuchs et al. 2002). This low minimum  $F_v/F_m$  may also be due to species or strain differences between the North Sea coastal and the North Atlantic Oceanic strains or species.

#### 5.4.4. Overview of community viability during the cruise

##### 5.4.4.1. SYTOX staining at stations 17 and 18

The viability of the phytoplankton assemblage at stations 17 and 18 was assessed using membrane permeability (using SYTOX-Green) and hydrolytic enzyme activity (using CMFDA) (Figure 5.3). As stations 17 and 18 were vastly dominated by one phytoplankton taxa (Figure 5.3.A) the interpretation of the cell staining results were simplified hence they have been included as a measure of phytoplankton population viability.

Less than 1% of the phytoplankton cells sampled from station 18 were labelled with the SYTOX-Green probe (Figure 5.3.B). There are no reports of SYTOX application to natural *Phaeocystis* blooms; hence this may be the first example. SYTOX has previously been applied to *Phaeocystis* in culture during viral infection (Brussaard et al. 2001). Even though the viral infection led to complete population collapse, a maximum of only 25% of cells were labelled SYTOX-positive. This low level of staining was due to a reduction in red fluorescence intensity in the infected cells (Brussaard et al. 2001). Therefore the proportions of SYTOX positive/negative cells did not represent the whole population, but rather, only cells that had also retained high red fluorescence. Hence in this case the proportion of cells with permeable membranes was probably underestimated. During *Phaeocystis* senescence up to 30% of cells were labelled (Brussaard et al. 2001), however the senescent cells did not have reduced red fluorescence and hence the proportion of SYTOX-positive/negative cells did represent the whole population. Therefore the interpretation of the SYTOX staining at stations 17 and 18 depends on the relative red fluorescence of the *Phaeocystis* cells and hence any environmental stress that may have led to reduced red fluorescence. The *Phaeocystis* cluster was tightly grouped within the cytogram (Figure 5.3.A) and no “low-red” sub-population was detected, adding confidence that the complete *Phaeocystis* spp. population was represented in the staining analysis. Hence the *Phaeocystis* spp. populations at stations 17 and 18 showed very low levels of membrane permeability.

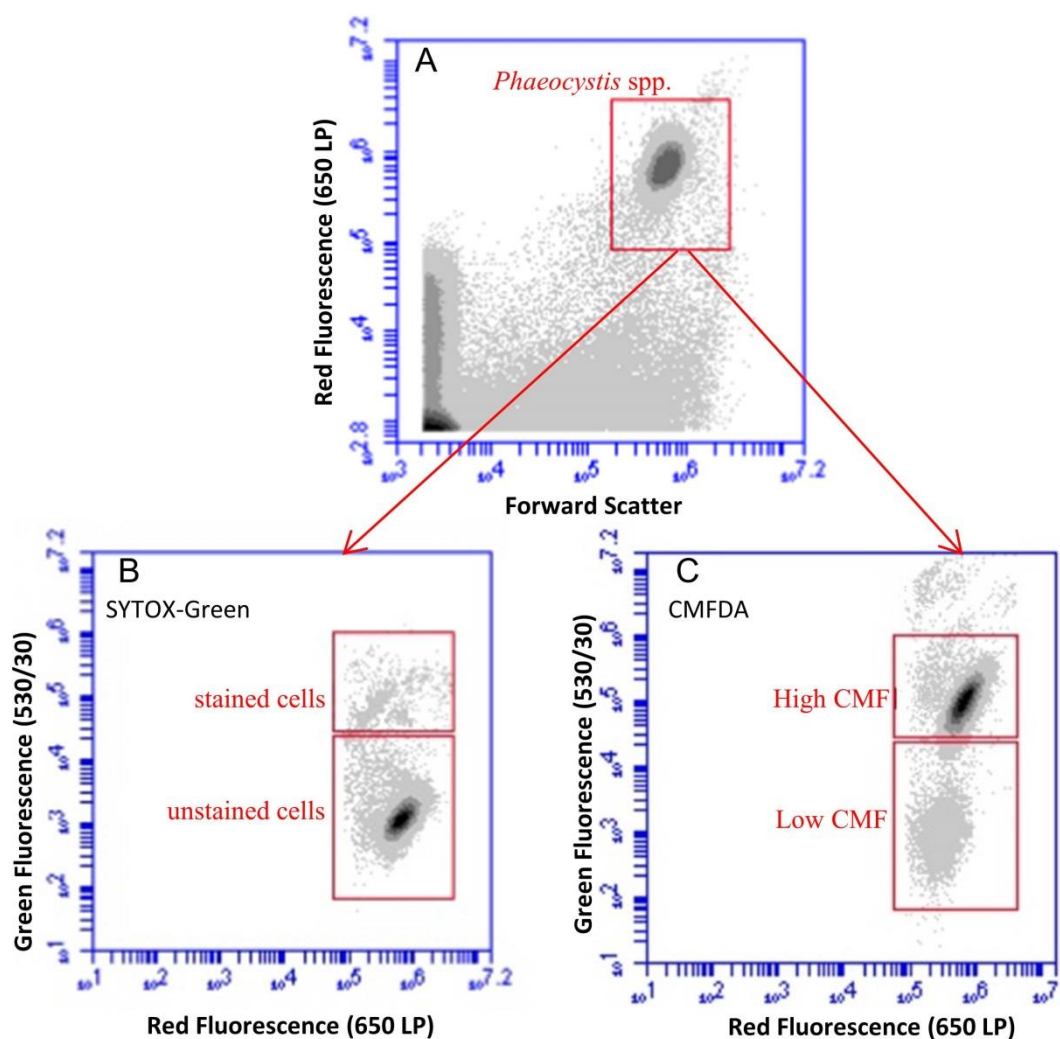


**Figure 5.3.** Cytogram plots from station 17, off Schevingen in the southern North Sea. The phytoplankton population was dominated by *Phaeocystis* spp. (A). Box encloses the *Phaeocystis* spp. population. The assemblage was stained for (B) membrane permeability (SYTOX-Green), and (C) hydrolytic enzyme activity (CMFDA), showing the *Phaeocystis* population only.

#### 5.4.4.2. CMFDA staining at stations 17 and 18

CMFDA staining of stations 17 and 18 resulted in 6% of cells with limited or no probe metabolism, 93% with substantial probe metabolism, and some even more (Figure 5.3.C, see chapter 1.5.2.3 for details of probe action). CMFDA has been tested for applicability to *Phaeocystis* cultures; for the 6 *Phaeocystis* stains tested, the probe response was moderate to high in all of the cultures in exponential and stationary phase (Peperzak and Brussaard 2011). Therefore, suggesting that the *Phaeocystis* population at stations 17 and 18 were active and viable, with high hydrolytic enzyme activity and near complete membrane integrity.

#### 5.4.5. Overview of chlorophyll, allomers and chl-*a* precursor measurements (by HPLC)

##### 5.4.5.1. Chlorophyll *a* concentration

Chlorophyll *a* concentration in the particulate samples from the water column (measured by HPLC) ranged from 0.056  $\mu\text{g L}^{-1}$  to 0.991  $\mu\text{g L}^{-1}$  (Figure 5.4), as expected in the central and southern North Sea (Gieskes and Kraay 1984, McQuatters-Gollop et al. 2007). However, chlorophyll *a* concentrations near the Dutch coast are known to exceed 20  $\mu\text{g L}^{-1}$  (Borges and Frankignoulle 1999, Petersen et al. 2008). To provide a more complete description of chlorophyll *a*, pre and post sampling, and through the water column, estimates of chl-*a* concentration were derived from satellite based ocean colour measurements and by fluorescence measurements from CTD casts. These data are discussed below in sections 5.4.9 and 5.4.8.

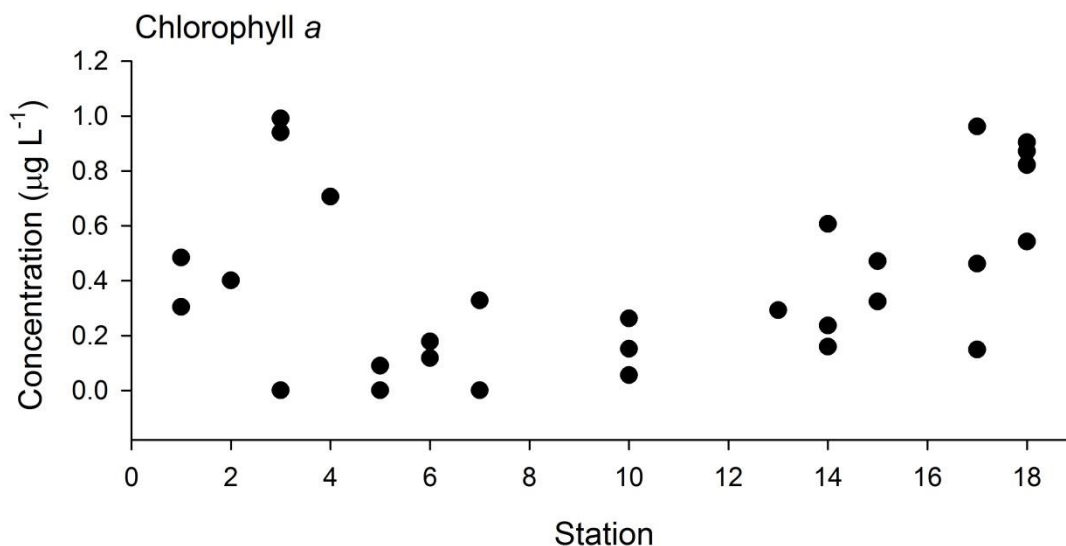


**Figure 5.4** Concentration of chlorophyll *a* in pelagic particulate samples throughout the water column, including replicates and multiple depths, from 18 stations in the central and southern North Sea during May 2011, determined by HPLC.

#### 5.4.5.2. Example pigment chromatogram from the North Sea

From HPLC analysis of pelagic particulate pigment samples, the methoxychlorophyll *a*-like allomer and the chlorophyll allomers hydroxychlorophyll *b* and hydroxychlorophyll *a* were detected along with the chlorophyll *a* precursor, chlorophyll *a*<sub>P276</sub> (Figure 5.5 & Table 5.2). These components were assigned by comparison of their main UV/vis absorption bands and retention times with the components presented in Chapter 3 (section 3.3.3) and Chapter 2 (section 2.6.1), and were confirmed by LCMS<sup>n</sup> analysis.

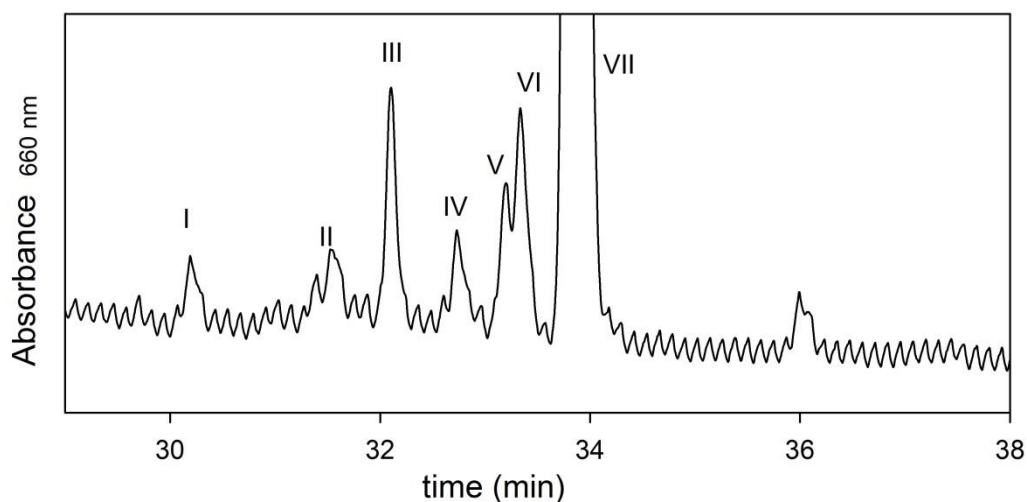


**Figure 5.5.** Partial HPLC-PDA chromatogram (660 nm) showing elution position relative to chl-*a* (VII) and chl-*b* (III) of chlorophyll allomers and precursor detected in the southern North Sea, at station 1 (at 6 m depth, located at lat: 53.518 and lon: 1.0722). For peak assignments, see Table 5.2.

**Table 5.2.** Peak assignment from 660 nm chromatogram resulting from HPLC separation of particulate photopigment samples from the central and southern North Sea.

Peak no.	Main UV/vis absorption bands (nm)	Assignment
I	429, 650	Methoxychlorophyll <i>a</i> -like allomer*
II	431, 650	Hydroxychlorophyll <i>b</i>
III	462, 647	Chlorophyll <i>b</i>
IV	431, 663	Chlorophyll <i>a</i> <sub>P276</sub>
V	425, 660	Hydroxychlorophyll <i>a</i>
VI	428, 660	Hydroxychlorophyll <i>a</i> epimer
VII	430, 663	Chlorophyll <i>a</i>

\* tentative assignment

#### 5.4.5.3. Hydroxychlorophyll *a* detected in the North Sea

Hydroxychlorophyll *a* was detected at all of the sampling stations and was maximum (relative to chl-*a*) at station 2, where the HO-chl-*a* to chl-*a* ratio was 0.129 (Figure 5.6.A). The minimum HO-chl-*a* to chl-*a* ratio (0.0139) was detected at station 4. This range of HO-chl-*a* to chl-*a* ratios was wider than that detected at station L4 in the Western English Channel, which had an annual range of 0.008 to 0.093 (chapter 4.3.5.1); and was also wider than the range recorded during a North Atlantic spring bloom which had a lower maximum ratio of ~0.05 (Bale 2010). The maximum HO-chl-*a* to chl-*a* ratio of 0.129, detected at station 2, was within the range which occurred during a spring bloom of *Chaetoceros* in the Celtic Sea (Walker & Keely, 2004). The range of the HO-chl-*a* to chl-*a* ratio during the *Chaetoceros* bloom can be calculated from the work of Walker and Keely (2004), as ~0.05 to ~0.5. The maximum ratio at station 2 is also similar to previous measurements of unidentified chlorophyll *a* allomers in the Baltic Sea, which accounted for 14% of the total chloropigments (Szymczak-Żyła and Kowalewska 2007).

The range of HO-chl-*a* to chl-*a* ratios detected during this cruise can also be compared to laboratory studies of algal cultures. The maximum HO-chl-*a* to chl-*a* ratios detected during an *Ostreococcus tauri* culture study were 0.18 during viral infection (chapter 3.3.4.2) and 0.014 during environmental limitation (chapter 3.3.4.4). Both of these maxima are within the range of HO-chl-*a* to chl-*a* ratios detected in the North Sea. In comparison, during *Thalassiosira pseudonana* nitrogen limitation the reported maximum ratio of HO-chl-*a* and chl-*a*<sub>P276</sub> combined, relative to chl-*a* was ~0.05 (Franklin et al. 2012). The maximum HO-chl-*a* to chl-*a* ratios detected in senescent cultures of *Pavlova gyrans* and *Isochrysis galbana* can be calculated as ~0.002 and ~0.007 respectively, from the work of Bale et al. (2011). In culture studies of *Emiliana huxleyi*, the HO-chl-*a* to chl-*a* ratios reached maxima of 0.036 in virally-infected (EhV86) cultures and 0.011 (Bale et al. 2013) and ~0.01 (Franklin et al. 2012) in senescent cultures.

The HO-chl-*a* to chl-*a* ratios measured during this cruise of the central and southern North Sea encompassed the wide range of ratios previously detected in 4 studies of pelagic marine sites and 4 culture studies involving a total of 5 species, and 2 applications of virus. This was due to the wide range of phytoplankton community compositions and environmental conditions encountered during the cruise.

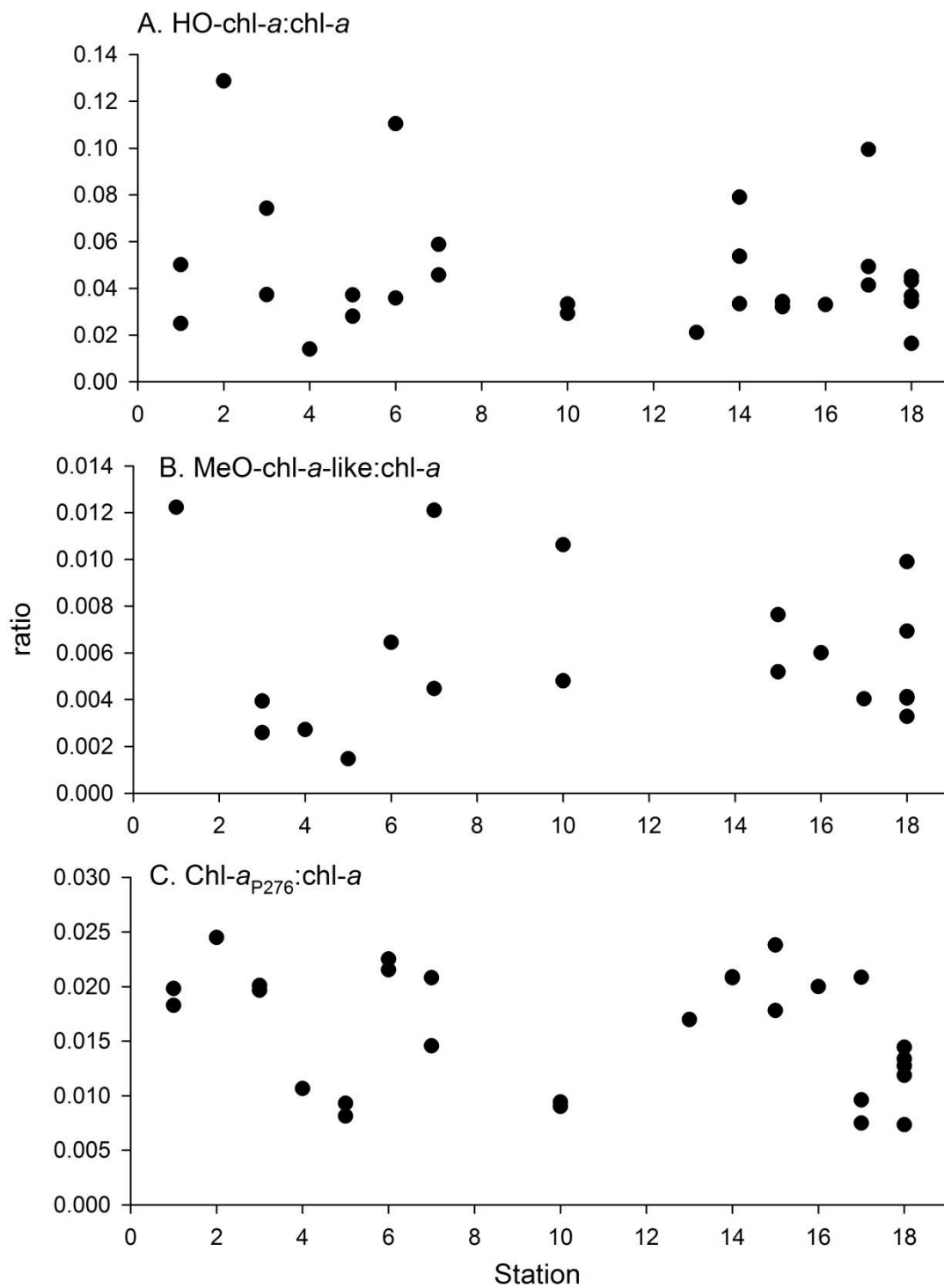


**Figure 5.6.** Ratios of allomers (A) hydroxychlorophyll *a* and (B) methoxychlorophyll *a*-like allomer, and precursor (C) chlorophyll  $a_{P276}$ , to chlorophyll *a* in pelagic particulate samples throughout the water column from 14 stations in the central and southern North Sea during May 2011, determined by HPLC.

#### 5.4.5.4. Methoxychlorophyll *a*-like allomer detected in the North Sea

The methoxychlorophyll *a*-like allomer was detected at 11 out of the 14 stations which were sampled for pigments (Figure 5.6.B). The maximum ratio of MeO-chl-*a*-like allomer to chl-*a* was 0.012, which occurred at stations 1 and 7. This chl-*a* allomer has been detected in phytoplankton pigment extracts on one previous occasion only; in a culture study of *O. tauri*. This allomer was not detected during growth limitation, but during viral infection only, with a ratio of MeO-chl-*a*-like allomer to chl-*a* between ~0.01 and ~0.02. The MeO-chl-*a*-like allomer to chl-*a* ratios at stations 1, 7, 10 and 18 are within the range detected during *O. tauri* viral infection. However, generally lower ratios were detected during this cruise than those detected during *O. tauri* viral infection. This is probably due to the natural marine environment containing a mixed assemblage of phytoplankton species. Higher concentrations of the MeO-chl-*a*-like allomer (relative to chl-*a*) were detected in culture because nearly all of the cells present were undergoing the same process of viral-infection.

#### 5.4.5.5. Chlorophyll $a_{p276}$ detected in the North Sea

The precursor chlorophyll  $a_{p276}$  was detected at every station sampled for pigments during the cruise (Figure 5.6.C). The ratios of chl- $a_{p276}$  to chl-*a* ranged from 0.0073 at station 18, to 0.025 at station 2. This is within the range of the chl- $a_{p276}$  to chl-*a* ratios detected at station L4 in the Western English Channel (from 0.003 to ~0.027, chapter 4.3.6).

This is only the second report of chlorophyll  $a_{p276}$  in the marine environment. However, chlorophyll  $a_{p276}$  has been previously detected during several culture studies. In exponentially growing *O. tauri* cultures, the maximum ratio of chl- $a_{p276}$  to chl-*a* was 0.014 (chapter 3.3.4.4). After population collapse due to viral infection, the chl- $a_{p276}$  to chl-*a* ratio greatly increased to 0.1, probably caused by the regrowth of a residual population.

Chlorophyll  $a_{p276}$  has also previously been detected in growing *Pavlova gyrans* cultures with a maximum chl- $a_{p276}$  to chl-*a* ratio of ~0.003 during exponential growth (Bale et al. 2010), which is consistent with the ratios measured during the cruise. Chl- $a_{p276}$  has also been detected in exponentially growing cultures of *E. huxleyi* and *Thalassiosira pseudonana* (Franklin et al. 2012), however the chl- $a_{p276}$  to chl-*a* ratios cannot be calculated as chlorophyll  $a_{p276}$  was quantified together with hydroxychlorophyll *a*.

The levels of chlorophyll allomers (relative to chl-*a*) encountered during this cruise transect are generally within ranges previously reported in marine (where they exist) and culture studies. The combined signal from the chlorophyll *a* allomers and precursor summates to between 2.7% (at station 4, Tyne) and 15.3% (at station 2, Outer Flamborough Front) of the total chl-*a* signal.

To begin to investigate the cause of the wide variation in the concentrations of the precursor and the chlorophyll allomers, relative to chlorophyll *a*, it is useful to further consider the biotic and environmental conditions of the sampling stations.

#### 5.4.6. *Multivariate analysis*

To enable comparisons of allomer measurements between stations, they were grouped by similarity of biota, nutrients, chlorophyll *a* concentration, allomer to chlorophyll ratios and the precursor (chl-*a*<sub>p276</sub>) to chl-*a* ratio. To try and explain variation in the phytoplankton assemblage by nutrient conditions and the variation in allomers by biotic and abiotic factors, MDS plots were compared and BEST analysis was carried out.

##### 5.4.6.1. Phytoplankton community compositions and nutrient concentration

The phytoplankton community compositions at the sampling stations were assessed for similarity. Cluster analysis was computed for the Bray-Curtis similarity of community composition, averaged across depths and replicate samples for each station. Four groups emanated at the 80% Bray-Curtis similarity level; cluster 1 included stations 7, 4 and 10; cluster 2 included stations 1, 2, 6, 13, 14 and 1; the remaining stations 3 and 18 were both isolated (Figure 5.7.A). Cluster analysis was computed for the Euclidian distance of nutrient conditions. Four groups emanated at the Euclidian distance 2 level; cluster 1 included stations 2, 3 and 15; cluster 2 included stations 4, 6, 7, 10, 14 and 18; the remaining stations 1 and 13 were isolated (Figure 5.7.B).

Grouping the sampling stations by biota and by nutrient conditions resulted in different clustering. Further, to assess any linkage between nutrient concentrations and biota at the sampling stations BEST analysis was carried out. When the similarity of the stations biota was compared to the nutrient conditions at each station, the best explanatory variables were combined ammonium and nitrite, however the correlation was weak ( $\rho=0.375$ ) and not statistically significant ( $p=0.247$ ). Hence the biota found at a station could not be explained fully by nutrient condition.

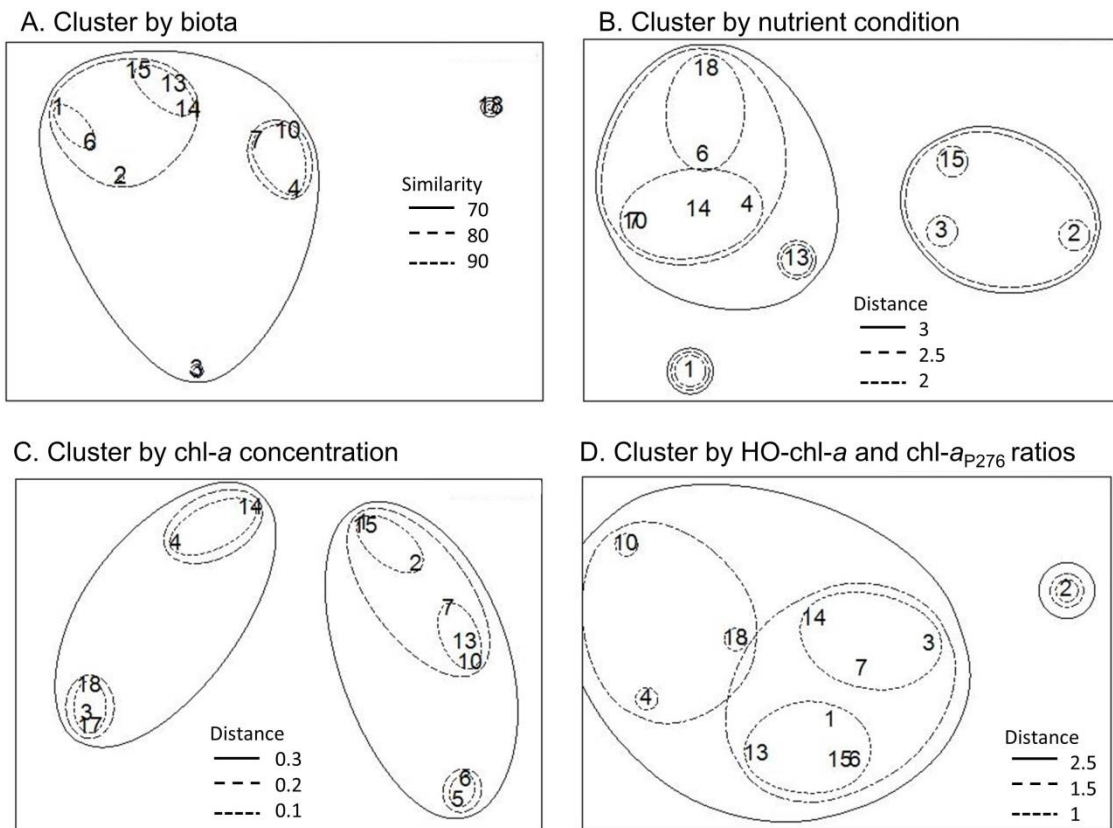


**Figure 5.7.** Multi-Dimensional Scaling (MDS) analysis of (A) phytoplankton community composition showing Bray-Curtis similarity, and (B) concentrations of nitrate, phosphate, nitrite, silicate, ammonium and silicate and N to P ratios, (C) chl-*a* concentration and (D) ratios of HO-chl-*a* and chl-*a*<sub>p276</sub> to chl-*a*, showing Euclidian distance.

The chlorophyll *a* concentrations at the sampling stations were assessed for similarity. Cluster analysis was computed for the Euclidian distance of chl-*a* concentrations, averaged across depths and replicate samples for each station. Four groups emanated at the Euclidian distance 0.2 level; cluster 1 included stations 4 and 14; cluster 2 included stations 18, 3 and 17; cluster 3 included stations 2, 15, 7, 13 and 10; cluster 4 included stations 5 and 6 (Figure 5.7.C). Cluster analysis was computed for the Euclidian distance of the ratios of HO-chl-*a* and chl-*a*<sub>p276</sub> to chl-*a*. Four groups emanated at the Euclidian distance 1 level; cluster 1 included stations 4, 10 and 18; cluster 2 included stations 1, 6, 13 and 15; cluster 3 included stations 3, 7 and 17; station 2 was isolated (Figure 5.7.D).

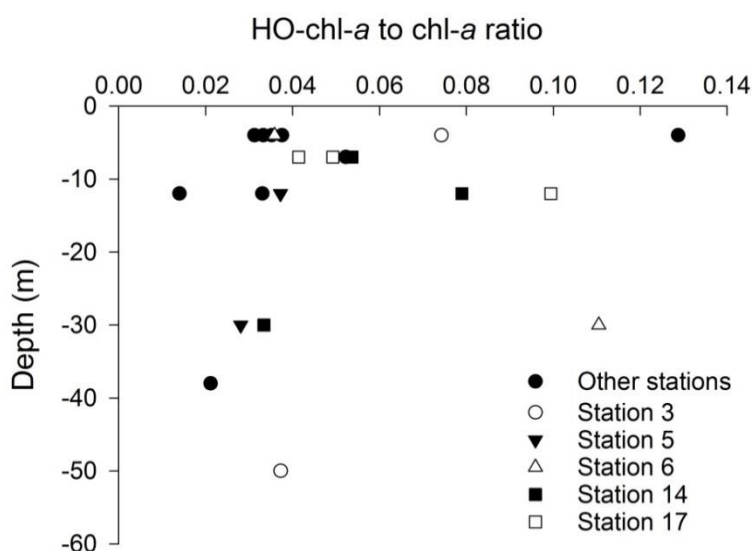
Grouping the stations by their ratios of HO-chl-*a* and chl-*a*<sub>p276</sub> to chl-*a* resulted in different clusters, compared to grouping by the biotic and abiotic factors. To assess the linkages between ratios of HO-chl-*a* and chl-*a*<sub>p276</sub> to chl-*a* and the biota and abiotic factors, BEST analysis was carried out. The similarity of the stations HO-chl-*a* and chl-*a*<sub>p276</sub> to chl-*a* ratios were compared

to the biotic and abiotic factors at each station. The best explanatory abiotic variables of the chl- $a_{p276}$  to chl- $a$  ratio were nitrate and chl- $a$ , however the correlation was weak ( $\rho=0.215$ ) and not statistically significant ( $p=0.59$ ). The best explanatory biotic variables were coccolithophore and *Phaeocystis* spp. abundance ( $\rho=0.454$ ), however this correlation was also not statistically significant ( $p=0.22$ ).

The best explanatory abiotic variables of the HO-chl- $a$  to chl- $a$  ratio were nitrate and silicate ( $\rho=0.613$ ), although the significance level was lower, it was still non-significant ( $p=0.07$ ). The best explanatory abiotic variables were *Micromonas*-like spp. and cryptophyte abundance ( $\rho=0.372$ ) however these correlations were also not statistically significant ( $p=0.59$ ).

#### 5.4.7. Hydroxychlorophyll $a$ through the water column

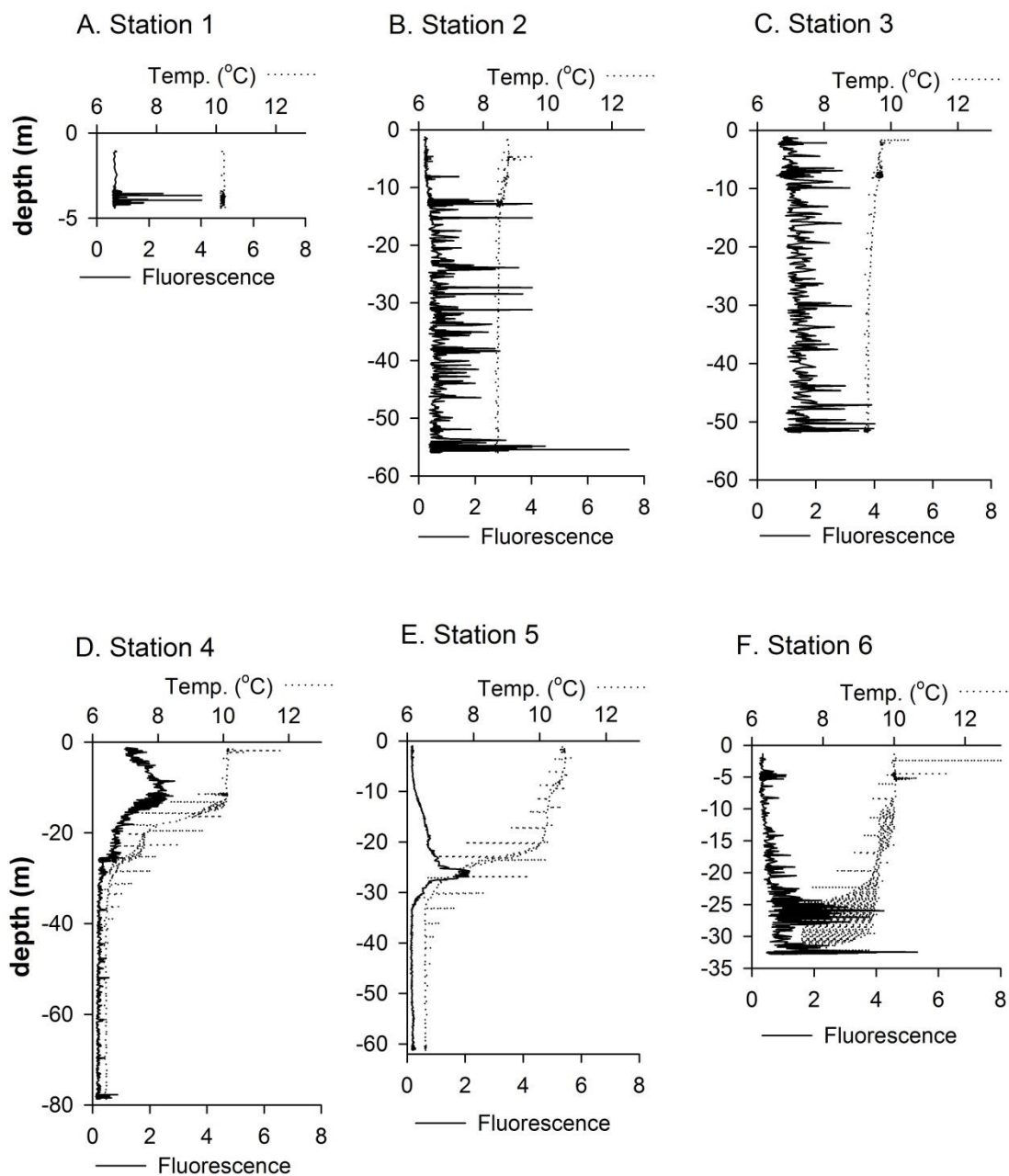
To establish if chl- $a$  allomers increase with depth (see section 5.1.1), as hypothesised by Walker and Keely (2004) photosynthetic pigment samples were collected from multiple depths at stations 3, 5, 14, 16 and 17. At stations 6 and 17 the ratio of HO-chl- $a$  to chl- $a$  increased with depth, however, at stations 3 and 5 the ratio of HO-chl- $a$  to chl- $a$  decreased with depth. When all samples were considered, regardless of station, there was no trend in the ratio of HO-chl- $a$  to chl- $a$  with depth (Figure 5.8). Hence there was no evidence to support the hypothesis that the ratio of HO-chl- $a$  to chl- $a$  increases with depth, when mixing/stratification of the water column is not considered. To further resolve this hypothesis, allomer occurrence through the water column was assessed at thermally stratified stations.



**Figure 5.8.** All measurements of hydroxychlorophyll  $a$  to chl- $a$  taken during a North Sea cruise in May 2011, through the depth profile.

5.4.8. Allomer to chlorophyll *a* ratios at thermally stratified stations

Thermal stratification was present at stations 4, 5, 7, 10 and 14 (Figure 5.9). Clear differences in chlorophyll *a* concentration above and below the thermocline also occurred at these stations (Figure 5.9). At the remaining stations, there was no obvious peak in chlorophyll fluorescence. To address the hypothesis that ratios of allomers to chlorophyll are maximal at depths below the chlorophyll maximum; only at stations 4, 5, 7, 10 and 14 were considered.



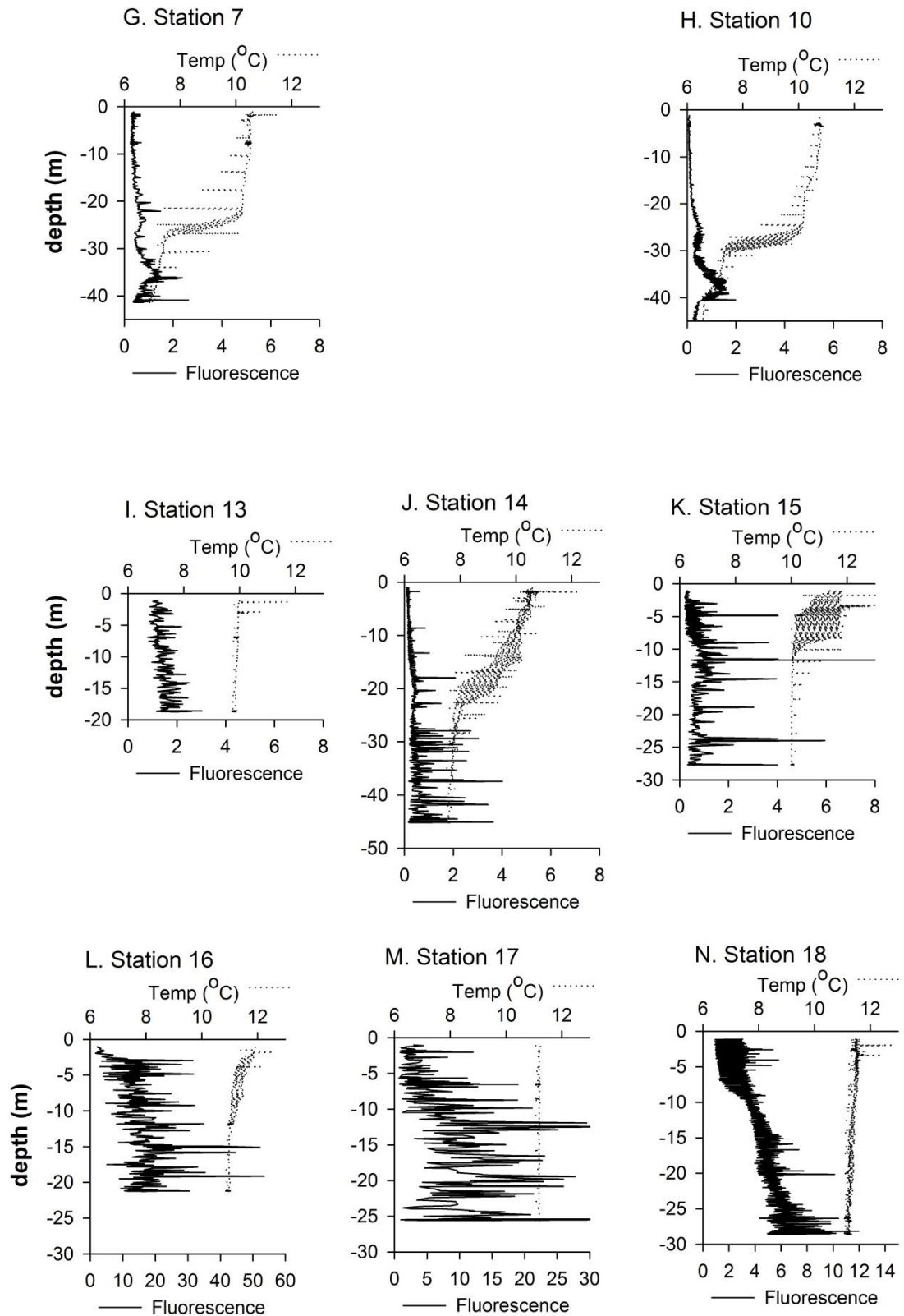


**Figure 5.9.** Continuous chlorophyll fluorescence (RFU) profiles through the water column at 14 sampling stations in the central and southern North Sea.

At station 5 chl-*a* concentration peaked at approximately 25-27m (Figure 5.9.E), which was located within the thermocline. Generally at this station, chlorophyll concentration was higher above the thermocline, than below. Samples for particulate photopigments were taken above the chl-*a* maximum (12 m), and just below the chl-*a* maximum at 30 m. The ratio of HO-chl-*a* to chl-*a* was 0.037 at 12 m and 0.028 at 30 m depth (Table 5.3). These values are respectively within and between the interquartile range of the HO-chl-*a* to chl-*a* ratios observed during this cruise. As a higher HO-chl-*a* to chl-*a* ratio occurred above the chl-*a* maximum, than below, this result provides evidence against the hypothesis that ratios of allomer to chl-*a* are increased at depths below the chlorophyll maximum. This is in contradiction to results by Walker and Keely (2004) where the HO-chl-*a* maximum was observed just below the chl-*a* maximum.

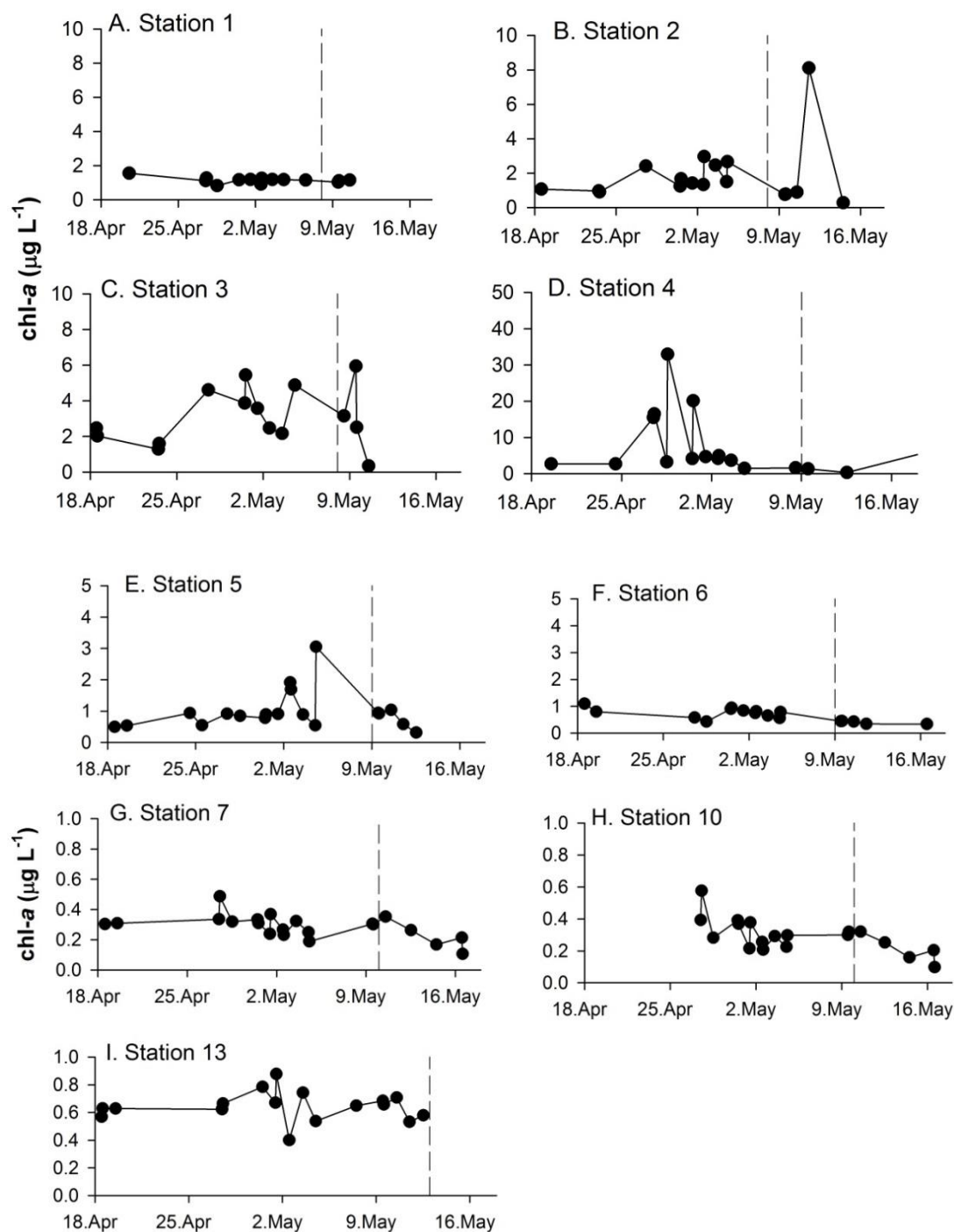
At station 14 the average chlorophyll *a* concentration was higher below the thermocline (from approximately 30 m), however chl-*a* concentration was variable, and no clear maximum peak in chl-*a* concentration occurred. The HO-chl-*a* to chl-*a* ratio was higher at 29 m (0.079), which was just below the thermocline compared to above the thermocline at 9 and 12 m, which had HO-chl-*a* to chl-*a* ratios of 0.054 and 0.033 respectively. This result is in agreement with measurements from the time series study at station L4 (Western English Channel) presented in chapter 4. At station L4, when the water column contained a thermocline, the HO-chl-*a* to chl-*a* ratio was higher at depths below the thermocline. This result also agrees with the hypothesis by Walker and Keely (2004), that the HO-chl-*a* to chl-*a* ratio is maximal below the chl-*a* maxima.

**Table 5.3.** Hydroxychlorophyll *a* ratios at stations sampled for photopigments at multiple depths.

Station	Sample depth (m)	Sample depth relative to chl- <i>a</i> maximum	HO-chl- <i>a</i> : chl- <i>a</i> ratio
5	12	above	0.037
5	30	below	0.028
14	9	above	0.054
14	12	above	0.033
14	29	at chl- <i>a</i> max.	0.079
4	12	at chl- <i>a</i> max.	0.014
7	6	above	0.0525
10	4	above	0.031

#### 5.4.9. Allomer to chlorophyll ratios in context of recent history of chlorophyll *a* (satellite derived)

To determine if the recent history of chlorophyll *a* in the water column influences the concentration of hydroxychlorophyll *a* or the precursor chl- $a_{p276}$  (relative to chl-*a*), the satellite derived chlorophyll *a* estimates were calculated for each station from the 20<sup>th</sup> April to the 20<sup>th</sup> May 2011 (Figure 5.10). These estimates were derived from ocean colour data on a 1 km resolution.



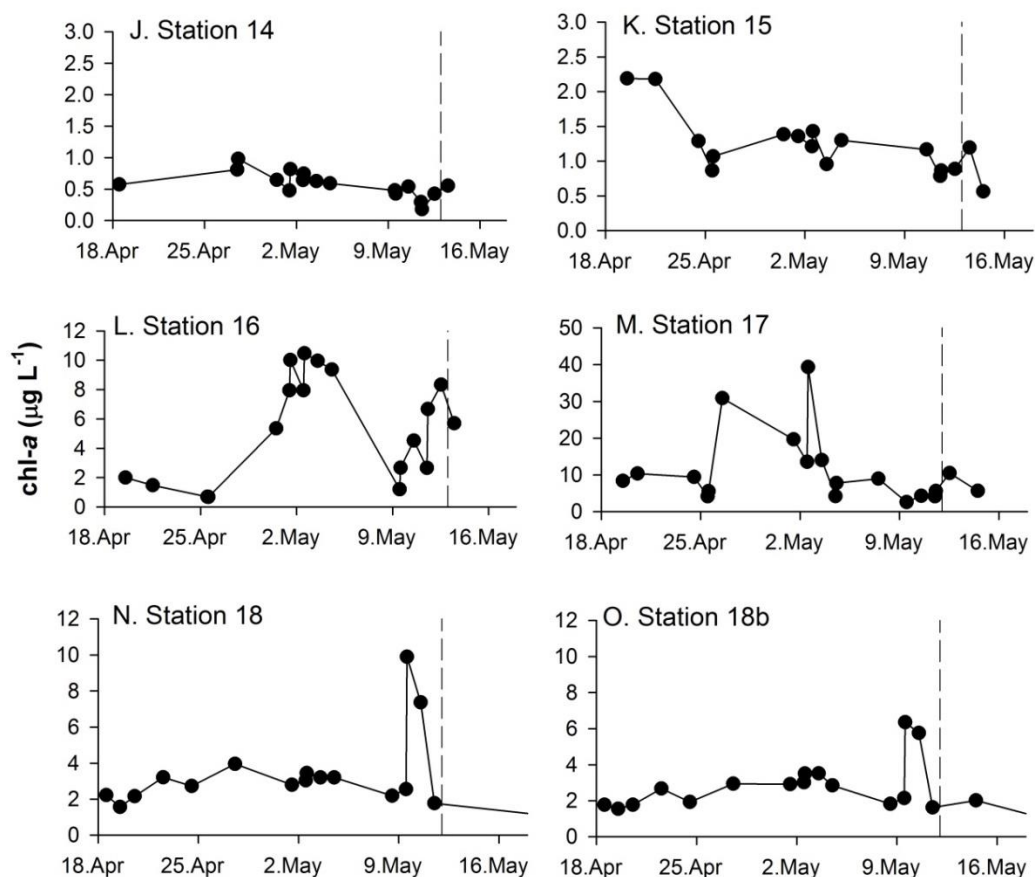


**Figure 5.10.** Satellite derived surface chlorophyll *a* concentration at 15 stations in the central and southern North Sea from 20<sup>th</sup> April to 20<sup>th</sup> May 2011. - - - indicates date of water column sampling.

From the historical satellite derived estimates, it is deduced that at the time of sampling, chl-*a* concentration was decreasing at stations 1, 2, 3, 4, 5, 6 and 16 (Figure 5.10). In particular, the historical chl-*a* data indicates that stations 5, 17, 18 and 18b were sampled immediately after phytoplankton blooms. Chlorophyll *a* concentration was increasing at stations 7, 10, 14, 15 and 17 (Figure 5.10).

The maximum HO-chl-*a* to chl-*a* ratio occurred at station 2, where chlorophyll *a* was decreasing, and a larger range of HO-chl-*a* to chl-*a* ratios occurred at stations with decreasing chl-*a* concentration (Figure 5.11.A), however this does not provide evidence to support the hypothesis that HO-chl-*a* to chl-*a* ratios are highest during periods of decreasing chl-*a* concentration.

A larger range in the ratios of the precursor chl- $a_{P276}$  to chl- $a$  was also measured at stations with decreasing chl- $a$  concentration. However, this study does not provide evidence in support of the hypothesis that chl- $a_{P276}$  to chl- $a$  ratios will be highest during periods of increasing chl- $a$  concentration.

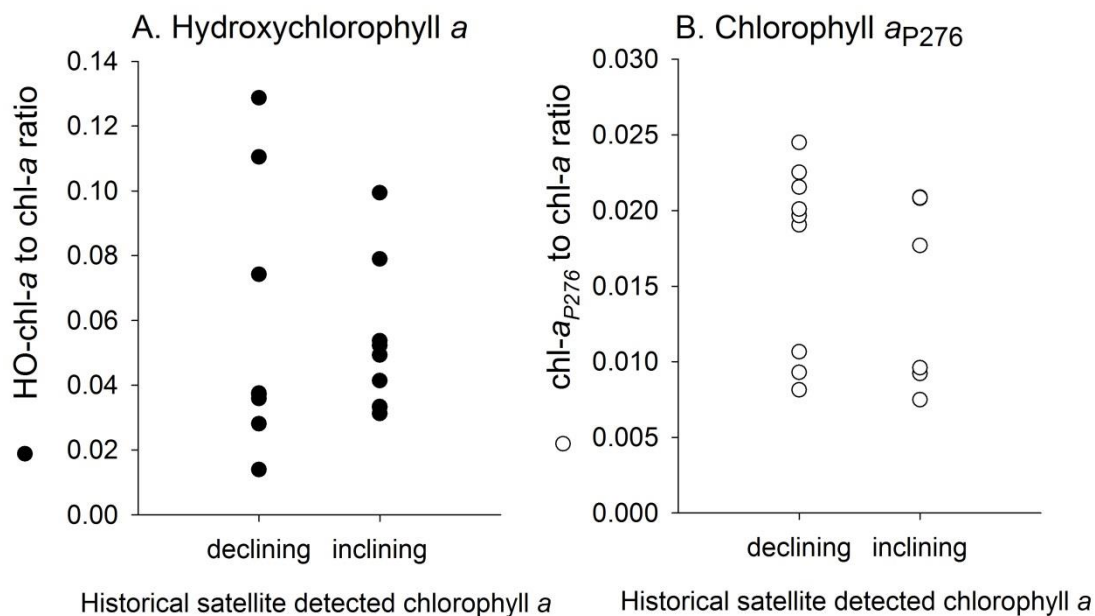


**Figure 5.11.** (A) HO-chl- $a$  to chl- $a$  ratio and (B) chl- $a_{P276}$  to chl- $a$  ratio, during periods of decreasing and increasing chl- $a$  concentration.

#### 5.4.10. Allomer to chlorophyll ratios in the context of $F_v/F_m$

As maximum  $F_v/F_m$  of mixed communities is known to reduce with increasing cell size (Cermeno et al. 2005, Suggett et al. 2009), it is expected that stations with limited nanoeukaryotes (stations 1, 2, 3, 6 and 15, Figure 5.2.C) may be expected to have higher  $F_v/F_m$  than stations with abundant nanoeukaryotes (stations 4, 7, 10, 16 and 18). However, this rough division of size class is not adequate to resolve the differences in  $F_v/F_m$  between stations.

Unfortunately no species identification was carried out during the cruise. Therefore it is impossible to accurately estimate the expected maximum possible  $F_v/F_m$  for the assemblages found at each station. The most reliable estimation can be made for stations 17 and 18 where abundant *Phaeocystis* occurred. The  $F_v/F_m$  ratio of stations 17 and 18 can be compared to the range of  $F_v/F_m$  ratios measured in culture studies of *Phaeocystis antarctica*; 0.61 to 0.7 under experimental growth irradiances (5-250  $\mu\text{mol photons m}^{-2} \text{s}^{-1}$ ) (Kropuenske et al. 2009), *P. globosa*: 0.6 (Baudoux et al. 2006) and *P. pouchetti*; 0.4 (Ray et al. 2014). With such variation between species it is not useful to compare the *Phaeocystis* spp. at station 17 and 18 with the above culture studies.

Without a thorough investigation of species contribution no conclusions can be drawn against the hypothesis that a higher ratio of allomers occurs when  $F_v/F_m$  is lower than the maximum expected for the phytoplankton assemblage. Without this data only general observations can be made: The maximum HO-chl-*a* to chl-*a* ratio of 0.129 occurred at station 2 (Figure 5.12), which had the median value of  $F_v/F_m$  observed (approximately). There is no evidence to support the hypothesis that the HO-chl-*a* to chl-*a* ratio will be highest at low  $F_v/F_m$ . The minimum HO-chl-*a* to chl-*a* ratio of 0.014 occurred at station 4 (at 12m), where the maximum surface  $F_v/F_m$  of 0.374 occurred (Figure 5.12). This supports the hypothesis that the HO-chl-*a* to chl-*a* ratio will be lowest at high  $F_v/F_m$ . Stations 1, 16 and 18 also support this hypothesis. However stations 5, 6, 7, 14, 15 and 18 are contrary.

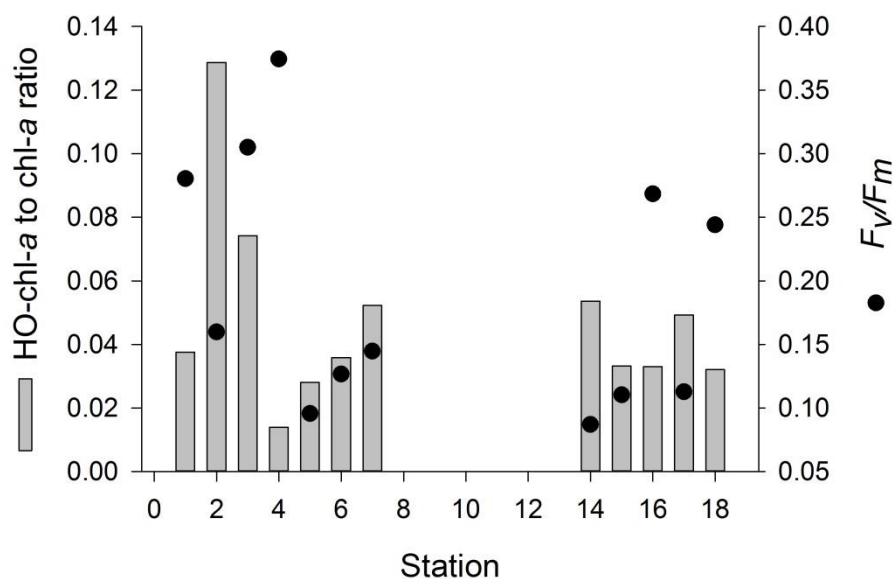


**Figure 5.12.** Surface  $F_v/F_m$  and maximum HO-chl-*a* to chl-*a* ratio at 12 sampling stations in the North Sea.

### 5.5. Chapter V conclusions

The chl-*a* signal originating from the chl-*a* allomers and precursor detected during the cruise (between 2.7% and 15.3%) was within the range measured over a year at the Western English Channel, from 3% in February to 12% in April 2012 (chapter 4.3.5). Although the cruise took place during April 2011, the sampling stations covered a wide variety of environmental and biological conditions and hence the range of allomer and precursor ratios matched that measured over a year in the Western English Channel.

Results from the novel dual staining technique indicated that phytoplankton cells were in an active and viable condition. Station 18 was sampled during a *Phaeocystis* spp. bloom and although historical chl-*a* concentration (determined by satellite observation) indicated that the peak abundance of *Phaeocystis* spp. had passed (Figure 5.10.N&O), the viability stains indicated the population was still viable and active. This was reflected in low HO-chl-*a* to chl-*a* ratios at station 18 (Figure 5.6.A). This unexpected result may be due to water movement, i.e. the chl-*a* concentrations measured at station 18 during April/May by satellite may not have been the same body of water.

This survey provided no evidence to support the hypothesis that the allomer to chl-*a* ratio is higher below the chlorophyll maxima, i.e. increased in sinking particles. However, only two thermally stratified stations were sampled at multiple depths during the cruise, Therefore the hypothesis that allomer to chl-*a* ratio is higher below the chlorophyll maxima, as supported by Walker and Keely (2004) and measurements at the Western English Channel (chapter 4.3.5.1), where the HO-chl-*a* to chl-*a* ratio was increased at depth, is not challenged.

The hypotheses that a high ratio of allomers to chl-*a* will occur during population decline, and a high ratio of chl-*a*<sub>p276</sub> to chl-*a* will occur during population increase could not be tested by this survey. Stations were only sampled once and historical chl-*a* concentration may be a poor representative of population dynamics due to movement of the water body. This hypothesis requires a high sampling resolution of the same body of water throughout population growth and decline.

As it is difficult to compare levels of  $F_v/F_m$  across varied phytoplankton assemblages, the hypothesis that a high allomer to chl-*a* ratio will occur in areas of low  $F_v/F_m$ , and a low allomer to chl-*a* ratio will occur in areas of high  $F_v/F_m$  remains untested. Finally, to provide conclusive evidence for the hypotheses addressed in this chapter, more critical and focused studies are required. For example species data is needed to provide expected  $F_v/F_m$  ranges, in order to relate allomer ratios to maximum photosynthetic efficiency. The ratio  $F_v/F_m$ , chl-*a* concentration and allomer to chl-*a* ratios are all bulk properties of a dynamic and heterogeneous community. Hence to test the hypotheses addressed in this study, further details need to be included, e.g. phytoplankton community composition and studies of sub-populations.

## **Chapter VI**

### ***Research Review***

### **Overview & Future Work**

#### **6.1. *Overview of Research***

This work has focused on the use of chlorophyll allomers as indicators of phytoplankton viability in culture populations and natural assemblages. Unlike previous studies of allomer occurrence in culture (Bale et al. 2011, Franklin et al. 2012, Bale et al. 2013) and *in situ* (Walker and Keely 2004, Bale 2010), this work included parallel measurements of cell physiology and photo-physiology. This was to allow comparison of allomer formation with the physiological changes which occur in the cells during population decline. As chlorophyll allomers were the main focus of this work, selection and optimisation of an HPLC method, specifically for the identification and quantification of allomers, was undertaken.

#### **6.2. *HPLC method selection and optimisation***

Initially, an HPLC method developed by Airs et al. (2001a) was chosen, based on its ability to resolve several allomers (Bale 2010), to be optimised for the separation of chl-*a* allomers. The eluent composition of the Airs et al. (2001a) method was modified to further separate the allomers (Method 1). However, artefact formation became evident during use of the Airs et al. (2001a) method and Method 1. As the artefacts were products of chlorophyll oxidation and the allomers of interest were also oxidation products of chlorophyll, steps to minimise artefact production were undertaken. To this end, the method of sample preparation was adjusted and alternative HPLC methods (Zapata et al. 2000, Saesaengseerung 2013) were assessed for artefact formation. The Zapata et al. (2000) method conceded the minimal and most repeatable level of allomers during analysis of chl-*a* standards. Hence, it was used for the analysis of chlorophyll allomers in the following work.

This report of artefact formation, resulting from the Airs et al. (2001a) method and Method 1, has implications for the measurement of pigments in phytoplankton, detritus and sediment. It highlights the importance of method optimisation, assessment of artefact formation and use of standards prior to analysis.

### 6.3. *O. tauri* senescence/viral-infection

There is evidence in the literature to suggest that allomer formation is dependent on mode of phytoplankton mortality (Franklin et al. 2012, Bale et al. 2013). A culture of *Ostreococcus tauri* was monitored for allomer formation during population decline due to both viral-lysis and environmental limitation. Detailed analysis of chlorophyll allomers was accompanied by assessment of cell membrane permeability by SYTOX-staining, reactive oxygen species (ROS) by CM-H<sub>2</sub>DCFDA-staining, and PSII efficiency ( $F_v/F_m$ ).

#### 6.3.1. Novelty of Study

To clarify the originality of this work – The Zapata et al. (2000) method for HPLC separation of photo-pigments was utilised for the first time to separate and identify chl-*a* allomers from phytoplankton culture. Previous studies of allomer production in virally infected, nutrient or environmentally limited algal cultures have utilised the Airs et al. (2001a) method (Bale et al. 2011, Franklin et al. 2012, Bale et al. 2013). In addition, intracellular ROS had not been measured previously in parallel with allomer occurrence. Further, during this study, ROS, membrane permeability and allomer occurrence were measured for the first time in *Ostreococcus* cultures.

#### 6.3.2. Novel Results

For the first time in microalgae, two chl-*a* allomers, methoxychlorophyll *a*-like (MeO-chl-*a*-like) and hydroxychlorophyll *a*-like (HO-chl-*a*-like) were detected solely in association with viral-infection, but not during environmental limitation, of *O. tauri*. Hydroxychlorophyll *a* (HO-chl-*a*) and hydroxychlorophyll *b* (HO-chl-*b*) were both produced during viral infection and environmental limitation of *O. tauri*. This was the first report of a chl-*b* allomer increasing with viral infection. Both HO-chl-*a* and HO-chl-*b* (relative to chl-*a* and chl-*b* respectively) increased by around 10-fold more during viral infection than during environmental limitation. Allomers had previously only been monitored during viral infection of *Emiliana huxleyi* CCMP 1516 cultures. An increase in HO-chl-*a* was associated with EhV86-infection of *E. huxleyi* but not with the decline of the control population (Bale et al. 2013).

The percentage of SYTOX-positive cells and CM-H<sub>2</sub>DCFDA-positive cells both increased during viral-infection. Interestingly, they also both had peaks prior of population decline due to environmental limitation, and at the later stage of population decline. However, HO-chl-*a* only increased at the later stage of population decline. Previously, the allomers methoxychlorophyll *a* and HO-chl-*a* were associated with the onset on *Thalassiosira pseudonana* decline due to nitrogen limitation and increase in SYTOX-positive cells (Franklin et al. 2012). This pre-decline peak in SYTOX-positive and CM-H<sub>2</sub>DCFDA-positive cells was a novel early warning sign of the impending population decline.

The component chl-*a*<sub>p276</sub> was most abundant (relative to chl-*a*) during growth of the *O. tauri* population. This provides evidence for chl-*a*<sub>p276</sub> as a biosynthetic precursor to chlorophyll *a*.

### 6.3.3. Further culture work

This culture section of the project was limited to one species only. Hence conclusions cannot be extended across phytoplankton taxa. This limits the inference for using chl-*a*<sub>p276</sub> and chlorophyll allomers as indicators of phytoplankton population growth and decline. A study of allomer and chl-*a*<sub>p276</sub> production in phytoplankton mono-cultures across classes would improve the prospects of this work to be utilised for monitoring natural marine assemblages. As the response of the cellular stain CM-H<sub>2</sub>DCFDA in the *O. tauri* cultures was limited, the ROS probe DCFH-DA could be optimised for use with *O. tauri* cultures and applied to future studies. In addition, to ascertain the sequence of events during cell mortality, other methods might include testing for degradation of DNA with deoxyuridine triphosphate nucleotides (f-dUTP) and enzyme activity measured by fluorescein diacetate (FDA).

## 6.4. Annual cycle of allomer and precursor occurrence in the Western English Channel

The occurrence of chlorophyll *a* allomers and the precursor chl-*a*<sub>p276</sub> were monitored over a year in the Western English Channel at time series station L4. Fluctuations in allomer abundance (relative to chl-*a*) were related to the seasonal community progression of phytoplankton. Hence, the potential sources of the allomers in the water column were resolved.

#### 6.4.1. Novelty of study

Previous measurements of HO-chl-*a* in the marine water column are limited to 2 studies, of 6 days (Walker and Keely 2004) and 16 days (Bale 2010) long. Hence, this is the first measurement of HO-chl-*a* and chl-*a*<sub>P276</sub> over an annual cycle. The parallel measurements of phyto- and microzooplankton abundance, nutrient concentrations, temperature and light levels were also unique to this study.

#### 6.4.2. Novel Results

HO-chl-*a* was quantified over the annual cycle and found to be primarily produced during the decline of phytoplankton blooms, at concentration in agreement with previous measurements (Walker and Keely 2004). Pelagic particulate HO-chl-*a* was associated with *Phaeocystis* spp, *Guinardia delicatula*, *E. huxleyi*, *Karenia mikimotoi* and *Chaetoceros socialis* abundance. However, alternate peaks in *G. delicatula* and *C. socialis* abundance were not associated with HO-chl-*a*. This indicated that the formation of HO-chl-*a* was not only dependant on taxa, but the reason for the population decline. HO-chl-*a* in the surface sediment was found to be around 10 times higher (relative to chl-*a*) than that found in the water column, indicating that most HO-chl-*a* was produced during the sedimentation of the phytoplankton cells. This follows on from results reported by Bale (2010), of higher HO-chl-*a* to chl-*a* ratios present in sinking particles. This study also provided evidence for the assignment of the component chl-*a*<sub>P276</sub> as a biosynthetic precursor to chl-*a* as it increased during high chl-*a* concentration. At the Western English Channel between 3% (Feb) and 12% (April) of compounds with chlorophyll *a* like absorption spectra were allomers or precursor.

#### 6.4.3. Further in situ work

The results of the time series study, along with *O. tauri* culture results add to previous evidence (Franklin et al. 2012, Bale et al. 2013) that the reason for population decline affects allomer formation. For the purpose of resolving this, measurement of virus particles in the water column would be useful. Further increasing the sampling resolution during the highly productive periods of the year (i.e. the spring bloom) would allow the timing of population declines to be related more closely to allomer occurrence. Further, thus far small amounts of HO-chl-*a* are always present in photo-pigment extracts; there are several possible reasons for its consistent

presence in extracts. This seemingly stable baseline level of HO-chl-*a* in the cell (relative to chl-*a*) may indicate it has a function within the photosystem. Alternatively, HO-chl-*a* may be produced as a component of chl-*a* turnover, and may arise from the proportion of the population in decline. Hence the investigation into the functionality of hydroxychlorophyll *a* may be of interest. Otherwise, this background level of HO-chl-*a* may be a small residual proportion produced during pigment extraction or analysis.

The time-series of allomer and chl-*a* precursor measurements from the Western English Channel could be incorporated into a basic productivity algorithm for coastal systems, based on ocean colour data. One approach could be to separate the year into “high productivity” and “low productivity” periods and use average percentages of “photosynthetically non-functional chl-*a* signal” to adjust productivity estimates; i.e. ~12% during the spring bloom and ~3% outside the spring bloom.

### **6.5. Allomer detection in the North Sea**

Chlorophyll allomers were analysed during a cruise, over a range of environmental conditions and phytoplankton community compositions. The occurrence of allomers and the component chl- $a_{p276}$  were related to bulk chlorophyll fluorescence measurement;  $F_v/F_m$ , and the recent history of chl-*a* concentration, as derived from satellite ocean colour measurements. The data was also used to test the hypothesis that allomers are increased (relative to chl-*a*) below the chlorophyll *a* maxima. Allomer and chl- $a_{p276}$  occurrence was also related to additional indicators of cell viability - cell membrane permeability and enzyme activity.

#### **6.5.1. Novelty of study**

Previous *in situ* studies of chlorophyll allomer occurrence in the water column have not included environmental measurements. This study is unique in that environmental and biological data were included. Unlike the time series study, this cruise data was also put into context of the recent history of chlorophyll *a* concentration. A novel dual cell staining technique was also used; CMFDA and SYTOX-Green were applied in combination, to assess phytoplankton assemblage viability.

### 6.5.2. Novel Results

Although data collected from the cruise did not provide evidence that allomers increase below the chl-*a* maxima, concentration of HO-chl-*a* (relative to chl-*a*) was higher below the thermocline compared to above. This result is in agreement with measurements from the time series study in the Western English Channel. The ratio of total chl-*a* allomers (and chl-*a*<sub>p276</sub>) to chl-*a* reached a maximum of 15% at the Flamborough Front.

### 6.5.3. Further *in situ* work

As up to 15% of the chlorophyll *a* signal originated from photosynthetically non-functional chl-*a*-like products, i.e. allomers and precursor, the confidence interval in chl-*a* estimates from ocean colour data may need to be re-assessed.

During further *in situ* measurements of allomers it would be beneficial to make parallel measurements of phytoplankton community function, i.e. quantification of carbon fixation by <sup>14</sup>C-labeling (Pinckney et al. 1996, Veldhuis et al. 2001). Combining *in situ* measurements of carbon fixation with quantification of the proportion of chl-*a* 'signal' that is produced by allomers or precursor would, at least, adjust ocean colour estimates of chl-*a* concentration to provide more accurate predictions of productivity. Satellite measurements of ocean colour are used to make estimates of oceanic chlorophyll biomass from which primary production is determined (Antoine and Morel 1996, Sathyendranath and Platt 2007). It is assumed, when modelling production in this way; that all the detected chlorophyll *a* is actively contributing to photosynthesis. However chlorophyll *a* allomers and precursor, which have similar spectral properties to chl-*a* are not contributing to photosynthesis. These primary productivity models are dependent on *in situ* truthing by quantification of carbon fixation by <sup>14</sup>C-labeling. Hence measurements of carbon fixation and allomer occurrence are appropriate.

## 6.6. Conclusions

Results from this study have demonstrated the allomer HO-chl-*a* to increase during population decline and the precursor chl-*a*<sub>P278</sub> to increase during population growth. It also introduces the MeO-chl-*a*-like allomer as a potential indicator of viral infection. The level of production of chlorophyll allomers in eukaryotic phytoplankton cells is dependent on species and the reason behind the population decline. Hence chlorophyll allomers and precursor are potential markers of phytoplankton population state.

[Blank Page]

## Chapter VII

### *Materials and Methods*

#### **7.1. *Materials for Biological use***

##### *7.1.1. Preparation of glassware*

Glassware for biological use was separate from that used for chemical purposes. Glassware was scrubbed and rinsed in tap water and soaked in 10% HCl (Fisher Scientific) overnight. Items were rinsed in Milli-Q (Synergy 185, Millipore, MA, USA) water 5 times. Bungs for culture flasks were soaked overnight in 1% Neutracon decontamination solution (Decon) (in Milli-Q water) and then rinsed in Milli-Q water until all noticeable Neutracon residues were removed. All glassware and bungs were sealed with foil and autoclaved.

##### *7.1.2. Algal and Viral stocks*

*Ostreococcus tauri* OTTH0595 and *Ostreococcus tauri* Virus 5 (OtV5) were provided by Nigel Grimsley (French National Centre for Scientific Research). The strain has been catalogued in the Roscoff Culture Collection as RCC 745. For strain details see Derelle et al. (2008).

##### 7.1.2.1. Preparation of OtV5 stock

On receipt, 5 mL of OtV5 lysate was applied to *O. tauri* cultures (1 L) in exponential growth phase ( $\mu \geq 0.69 \text{ d}^{-1}$ ). *O. tauri* population abundance was monitored daily by flow cytometry (section 7.2.2). When the *O. tauri* population had declined by more than 95%, the culture was processed to create fresh viral lysate under sterile conditions. Lysed cell particles were removed from the lysate by filtration (0.2  $\mu\text{m}$ , Millipore Express) into sterile flasks (1 L), aided by vacuum pump (at  $\sim 15 \text{ kg cm}^{-3}$ ). The fresh lysate was stored at 5 °C in the dark. Aliquots were brought to culture temperature prior to use.

#### 7.1.2.2. Algal maintenance

*O. tauri* was maintained in an artificial seawater base (ASW) enriched with F/2 (recipes can be found in section 7.1.3.1), using sterile technique. Sub-culturing was carried-out weekly, where 1 mL of culture was transferred into triplicate 250 mL conical flasks containing 50 mL of freshly filter-sterilised culture media, to maintain cells in exponential growth phase. Prior to use in experiments, *O. tauri* was closely monitored and kept growing in semi-continuous batch culture populations with a specific growth rate ( $\mu$  d<sup>-1</sup>) between 0.3 and 0.7. During this time, cultures consistently reached a final yield of  $7.5 \times 10^7$  cells ml<sup>-1</sup> before declining. Assuming cells were using nutrients in the Redfield ratio, by calculation phosphate was limiting (F/2 media has 24:1 N:P) (Guillard and Ryther 1962).

#### 7.1.2.3. Culture conditions

Cultures of *O. tauri* during the maintenance and study periods were incubated at 20 °C in a constant temperature room. Illumination from cool white fluorescent tubes was provided at 100 - 130  $\mu\text{mol photons m}^{-2} \text{s}^{-1}$  between 07:00 h and 23:00 h on a 16 : 8 h light : dark cycle.

#### 7.1.3. *Preparation of Growth Media*

Growth media for the *O. tauri* cultures used the ASW base from the ESAW formulation (Harrison and Berges 2005) enriched with F/2 nutrients (Guillard and Ryther 1962). Recipes and preparation instructions were accessed from Andersen (2005). The anhydrous and hydrated salt solutions (Tables 7.1 & 7.2) were prepared separately in Milli-Q water, in 5 L volumes (in 10 L carboys) and autoclaved at 121 °C for 90 min. The vitamin (Table 7.3) and Iron-EDTA (Table 7.4) stock solutions were filter sterilised through pre-autoclaved cellulose nitrate filters (47 mm diameter, 0.2  $\mu\text{m}$  pore size, Whatman, Chiltern, UK) and the Trace Metal stock solution (Table 7.5) was autoclaved at 120.8 °C for 20 min. These components were stored at -20 °C in 10 mL aliquots. The F/2 nutrients were prepared in 50 mL batches, autoclaved at 120.8 °C for 20 min and stored at 5 °C.

The stored components were brought to room temperature prior to preparation of the growth media. All components were added together (quantities can be found in Table 7.7) and the final volume was brought to 1 L with dH<sub>2</sub>O. Each litre of media was filter sterilised through pre-autoclaved cellulose nitrate filters (as above) prior to use.

7.1.3.1. ASW and media recipes

The components of each solution were dissolved in 5 L of Milli-Q water.

**Table 7.1.** Components of ESAW Salt solution I: Anhydrous salts. Quantity to produce 5 L of stock.

Component	Quantity used for 5 L stock (g)	Salt Supplier
NaCl	176.62	Sigma
Na <sub>2</sub> SO <sub>4</sub>	29.58	Sigma
KCl	4.9917	Sigma
NaHCO <sub>3</sub>	1.45	Sigma
KBr	0.7192	Fluka
H <sub>3</sub> BO <sub>3</sub>	0.1917	Sigma
NaF	0.2333	Sigma

**Table 7.2.** Components of ESAW Salt solution II: Hydrated salts. Quantity to produce 5 L of stock.

Component	Quantity used for 5 L working stock (g)	Salt Supplier
MgCl <sub>2</sub> · 6H <sub>2</sub> O	79.93	Fisher Scientific
CaCl <sub>2</sub> · 2H <sub>2</sub> O	11.2	Sigma
SrCl <sub>2</sub> · 6H <sub>2</sub> O	0.1816	Fisher Scientific

Table 7.3. Components to produce Vitamins for ESAW media

Component	Primary stock g L <sup>-1</sup> dH <sub>2</sub> O	Quantity used for 1 L working stock	Salt Supplier
Thiamine · HCl (vitamin B <sub>1</sub> )		0.1 g	Sigma
Biotin (vitamin H)	1.0	1 mL	Sigma
Cyanocobalamin (vitamin B <sub>12</sub> )	2.0	1 mL	Sigma

**Table 7.4.** Components to produce Iron-EDTA stock solution for ESAW media.

Component	Quantity used for 1 L working stock (g)	Salt Supplier
Na <sub>2</sub> EDTA · 2H <sub>2</sub> O	2.44	Sigma
FeCl <sub>3</sub> · 6H <sub>2</sub> O	1.77	Sigma

**Table 7.5.** Components to produce Trace Metals Solution II for ESAW media.

Component	Primary stock g L <sup>-1</sup> dH <sub>2</sub> O	Quantity used for 1 L working stock	Salt Supplier
Na <sub>2</sub> EDTA · 2H <sub>2</sub> O		3.09 g	Sigma
ZnSO <sub>4</sub> · 7H <sub>2</sub> O		0.073 g	Sigma
CoSO <sub>4</sub> · 7H <sub>2</sub> O		0.016 g	Sigma
MnSO <sub>4</sub> · 4H <sub>2</sub> O		0.54 g	Fisher Scientific
Na <sub>2</sub> MoO <sub>4</sub> · 2H <sub>2</sub> O	1.48	1 mL	Sigma
Na <sub>2</sub> SeO <sub>3</sub>	0.173	1 mL	Sigma
NiCl <sub>2</sub> · 6H <sub>2</sub> O	1.49	1 mL	Sigma

**Table 7.6.** Additions for F/2 enriched media

Component	Quantity used for 50 mL working stock (g)	Salt Supplier
NaNO <sub>3</sub>	3.75	Sigma
NaH <sub>2</sub> PO <sub>4</sub> · H <sub>2</sub> O	0.25	Fluka
Na <sub>2</sub> SiO <sub>3</sub> · 9H <sub>2</sub> O	1.5	Sigma

**Table 7.7.** Growth Media components

Stock solution	Quantity stock used for 1 L media (mL)
Anhydrous salts	600
Hydrated Salts	300
Trace Metals	1
Iron-EDTA	1
Vitamins	1
NaNO <sub>3</sub>	1
NaH <sub>2</sub> PO <sub>4</sub> · H <sub>2</sub> O	1
Na <sub>2</sub> SiO <sub>3</sub> · 9H <sub>2</sub> O	1

## 7.2. *Biological measurements for culture study (Chapter III)*

### 7.2.1. *Maximum quantum efficiency of Photosystem II photochemistry ( $F_v/F_m$ )*

Variable fluorescence ( $F_v$ ) of the *O. tauri* cultures was measured using a fluorescence induction and relaxation Fluorometer (FIRE) (Satlantic, Halifax, Canada) as in Kimmance et al. (2014), by measurement of the minimum ( $F_o$ ) and maximum ( $F_m$ ) fluorescence. Culture samples (2 mL) were incubated at growth temperature in the dark for 15 minutes. Filtered, non-enriched ASW media (0.2  $\mu\text{m}$ ) was used as the blank. Excitation was provided by a high luminosity blue (450 nm) and green (530 nm) LED array (each with 30 nm bandwidth), computer controlled to generate pulses. Chl-*a* fluorescence was isolated by red interference filters (678 nm with 20 nm bandwidth) and detected by a sensitive avalanche photodiode module. The gain of the detector unit was adjusted depending on chlorophyll content of the sample. An estimation of the maximum quantum efficiency of photosystem II (PSII) photochemistry was calculated by  $F_v/F_m$ , where  $F_v$  (variable fluorescence) =  $F_m - F_o$  (Genty et al. 1989).

Settings:

LED colour	blue
Gain	0-2400
Sample delay	1000
Number samples	20
STF	80
STRP	40
STRI	60
MTF	20
MTRP	40
MTRI	100

### 7.2.2. *Population density of cultures by flow cytometry*

Phytoplankton cells were enumerated using flow cytometry (Accuri C6), Milli-Q was used as sheath fluid and analysis was triggered on forward scatter and red (chlorophyll) fluorescence. A core size of 22  $\mu\text{m}$  was used and the event rate was kept below 5000 events  $\text{s}^{-1}$  to avoid coincidence (Tarran pers. Comm.); when necessary samples were diluted with filtered ASW

(0.2  $\mu\text{m}$ ). Flow rate was set to 66  $\mu\text{l min}^{-1}$  and measured daily by uptake of Milli-Q over 5 min (by mass). Cells were identified on red fluorescence vs. side scatter plots (Figure 7.1.A).

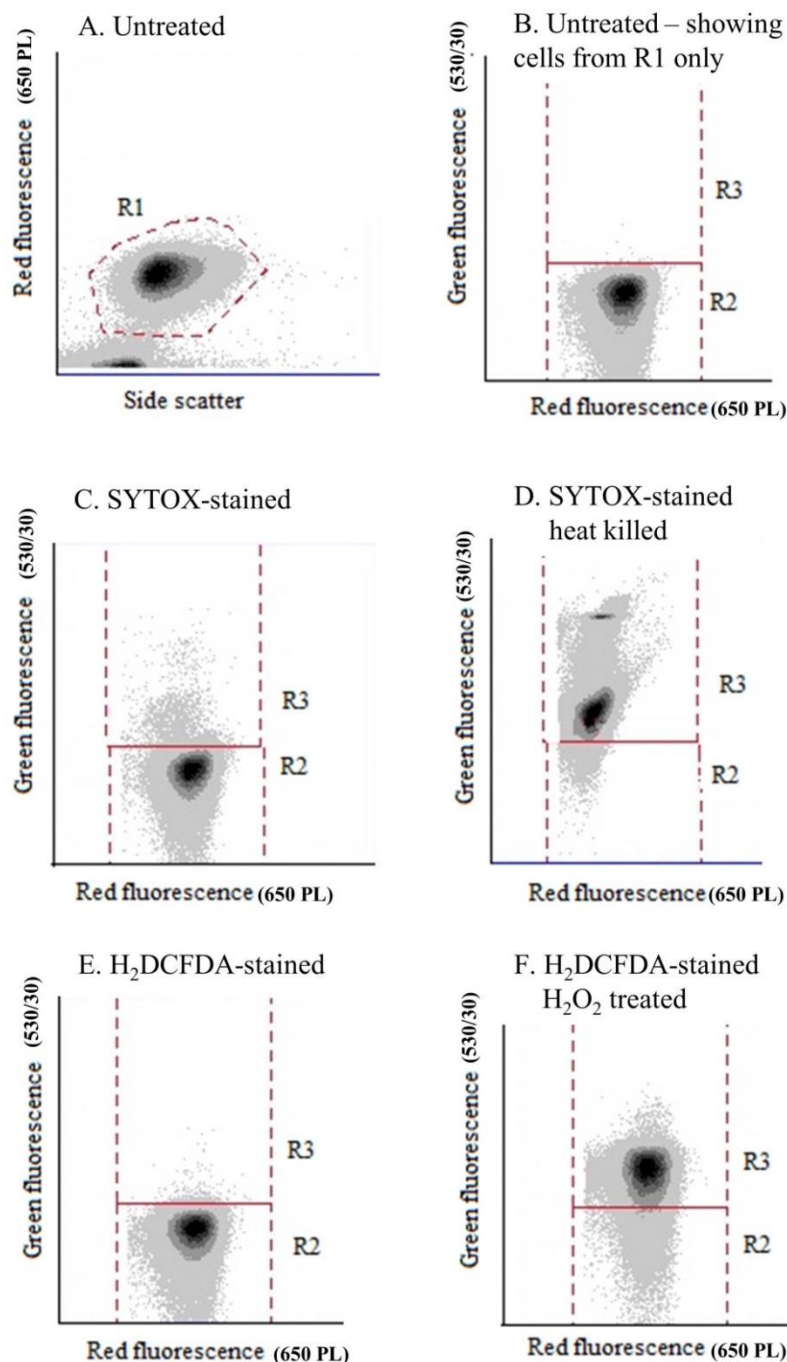


**Figure 7.1.** Example cytograms of *Ostreococcus tauri* culture after 5 days of growth (A) and (B). Cellular stains SYTOX-Green for membrane permeability (C and D) and H<sub>2</sub>DCFDA (E and F) were applied to untreated cultures (left side) and positive controls (right side). Region R2 contains non-stained cells, region R3 contains stained cells.

### 7.2.3. Membrane permeability probe (SYTOX-Green)

The commercial stock of SYTOX-Green (Invitrogen S7020, 5 mM) was diluted in Mill-Q water to yield 50  $\mu$ M working stock solutions. The working stock was stored at -20 °C in aliquots of 1 mL until use. The working stock aliquots were not re-frozen after their first use. One mL samples of culture were diluted to an appropriate population density for flow cytometry (Accuri C6) with ASW. SYTOX-Green was applied to the diluted aliquots at a final concentration of 0.5  $\mu$ M. Cells were incubated with the stain, in the dark, at growth temperature for 15 min. Incubation and staining conditions were optimised prior to the study using positive controls consisting of heat-killed cells (80 °C, 5 min) (Peperzak and Brussaard 2011). The sample was then processed by flow cytometry (Accuri C6) and the *O. tauri* population was identified as described in section 7.2.2. Uptake of the probe was assessed on a green (stain) vs. red fluorescence plot. Cytograms were compared to stained positive controls. Example cytograms of SYTOX-stained culture samples and the SYTOX-stained, heat-killed controls are displayed in Figure 7.1.C&D.

### 7.2.4. Reactive Oxygen Species probe (CM-H<sub>2</sub>DCFDA)

The commercial stock of 5-(and-6)-chloromethyl-2',7'-dichlorodihydrofluorescein diacetate (CM-H<sub>2</sub>DCFDA, Invitrogen, C-6827) was supplied in 50  $\mu$ g aliquots and was stored at -20 °C until required. Before use, aliquots were diluted in ethanol (100%, 86.54  $\mu$ L) to the working stock concentration of 1 mM.

The culture samples were diluted to an appropriate population density for flow cytometry (Accuri C6) with ASW. The CM-H<sub>2</sub>DCFDA (1 mM) was applied to the diluted culture (1 mL) to give a final concentration of 5  $\mu$ M. Samples were then incubated in the dark at growth temperature for 30 min. Incubation conditions were optimised prior to the study using positive controls; hydrogen peroxide (Sigma) inoculated cells (10  $\mu$ M final concentration). Uptake of the stain was compared with unstained and stained controls by flow cytometry (Accuri C6). Analysis of stain uptake was the same as for SYTOX-Green (section 7.2.3). Example cytograms of CM-H<sub>2</sub>DCFDA-stained culture samples and the CM-H<sub>2</sub>DCFDA-stained, hydrogen peroxide treated controls are displayed in Figure 7.1.E&F.

### 7.2.5. *Viral enumeration*

OtV5 particles were enumerated using a FACScan (Becton Dickinson) flow cytometer. One mL culture samples were fixed (0.5% TEM-grade glutaraldehyde final concentration), flash frozen and stored at -80 °C until analysis. Defrosted samples were diluted in TE buffer (10 mM Tris HCL, 1 mM EDTA, pH=8) and stained with SYBR Green I (Invitrogen, S7585) at a final concentration of  $5 \times 10^{-5}$  commercial stock (Brussaard et al. 2000) and incubated for 10 min in the dark, at 80 °C. Analyses were run on a FACScan flow cytometer with Milli-Q water as the sheath fluid, triggered on green fluorescence and set to “low” flow ( $\sim 20 \mu\text{L min}^{-1}$ ) for 1 min. Samples were diluted with 0.2  $\mu\text{m}$  filtered (cellulose nitrate filters, as in section 7.1.4) ASW to give event rates between 100 and 500 particles  $\text{s}^{-1}$ . Viral particles were identified using a green fluorescence vs. side scatter plot.

## 7.3. *Sampling procedure for Station L4 (Chapter IV)*

### 7.3.1. *Sample collection, PAR and temperature*

Surface photosynthetically active radiation (PAR) was calculated from continuous measurements by a hyperspectral irradiance sensor (Satlantic, Halifax, Canada) from an Autonomous Buoy moored at station L4 (50° 15.00' N, 4° 13.02' W). Water samples were collected from 2, 10, 25 and 50 m depth using 10 L Niskin bottles mounted on a rosette and temperature was measured simultaneously by Seabird 19+ CTD casts (Sea-Bird Electronics, Washington, USA), collected on a weekly basis using the Plymouth Marine Laboratory Vessel, RV *Quest*.

### 7.3.2. *Nutrients*

Measurement of the major nutrients including nitrate, phosphate and silicate were taken weekly from fresh samples throughout the depth profile (2, 10, 25 and 50 m); water samples were stored in cool boxes prior to analysis. Samples were collected using a 60 mL syringe, and filtered through an Acrodisc Supor PF membrane filter (with pore size 0.8/0.2  $\mu\text{m}$ ) (Pall Corporation, NY, USA) into 50 mL acid-washed high density poly-ethylene (HDPE) bottles. Sample collection and analysis were carried out by Carolyn Harris at the Plymouth Marine Laboratory. Nutrient concentrations were determined using the procedures described in

Woodward and Rees (2001) as follows; phosphate (Zhang and Chi 2002), silicate (Kirkwood 1989), nitrate and nitrite ions (Brewer and Riley 1965) and nitrite analysis (Grasshoff 1976).

### 7.3.3. *Phytoplankton enumeration and identification*

#### 7.3.3.1. Enumeration by flow cytometry

Triplicate samples from 2, 10, 25 and 50 m depth were collected into 0.25 L polycarbonate bottles (rinsed first with seawater) and were stored in a cool box until analysis in the laboratory. The time between collection and analysis is between 3.5 and 5.5 h. The phytoplankton assemblage was analysed on an Accuri C6 flow cytometer (BD Biosciences, CA, USA) with Milli-Q (Millipore) sheath fluid, triggered on forward scatter and red fluorescence. A 500  $\mu\text{L}$  sample volume was processed at  $100 \mu\text{L min}^{-1}$ . Cells were separated into 7 groups according to red and orange fluorescence and side scatter; *Synechococcus*, picoeukaryotes, coccolithophores, cryptophytes, *Phaeocystis* single cells, small dinoflagellates ( $< 20 \mu\text{m}$ ) and other nanoeukaryotes. The flow cytometry data for the *Phaeocystis* single cells and small dinoflagellates are speculative, and relied on verification of the significant presence of *Phaeocystis* or small dinoflagellates by microscopy at the same time as the appearance of clusters of events in flow cytometric density plots of forward light scatter versus red fluorescence, used to discriminate other nanophytoplankton groups. Analysis of L4 samples was performed by Glen Tarran at the Plymouth Marine Laboratory.

#### 7.3.3.2. Identification by microscopy

Water samples (100 mL) from 10 m depth were fixed upon collection with 2% (final concentration) Lugol's iodine (Widdicombe et al. 2010). Phytoplankton were identified by microscopy (DMI4000B, Leica, Wetzlar, Germany) to species level where possible, following the protocol of Widdicombe et al. (2010) and enumerated using the Utermöhl (1958) technique.

## 7.4. Sampling procedure for North Sea Cruise (Chapter V)

### 7.4.1. Sample collection

Water samples were collected throughout the depth-profile in 10 L niskin bottles mounted on an on-board CTD rosette sampler. Water was also collected continuously from 6 m depth (via an underway system) and entered a Pocket Ferry Box at max. 1 bar pressure.

### 7.4.2. $F_v/F_m$

Estimation of  $F_v/F_m$  were made semi-continuously by Phytoflash (Turner Designs, CA, USA) measurements within the Pocket Ferry Box.

### 7.4.3. Nutrients

Water was analysed for nitrite, nitrate, phosphate and silicate by Rodney Forster at Cefas (UK), following the protocol of Greenwood et al. (2011).

### 7.4.4. Phytoplankton abundance and community composition

Water samples from the depth profile were analyzed for phytoplankton abundance and identification using a Cytosense scanning flow cytometer (SCF, Cytobuoy, Woerden, the Netherlands), equipped with the Image in Flow system and 2 sets of photomultiplier tubes to resolve optical signals from small (<10  $\mu\text{m}$ ) to large particles (<800  $\mu\text{m}$ ) as in Thyssen et al. (2014). Two instrument settings (both triggered on red fluorescence) were used to discriminate cells within the populations of picoplankton and cyanobacteria (threshold level of red fluorescence: 10 mV; acquisition time: 180 s; sample flow rate: 4.5  $\text{mL s}^{-1}$ ) and within the nano- and microphytoplankton populations (trigger level: Red Fluorescence 25 mV, acquisition time: 400 s; sample flow rate: 9  $\text{mL s}^{-1}$ ). Analysis was carried out by Melilotus Thyssen (Laboratoire d'Océanographie et de Géoscience, Wimereux, France) (Thyssen et al. 2014).

#### 7.4.5. Cellular staining

The probe for enzyme activity, 5-chloromethylfluorescein diacetate (CMFDA, Invitrogen) was diluted in acetone to working stock concentration prior to use. The stain was added to water samples at a final concentration of 5  $\mu\text{M}$  and incubated in low light/cool conditions for 60 minutes. A separate sample was incubated with SYTOX-Green (Invitrogen cat no. S7020) at a final concentration of 0.5  $\mu\text{M}$  in a 15 minute dark/cool incubation. Analysis was carried out by Daniel Franklin (Bournemouth University, UK). Stain up-take was analysed on an Accuri C6 flow cytometer with Milli-Q sheath fluid, triggered on forward scatter and red fluorescence with a core size of 15  $\mu\text{m}$ . A 500  $\mu\text{L}$  sample volume was processed at 100  $\mu\text{L min}^{-1}$ .

#### 7.4.6. Satellite data

Ocean colour, detected by the polar-orbiting sensor Aqua-MODIS at a 1 km resolution, was processed by NEODAAS ([www.neodaas.ac.uk](http://www.neodaas.ac.uk)) to estimate chlorophyll *a* concentration. For each sampling station of the cruise, the ocean colour data was extracted from the relevant square kilometre, from individual passes of the MODIS sensor, between the 18<sup>th</sup> of April and the 18<sup>th</sup> of May, 2011. Data processing was specific for coastal waters and involved calibration and UK-specific atmospheric correction and used algorithms for chl-*a* estimation (Shutler et al. 2007) and the inherent optical properties of the water (Smyth et al. 2006).

### 7.5. Materials for Analytical use

#### 7.5.1. Solvents for HPLC/MS

All solvents used were either HPLC grade (Fisher Scientific) or LC/MS grade (CHROMASOLV, Sigma Aldrich Company Ltd, Dorset, UK). The water used was processed by an ELGA (ELGA Labwater, International) system.

#### 7.5.2. Preparation of HPLC/MS eluents

Glassware for HPLC use were separate from those for biological use. Glassware was rinsed in ELGA water 3 times and then rinsed in the solvent to be used.

### 7.5.3. Preparation of chlorophyll *a* standard

Chlorophyll *a* standards (Sigma, C6144-1MG) were used for assessing alterations to the HPLC method, for quantification and for checking system stability. A stock solution was made by diluting 1 mg chlorophyll *a* into acetone (100%), with a final volume of 100 mL, this was stored at -20 °C and replaced after 3 months. A Working Standard solution was made by diluting 3 mL stock solution into acetone (90 %) with a final volume of 100 mL, this was stored at -20 °C and replaced after 1 month. The working standard and stock solution were routinely quantified by spectrophotometry (Lambda 800, PerkinElmer Inc., Waltham, MA, USA) using the absorbance (abs) at 663 nm and 750 nm follows;

$\text{Chl-}a \text{ conc (gL}^{-1}\text{)} = (\text{abs } 663 - \text{abs } 750^{\text{b}}) / \text{extinction coefficient}^{\text{a}}$ .

<sup>a</sup> Extinction coefficient for chl-*a* in 90% acetone = 88.67 L g<sup>-1</sup> cm<sup>-1</sup> (Jeffrey et al. 1997)

<sup>b</sup> If absorbance at 750 nm is non-negligible (e.g. >0.002), absorbance reading at 700 nm may be used.

## 7.6. Analytical Procedures

### 7.6.1. Sampling procedure for pigments

#### 7.6.1.1. From phytoplankton culture

Culture samples (7 – 50 mL) were centrifuged using a Beckman Coulter Avanti J-26xP (CA, USA) equipped with a JS 5.3 rotor, at 5300 x g for 20 min in a cooled environment (8 °C), the pellet was flash frozen in liquid N<sub>2</sub> and stored at -80 °C until analysis. Exhaustive extraction of pigments used acetone (90% in ELGA water) under dim light by sonication (Sonics Vibracell probe, CT, USA) for 40 s at 40 W. The extract was clarified by centrifugation at 17000 x g (Heraeus Pico17, Thermo Scientific).

#### 7.6.1.2. From marine water samples

Between 0.5 and 1 L water samples were filtered through 25 mm GF/F filters immediately after sampling. The filters were snap frozen in liquid nitrogen and stored in liquid nitrogen (L4 samples, chapter 4) or at -80 °C (Cruise samples, chapter 5) at Plymouth Marine Laboratory until analysis. Samples were extracted under dim light conditions on ice, in 2 mL 90% acetone

by sonication (for 35 s at 40 W), followed by a soaking period (total extraction time = 1h). Extracts were clarified by centrifugation at 4000 rpm for 5 min (Centaur 2, MES, UK), and by filtration (0.2  $\mu$ m, 17mm Teflon syringe filters, DHI, Denmark). Analysis of samples from station L4 was carried out by Ruth Airs, Denise Cummings and Gunjan Motwani at the Plymouth Marine Laboratory.

#### 7.6.1.3. From marine surface sediment samples

Sediment samples were collected from site L4. A multicorer was used to collect eight replicate cores. Surface sediment samples (~1 mL) were taken using the barrel of a 2.5 mL syringe and immediately frozen at -20° C in the dark. Samples of semi-thawed surface sediment (2-3 g) were sliced off and thawed completely before being centrifuged to remove excess water. Sediment was transferred to a pre-weighed extraction tube and 3 mL of acetone (90%) was added. Extracts were kept on ice in the dark during extraction. Samples were sonicated for 35 s at 40 W before centrifugation (Centaur 2) at 4000 rpm for 5 min at 4 °C, and the supernatant decanted. The procedure was repeated until no additional pigment was extracted. Sampling and processing was carried out by Ruth Airs at the Plymouth Marine Laboratory.

#### 7.6.2. *Concentration by SPE primed in methanol*

Where necessary, pigment extracts from the cruise samples (chapter 5) were concentrated by SPE using C18 cartridges (Strata C18-E, 200 mg, 3 mL, Phenomenex, CA, USA), primed with methanol (2 mL), water (2 mL) and acetone (50 %, 2 mL) as in Bale (2010). Extracts were mixed 1:1 with MilliQ water (Synergy 185, Millipore, MA, USA) and loaded onto the cartridge. Acetone (100%) was used to elute the pigments. The first 300  $\mu$ L of acetone loaded acted to bring the chlorophyll towards the cartridge nozzle, the resulting eluent was not collected. A further 400  $\mu$ L acetone (100%) was loaded, to elute the pigment extract, this fraction was collected and the volume measured.

### 7.6.3. Pigment analysis

Extracts were analysed on an Accela HPLC instrument (ThermoScientific, UK), comprising an Accela quarternary pump, thermostated autosampler, thermostated column compartment and photodiode array detector using a method based on Zapata et al. (2000). A 200  $\mu\text{L}$  aliquot of extract was mixed with 80  $\mu\text{L}$  water in the autosampler (Table 2.2), and 25  $\mu\text{L}$  of this mix was injected onto the column. A Waters  $\text{C}_8$  Symmetry column (150 x 2.1 mm; 3.5  $\mu\text{m}$  particle size) was used at a flow rate of 200  $\mu\text{L min}^{-1}$ . Elution used a mobile phase gradient composed of methanol, acetonitrile, aqueous pyridine (0.25 M) and acetone as described in Zapata et al. (2000). Samples were analysed within 24 hours of extraction during which time they were maintained at 4  $^{\circ}\text{C}$  in the dark in the autosampler. The following quality assurance protocols are adhered to for pigment analysis: A mixed pigment standard (DHI, Denmark) was analysed daily before sample extraction to check resolution of pigment critical pairs and consistency of retention times (Hooker and Van Heukelem 2011); During analyses, triplicate injections of chl-*a* standard were performed to check response factor. Accuracy of the repipette was checked daily by weighing aliquots of extraction solution expelled by the repipette. Multipoint calibration of 19 pigments is performed annually by injection of pigments standards obtained from DHI. For calibration curves, the standards were used to prepare a dilution series, comprising three solutions bracketing the limit of quantification (LOQ), and three bracketing the expected sample concentration.

Additional U/HPLC (Ultra-high Performance Liquid Chromatography) methods used during method selection and optimisation are described in Chapter 2.

### 7.6.4. Pigment HPLC calibration

The Zapata et al (2000) method was calibrated on the Symmetry  $\text{C}_8$  column and Accela HPLC instrument by Ruth Airs during July 2012. The limit of detection for chlorophyll *a* is 0.07 ng injected onto the column. The response calibration was determined within the range 0.62 to 14 ng of injected chlorophyll (quantified by spectrophotometer);  $y = 86134x + 4724.9$  where  $y$ =peak area and  $x$ =ng injected,  $R^2=0.9996$  (linear regression). The linearity of response extends past 80 ng of injected chlorophyll. However the proportion of allomers is increased in injections of more than 13.65 ng chlorophyll *a*. For between 3 ng and 13.9 ng of chlorophyll *a* injected;  $y = 0.00348x - 0.00739$  where  $y$  = ratio of allomers to chlorophyll *a* and  $x$  = ng injected,  $R^2 = 0.959$  (linear regression).

#### 7.6.5. HPLC/MS of selected samples

Selected samples were analysed by LC/MS<sup>n</sup> (replicate samples freshly extracted for LC/MS analysis) for assignment of components. LC/MS<sup>n</sup> was performed using an Agilent 1200 HPLC comprising a G1313A binary pump, a G1377B thermostated autosampler, a G1317A thermostated column compartment and a G1316B photodiode array detector coupled to an Agilent 6330 ion trap mass spectrometer via an atmospheric pressure chemical ionisation (APCI) source. HPLC conditions were as for Zapata et al. (2000) described above in section 7.6.3. Post column addition of formic acid (5  $\mu\text{L min}^{-1}$ ) was used to aid ionisation of metallated components (Airs and Keely 2000). MS settings were as follows: Ionisation mode: positive, drying temperature 350 °C, vaporiser temperature 450°C, nebuliser pressure 60 PSI, drying gas flow rate 5 L min<sup>-1</sup>, capillary voltage -4500 V. The scan range was  $m/z$  400-1100. MS<sup>n</sup> utilised an ion trap to select ions of interest for fragmentation to aid component assignment. MS<sup>n</sup> settings were used as follows: Synchronous Precursor Selection (SPS) on, number of precursor ions 2, and isolation width 3  $m/z$ . Components were assigned based on relative retention time, on-line UV/vis spectra, protonated molecule and fragmentation data (Airs et al. 2001a).

## References

- Admiraal, W. and Venekamp, L.A.H., 1986. Significance of tintinnid grazing during blooms of *Phaeocystis pouchetii* (Haptophyceae) in Dutch coastal waters. *Netherlands Journal of Sea Research*, 20 (1), 61-66.
- Agusti, S., Duarte, C.M., Vaqué, D., Hein, M., Gasol, J.M. and Vidal, M., 2001. Food-web structure and elemental (C, N and P) fluxes in the eastern tropical North Atlantic. *Deep Sea Research Part II: Topical Studies in Oceanography*, 48 (10), 2295-2321.
- Agustí, S., Satta, M.P., Mura, M.P. and Benavent, E., 1998. Dissolved esterase activity as a tracer of phytoplankton lysis: evidence of high phytoplankton lysis rates in the northwestern Mediterranean. *Limnology and Oceanography*, 43 (8), 1836-1849.
- Agustí, S. and Duarte, C.M., 2000. Strong seasonality in phytoplankton cell lysis in the NW Mediterranean littoral. *Limnology and Oceanography*, 45 (4), 940-947.
- Agustí, S. and Sánchez, M.C., 2002. Cell viability in natural phytoplankton communities quantified by a membrane permeability probe. *Limnology and Oceanography*, 47 (3), 818-828.
- Agustí, S., 2004. Viability and niche segregation of *Prochlorococcus* and *Synechococcus* cells across the Central Atlantic Ocean. *Aquatic Microbial Ecology*, 36 (1), 53-59.
- Agustí, S. and Duarte, C.M., 2013. Phytoplankton lysis predicts dissolved organic carbon release in marine plankton communities. *Biogeosciences*, 10, 1259-1264.
- Airs, R.L., Jie, C. and Keely, B.J., 2000. A novel sedimentary chlorin: structural evidence for a chlorophyll origin for aetioporphyryns. *Organic Geochemistry*, 31 (11), 1253-1256.
- Airs, R.L. and Keely, B.J., 2000. A novel approach for sensitivity enhancement in atmospheric pressure chemical ionisation liquid chromatography/mass spectrometry of chlorophylls. *Rapid Communications in Mass Spectrometry*, 14 (3), 125-128.
- Airs, R.L., Atkinson, J.E. and Keely, B.J., 2001a. Development and application of a high resolution liquid chromatographic method for the analysis of complex pigment distributions. *Journal of Chromatography*, 917 (1-2), 167-177.
- Airs, R.L., Borrego, C.M., Garcia-Gil, J. and Keely, B.J., 2001b. Identification of the bacteriochlorophyll homologues of *Chlorobium phaeobacteroides* strain UdG6053 grown at low light intensity. *Photosynthesis Research*, 70 (2), 221-230.
- Airs, R.L. and Keely, B.J., 2002. Atmospheric pressure chemical ionisation liquid chromatography/mass spectrometry of bacteriochlorophylls from Chlorobiaceae: characteristic fragmentations. *Rapid communications in Mass Spectrometry*, 16 (5), 453-461.
- Airs, R.L. and Keely, B.J., 2003. A high resolution study of the chlorophyll and bacteriochlorophyll pigment distributions in a calcite/gypsum microbial mat. *Organic Geochemistry*, 34 (4), 539-551.
- Airs, R.L. and Llewellyn, C.A., 2006. Improved detection and characterization of fucoxanthin-type carotenoids: Novel pigments in *Emiliania huxleyi* (Prymnesiophyceae). *Journal of phycology*, 42 (2), 391-399.

- Alonso-Laita, P. and Agustí, S., 2006. Contrasting patterns of phytoplankton viability in the subtropical NE Atlantic Ocean. *Aquatic Microbial Ecology*, 43 (1), 67-78.
- Andersen, R.A., 2005. *Algal culturing techniques*. London, UK: Elsevier Academic Press.
- Antoine, D. and Morel, A., 1996. Oceanic primary production. 1 - Adaptation of a spectral light-photosynthesis model in view of application to satellite chlorophyll observations. *Global Biogeochemistry Cycles*, 10 (1), 43-55.
- Apel, K. and Hirt, H., 2004. Reactive oxygen species: metabolism, oxidative stress, and signal transduction. *Annual Review of Plant Biology*, 55, 373-399.
- Asada, K., 2006. Production and scavenging of reactive oxygen species in chloroplasts and their functions. *Plant physiology*, 141 (2), 391-396.
- Balachandran, S., Hull, R.J., Martins, R.A., Vaadia, Y. and Lucas, W.J., 1997. Influence of environmental stress on biomass partitioning in transgenic tobacco plants expressing the movement protein of tobacco mosaic virus. *Plant physiology*, 114 (2), 475-481.
- Bale, N., 2010. *Type I and Type II chlorophyll a transformation products associated with phytoplankton fate processes*. Thesis (PhD), University of Bristol.
- Bale, N.J., Llewellyn, C.A. and Airs, R.L., 2010. Atmospheric pressure chemical ionisation liquid chromatography/mass spectrometry of type II chlorophyll a transformation products: Diagnostic fragmentation patterns. *Organic Geochemistry*, 41 (5), 473-481.
- Bale, N.J., Airs, R.L. and Llewellyn, C.A., 2011. Type I and Type II chlorophyll a transformation products associated with algal senescence. *Organic Geochemistry*, 42 (5), 451-464.
- Bale, N.J., Airs, R.L., Kimmance, S. and Llewellyn, C.A., 2013. Transformation of chlorophyll a during viral infection of *Emiliania huxleyi*. *Aquatic Microbial Ecology*, 69 (3), 205-210.
- Barlow, R.G., Cummings, D.G. and Gibb, S.W., 1997. Improved resolution of mono- and divinyl chlorophylls a and b and zeaxanthin and lutein in phytoplankton extracts using reverse phase C-8 HPLC. *Marine Ecology Progress Series*, 161 (8), 303-307.
- Baudoux, A.-C., Noordeloos, A.A.M., Veldhuis, M.J.W. and Brussaard, C.P.D., 2006. Virally induced mortality of *Phaeocystis globosa* during two spring blooms in temperate coastal waters. *Aquatic Microbial Ecology*, 44 (3), 207-217.
- Baudoux, A.-C., 2007. *The role of viruses in marine phytoplankton mortality*. Thesis (PhD), Royal Netherlands Institute for Sea Research.
- Baudoux, A.-C., Veldhuis, M.J.W., Noordeloos, A.A.M., van Noort, G. and Brussaard, C.P.D., 2008. Estimates of virus vs. grazing induced mortality of picophytoplankton in the North Sea during summer. *Aquatic Microbial Ecology*, 52 (1), 69-82.
- Becker, G.A. and Pauly, M., 1996. Sea surface temperature changes in the North Sea and their causes. *ICES Journal of Marine Science*, 53, 887-898.
- Behrenfeld, M.J., Worthington, K., Sherrell, R.M., Chavez, F.P., Strutton, P., McPhaden, M. and Shea, D.M., 2006. Controls on tropical Pacific Ocean productivity revealed through nutrient stress diagnostics. *Nature*, 442 (7106), 1025-1028.

- Berges, J.A. and Falkowski, P.G., 1998. Physiological stress and cell death in marine phytoplankton: Induction of proteases in response to nitrogen or light limitation. *Limnology and Oceanography*, 43 (1), 129-135.
- Berman-Frank, I., Bidle, K.D., Haramaty, L. and Falkowski, P.G., 2004. The demise of the marine cyanobacterium, *Trichodesmium* spp., via an autocatalyzed cell death pathway. *Limnology and Oceanography*, 49 (4), 997-1005.
- Bidle, K.D., Haramaty, L., e Ramos, J.B. and Falkowski, P., 2007. Viral activation and recruitment of metacaspases in the unicellular coccolithophore, *Emiliania huxleyi*. *Proceedings of the National Academy of Sciences*, 104 (14), 6049-6054.
- Bidle, K.D. and Bender, S.J., 2008. Iron starvation and culture age activate metacaspases and programmed cell death in the marine diatom *Thalassiosira pseudonana*. *Eukaryotic Cell*, 7 (2), 223-236.
- Bidle, K.D. and Vardi, A., 2011. A chemical arms race at sea mediates algal host-virus interactions. *Current Opinion in Microbiology*, 14 (4), 449-457.
- Borges, A.V. and Frankignoulle, M., 1999. Daily and seasonal variations of the partial pressure of CO<sub>2</sub> in surface seawater along Belgian and southern Dutch coastal areas. *Journal of Marine Systems*, 19 (4), 251-266.
- Bouchard, J.N. and Purdie, D.A., 2011. Effect of elevated temperature, darkness and hydrogen peroxide treatment on oxidative stress and cell death in the bloom-forming toxic cyanobacteria *Microcystis aeruginosa*. *Journal of Phycology*, 47 (6), 1-10.
- Bratbak, G., Egge, J.K. and Heldal, M., 1993. Viral mortality of the marine alga *Emiliania huxleyi* (Haptophyceae) and termination of algal blooms. *Marine Ecology Progress Series*, 93, 39-48.
- Brewer, P.G. and Riley, J.P., 1965. The automatic determination of nitrate in sea water. *Deep Sea Research and Oceanographic Abstracts*, 12 (6), 765-772.
- Brewin, R.J.W., Lavender, S.J. and Hardman-Mountford, N.J., 2010. Mapping size-specific phytoplankton primary production on a global scale. *Journal of Maps Student Edition*, 12-25.
- Brussaard, C.P.D., Riegman, R., Noordeloos, A.A.M., Cadeé, G.C., Witte, H., Kop, A.J., Nieuwland, G., Van Duyl, F.C. and Bak, R.P.M., 1995. Effects of grazing, sedimentation and phytoplankton cell lysis on the structure of a coastal pelagic food web. *Marine Ecology Progress Series*, 123 (1), 259-271.
- Brussaard, C.P.D., Marie, D. and Bratbak, G., 2000. Flow cytometric detection of viruses. *Journal of virological methods*, 85 (1), 175-182.
- Brussaard, C.P.D., Marie, D., Thyraug, R. and Bratbak, G., 2001. Flow cytometric analysis of phytoplankton viability following viral infection. *Aquatic Microbial Ecology*, 26 (2), 157-166.
- Brussaard, C.P.D., 2004. Viral Control of Phytoplankton Populations - A Review. *Journal of Eukaryotic Microbiology*, 51 (2), 125-138.
- Cariou-Le Gall, V., Rosell-Mele, A. and Maxwell, J., 1998. Data report: Characterization of distributions of photosynthetic pigments in sapropels from holes 966D and 969C<sup>1</sup>. In: Robertson, A.H.F., Emeis, K.-C., Richter, C. and Camerlenghi, A., eds. *Proceedings of the Ocean Drilling Program, Scientific Results*, 160, 297-302.

- Cermeno, P., Estévez-Blanco, P., Marañón, E. and Fernández, E., 2005. Maximum photosynthetic efficiency of size-fractionated phytoplankton assessed by  $^{14}\text{C}$  uptake and fast repetition rate fluorometry. *Limnology and Oceanography*, 50 (5), 1438.
- Chen, N., Bianchi, T.S. and Bland, J.M., 2003. Implications for the role of pre- versus post-depositional transformation of chlorophyll *a* in the Lower Mississippi River and Louisiana shelf. *Marine Chemistry*, 81 (1-2), 37-55.
- Chrétiennot-Dinet, M., Courties, C., Vaquer, A., Neveux, J., Claustre, H., Lautier, J. and Machado, M., 1995. A new marine picoeucaryote: *Ostreococcus tauri* gen. et sp. nov. (Chlorophyta, Prasinophyceae). *Phycologia*, 34 (4), 285-292.
- Clarke, K.R. and Gorley, R.N., 2006. *PRIMER v6: User Manual / Tutorial*. Plymouth, UK: Primer-E Ltd.
- Countway, P.D. and Caron, D.A., 2006. Abundance and distribution of *Ostreococcus* sp. in the San Pedro Channel, California, as revealed by quantitative PCR. *Applied and Environmental Microbiology*, 72 (4), 2496-2506.
- Crow, J.P., 1997. Dichlorodihydrofluorescein and dihydrorhodamine 123 are sensitive indicators of peroxynitrite in vitro: Implications for intracellular measurement of reactive nitrogen and oxygen species. *Nitric Oxide*, 1 (2), 145-157.
- Cullen, J.J., 1982. The deep chlorophyll maximum: comparing vertical profiles of chlorophyll *a*. *Canadian Journal of Fisheries and Aquatic Sciences*, 39 (5), 791-803.
- Cullen, J.J. and Davis, R.F., 2003. The blank can make a big difference in oceanographic measurements. *Limnology and Oceanography Bulletin*, 12 (2), 29-35.
- Darzynkiewicz, Z., Li, X. and Gong, J., 1994. Assays of cell viability. Discrimination of cells dying by apoptosis. In: Darzynkiewicz, Z., Robinson, J.P. and Crissman, H.A., eds. *Methods in Cell Biology*. San Diego: Academic Press, 15-38.
- Davey, H.M., 2011. Life, death, and in-between: Meanings and methods in microbiology. *Applied and Environmental Microbiology*, 77 (16), 5571-5576.
- De Gara, L., de Pinto, M.C. and Tommasi, F., 2003. The antioxidant systems vis-à-vis reactive oxygen species during plant-pathogen interaction. *Plant Physiology and Biochemistry*, 41 (10), 863-870.
- Demmig-Adams, B., 1990. Carotenoids and photoprotection in plants: a role for the xanthophyll zeaxanthin. *Biochimica et Biophysica Acta (BBA)-Bioenergetics*, 1020 (1), 1-24.
- Derelle, E., Ferraz, C., Escande, M.L., Eychenié, S., Cooke, R., Piganeau, G., Desdevises, Y., Bellec, L., Moreau, H. and Grimsley, N., 2008. Life-cycle and genome of OtV5, a large DNA virus of the pelagic marine unicellular green alga *Ostreococcus tauri*. *PLoS One*, 3 (5), e2250.
- Doke, N., 1985. NADPH-dependent  $\text{O}_2^-$  generation in membrane fractions isolated from wounded potato tubers inoculated with *Phytophthora infestans*. *Physiological Plant Pathology*, 27 (3), 311-322.
- Duarte, C.M., Agustí, S., Kennedy, H. and Vaqué, D., 1999. The Mediterranean climate as a template for Mediterranean marine ecosystems: the example of the northeast Spanish littoral. *Progress in Oceanography*, 44 (1-3), 245-270.

- Ebata, T. and Fujita, Y., 1971. Changes in photosynthetic activity of the diatom *Phaeodactylum tricorutum* in a culture of limited volume. *Plant Cell Physiology*, 12 (4), 533-541.
- Ellis, R.E., Yuan, J. and Horvitz, H.R., 1991. Mechanisms and functions of cell death. *Annual Review of Cell Biology*, 7 (1), 663-698.
- Evans, C., Malin, G., Mills, G.P. and Wilson, W.H., 2006. Viral infection of *Emiliania huxleyi* (Prymnesiophyceae) leads to elevated production of reactive oxygen species. *Journal of Phycology*, 42 (5), 1040-1047.
- Falkowski, P. and Kolber, Z., 1995. Variations in chlorophyll fluorescence yields in phytoplankton in the world oceans. *Functional Plant Biology*, 22 (2), 341-355.
- Field, C.B., Behrenfeld, M.J., Randerson, J.T. and Falkowski, P., 1998. Primary production of the biosphere: integrating terrestrial and oceanic components. *Science*, 281 (5374), 237-240.
- Fileman, E., Petropavlovsky, A. and Harris, R., 2010. Grazing by the copepods *Calanus helgolandicus* and *Acartia clausi* on the protozooplankton community at station L4 in the Western English Channel. *Journal of Plankton Research*, 32 (5), 709-724.
- Fogg, G.E. and Thake, B., 1987. *Algal cultures and phytoplankton ecology*. Wisconsin, USA: University of Wisconsin Press.
- Förster, T., 1967. Mechanisms of energy transfer. In: Stotz, E.H., ed. *Comprehensive biochemistry*. Amsterdam: Elsevier, 61-80.
- Franklin, D.J., Brussaard, C.P.D. and Berges, J.A., 2006. What is the role and nature of programmed cell death in phytoplankton ecology? *European Journal of Phycology*, 41 (1), 1-14.
- Franklin, D.J., Choi, C.J., Claire, H. and Gill, M., 2009a. Effect of dead phytoplankton cells on the apparent efficiency of photosystem II. *Marine Ecology Progress Series*, 382, 35-40.
- Franklin, D.J., Poulton, A.J., Steinke, M., Young, J., Peeken, I. and Malin, G., 2009b. Dimethylsulphide, DMSP-lyase activity and microplankton community structure inside and outside of the Mauritanian upwelling. *Progress in Oceanography*, 83 (1), 134-142.
- Franklin, D.J., Airs, R.L., Fernandes, M., Bell, T., Bongaerts, R.J., Berges, J.A. and Malin, G., 2012. Identification of senescence and death in *Emiliania huxleyi* and *Thalassiosira pseudonana*: cell staining, chlorophyll alterations and dimethylsulfoniopropionate (DMSP) metabolism. *Limnology and Oceanography*, 57 (1), 305-317.
- Fuchs, E., Zimmerman, R.C. and Jaffe, J.S., 2002. The effect of elevated levels of phaeophytin in natural water on variable fluorescence measured from phytoplankton. *Journal of Plankton Research*, 24 (11), 1221-1229.
- Fuhrman, J.A., 1992. Bacterioplankton roles in cycling of organic matter: the microbial food web. In: Falkowski, P.G. and Woodhead, A.D., eds. *Primary productivity and biogeochemical cycles in the sea*. New York, USA: Plenum, 361-383.
- Fuhrman, J.A., 1999. Marine viruses and their biogeochemical and ecological effects. *Nature*, 399 (6736), 541-548.
- Gadjev, I., Stone, J.M. and Gechev, T.S., 2008. Programmed Cell Death in Plants: New Insights into Redox Regulation and the Role of Hydrogen Peroxide. *International Review of Cell and Molecular Biology*, 270, 87-144.

- Garvey, M., Moriceau, B. and Passow, U., 2007. Applicability of the FDA assay to determine the viability of marine phytoplankton under different environmental conditions. *Marine Ecology Progress Series*, 352, 17-26.
- Geider, R.J., Greene, R.M., Kolber, Z., MacIntyre, H.L. and Falkowski, P.G., 1993a. Fluorescence assessment of the maximum quantum efficiency of photosynthesis in the western North Atlantic. *Deep Sea Research Part I: Oceanographic Research Papers*, 40 (6), 1205-1224.
- Geider, R.J., Roche, J., Greene, R.M. and Olaizola, M., 1993b. Response of the photosynthetic apparatus of *Phaeodactylum tricornutum* (Bacillariophyceae) to nitrate, phosphate or iron starvation. *Journal of Phycology*, 29 (6), 755-766.
- Geider, R.J., Delucia, E.H., Falkowski, P.G., Finzi, A.C., Grime, J.P., Grace, J., Kana, T.M., La Roche, J., Long, S.P., Osborne, B.A., Platt, T., Prentice, I.C., Raven, J.A., Schlesinger, W.H., Smetacek, V., Stuart, V., Sathyendranath, S., Thomas, R.B., Vogelmann, T.C., Williams, P. and Woodward, F.I., 2001. Primary productivity of planet earth: biological determinants and physical constraints in terrestrial and aquatic habitats. *Global Change Biology*, 7 (8), 849-882.
- Genty, B., Briantais, J.-M. and Baker, N.R., 1989. The relationship between the quantum yield of photosynthetic electron transport and quenching of chlorophyll fluorescence. *Biochimica et Biophysica Acta (BBA)-General Subjects*, 990 (1), 87-92.
- Gich, F., Airs, R.L., Danielsen, M., Keely, B.J., Abella, C.A., Garcia-Gil, J., Miller, M. and Borrego, C.M., 2003. Characterization of the chlorosome antenna of the filamentous anoxygenic phototrophic bacterium *Chloronema* sp. strain UdG9001. *Archives of Microbiology*, 180 (6), 417-426.
- Gich, F. and Overmann, J., 2006. *Sandarakinorhabdus limnophila* gen. nov., sp. nov., a novel bacteriochlorophyll a-containing, obligately aerobic bacterium isolated from freshwater lakes. *International journal of systematic and evolutionary microbiology*, 56 (4), 847-854.
- Gieskes, W. and Kraay, G., 1984. Phytoplankton, its pigments, and primary production at a central North Sea station in May, July and September 1981. *Netherlands Journal of Sea Research*, 18 (1), 51-70.
- Gobler, C.J., Hutchins, D.A., Fisher, N.S., Cosper, E.M. and Sanudo-Wilhelmy, S.A., 1997. Release and bioavailability of C, N, P, Se, and Fe following viral lysis of a marine chrysophyte. *Limnology and Oceanography*, 42 (7), 1492-1504.
- Grasshoff, K., 1976. *Methods of Seawater Analysis*. Weinheim, Germany: Verlag Chemie.
- Greenwood, N., Hydes, D.J., Mahaffey, C., Wither, A., Barry, J., Sivy, D.B., Pearce, D.J., Hartman, S.E., Andres, O. and Lees, H.E., 2011. Spatial and temporal variability in nutrient concentrations in Liverpool Bay, a temperate latitude region of freshwater influence. *Ocean Dynamics*, 61 (12), 2181-2199.
- Grob, C., Hartmann, M., Zubkov, M.V. and Scanlan, D.J., 2011. Invariable biomass specific primary production of taxonomically discrete picoeukaryote groups across the Atlantic Ocean. *Environmental Microbiology*, 13 (12), 3266-3274.
- Guillard, R.R.L. and Ryther, J.H., 1962. Studies of marine plankton diatoms: I. *Cyclotella nana* Hustedt and *Detonula confervacea* Cleve. *Canadian Journal of Microbiology*, 8 (2), 229-239.

- Hallegraeff, G.M., 1981. Seasonal study of phytoplankton pigments and species at a coastal station off Sydney: importance of diatoms and the nanoplankton. *Marine Biology*, 61 (2), 107-118.
- Harrison, P.J. and Berges, J.A., 2005. Marine Culture Media. In: Anderson, R.A., ed. *Algal Culturing Techniques*. London, UK: Elsevier Academic Press, 21-33.
- Haugland, R.P., 2002. *Handbook of fluorescent probes and research products*. 9<sup>th</sup> edition. Eugene, USA: Molecular Probes.
- Hayakawa, M., Suzuki, K., Saito, H., Takahashi, K. and Ito, S., 2008. Differences in cell viabilities of phytoplankton between spring and late summer in the northwest Pacific Ocean. *Journal of Experimental Marine Biology and Ecology*, 360 (2), 63-70.
- Head, E.J.H. and Horne, E.P.W., 1993. Pigment transformation and vertical flux in an area of convergence in the North Atlantic. *Deep Sea Research Part II: Topical Studies in Oceanography*, 40 (1-2), 329-346.
- Head, E.J.H., Hargrave, B.T. and Rao, D.V.S., 1994. Accumulation of a pheophorbide-*a* like pigment in sediment traps during late stages of a spring bloom: a product of dying algae? *Limnology and Oceanography*, 39 (1), 176-181.
- Hodgson, D.A., McMinn, A., Kirkup, H., Cremer, H., Gore, D., Melles, M., Roberts, D. and Montiel, P., 2003. Colonization, succession, and extinction of marine floras during a glacial cycle: A case study from the Windmill Islands (east Antarctica) using biomarkers. *Paleoceanography*, 18 (3), 12-26.
- Hodgson, D.A., Roberts, D., McMinn, A., Verleyen, E., Terry, B., Corbett, C. and Vyverman, W., 2006. Recent rapid salinity rise in three East Antarctic lakes. *Journal of Paleolimnology*, 36 (4), 385-406.
- Holligan, P.M. and Harbour, D.S., 1977. The vertical distribution and succession of phytoplankton in the western English Channel in 1975 and 1976. *Journal of the Marine Biological Association of the United Kingdom*, 57 (4), 1075-1093.
- Hooker, S.B., Van Heukelem, L., Thomas, C.S., Claustre, H., Ras, J., Barlow, R., Sessions, H., Schlüter, L., Perl, J., Trees, C., Head, E., L, C., Fishwick, J., Llewellyn, C.A. and Aiken, J., 2005. *Second SeaWiFS HPLC Analysis Round-robin Experiment (SeaHARRE-2)*. Maryland, USA: National Aeronautics and Space Administration, Goddard Space Flight Center.
- Hooker, S.B. and Van Heukelem, L., 2011. *An investigation into HPLC data quality problems*. Maryland, USA: National Aeronautics and Space Administration, Goddard Space Flight Center.
- Horton, P. and Hague, A., 1988. Studies on the induction of chlorophyll fluorescence in isolated barley protoplasts. IV. Resolution of non-photochemical quenching. *Biochimica et Biophysica Acta (BBA)-Bioenergetics*, 932, 107-115.
- Hutchins, D.A., Pustizzi, F., Hare, C.E. and DiTullio, G.R., 2003. A shipboard natural community continuous culture system for ecologically relevant low-level nutrient enrichment experiments. *Limnology and Oceanography: Methods*, 1, 82-91.
- Hynninen, P.H., 1991. Chemistry of chlorophylls: Modifications. In: Scheer, H., ed. *Chlorophylls*. Boca Raton, Florida, USA: CRC Press, 145-210.

- Hyvärinen, K. and Hynninen, P.H., 1999. Liquid chromatographic separation and mass spectrometric identification of chlorophyll *b* allomers. *Journal of Chromatography A*, 837 (1), 107-116.
- Jacobsen, A., Bratbak, G. and Heldal, M., 1996. Isolation and characterization of a virus infecting *Phaeocystis pouchetii* (Prymnesiophyceae). *Journal of Phycology*, 32 (6), 923-927.
- Jeffrey, S.W. and Hallegraeff, G.M., 1987. Chlorophyllase distribution in ten classes of phytoplankton: a problem for chlorophyll analysis. *Marine Ecology Progress Series*, 35 (3), 293-304.
- Jeffrey, S.W., Mantoura, R.F.C. and Wright, S.W., 1997. *Phytoplankton pigments in oceanography: guidelines to modern methods*. Paris, France: UNESCO Publishing.
- Jiao, N., Herndl, G.J., Hansell, D.A., Benner, R., Kattner, G., Wilhelm, S.W., Kirchman, D.L., Weinbauer, M.G., Luo, T. and Chen, F., 2010. Microbial production of recalcitrant dissolved organic matter: long-term carbon storage in the global ocean. *Nature Reviews Microbiology*, 8 (8), 593-599.
- Jie, C., Walker, J.S. and Keely, B.J., 2002. Atmospheric pressure chemical ionisation normal phase liquid chromatography mass spectrometry and tandem mass spectrometry of chlorophyll *a* allomers. *Rapid Communications in Mass Spectrometry*, 16 (5), 473-479.
- Juneau, P., Lawrence, J.E., Suttle, C.A. and Harrison, P.J., 2003. Effects of viral infection on photosynthetic processes in the bloom-forming alga *Heterosigma akashiwo*. *Aquatic Microbial Ecology*, 31 (1), 9-17.
- Kaneshiro, E.S., Wyder, M.A., Wu, Y.P. and Cushion, M.T., 1993. Reliability of calcein acetoxy methyl ester and ethidium homodimer or propidium iodide for viability assessment of microbes. *Journal of Microbiological Methods*, 17 (1), 1-16.
- Kashiyama, Y., Yokoyama, A., Kinoshita, Y., Shoji, S., Miyashiya, H., Shiratori, T., Suga, H., Ishikawa, K., Ishikawa, A. and Inouye, I., 2012. Ubiquity and quantitative significance of detoxification catabolism of chlorophyll associated with protistan herbivory. *Proceedings of the National Academy of Sciences*, 109 (43), 17328-17335.
- Keely, B.J., 2006. Geochemistry of chlorophylls. In: Grimm, B., Porra, R.J., Rüdiger, W. and Scheer, H., eds. *Advances in Photosynthesis and Respiration*. Dordrecht, The Netherlands: Springer, 535-561.
- Kimmance, S.A., Allen, M.J., Pagarete, A., Martínez, J.M. and Wilson, W.H., 2014. Reduction in photosystem II efficiency during a virus-controlled *Emiliania huxleyi* bloom. *Marine Ecology Progress Series*, 495, 65-76.
- Kirchman, D.L., 1999. Oceanography: Phytoplankton death in the sea. *Nature*, 398 (6725), 293-294.
- Kirk, J.T.O., 1994. *Light and photosynthesis in aquatic ecosystems*. 2<sup>nd</sup> edition. Cambridge, UK: Cambridge University Press.
- Kirkwood, D.S., 1989. Simultaneous determination of selected nutrients in sea water. *International Council for the Exploration of the Sea (ICES)*, CM(100)/C:29.

- Koblížek, M., Bějč, O., Bidigare, R.R., Christensen, S., Benitez-Nelson, B., Vetriani, C., Kolber, M.K., Falkowski, P.G. and Kolber, Z.S., 2003. Isolation and characterization of *Erythrobacter* sp. strains from the upper ocean. *Archives of microbiology*, 180 (5), 327-338.
- Kolber, Z., Zehr, J. and Falkowski, P., 1988. Effects of growth irradiance and nitrogen limitation on photosynthetic energy conversion in photosystem II. *Plant physiology*, 88 (3), 923-929.
- Kolber, Z. and Falkowski, P.G., 1993. Use of active fluorescence to estimate phytoplankton photosynthesis in situ. *Limnology and Oceanography*, 38 (8), 1646-1665.
- Kolber, Z.S., Barber, R.T., Coale, K.H., Fitzwater, S.E., Greene, R.M., Johnson, K.S., Lindley, S. and Falkowski, P.G., 1994. Iron limitation of phytoplankton photosynthesis in the equatorial Pacific Ocean. *Nature*, 371 (6493), 145-149.
- Kolber, Z.S., Prášil, O. and Falkowski, P.G., 1998. Measurements of variable chlorophyll fluorescence using fast repetition rate techniques: defining methodology and experimental protocols. *Biochimica et Biophysica Acta (BBA)-Bioenergetics*, 1367 (1), 88-106.
- Kovala, P.E. and Larrance, J.D., 1966. Computation of phytoplankton cell numbers, cell volume, cell surface and plasma volume per liter, from microscopical counts. Seattle: University of Washington: Report 38. DTIC Document, 21.
- Kramer, D.M., Robinson, H.R. and Crofts, A.R., 1990. A portable multi-flash kinetic fluorimeter for measurement of donor and acceptor reactions of Photosystem II in leaves of intact plants under field conditions. *Photosynthesis Research*, 26 (3), 181-193.
- Kroemer, G., Petit, P., Zamzami, N., Vayssiere, J.L. and Mignotte, B., 1995. The biochemistry of programmed cell death. *Federation of American Societies for Experimental Biology*, 9 (13), 1277-1287.
- Kromkamp, J.C. and Forster, R.M., 2003. The use of variable fluorescence measurements in aquatic ecosystems: differences between multiple and single turnover measuring protocols and suggested terminology. *European Journal of Phycology*, 38 (2), 103-112.
- Kropuenske, L.R., Mills, M.M., van Dijken, G.L., Bailey, S., Robinson, D.H., Welschmeyer, N.A. and Arrigo, K.R., 2009. Photophysiology in two major Southern Ocean phytoplankton taxa: photoprotection in *Phaeocystis antarctica* and *Fragilariopsis cylindrus*. *Limnology and Oceanography*, 54 (4), 1176-1196.
- Kruskopf, M. and Flynn, K.J., 2006. Chlorophyll content and fluorescence responses cannot be used to gauge reliably phytoplankton biomass, nutrient status or growth rate. *New Phytologist*, 169 (3), 525-536.
- Kulk, G., van de Poll, W.H., Visser, R.J. and Buma, A.G., 2013. Low nutrient availability reduces high-irradiance-induced viability loss in oceanic phytoplankton. *Limnology and Oceanography*, 58 (5), 1747-1760.
- Kuronen, P., Hyvarinen, K., Hynninen, P.H. and Kilpelainen, I., 1993. High-performance liquid chromatographic separation and isolation of the methanolic allomerization products of chlorophyll *a*. *Journal of Chromatography*, 654 (1), 93-104.
- Lancelot, C., 1983. Factors affecting phytoplankton extracellular release in the Southern Bight of the North Sea. *Marine Ecology Progress Series*, 12 (2), 115-121.

- Lane, N., 2008. Marine microbiology: origins of death. *Nature*, 453 (7195), 583-585.
- Lasternas, S., Agustí, S. and Duarte, C.M., 2010. Phyto- and bacterioplankton abundance and viability and their relationship with phosphorus across the Mediterranean Sea. *Aquatic Microbial Ecology*, 60 (2), 175-191.
- Latasa, M. and Bidigare, R.R., 1998. A comparison of phytoplankton populations of the Arabian Sea during the Spring Intermonsoon and Southwest Monsoon of 1995 as described by HPLC-analyzed pigments. *Deep-Sea Research Part II*, 45 (10-11), 2133-2170.
- Latasa, M., Scharek, R., Gall, F.L. and Guillou, L., 2004. Pigment suites and taxonomic groups in Prasinophyceae. *Journal of Phycology*, 40 (6), 1149-1155.
- Latifi, A., Ruiz, M. and Zhang, C.C., 2009. Oxidative stress in cyanobacteria. *FEMS Microbiology Reviews*, 33 (2), 258-278.
- Lawrence, J.E. and Suttle, C.A., 2004. Effect of viral infection on sinking rates of *Heterosigma akashiwo* and its implications for bloom termination. *Aquatic Microbial Ecology*, 37 (1), 1-7.
- Lesser, M.P., 1996. Elevated temperatures and ultraviolet radiation cause oxidative stress and inhibit photosynthesis in symbiotic dinoflagellates. *Limnology and Oceanography*, 41 (2), 271-283.
- Li, W.K.W., 1994. Primary production of prochlorophytes, cyanobacteria, and eucaryotic ultraphytoplankton: measurements from flow cytometric sorting. *Limnology and Oceanography*, 39 (1), 169-175.
- Liu, W., Ming, Y., Huang, Z. and Li, P., 2012a. Impacts of florfenicol on marine diatom *Skeletonema costatum* through photosynthesis inhibition and oxidative damages. *Plant Physiology and Biochemistry*, 60, 165-170.
- Liu, W., Ming, Y., Li, P. and Huang, Z., 2012b. Inhibitory effects of hypo-osmotic stress on extracellular carbonic anhydrase and photosynthetic efficiency of green alga *Dunaliella salina* possibly through reactive oxygen species formation. *Plant Physiology and Biochemistry*, 54, 43-48.
- Llabrés, M. and Agustí, S., 2006. Picophytoplankton cell death induced by UV radiation: evidence for oceanic Atlantic communities. *Limnology and Oceanography*, 51 (1), 21-29.
- Llabrés, M., Agustí, S., Alonso-Laita, P. and Herndl, G.J., 2010. *Synechococcus* and *Prochlorococcus* cell death induced by UV radiation and the penetration of lethal UVR in the Mediterranean Sea. *Marine Ecology Progress Series*, 399, 27-37.
- Llabrés, M., Dachs, J. and Agustí, S., 2012. Transference of atmospheric hydroxyl radical to the ocean surface induces high phytoplankton cell death. *Photochemistry and Photobiology*, 88 (6), 1473-1479.
- Llewellyn, C.A., Mantoura, R.F.C. and Brereton, R.G., 1990. Products of chlorophyll photodegradation 2. Structural identification. *Photochemistry and Photobiology*, 52 (5), 1043-1047.

- Llewellyn, C.A., Evans, C., Airs, R.L., Cook, I., Bale, N. and Wilson, W.H., 2007. The response of carotenoids and chlorophylls during virus infection of *Emiliania huxleyi* (Prymnesiophyceae). *Journal of Experimental Marine Biology and Ecology*, 344 (1), 101-112.
- Lønborg, C., Middelboe, M. and Brussaard, C.P., 2013. Viral lysis of *Micromonas pusilla*: impacts on dissolved organic matter production and composition. *Biogeochemistry*, 116 (1-3), 231-240.
- Longhurst, A., Sathyendranath, S., Platt, T. and Caverhill, C., 1995. An estimate of global primary production in the ocean from satellite radiometer data. *Journal of Plankton Research*, 17 (6), 1245-1271.
- Louda, J.W., Li, J., Liu, L., Winfree, M.N. and Baker, E.W., 1998. Chlorophyll *a* degradation during cellular senescence and death. *Organic Geochemistry*, 29 (5-7), 1233-1251.
- Louda, J.W., Mongkhonsri, P. and Baker, E.W., 2011. Chlorophyll degradation during senescence and death-III: 3–10yr experiments, implications for ETIO series generation. *Organic Geochemistry*, 42 (6), 688-699.
- Louda, W.J., Loitz, J.W., Rudnick, D.T. and Baker, E.W., 2000. Early diagenetic alteration of chlorophyll *a* and bacteriochlorophyll *a* in a contemporaneous marl ecosystem; Florida Bay. *Organic Geochemistry*, 31 (12), 1561-1580.
- Louda, W.J., Liu, L. and Baker, E.W., 2002. Senescence and death related alteration of chlorophylls and carotenoids in marine phytoplankton. *Organic Geochemistry*, 33 (12), 1635-1653.
- Malkin, S. and Kok, B., 1966. Fluorescence induction studies in isolated chloroplasts I. Number of components involved in the reaction and quantum yields. *Biochimica et Biophysica Acta (BBA)-Biophysics including Photosynthesis*, 126 (3), 413-432.
- Marin, B., 2014. Reduction to essentials: *Ostreococcus*, the smallest free-living eukaryote. *Perspectives in Phycology*, 1, 7-10.
- McQuatters-Gollop, A., Raitos, D.E., Edwards, M., Pradhan, Y., Mee, L.D., Lavender, S.J. and Attrill, M.J., 2007. A long-term chlorophyll data set reveals regime shift in North Sea phytoplankton biomass unconnected to nutrient trends. *Limnology and Oceanography*, 52 (2), 635.
- Menden-Deuer, S. and Lessard, E.J., 2000. Carbon to volume relationships for dinoflagellates, diatoms, and other protist plankton. *Limnology and Oceanography*, 45 (3), 569-579.
- Middelboe, M. and Lyck, P.G., 2002. Regeneration of dissolved organic matter by viral lysis in marine microbial communities. *Aquatic Microbial Ecology*, 27 (2), 187-194.
- MolecularProbes, 2010. *Product Information - SYTOX® Green Nucleic Acid Stain (S-7020)* [online]. Thermo Fisher Scientific. Available from: <http://www.lifetechnologies.com/order/catalog/product/S7020>
- Montalbini, P. and Lupattelli, M., 1989. Effect of localized and systemic tobacco mosaic virus infection on some photochemical and enzymatic activities of isolated tobacco chloroplasts. *Physiological and molecular plant pathology*, 34 (2), 147-162.

- Moore, C.M., Suggett, D., Holligan, P.M., Sharples, J., Abraham, E.R., Lucas, M.I., Rippeth, T.P., Fisher, N.R., Simpson, J.H. and Hydes, D.J., 2003. Physical controls on phytoplankton physiology and production at a shelf sea front: a fast repetition-rate fluorometer based field study. *Marine Ecology Progress Series*, 259, 29-45.
- Moore, C.M., Lucas, M.I., Sanders, R. and Davidson, R., 2005. Basin-scale variability of phytoplankton bio-optical characteristics in relation to bloom state and community structure in the Northeast Atlantic. *Deep Sea Research Part I: Oceanographic Research Papers*, 52 (3), 401-419.
- Moore, C.M., Mills, M.M., Arrigo, K.R., Berman-Frank, I., Bopp, L., Boyd, P.W., Galbraith, E.D., Geider, R.J., Guieu, C. and Jaccard, S.L., 2013. Processes and patterns of oceanic nutrient limitation. *Nature Geoscience*, 6, 701-710.
- Mulders, K.J.M., Weesepoel, Y., Lamers, P.P., Vincken, J.-P., Martens, D.E. and Wijffels, R.H., 2013. Growth and pigment accumulation in nutrient-depleted *Isochrysis* aff. *galbana* T-ISO. *Journal of Applied Phycology*, 25 (5), 1421-1430.
- Murata, N., Nishimura, M. and Takamiya, A., 1966. Fluorescence of chlorophyll in photosynthetic systems II. Induction of fluorescence in isolated spinach chloroplasts. *Biochimica et Biophysica Acta (BBA)-Biophysics including Photosynthesis*, 120 (1), 23-33.
- Murray, A.G. and Jackson, G.A., 1992. Viral dynamics: a model of the effects of size, shape, motion and abundance of single-celled planktonic organisms and other particles. *Marine Ecology Progress Series*, 89 (2), 103-116.
- Naganuma, T., 1996. Differential enumeration of intact and damaged marine planktonic bacteria based on cell membrane integrity. *Journal of Aquatic Ecosystem Stress and Recovery*, 5 (4), 217-222.
- Not, F., Massana, R., Latasa, M., Marie, D., Colson, C., Eikrem, W., Pedrós-Alió, C., Vaultot, D. and Simon, N., 2005. Late summer community composition and abundance of photosynthetic picoeukaryotes in Norwegian and Barents Seas. *Limnology and Oceanography*, 50 (5), 1677.
- Olaizola, M., Geider, R.J., Harrison, W.G., Graziano, L.M., Ferrari, G.M. and Schlittenhardt, P.M., 1996. Synoptic study of variations in the fluorescence-based maximum quantum efficiency of photosynthesis across the North Atlantic Ocean. *Limnology and Oceanography*, 41 (4), 755-765.
- Peperzak, L. and Brussaard, C.P.D., 2011. Flow cytometric applicability of fluorescent vitality probes on phytoplankton. *Journal of Phycology*, 47 (3), 692-702.
- Petersen, W., Wehde, H., Krasemann, H., Colijn, F. and Schroeder, F., 2008. *FerryBox* and *MERIS*—Assessment of coastal and shelf sea ecosystems by combining *in situ* and remotely sensed data. *Estuarine, Coastal and Shelf Science*, 77 (2), 296-307.
- Pickney, J.L., Millie, D.F. and Van Heukelem, L., 2011. Appendix A: Update on filtration, storage and extraction solvents. In: Roy, S., Llewellyn, C.A., Egeland, E.S. and Johnsen, G., eds. *Phytoplankton pigments: characterization, chemotaxonomy and applications in oceanography*. New York, USA: Cambridge University Press, 627-635.
- Pinckney, J.L., Millie, D.F., Howe, K.E., Paerl, H.W. and Hurley, J.P., 1996. Flow scintillation counting of <sup>14</sup>C-labeled microalgal photosynthetic pigments. *Journal of Plankton Research*, 18 (10), 1867-1880.

- Poorvin, L., Rinta-Kanto, J.M., Hutchins, D.A. and Wilhelm, S.W., 2004. Viral release of iron and its bioavailability to marine plankton. *Limnology and Oceanography*, 49 (5), 1734-1741.
- Porter, J., Diaper, J., Edwards, C. and Pickup, R., 1995. Direct measurements of natural planktonic bacterial community viability by flow cytometry. *Applied and Environmental Microbiology*, 61 (7), 2783-2786.
- Poulton, A.J., Moore, M.C., Seeyave, S., Lucas, M.I., Fielding, S. and Ward, P., 2007. Phytoplankton community composition around the Crozet Plateau, with emphasis on diatoms and *Phaeocystis*. *Deep Sea Research Part II: Topical Studies in Oceanography*, 54 (18), 2085-2105.
- Rastogi, R.P., Singh, S.P., Häder, D.-P. and Sinha, R.P., 2010. Detection of reactive oxygen species (ROS) by the oxidant-sensing probe 2', 7'-dichlorodihydrofluorescein diacetate in the cyanobacterium *Anabaena variabilis* PCC 7937. *Biochemical and Biophysical Research Communications*, 397 (3), 603-607.
- Rastogi, R.P., Singh, S.P., Incharoensakdi, A., Häder, D.-P. and Sinha, R.P., 2014. Ultraviolet radiation-induced generation of reactive oxygen species, DNA damage and induction of UV-absorbing compounds in the cyanobacterium *Rivularia* sp. HKAR-4. *South African Journal of Botany*, 90, 163-169.
- Ray, J.L., Haramaty, L., Thyrraug, R., Fredricks, H.F., Van Mooy, B.A., Larsen, A., Bidle, K.D. and Sandaa, R.-A., 2014. Virus infection of *Haptolina ericina* and *Phaeocystis pouchetii* implicates evolutionary conservation of programmed cell death induction in marine haptophyte-virus interactions. *Journal of Plankton Research*, 36 (4), 943-955.
- Rees, A.P., Hope, S.B., Widdicombe, C.E., Dixon, J.L., Woodward, E.M.S. and Fitzsimons, M.F., 2009. Alkaline phosphatase activity in the Western English Channel: elevations induced by high summertime rainfall. *Estuarine, Coastal and Shelf Science*, 81 (4), 569-574.
- Rijstenbil, J.W., Derksen, J.W.M., Gerringa, L.J.A., Poortvliet, T.C.W., Sandee, A., Van den Berg, M., Van Drie, J. and Wijnholds, J.A., 1994. Oxidative stress induced by copper: defense and damage in the marine planktonic diatom *Ditylum brightwellii*, grown in continuous cultures with high and low zinc levels. *Marine Biology*, 119 (4), 583-590.
- Rijstenbil, J.W., 2002. Assessment of oxidative stress in the planktonic diatom *Thalassiosira pseudonana* in response to UVA and UVB radiation. *Journal of Plankton Research*, 24 (12), 1277-1288.
- Rodríguez, F., Varela, M., Fernández, E. and Zapata, M., 2003. Phytoplankton and pigment distributions in an anticyclonic slope water oceanic eddy (SWODDY) in the southern Bay of Biscay. *Marine Biology*, 143 (5), 995-1011.
- Roy, S., Llewellyn, C.A., Egeland, E.S. and Johnsen, G., 2011. *Phytoplankton pigments: characterization, chemotaxonomy and applications in oceanography*. Cambridge, UK: Cambridge University Press.
- Rüdiger, W., 2006. Biosynthesis of chlorophylls *a* and *b*: the last steps. In: Grimm, B., Porra, R.J., Rudiger, W. and Scheer, H., eds. *Chlorophylls and bacteriochlorophyll*. The Netherlands: Springer, 189-200.
- Saesaengseerung, N., 2013. *High-throughput methods for the analysis of pigments in aquatic sediments*. Thesis (PhD), University of York.

- Samson, G. and Bruce, D., 1995. Complementary changes in absorption cross-sections of Photosystems I and II due to phosphorylation and Mg<sup>2+</sup>-depletion in spinach thylakoids. *Biochimica et Biophysica Acta (BBA)-Bioenergetics*, 1232 (1), 21-26.
- Sathyendranath, S. and Platt, T., 2007. Spectral effects in bio-optical control on the ocean system. *Oceanologia*, 49 (1), 5-39.
- Schreiber, U., Bilger, W. and Schliwa, U., 1986. Continuous recording of photochemical and non-photochemical chlorophyll fluorescence quenching with a new type of modulation fluorometer. *Photosynthesis Research*, 10 (1-2), 51-62.
- Schroeder, D., Oke, J., Malin, G. and Wilson, W., 2002. Coccolithovirus (Phycodnaviridae): characterisation of a new large dsDNA algal virus that infects *Emiliana huxleyi*. *Archives of Virology*, 147 (9), 1685-1698.
- Schwarz, K.B., 1996. Oxidative stress during viral infection: a review. *Free Radical Biology and Medicine*, 21 (5), 641-649.
- Seaton, G.G.R., Lee, K. and Rohozinski, J., 1995. Photosynthetic shutdown in *Chlorella* NC64A associated with the infection cycle of *Paramecium bursaria Chlorella* virus. *Plant Physiology*, 108 (4), 1431-1438.
- Segovia, M. and Berges, J.A., 2009. Inhibition of caspase-like activities prevents the appearance of reactive oxygen species and dark induced apoptosis in the unicellular chlorophyte *Dunaliella tertiolecta*. *Journal of Phycology*, 45 (5), 1116-1126.
- Shutler, J.D., Land, P.E., Smyth, T.J. and Groom, S.B., 2007. Extending the MODIS 1 km ocean colour atmospheric correction to the MODIS 500 m bands and 500 m chlorophyll *a* estimation towards coastal and estuarine monitoring. *Remote Sensing of Environment*, 107 (4), 521-532.
- Smyth, T.J., Pemberton, K.L., Aiken, J. and Geider, R.J., 2004. A methodology to determine primary production and phytoplankton photosynthetic parameters from fast repetition rate fluorometry. *Journal of Plankton Research*, 26 (11), 1337-1350.
- Smyth, T.J., Moore, G.F., Hirata, T. and Aiken, J., 2006. Semianalytical model for the derivation of ocean color inherent optical properties: description, implementation, and performance assessment. *Applied Optics*, 45 (31), 8116-8131.
- Smyth, T.J., Fishwick, J.R., Lisa, A.-M., Cummings, D.G., Harris, C., Kitidis, V., Rees, A., Martinez-Vicente, V. and Woodward, E.M., 2010. A broad spatio-temporal view of the Western English Channel observatory. *Journal of Plankton Research*, 32 (5), 585-601.
- Sosik, H.M., 1999. Storage of marine particulate samples for light-absorption measurements. *Limnology and Oceanography*, 44 (4), 1139-1141.
- Southward, A.J., Langmead, O., Hardman-Mountford, N.J., Aiken, J., Boalch, G.T., Dando, P.R., Genner, M.J., Joint, I., Kendall, M.A. and Halliday, N.C., 2004. Long-term oceanographic and ecological research in the western English Channel. *Advances in Marine Biology*, 47, 1-105.
- Spooner, N., Harvey, R., H., Pearce, G.E.S., Eckardt, C.B. and Maxwell, J.R., 1994a. Biological defunctionalisation of chlorophyll in the aquatic environment II: action of endogenous algal enzymes and aerobic bacteria. *Organic Geochemistry*, 22 (3-5), 773-780.

- Spooner, N., Keely, B.J. and Maxwell, J.R., 1994b. Biologically mediated defunctionalization of chlorophyll in the aquatic environment - I. Senescence/decay of the diatom *Phaeodactylum tricornutum*. *Organic Geochemistry*, 21 (5), 509-516.
- Spooner, N., Harvey, R.H., Pearce, G.E.S., Eckardt, C.B. and Maxwell, J.R., 1994c. Biological defunctionalisation of chlorophyll in the aquatic environment II: action of endogenous algal enzymes and aerobic bacteria. *Organic Geochemistry*, 22 (3-5), 773-780.
- Spooner, N., Getliff, J.M., Teece, M.A., Parkes, R.J., Leftley, J.W., Harris, P.G. and Maxwell, J.R., 1995. Formation of mesopyropheophorbide *a* during anaerobic bacterial degradation of the marine prymnesiophyte *Emiliana huxleyi*. *Organic Geochemistry*, 22 (1), 225-229.
- Squier, A.H., Hodgson, D.A. and Keely, B.J., 2004. Structures and profiles of novel sulfur-linked chlorophyll derivatives in an Antarctic lake sediment. *Organic geochemistry*, 35 (11), 1309-1318.
- Suggett, D., Kraay, G., Holligan, P., Davey, M., Aiken, J. and Geider, R., 2001. Assessment of photosynthesis in a spring cyanobacterial bloom by use of a fast repetition rate fluorometer. *Limnology and Oceanography*, 46 (4), 802-810.
- Suggett, D.J., Oxborough, K., Baker, N.R., MacIntyre, H.L., Kana, T.M. and Geider, R.J., 2003. Fast repetition rate and pulse amplitude modulation chlorophyll *a* fluorescence measurements for assessment of photosynthetic electron transport in marine phytoplankton. *European Journal of Phycology*, 38 (4), 371-384.
- Suggett, D.J., MacIntyre, H.L. and Geider, R.J., 2004. Evaluation of biophysical and optical determinations of light absorption by photosystem II in phytoplankton. *Limnology and Oceanography*, 2, 316-332.
- Suggett, D.J., Moore, C.M., Marañón, E., Omachi, C., Varela, R.A., Aiken, J. and Holligan, P.M., 2006. Photosynthetic electron turnover in the tropical and subtropical Atlantic Ocean. *Deep Sea Research Part II: Topical Studies in Oceanography*, 53 (14), 1573-1592.
- Suggett, D.J., Moore, C.M., Hickman, A.E. and Geider, R.J., 2009. Interpretation of fast repetition Rate (FRR) fluorescence: signatures of community structure versus physiological state. *Marine Ecology Progress Series*, 376, 1-19.
- Suttle, C.A., Chan, A.M. and Cottrell, M.T., 1990. Infection of phytoplankton by viruses and reduction of primary productivity. *Nature*, 347 (6292), 467-469.
- Suttle, C.A. and Chan, A.M., 1993. Marine cyanophages infecting oceanic and coastal strains of *Synechococcus*: abundance, morphology, cross-infectivity and growth characteristics. *Marine Ecology Progress Series*, 92, 99-109.
- Suttle, C.A., 2005. Viruses in the sea. *Nature*, 437 (7057), 356-361.
- Suttle, C.A., 2007. Marine viruses—major players in the global ecosystem. *Nature Reviews Microbiology*, 5 (10), 801-812.
- Szymczak-Żyła, M. and Kowalewska, G., 2007. Chloropigments *a* in the Gulf of Gdańsk (Baltic Sea) as markers of the state of this environment. *Marine pollution bulletin*, 55 (10), 512-528.

- Szymczak-Żyła, M., Kowalewska, G. and Louda, J.W., 2008. The Influence of microorganisms on chlorophyll *a* degradation in the marine environment. *Limnology and Oceanography*, 53 (2), 851-862.
- Szymczak-Żyła, M., Kowalewska, G. and Louda, J.W., 2011. Chlorophyll *a* and derivatives in recent sediments as indicators of productivity and depositional conditions. *Marine Chemistry*, 125 (1), 39-48.
- Tait, K., Airs, R.L., Widdicombe, C.E., Tarran, G.A., Jones, M.R. and Widdicombe, S., in review. Dynamic responses of the benthic bacterial community at the Western English Channel observatory site L4 are driven by deposition of fresh phytodetritus. *Progress in Oceanography*.
- Teklemariam, T.A., Demeter, S., Deák, Z., Surányi, G. and Borbély, G., 1990. AS-1 cyanophage infection inhibits the photosynthetic electron flow of photosystem II in *Synechococcus* sp. PCC 6301, a cyanobacterium. *Federation of European Biochemical Societies letters*, 270 (1), 211-215.
- Thomas, H., Huang, L., Young, M. and Ougham, H., 2009. Evolution of plant senescence. *BioMedCentral Evolutionary Biology*, 9 (1), 163-196.
- Thomas, R., Grimsley, N., Escande, M.-l., Subirana, L., Derelle, E. and Moreau, H., 2011. Acquisition and maintenance of resistance to viruses in eukaryotic phytoplankton populations. *Environmental Microbiology*, 13 (6), 1412-1420.
- Thyssen, M., Alvain, S., Lefèbvre, A., Dessailly, D., Rijkeboer, M., Guiselin, N., Creach, V. and Artigas, L.-F., 2014. Phytoplankton community structure in the North Sea: coupling between remote sensing and automated in situ analysis at the single cell level. *Biogeosciences Discussions*, 11, 15621-15662.
- Timmermans, K., Van der Wagt, B., Veldhuis, M., Maatman, A. and De Baar, H., 2005. Physiological responses of three species of marine pico-phytoplankton to ammonium, phosphate, iron and light limitation. *Journal of sea research*, 53 (1), 109-120.
- Timmermans, K.R., Veldhuis, M.J.W. and Brussaard, C.P.D., 2007. Cell death in three marine diatom species in response to different irradiance levels, silicate, or iron concentrations. *Aquatic Microbial Ecology*, 46 (3), 253-261.
- Tomaru, Y., Takao, Y., Suzuki, H., Nagumo, T. and Nagasaki, K., 2009. Isolation and characterization of a single-stranded RNA virus infecting the bloom-forming diatom *Chaetoceros socialis*. *Applied and Environmental Microbiology*, 75 (8), 2375-2381.
- Treibs, A., 1936. Chlorophyll and hemin derivatives in organic material. *Angewandte Chemie, International Edition* 49, 682-686.
- Utermöhl, H., 1958. Zur vervollkommnung der quantitativen phytoplankton methodik. *Mitteilungen Internationale Vereinigung für Theoretische und Angewandte Limnologie*, 9, 1-38.
- van Bleijswijk, J.D.L., Kempers, R.S., Veldhuis, M.J. and Westbroek, P., 1994. Cell and growth characteristics of types A and B of *Emiliana huxleyi* (Prymnesiophyceae) as determined by flow cytometry and chemical analyses. *Journal of Phycology*, 30 (2), 230-241.

- van der Woerd, H.J., Blauw, A., Peperzak, L., Pasterkamp, R. and Peters, S., 2011. Analysis of the spatial evolution of the 2003 algal bloom in the Voordelta (North Sea). *Journal of Sea Research*, 65 (2), 195-204.
- Van Heukelem, L. and Thomas, C.S., 2001. Computer-assisted high-performance liquid chromatography method development with applications to the isolation and analysis of phytoplankton pigments. *Journal of Chromatography A*, 910 (1), 31-49.
- Vardi, A., Formiggini, F., Casotti, R., De Martino, A., Ribalet, F., Miralto, A. and Bowler, C., 2006. A stress surveillance system based on calcium and nitric oxide in marine diatoms. *PLoS Biology*, 4 (3), 411-419.
- Vardi, A., Van Mooy, B.A.S., Fredricks, H.F., Pependorf, K.J., Ossolinski, J.E., Haramaty, L. and Bidle, K.D., 2009. Viral glycosphingolipids induce lytic infection and cell death in marine phytoplankton. *Science*, 326 (5954), 861-865.
- Vardi, A., Haramaty, L., Van Mooy, B.A.S., Fredricks, H.F., Kimmance, S.A., Larsen, A. and Bidle, K.D., 2012. Host-virus dynamics and subcellular controls of cell fate in a natural coccolithophore population. *Proceedings of the National Academy of Sciences*, 109 (47), 19327-19332.
- Veldhuis, M., Colijn, F. and Venekamp, L., 1986. The spring bloom of *Phaeocystis pouchetii* (Haptophyceae) in Dutch coastal waters. *Netherlands Journal of Sea Research*, 20 (1), 37-48.
- Veldhuis, M.J.W. and Kraay, G.W., 2000. Application of flow cytometry in marine phytoplankton research: current applications and future perspectives. *Scientia Marina*, 64 (2), 121-134.
- Veldhuis, M.J.W., Kraay, G.W. and Timmermans, K.R., 2001. Cell death in phytoplankton: correlation between changes in membrane permeability, photosynthetic activity, pigmentation and growth. *European Journal of Phycology*, 36 (2), 167-177.
- Venn, A.A., Wilson, M.A., Trapido-Rosenthal, H.G., Keely, B.J. and Douglas, A.E., 2006. The impact of coral bleaching on the pigment profile of the symbiotic alga, *Symbiodinium*. *Plant, Cell & Environment*, 29 (12), 2133-2142.
- Vidussi, F., Claustre, H., Bustillos-Guzmán, J., Cailliau, C. and Marty, J.-C., 1996. Determination of chlorophylls and carotenoids of marine phytoplankton: Separation of chlorophyll *a* from divinylchlorophyll *a* and zeaxanthin from lutein. *Journal of Plankton Research*, 18 (12), 2377-2382.
- Walker, J.S., Jie, C. and Keely, B.J., 2003. Identification of diastereomeric chlorophyll allomers by atmospheric pressure chemical ionisation liquid chromatography/tandem mass spectrometry. *Rapid Communications in Mass Spectrometry*, 17 (11), 1125-1131.
- Walker, S.J., Squier, A.H., Hodgson, D.A. and Keely, B.J., 2002. Origin and significance of <sup>13</sup>C-hydroxychlorophyll derivatives in sediments. *Organic Geochemistry*, 33 (12), 1667-1674.
- Walker, S.J. and Keely, B.J., 2004. Distribution and significance of chlorophyll derivatives and oxidation products during the spring phytoplankton bloom in the Celtic Sea April 2002. *Organic Geochemistry*, 35 (11-12), 1289-1298.
- Walsh, J., 1983. Death in the sea: enigmatic phytoplankton losses. *Progress in Oceanography*, 12 (1), 1-86.

- Wang, J., Zhu, J., Liu, S., Liu, B., Gao, Y. and Wu, Z., 2011. Generation of reactive oxygen species in cyanobacteria and green algae induced by allelochemicals of submerged macrophytes. *Chemosphere*, 85 (6), 977-982.
- Waterbury, J.B. and Valois, F.W., 1993. Resistance to co-occurring phages enables marine *Synechococcus* communities to coexist with cyanophages abundant in seawater. *Applied and Environmental Microbiology*, 59 (10), 3393-3399.
- Waters, R.E. and Chan, A.T., 1982. *Micromonas pusilla* virus: the virus growth cycle and associated physiological events within the host cells; host range mutation. *Journal of General Virology*, 63 (1), 199-206.
- Weinbauer, M.G. and Rassoulzadegan, F., 2004. Are viruses driving microbial diversification and diversity? *Environmental Microbiology*, 6 (1), 1-11.
- Weis, E. and Berry, J.A., 1987. Quantum efficiency of photosystem II in relation to 'energy'-dependent quenching of chlorophyll fluorescence. *Biochimica et Biophysica Acta (BBA)-Bioenergetics*, 894 (2), 198-208.
- Werdell, P.J. and Bailey, S.W., 2005. An improved in-situ bio-optical data set for ocean color algorithm development and satellite data product validation. *Remote Sensing of Environment*, 98 (1), 122-140.
- Weston, K., Jickells, T.D., Fernand, L. and Parker, E.R., 2004. Nitrogen cycling in the southern North Sea: consequences for total nitrogen transport. *Estuarine, Coastal and Shelf Science*, 59 (4), 559-573.
- Widdicombe, C.E., Eloire, D., Harbour, D., Harris, R.P. and Somerfield, P.J., 2010. Long-term phytoplankton community dynamics in the Western English Channel. *Journal of Plankton Research*, 32 (5), 643-655.
- Wilhelm, S.W. and Suttle, C.A., 1999. Viruses and nutrient cycles in the sea viruses play critical roles in the structure and function of aquatic food webs. *Bioscience*, 49 (10), 781-788.
- Willstätter, R. and Stoll, A., 1913. *Untersuchungen über chlorophyll*. Berlin, Germany: Springer.
- Wilson, M.A., Airs, R.L., Atkinson, J.E. and Keely, B.J., 2004. Bacterioviridins: novel sedimentary chlorins providing evidence for oxidative processes affecting palaeobacterial communities. *Organic Geochemistry*, 35 (2), 199-202.
- Wilson, W.H., Tarran, G. and Zubkov, M.V., 2002. Virus dynamics in a coccolithophore-dominated bloom in the North Sea. *Deep Sea Research Part II: Topical Studies in Oceanography*, 49 (15), 2951-2963.
- Wood, A.M., Everroad, R.C. and Wingard, L.M., 2005. Measuring growth rates in microalgal cultures. In: Anderson, R.A., ed. *Algal Culturing Techniques*. London, UK: Elsevier Academic Press, 269-285.
- Woodward, E.M.S. and Rees, A.P., 2001. Nutrient distributions in an anticyclonic eddy in the northeast Atlantic Ocean, with reference to nanomolar ammonium concentrations. *Deep Sea Research Part II: Topical Studies in Oceanography*, 48 (4), 775-793.
- Worden, A.Z., Nolan, J.K. and Palenik, B., 2004. Assessing the dynamics and ecology of marine picophytoplankton: the importance of the eukaryotic component. *Limnology and Oceanography*, 49 (1), 168-179.

- Wright, S.W., van den Enden, R.L., Pearce, I., Davidson, A.T., Scott, F.J. and Westwood, K.J., 2010. Phytoplankton community structure and stocks in the Southern Ocean (30–80 E) determined by CHEMTAX analysis of HPLC pigment signatures. *Deep Sea Research Part II: Topical Studies in Oceanography*, 57 (9), 758-778.
- Wyllie, A.H., Kerr, J.F.R. and Currie, A.R., 1980. Cell death: the significance of apoptosis. *International Reviews in Cytology*, 68, 251-306.
- Xie, J., Bai, X., Li, Y., Sun, C., Qian, H. and Fu, Z., 2014. The effect of glufosinate on nitrogen assimilation at the physiological, biochemical and molecular levels in *Phaeodactylum tricorutum*. *Ecotoxicology*, 23, 1-9.
- Yao, P., Yu, Z., Deng, C., Liu, S. and Zhen, Y., 2010. Spatial-temporal distribution of phytoplankton pigments in relation to nutrient status in Jiaozhou Bay, China. *Estuarine, Coastal and Shelf Science*, 89 (3), 234-244.
- Zapata, M., Rodríguez, F. and Garrido, J.L., 2000. Separation of chlorophylls and carotenoids from marine phytoplankton: a new HPLC method using a reversed phase C8 column and pyridine-containing mobile phases. *Marine Ecology Progress Series*, 195, 29-45.
- Zapata, M., Edvardsen, B., Rodríguez, F., Maestro, M.Á. and Garrido, J.L., 2001. Chlorophyll  $c_2$  monogalactosyldiacylglyceride ester (chl  $c_2$ -MGDG). A novel marker pigment for *Chrysochromulina* species (Haptophyta). *Marine Ecology Progress Series*, 219, 85-98.
- Zapata, M., Rodríguez, F., Barra, L. and Ruggiero, V., 2011. Chlorophyll  $c$  pigment patterns in 18 species (51 strains) of the genus *Pseudo-nitzschia* (Bacillariophyceae). *Journal of Phycology*, 47 (6), 1274-1280.
- Zetsche, E.-M. and Meysman, F.J.R., 2012. Dead or alive? Viability assessment of micro- and mesoplankton. *Journal of Plankton Research*, 34 (6), 493-509.
- Zhang, J.-Z. and Chi, J., 2002. Automated analysis of nanomolar concentrations of phosphate in natural waters with liquid waveguide. *Environmental Science & Technology*, 36 (5), 1048-1053.
- Zhu, F., Massana, R., Not, F., Marie, D. and Vault, D., 2005. Mapping of picoeucaryotes in marine ecosystems with quantitative PCR of the 18S rRNA gene. *FEMS Microbiology Ecology*, 52 (1), 79-92.